Biophysical & molecular characterisation of P2X7 receptors & TMEM16F channels complex unravel novel immunoregulatory targets

Federico Cevoli

Université de Strasbourg

École Doctorale des Sciences de la Vie et de la Santé STRASBOURG

UNIVERSITÉ DE STRASBOURG

ÉCOLE DOCTORALE DES SCIENCES DE LA VIE ET DE LA SANTÉ

Laboratoire de **Conception et Application de Molécules Bioactives**

Equipe de **Chimie et Neurobiologie Moléculaire**

[UMR 7199 CNRS]

THÈSE présentée par :

Federico CEVOLI

Soutenue le : **26 septembre 2022**

Pour obtenir le grade de : **Docteur de l'université de Strasbourg**

Discipline/ Spécialité : Molecular and cellular aspects of biology

Biophysical & Molecular Characterisation of P2X7 Receptors & TMEM16F Channels Complex Unravel Novel Immunoregulatory Targets

THÈSE dirigée par :

Dr. GRUTTER Thomas	Directeur de recherche, DR1, CNRS, Université de Strasbourg.

PRÉSIDENT du jury :

Dr. GASMAN Stéphane	Directeur de recherche, INSERM, Université de Strasbourg.

RAPPORTEURS :

Dr. NICKE Annette	Professor, Ludwig-Maximilians Universität München.
Dr. MONY Laetitia	Chargée de recherches, INSERM, École normale supérieure Paris.

MEMBRES EXTÉRNE du jury :

Dr. DI VIRGILIO Francesco	Professor, Università degli Studi di Ferrara.

Table of contents

Acknowledgement

I am very grateful to all my jury members for accepting to evaluate this research work; particularly, I would like to thank Prof. Dr. Nicke and Dr. Mony as examiners, Prof. Dr. Di Virgilio as external member, and Prof. Dr. Gasman as internal president of the jury.

First of all, I would like to thank my Ph.D. supervisor, Prof. Thomas Grutter for the trust and guidance he has given me throughout the research projects, his mentoring and freedom to conduct research really allowed me to gain a huge confidence in my professional as well as developmental skills. Thanks for your support and enthusiasm toward science, and to have built an excellent research environment in which to discuss, explore, and execute news ideas. It has been such an amazing journey – Thank you!!!

To my colleague Adeline Martz, Dr. Peralta and ex-colleagues Dr. Arnould and Dr. Morville, with who I spent incredible moments. To Dr. Arnould from who I learnt that you can actually drink 10 cups of coffee in half-a-day and be fine, thanks for all the chit-chats; to Dr. Morville for all the good laughs; to Dr. Peralta for the huge help in electrophysiology and for the support throughout the years. A particular thanks goes to Adeline, from who I learnt lots of different techniques, thank you so much for the help and for all the good laughs. Thank you to all of you for reassuring me when I had problems. We really had such a great team spirit!!

Finally, and most importantly, to my family, my Mamma and Papà che mi hanno sempre sostenuto e sono stati li per me in qualsiasi momento e qualsiasi distanza, grazie mille di cuore. To my other half, I appreciate everything you have done for me throughout all these years, I love you and I could not have possibly done it without your help – Merci beaucoup!

List of tables and figures:

Abbreviations

7-TMR: 7-transmembrane receptor

9-AC: 9-anthracene carboxylic acid

Å: angstrom

AAV: adeno-associated virus

ABC: ATP-binding cassette

ABP: actin-binding protein

AC: adenylyl cyclase

ADA: adenosine deaminase

ADK: adenosine kinase

ADAM: A-desintegrin metalloproteinase member

AKAP: A kinase anchoring protein

Ado: adenosine

ADP: adenosine diphosphate

AF: actin filament

AIR: aminoimidazole ribonucleotide

AMP: adenosine monophosphate

AMP-PNP: adenylyl imidodiphosphate

ANO: anoctamin

AP2: adaptor protein 2

APAF1: apoptotic protease activator factor 1

APRT: adenine phosphoribosyltransferase

ATF-1: activation transcription factor 1

ATP: adenosine triphosphate

AZ: AstraZeneca P2X7 antagonist

bp: base pair

BSA: bovine serum albumin

BzATP: 2'(3')-O-(4-benzoylbenzoyl) adenosine-5'-triphosphate

CaCC: calcium activated chloride channel

cAMP: cyclic adenosine monophosphate

CAIRS: carboxy-aminoimidazole ribonucleotide synthase

CASP: caspase

CBP: CREB binding protein

C-cys: cytoplasmic cysteine residues

CF: cystic fibrosis

CFTR: cystic fibrosis transmembrane regulator

CNS: central nervous system

CNT: concentrative nucleoside transporter

CRE: cAMP responsive element

CREB: cAMP responsive element binding protein

CREM: cAMP responsive element modulator

Cryo-EM: cryo electron microscopy

Da: Dalton

DAG: diacyl glycerol

DAMP: damage associated molecular pattern

DC: dendritic cell

DNA: deoxyribose nucleic acid

dNTP: deoxynucleotides

dsDNA: double-stranded deoxyribose nucleic acid

DTT: dithiothreitol

E: glutamic acid

EAE: experimental autoimmune encephalomyelitis

eATP: extracellular ATP

ECL1-3: extracellular loop 1-3

E-NPP: ecto-nucleoside pyrophosphatase-phosphodiesterase

E-NTPDase: ecto-nucleoside triphosphate diphosphohydrolase

ENT: equilibrative nucleoside transporter

EPSC: excitatory postsynaptic current

ER: endoplasmic reticulum

EV: extracellular vesicles

FACS: fluorescence activated cell sorting

FCS: fluorescence correlation spectroscopy

FGAR: formyl-glycinamide ribonucleotide GAR

FLIM: fluorescence lifetime imaging microscopy

FRET: fluorescence resonance energy transfer

GAR: glycinamide ribonucleotide

GARS: glycinamide ribonucleotide synthase

GBM: glioblastoma

GEF: guanine nucleoside exchanger

GMP: guanosine monophosphate

GP1: glycosyl phosphatidylinositol

GPCR: G-protein coupled receptor

HPRT: hypoxanthine-guanine phosphoribosyltransferase

ICAM: intracellular adhesion molecule 1

ICER: inducible cAMP early repressor

ICL1-3: intracellular loop 1-3

IKDC: interferon killer dendritic cell

IL: interleukin

IMP: inosine monophosphate

INF-γ: interferon gamma

IP3: inositol triphosphate

KO: knockout

LAK: lymphokine activated killer

LPS: lipopolysaccharide

LTB4: leukotriene-B4

Mac-1: macrophage integrin

MAPK: mitogen activated protein kinase

MC: Monte-Carlo

MOMP: mitochondrial outer membrane permeabilization

MP: mononuclear phagocyte

mRNA: messenger ribonucleic acid

MS: multiple sclerosis

mTOR: mammalian target of rapamycin

MW: molecular weight

NBD: nucleotide-binding domain

NCCD: nomenclature committee cell death

NEK7: NIMA-related kinase 7

NF-κB: nuclear factor Kappa B

NK: natural killer

NLRP3: NOD-like receptor family, pyrin domain containing 3

NMDAR: N-methyl-D-aspartate receptor

$NMDG^{+}$: N-methyl-D-glucamine

NSDAID: non-steroidal anti-inflammatory drug

NT: nucleoside transporter protein

PAMP: pathogen associated molecular pattern

PBS: phosphate buffered saline

PC: phosphatidylcholine

PCD: programmed cell death

PDC: plasmacytoid dendritic cell

PDE: phosphodiesterase

PE: phosphatidylethanolamine

PG: prostaglandin

PI: phosphatidylinositol

PKA: protein kinase A

PLC: phospholipase C

PM: plasma membrane

PMN: polymorphonuclear leukocyte

PNS: peripheral nervous system

PPAT: PRPP amidotransferase

PPI: protein-protein interaction

PRA: phospho-ribosylamine

PRPP: phospho-ribosyl-pyrophosphate

PS: phosphatidylserine

PYD: pyrin domain

R: arginine

RCD: regulated cell death

RNA: ribonucleic acid

RNR: ribonucleotide reductase

RNS: reactive nitrogen species

ROS: reactive oxygen species

SAICARS: succinyl- aminoimidazole carboxamide ribonucleotide synthetase

SCID: severe combined immunodeficiency

SF2: super family 2

SLC: solute carrier

SM: sphingomyelin

SPCM: single photon counting module

TCSPC: time correlated single photon counting

TGF-β: tissue growth factor β

Th: T helper 1

TLR: toll-like receptor

TM: transmembrane

TMD: transmembrane domain

TMEM16: transmembrane protein 16 family

TMEM16FΔ: 16F knockout

TNF-α: Tumour necrosis factor alpha

UDP: uridine diphosphate

UTP: uridine triphosphate

trifGART: trifunctional purine biosynthetic protein adenosine 3

VCAM-1: vascular cell adhesion molecule-1

VLA-4: very late antigen-4

WT: wildtype

Xkr: Xk related protein

α,β-MeATP: α, β-methylene adenosine 5′-triphosphate

β,γ-MeATP: β,γ-methylene adenosine 5′-triphosphate

Chapter 1

Introduction

Purine biosynthetic enzymes can organise themselves into dynamic cellular bodies referred to as purinosome. Understanding the concept within which altered purinosome function controls purinergic transmitter network with other proteins – coordinating the multitude aspects of cell behaviour – requires a synopsis of purine biogenesis and metabolism, with a focus on the relevant cellular functions and molecular pathways involved. As ATP is the primordial form of chemical signalling patrolling the whole purinergic system, this introduction will illustrate the fundamental elements implicated in complex system interactions providing an in-depth, up-to-date, review on current literature.

1.1 Cell homoeostasis, movement, and metabolism

1.1.1 Extracellular nucleotides

Cells display a variety of different shapes in order to optimise their functions. Regulation of cell geometry features a steady-state flux of ubiquitous adenosine triphosphate (ATP) energy supply as well as adenosine (adenine riboside) underling important implications in

cellular organisation, compartmentalisation, and function. While the intracellular role of ATP has been established many years ago (Gordon, 1986; El-Moatassim et al., 1992; Khakh & Burnstock, 2009) as the reservoir of potential chemical energy, at the cytosolic level, extracellular ATP and adenosine have been suggested to participate in vital biological processes including neurotransmission excitability, platelet activation, cardiac function, tissue injury, chronic inflammation, lymphocyte activation, signal transduction such as phospholipid scrambling and secretion in many cell types (Skrabanja et al., 2005; Faulds et al., 1991; Gordon, 1986; El-Moatassim et al., 1992).

Following the release of ATP and adenosine into the extracellular milieu, many cells may express different subclassifications of purinergic and/or nucleotide receptors, such as P2 for ATP or P1 for adenosine (Burnstock, 1990), according to their ligand affinity and specificity (Table 1.1). Specifically, to date, there are four subsets of P1 receptors (A1, A2A, A2B, A3), a family of G-protein coupled receptors (GPCR; 7-transmembrane receptor, 7-TMR), whereas P2 receptors can be classified into two additional receptor subfamilies – ligand-gated ion channels P2X1-7 and GPCR/7-TM receptors $P2Y_{1,2,3,6,11-14}$ (discussed in chapter 1.2). Ultimately, they elicit a variety of intracellular responses of physiological as well as pathological importance. In the extracellular milieu, ATP and adenosine balance is tightly regulated by the concerted activity of ectoenzymes CD39 and CD73. This is vital for the production of adenosine through the degradation of extracellular ATP and whether or not tolerance/immunity are ensued (Silva-Vilches et al., 2018; Mizumoto et al., 2002).

Table 1.1: Purinoceptor subtypes affinity & specificity

Receptor subtype		Distribution	Signalling	Agonists	Antagonists	Diseases
P2X	$P2X_1$	Platelets, spinal dorsal horn neurons, cerebellum, smooth muscle	Intrinsic cation channel (Ca^{2+} and Na^{+})	ATP, ADP, BzATP, α,β-meATP, β,g-meATP, 2-me-ATP, ATPγS	Suramin, PPADS, NF023, NF157, NF279, NF449, NF110, Spinorpin, TNT-ATP	Hypertension, arterial thrombosis
	$P2X_2$	CNS, retina, smooth muscle, autonomic and sensory ganglia, pancreas, pheochromocytes	Intrinsic ion channel	ATP, ADP, BzATP, α,β-meATP, β,g-meATP, 2-me-ATP, ATPγS	Suramin, PPADS, NF023, NF157, NF279, NF449, NF110, TNT-ATP	Bone tumor pain, hearing loss
	$P2X_3$	NTS, sensory and (some) sympathetic neurons	Intrinsic cation channel	ATP, ADP, BzATP, α,β-meATP, β,g-meATP, 2-me-ATP, ATPγS	Suramin, PPADS, NF023, NF157, NF279, NF449, NF110,Spinorpin , TNT-ATP	Cystitis, neuropathic/inflammatory pain
	$P2X_4$	CNS, microglia, endothelial cells, colon, testis	Intrinsic ion channel	ATP, ADP, BzATP, α,β-meATP, β,g-meATP, 2-me-ATP	Suramin, PPADS, NF023, NF157, NF279, NF449, NF110, TNT-ATP	neuropathic/inflammatory pain
	$P2X_5$	Proliferating cells in spinal cord, adrenal medulla, thymus, heart, gut, bladder, skin	Intrinsic ion channel	ATP, ADP, BzATP, α,β-meATP, β,g-meATP, 2-me-ATP	Suramin, PPADS	Bone loss
	$P2X_6$	CNS, motor neurons in spinal cord	Intrinsic ion channel	Function only as heteromultimer	-	-
	$P2X_7$	Immune cells (DC, mast cells, macrophages), pancreas, skin, macroglia	Intrinsic cation channel	ATP, ADP, BzATP, α,β-meATP, β,g-meATP, 2-me-ATP	Suramin, PPADS, NF157, NF279, NF449, NF110, Spinorpin, AZ10606120, GSK-1370319	Neuropathic/inflammatory pain, neurodegenerative and psychiatric diseases, cystitis, cancer, heart diseases and stroke.
P2Y	$P2Y_1$	Epithelial and endothelial cells, immune cells, palates, osteoclasts	PLC-β activation, G_q/G_{11} ↑ IP3	ADP , 2- MeSADP, ADP -β-S	MRS2500, MRS2279, MRS2179	Chronic inflammatory vascular disease, cancer progression
	$P2Y_2$	Epithelial and endothelial cells, immune cells, osteoblasts, kidney tubules	PLC-β activation, G_q/G_{11} ↑ IP3	UTP, ATP, UTPγS, MRS2698, INS37217	AR-C126313, suramin	Metastasis, cystitis, dry eye disease
	$P2Y_4$	Endothelial cells, placenta, spleen, thymus	PLC-β activation, G_q/G_{11} ↑ IP3	UTP, (ATP in rodents), 2' -azido-dUTP	ATP (human), suramin, PPADS	N/A
	$P2Y_6$	T-cells, thymus, activated microglia, placenta, airway and intestinal epithelial cells	PLC-β activation, G_q/G_{11} ↑ IP3	UTP, UDP-β-S, MRS2693	MRS2578, PPADS	Chronic inflammatory vascular disease, hypertension, migraine and vascular pain
	$P2Y_{11}$	Spleen, intestine, granulocytes	PLC-β activation, G_q/G_{11} ↑ IP3, G_s ↑ cAMP	ATP,ATP γS,BzATP,	Suramin, AMP -α-5	Chronic inflammatory vascular disease, myocardial fraction,
	$P2Y_{12}$	Platelets, glial cells	$G\alpha_i$ ↓ cAMP	ADP, ADP-β-S, 2-MeSADP	AR-C69931MX, 2-MeSAMP, clopidogrel	Chronic inflammatory vascular disease, coronary heart disease
	$P2Y_{13}$	Spleen, brain, lymph nodes, erythrocytes, bone marrow	G_i/G_o ↓ cAMP	ADP	AR-C69931MX, 2-MeSAMP	Osteoporosis , diabetes
	$P2Y_{14}$	Stomach, adipose tissue, Placenta	G_q/G_{11} IP3	UDP-glucose, UDP-galagtose, UDP-glucosamine	PPTN, UDP	N/A
P1	$P1A_1$	Automatic nerve terminals, testis, heart, spinal cord, brain	G_i/G_o ↓ cAMP	Adenosine,ionosine , AMP	DPCPX, MRS1754	Atherosclerosis
	$P1A_{2A}$	Lungs, heart, bran, spleen	G_s ↑ cAMP	Adenosine,ionosine , Regadenoson	KF17827	Atherosclerosis, chronic autoimmune disease,
	$P1A_{2B}$	Bladder, large intestine	G_s ↑ cAMP	Adenosine, NECA	MRS1754, MRS1706, Alloxazine	coronary heart disease
	$P1A_3$	Testis, liver, brain, heart, lung	G_i/G_o, G_q/G_{11}, ↓cAMP, PLC-β activation	Adenosine,ionosine , IB-MECA	MRS1220, L-268605, MRS11891	Chronic autoimmune disease

Source: (Burnstock, 1990, 2018b; Dou et al., 2018; Erlinge, 2011; Faas et al., 2017; Jacobson et al., 2009; Zeiser et al., 2016).

In addition, central to cell plasticity, cell motility and phagocytosis is the spatially controlled polymerisation of ATP-bound globular [G] actin monomers to the barbed (+) end of actin filaments (AFs) creating a dense network called actin cortex (Horssen et al., 2009; Chhabra & Higgs, 2007). Notably, although ATP is not required for polymerisation, the addition of ATP-bound G-actin monomers elongates approximately 10-fold faster at the barbed end, as compared to ADP-bound G-actin monomers at the pointed (-) end. Consequently, ADP-actin dissociates more readily than ATP-actin. Because of this difference, for the system to be in a steady state, there is a net loss of actin monomers from the pointed end, which is, in turn, balanced by a net addition of ATP-actin from the barbed end. This process is described as treadmilling. Together, this strengthens the importance of adequate ATP as well as adenosine supplies for the mechanism of cell assembly and disassembly, cell movement, including cell division after mitosis, and changes in cell structure.

Interestingly, actin bundles containing dense, closely spaced same polarity AFs with barbed ends are located adjacent to the plasma membrane (PM). Such synergy provides structural and functional support to lipid organisation (Cooper, 2000) and lipid phase separation (Honigmann et al., 2014) within the PM. This supports the fundamental principle of lipid raft theory, influencing receptors trafficking and regulation at the PM through interactions between cholesterol, sphingolipids, and saturated phospholipids (Honigmann et al., 2014; Simons & Ikonen, 1997; Simons & Sampaio, 2011). Furthermore, recent mass spectroscopy tools have allowed unprecedented data on the lipidome compositions of the two PM leaflets in human erythrocytes (Lorent et al., 2020). The results confirmed PM asymmetry transbilayer composition, showing phosphatidylcholine (PC), choline-containing phospholipids and sphingomyelin (SM) in the exoplasmic (outer) leaflet of the PM, whereas phosphatidylethanolamine (PE), phosphatidylserine (PS) and phosphatidylinositol (PI) occupy the cytoplasmic (inner) leaflet (Figure 1.1a). It has been shown that this segregation of charged lipids to the inner leaflet may have functional implications for the folding, insertion, and orientation of transmembrane proteins (Doktorova et al., 2020; Dowhan et al., 2019; Entova et al., 2018). The PM is therefore in a constant state of flux whereby lipids are continuously shuffled

between leaflets by ATP-consuming asymmetry-driven enzymes (flippases and floppase) and ATP-independent phospholipid scramblases (as detailed in 1.3.2). Together, these transporters mediate the bidirectional trasnbilayer of lipids flow responsible for maintaining specific lipid distributions in the PM. Recent insights have identified two major families of PM phospholipid scramblases belonging to TMEM16 (most notable is TMEM16F or ANO6) as bona fide lipid channels and Xk-related proteins (Figure 1.1b). Immune cells are a perfect example for understanding ATP-gated P2X7 receptor and TMEM16F channel implications in the regulation of PM asymmetry and diseases. Dissipation or loss of PM lipid asymmetry induced by elevated extracellular ATP or nucleotides escaping dying cells can trigger the activation of the ATP-gated P2X7 receptors, resulting in a high intracellular Ca^{2+} level and subsequent membrane blebbing. It is likely that this mode of activation, ATP→ P2X7 → PS exposure → bleb, is orchestrated by a synergistic interaction with TMEM16. Remarkably, defects in TMEM16F activation following an increase in cytosolic Ca^{2+} prevent PS exposure, resulting in the bleeding disorder known as Scott Syndrome. This research thesis pivots on understanding the underlying regulatory mechanisms taking place between P2X7 receptors and TMEM16F channels following immune cell activation.

1.1.1.1 The biology of adenosine triphosphate

ATP is one of the most evolutionary conserved nucleotides, acting as a universal energy source in living cells and commonly employed as a phosphate donor for around 200 different kinases (Traut, 1994). Under physiological conditions, it has been estimated that a human being contains a total ATP concentration of about 0.4-1 μM (Bakker et al., 2007; Faas et al., 2017; Ryan et al., 1996), which can be recycled up to 750 times per day to provide a steady supply of energy throughout the day (H. Chen & Zhang, 2021). Cells display complex mechanisms for synthesising ATP, making its interactions with other signalling systems central to understanding various aspects of cell metabolism, motility, structure, and signalling. Indeed, the hydrolysis of ATP is essential for the active transport of diverse macromolecules, including proteins, lipids, and large-size carbohydrates across the cellular membrane.

(a)

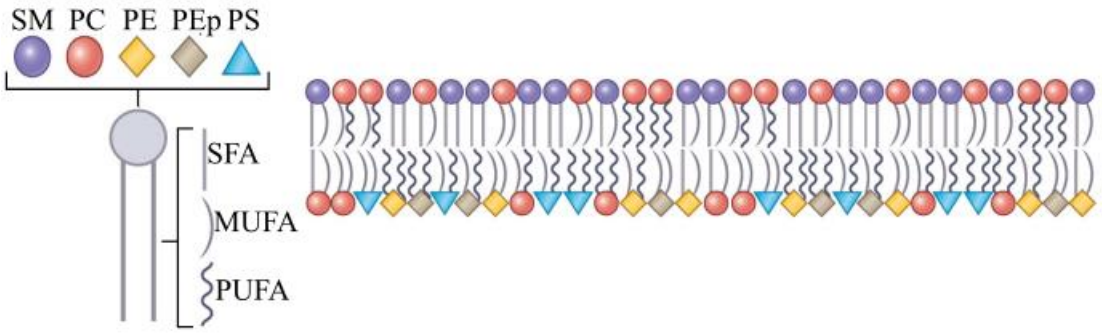

(b)

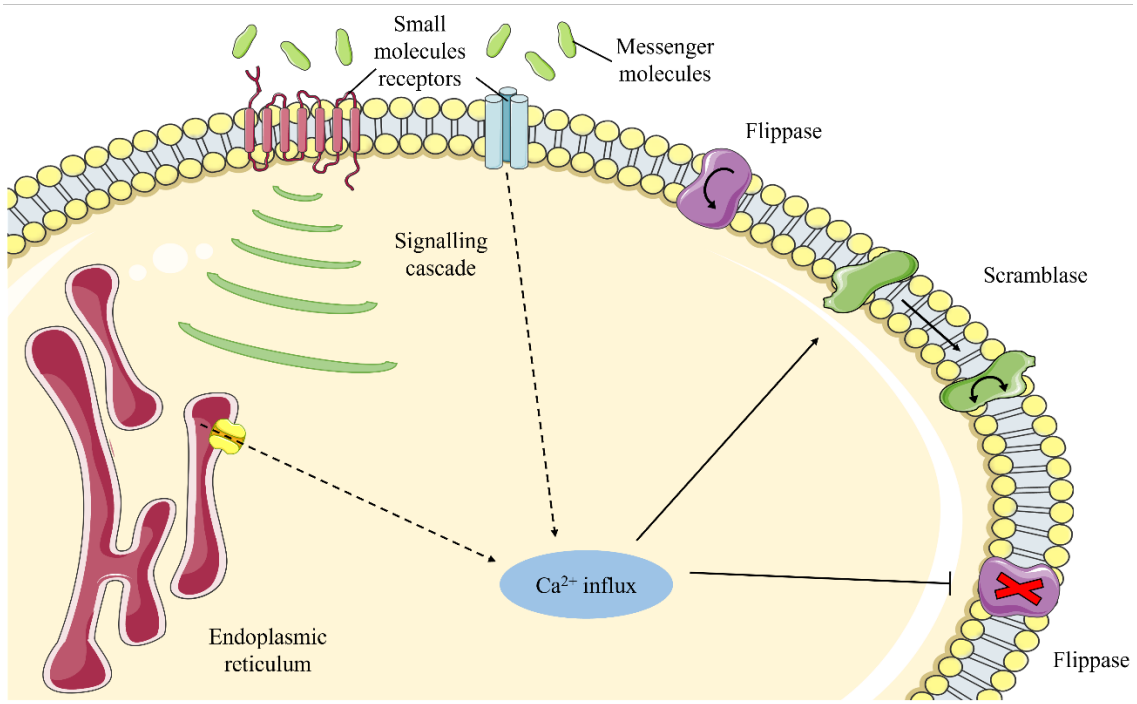

Figure 1.1: Plasma membrane lipid asymmetry and functional roles.
(**a**) Illustration of asymmetric transbilayer lipids composition of PM showing sphingomyelin (SM; blue), phosphatidylcholine (PC; red) present in the exoplasmic leaflet of the plasma membrane, whereas phosphatidylethanolamine (PE; yellow) and phosphatidylserine (PS; light blue) occupy the inner leaflet of the PM. SFA: saturated fatty acid; MUFA: monounsaturated fatty acid; PUFA: polyunsaturated fatty acid. (**b**) Schematic representation of non-apoptotic events regulating PM lipid asymmetry. Examples include small molecule receptors inducing signalling cascade leading to changes in PM asymmetry; ATP released at sites of cells/tissues injury increase cytosolic calcium, which inhibits flippases activation scramblases resulting in loss of lipid asymmetry. (Image source: Doktorova et al., 2020).

The rapidly growing class of ATP-binding cassette (ABC) transporters falls into this category. These are ubiquitous membrane proteins coupling the energy derived from the hydrolysis of ATP to the translocation of solutes across lipid bilayers against a concentration gradient (Holland et al., 2003; Hollenstein et al., 2007; Schneider & Hunke, 1998). In eukaryotic cells, this proteinaceous transporter has been associated with cystic fibrosis (Ambudkar et al., 2003), extrusion of chemotherapeutic drugs, resulting in multidrug resistance in cancer cells (Deeley et al., 2006), and antigen presentation (Higgins, 1992). Moreover, in bacteria, ABC transports aid in extruding toxic substances, contributing to antibiotic resistance (Davidson & Chen, 2004). Typically, the domain organisation of an ABC transporter consists of two hydrophobic transmembrane domains (TMDs) containing six membrane-spanning segments and two highly conserved ATP-hydrolysing domains referred to as nucleotide-binding domains (NBDs) (Higgins, 1992). In eukaryotic systems, TMD and NBD modules are expressed together, yielding a single polypeptide chain, whilst in bacteria, one TMD is fused to one NBD, generating individual functional subunits (Higgins, 1992; Hollenstein et al., 2007). Together, TMD domains are believed to dictate the substrate specificity of ABC transporters.

On the contrary, the highly hydrophilic NBDs can be viewed as the motor domains of the ABC proteins, consisting of RecA-like and helical subdomains, and would normally be located at the cytoplasmic face of the membrane (Hollenstein et al., 2007). The conserved primary structures of the ATP-binding domains comprise two short motifs known as the Walker sites, associated with many nucleotide-binding proteins, and the Q, D, and A loops (Higgins, 1992; Higgins et al., 1982; Walker et al., 1982). Together, they mediate ATP binding, hydrolysis, and interfaces in the assembled transporter (Hollenstein et al., 2007; Schneider & Hunke, 1998). Nucleotide binding occurs in the Walker-A motif, whereas the Walker-B motif, or the catalytic base, contains a conserved glutamate residue orchestrating the nucleophilic attack on ATP through a water molecule. The latter is preceded by a linker peptide or signature motif LSGGQ, recognising the nucleotide in the ATP-bound state. Crystal structure studies have provided key aspects on the role of the Q-loop as a water sensor connecting the γ-phosphate ATP moiety with Q550 of the Q-loop (Zaitseva et al., 2005) and contributing to NBD-TMD coupling inducing important

conformational changes transmission (Hollenstein et al., 2007). Though, the D-loop sequence is not well characterised, Zaitseva et al., suggested that it might be involved in the monomer-monomer contact interface between the two NBDs communicating the functional state of one ATPase-binding site to the other (Zaitseva et al., 2005).

Insights into the A-loop showed 25 highly conserved aromatic residues upstream of the Walker A motif stack against the adenine ring of ATP (Ambudkar et al., 2006). Thus, given the complexity of such a system, it is not surprising that 18 out of 48 ABC genes present in the human genome have been involved in clinical manifestations of illnesses. For instance, in humans, the product of the cystic fibrosis transmembrane conductance regulator (CFTR) gene consists of a deletion of F508 located in the NBDs (Annereau et al., 1997; Tsui, 1992). The primary evidence demonstrating that the CFTR was responsible for cystic fibrosis (CF) came from a mutation study that showed that 68-70% of CF cases resulted from a deletion of phenylalanine at position 508 (Riordan et al., 1989; Rommens et al., 1989). It is believed that the cause may arise from the inability of the mutant to fold efficiently, leading to the proteolytic degradation of the protein (Welsh & Smith, 1993).

1.1.1.2 Energy transduction mechanisms in cells

In humans, ATP energises the transduction of chemicals into mechanical movement. Key to this mechanochemical structure is myosin, orchestrating along with AFs muscle contractions (Smith, 1988). Cells contain numerous actin-binding proteins (ABPs) that strongly govern cyclic polymerisation and de-polymerisation of actin, as described in the aforementioned “treadmilling” process. Myosin motors belonging to the fourth class of ABPs commonly comprise a conserved motor domain containing actin-activated ATPase and a converter subdomain that amplifies and transmits structural rearrangements from the motor domain to the lever arm. The latter region is composed of IQ motifs, forming a helix specialised for the binding of calmodulin and calmodulin-like light chains. Adjacent to this is a variable coiled-coil dimerisation domain involved in protein folding, followed by the cargo-binding domain (Sweeney & Houdusse, 2010).

Over 35 classes of myosin have been characterised in mammalian cells (Odronitz & Kollmar, 2007), all elongating toward the barbed end of AFs, with the exception of myosin VI, which is pointed end directed (Wells et al., 1999). When the muscle contracts, either actively during contraction or passively by stretching, mutual sliding arrays of thick myosin filaments and thin AFs occur, resulting in the shortening of sarcosomes – the contractile regulatory units found on muscle cells (Brenner & Eisenberg, 1987; Huxley, 1969). Importantly, this sliding force is originated in the motor domain of myosin filaments through cyclic interactions with actin molecules (Fujii & Namba, 2017). Here, it is the ATPase site of the myosin head that regulates the cyclic interactions (association and dissociation) of myosin with AFs (Lymn & Taylor, 1971), leading to the so-called actomyosin ATPase cycle. Briefly, binding of MgATP induces myosin to rapidly hydrolyse ATP in the absence of actin; however, the release of the hydrolysis products phosphate (P_i) and ADP only occurs in the actin-bound myosin conformational change. The rate of P_i and ADP release dictates kinetic tuning differences among myosin motors determining the ratio spent between the actin-binding states, known as the duty ratio (Sweeney & Houdusse, 2010). This ATPase-coupled reaction cycle of actomyosin is central to the cellular function of the contractile apparatus. Indeed, mutations occurring within these genes may result in the development of diseases such as nemaline myopathy, in which the regulation of the sarcomere thin filament is impaired leading to weakness of skeletal muscles, respiratory insufficiency, and death (González-Jamett et al., 2018). Molecular dynamics studies have also found that ATP energises the flagellum protein export apparatus of *Escherichia coli* and *Salmonella* through an ATPase ring complex involving FliI6 export protein (Bai et al., 2014; Kitao & Hata, 2018; Nakamura & Minamino, 2019). The latter is thought to hydrolyse ATP, thus activating the transmembrane export gate complex (Nakamura & Minamino, 2019).

Thirdly, high levels of ATP are central to DNA and RNA synthesis processes (Conaway & Conaway, 1988, 1989; Enomoto et al., 1981; Gershowitz et al., 1978). ATP serves essentially as a precursor for all nucleotide biosynthesis. Indeed, it is required for the *de novo* pathway, which is involved in the synthesis of purine and pyrimidine through phosphoribosyl-pyrophosphate (PRPP), and for the salvage pathway, in which purines are

synthesised to their respective nucleotides through the PRPP ribose-phosphate group transfer to their base (Bhagavan & Ha, 2015). The PRPP is a high-energy substrate that is synthesised from ribose 5-phosphate in a reaction powered by the pyrophosphate moiety of ATP (Bhagavan & Ha, 2015). Structural features of the *de novo* and salvage pathways are discussed in section 1.1.2.3. Mutations occurring in the gene coding for the PRPP synthase induce an X chromosome-linked disorder of purine metabolism, leading to hyperuricemia and hyperuricosuria (Zikánová et al., 2018). Furthermore, ATP is generally present in higher concentrations when compared to other nucleoside triphosphates, thus acting as a primary source of transferred phosphate. This peculiar aspect of ATP is of particular interest as the triphosphates of deoxy-nucleosides and nucleosides are substrates for DNA and RNA polymerases, respectively (Bhagavan & Ha, 2015). In addition, the adenine of ATP is directly added to RNA molecules during RNA polymerases, thus acting as a building block of RNA (H. Chen & Zhang, 2021). During DNA synthesis, binding of ATP to ribonucleotide reductase (RNR) regulates the balance of deoxynucleotides (dNTPs) production in cells: a low dNTP concentration inhibits DNA synthesis, whereas a high concentration can lead to deleterious effects (Pai & Kearsey, 2017; Torrents, 2014). Early studies have also elucidated multiple roles for ATP in transcription initiation and processing of RNA. Gershowitz's et al., 1978 work using a purified vaccina virus model provided considerable information on mRNA biosynthesis. This is because the DNA virus contains all the machinery required for synthesising capped, methylated, and polyadenylated mRNA molecules in vitro, leading to actual protein production. In this study, they employed an ATP analogue named AMP-PNP containing an imido group that substitutes the oxygen bridging the γ-phosphate, which prevents the hydrolysis to ADP and P_i by phosphohydrolase enzymes (Yount et al., 1971). They showed that in the presence of AMP-PNP, four critical points of vaccina virus transcription were altered, including RNA synthesis initiation, nascent RNA chain termination, post-transcriptional polyadenylation of the 3'-end of nascent RNA and, lastly, RNA extrusion (Gershowitz et al., 1978). Together, the results argued that ATP hydrolysis may be the essential requirement preceding synthesis initiation of all RNA chains. This notion was later supported by the work led by Conaway and Conaway, in which they argued that the ATP

and magnesium equilibrium reversibly trigger the activation and inactivation of the transcription system prior to RNA synthesis (Conaway & Conaway, 1988).

1.1.1.3 ATP effects on global genome structure

Other important molecular aspects of ATP include, but not limited to, regulation of genome topology, activation of autocrine-paracrine signalling, synthesis of cyclic adenosine monophosphate (cAMP; discussed below in 1.1.2.1), biosynthesis of a plethora of biological compounds, immune system activation, and regulation of ion channels. In this section, we begin by considering chromosome organisation shifting eventually our focus on extracellular ATP role and implications in major cell-types involved in innate and adaptive immunity including neutrophils, monocytes, dendritic cells and lymphocytes.

All nucleated cells share the same complement of genetic material – their genome. To counteract the repeated effects of transcription and replication, cells have specialised ATP-dependent molecular machinery that aids in altering the local and global genome topology (Hauk & Berger, 2016). Thus, positioning chromosomes at the centre of numerous critical processes. Chromosomes can be thought of as the information repository of an organism, containing a myriad of genes and intergenomic tracts of DNA. For instance, the yeast *Saccharomyces cerevisiae* consists of a relatively small genome made of 16 chromosomes with molecular masses varying between 1.5×10^8 and 1×10^9 Daltons (Da), carrying DNA molecules ranging from 2.3×10^5 to 1.532×10^6 contiguous base pairs (bp), whereas, in human they may contain over 270 million bp (Lehninger et al., 2008). Given the very size of a cell, the apportionment of DNA molecules poses an intriguing biological puzzle. ATP-dependent chromatin remodelling enzymes organise histone octamers, located at the centre of a nucleosome core particle, bound to DNA (Hauk & Berger, 2016). These chromatin remodelers harbour an ATPase subunit belonging to SNF2 of the super-family 2 (SF2) helicases employing the energy derived from ATP hydrolysis to alter chromatin structures, resulting in nucleosome sliding, eviction, assembly and histone exchange, exposing the corresponding DNA (Hauk

& Berger, 2016; Hogan & Varga-Weisz, 2007; A. Lin et al., 2020). Four subfamilies of SNF2 motor proteins have been characterised so far, including SWI/SNF, CHD/Mi2, ISWI and Ino80 – based on ATPase sites and accessory domains (Clapier & Cairns, 2009; Flaus, 2006). Furthermore, X-ray work by Durr et al., on *Sulfolobus solfactaricus* has solved the crystallographic structure of the Rad54 translocase enzyme of the SNF2 motor protein family. Several sequence motifs were found to be implicated in ATP hydrolysis and DNA binding of helicases in the two RecA-type Rad54 domains. Thus, suggesting an ATP-dependent cycle of open/closed transition of "RecA" subdomains involved in coupling tight and weak double-stranded DNA (dsDNA)-binding events, ratcheting the duplex DNA through the motor (Dürr et al., 2005). Alterations in ATP-dependent chromatin remodelers have been associated to X-linked mental retardation syndrome and Cockayne, among others (Cho, 2004). Additionally, in bacteria ATP binding to initiator protein, DnaA was found to be central in triggering initiation of chromosome replication – the orisome (Grimwade et al., 2018). DnaA consists of four domains, and tightly binds to ATP and ADP in domain III, which has been implicated in oligomerisation and helicase loading (Kaguni, 2006; Katayama et al., 2017).

1.1.1.4 ATP as a "danger" signal

Cellular release of ATP into the extracellular milieu also acts as a primary signalling molecule in response to mechanical stimuli including osmotic swelling, shrinkage, and lysis (Darby et al., 2003), physical perturbation (Riddle et al., 2007), and to extracellular biochemical cues such as host-pathogen interactions (Bours et al., 2006). To avoid potent ATP-induced immune stimulatory effects, extracellular concentrations of ATP are kept in check by a cascade of enzymes rapidly digesting ATP into adenosine and phosphate (Silva-Vilches et al., 2018b; Yegutkin, 2008). Hence, the interrelation between ATP and Ado is central to determining the final effects on major cell types involved in innate and adaptive immunity, and their concentrations in the extracellular compartment are tightly regulated by ectoenzymes (discussed in 1.1.2.2) catalysing their conversion (Bours et al., 2006). In neutrophils, the body's first line of defence against infections, ATP has been shown to contribute to their effector functions following inflammatory activation

through the expression and regulation of CD39, CD73, P2Y- and P2X7-receptor subtypes (Bours et al., 2006; X. Wang & Chen, 2018). During early stages of inflammation, extracellular ATP stimulates neutrophil adhesion to the vascular endothelial cells and ensuing extravasation by tethering circulating neutrophils to inflammatory sites (Zarbock & Ley, 2009). Extracellular ATP also mediates neutrophil migration to sites of tissue damage by modulating neutrophil accumulation through P2Y2 receptor activation, acting either directly as chemoattractants or indirectly as modulators of the potent neutrophil leukotriene (LT)-B_4 production (Bours et al., 2006). Moreover, ATP-induced chemokine release from cells surrounding inflammation sites may also assist in recruiting neutrophils to these sites, where ATP concentrations are now at their highest. This would now allow neutrophils to exert their bactericidal function without being affected or inhibited by ATP (Bours et al., 2006). The latter mechanism has also been suggested to be stimulated in an ATP-driven manner via activation of the macrophage antigen (Mac)-1, degranulation, and oxidative burst in neutrophils (Miyabe et al., 2004). Micromolar concentrations of extracellular ATP acting through P2Y2 is required for pathogen destruction due to mobilisation of degranulation into the phagolysosome or extracellular compartment in human neutrophils (Faurschou & Borregaard, 2003; Meshki et al., 2004). Enhanced neutrophils granule secretion during inflammation can also be achieved in an autocrine manner via P2Y2-mediated LTB4 generation (Kannan, 2002). Additionally, several studies demonstrated the contribution of extracellular ATP to increased reactive oxygen species production in ATP-primed neutrophils (Bours et al., 2006; Melloni et al., 1986; Sheshachalam et al., 2014), as well as to extend the functional life span of neutrophils by delaying the granulocyte macrophage colony-stimulating survival factor (GM-CSF) (Gasmi et al., 1996; Raiden et al., 2003).

In contrast to neutrophils participating chiefly in acute inflammation, mononuclear phagocytes (MP) are major components of chronic inflammation, comprising committed marrow progenitors giving rise to blood stream monocytes and tissue macrophages. Early during embryogenesis, monocyte-like precursors colonise peri- and extra-vascular sites, becoming resident macrophages, acquiring morphological and functional features representative of the tissue in which they reside (Hume et al., 2019) –

microglia in the brain. The postnatal surge of monocyte migration is a major source of inflammatory response to the wave of apoptotic cell death events occurring in different tissues at that time (Askew et al., 2017; Perry et al., 1985). This changes their functional phenotype as a result of events developing in the tissue microenvironment (Stout et al., 2005). The physiological basis of macrophages' functional heterogeneity enabled the identification of inflammatory monocytes in either classically activated – induced by IFN-γ, TNFα, toll-like receptor – or alternatively activated – triggered by phagocytosis of apoptotic cells or anti-inflammatory cytokines, among others (Stout & Suttles, 2004). Classical macrophages, however, are equipped with gene-expression programmes allowing them to migrate into tissues under homeostatic conditions (Guilliams et al., 2018). If left unchecked, this may result in uncontrolled excessive inflammation events leading to the destruction of healthy tissues. The adhesion of inflammatory monocytes to vascular endothelial cells is the first step in their migration to the vessel wall. A study by Ventura & Thomopoulos, suggested that extracellular ATP increases the adhesiveness of U-937 promonocyte cells with an estimated EC_{50} of 6-10 M contributing to the adhesion of inflammatory to the vascular endothelium (Ventura & Thomopoulos, 1991).

Additionally, extracellular ATP has been shown to upregulate E-selectin adhesion receptor expression on the cell membrane and apoptosis through P2X7-mediated activation of transcription factor NFkB, reducing the rapid flow of monocytes – the monocyte rolling (von Albertini et al., 1998). This is augmented upon TNFα release from endothelial cells (von Albertini et al., 1998). At high extracellular levels, ATP may facilitate transmigration of monocytes between adjacent endothelial cell barriers by either apoptosis, disturbing the endothelium wall integrity (Goepfert et al., 2000, 2001; von Albertini et al., 1998) or by P2Y-mediated shrinkage of the endothelial cells (Tanaka et al., 2004). Similarly to neutrophils, low micromolar concentrations of ATP have been described to enhance the expression of Mac-1 in monocytes, leading to firm adhesion (Goepfert et al., 2001) as well as stimulation of chemokinesis (random cell motility) central to immune cell mobilisation and deployment (Kaufmann et al., 2001; Keller, 1983; Salentin et al., 2003). Both mechanisms have been shown to be G-protein dependent, indicating perhaps P2Y receptor involvement (Honda et al., 2001). Together, the

monocytic lineage (monocytes and macrophages) represents a major group of cytokine-producing cells linking innate and adaptive immunity through a dynamic network, in which extracellular ATP has been shown to regulate the production of IL-1α, IL-1β, IL-6, IL-18, TNFα and others (Figure 1.2) (Bours et al., 2006; Parihar et al., 2010). Lastly, extracellular ATP has also been shown to bi-directionally modulate macrophages-induced phagocytosis of harmful pathogens, allowing the secretions of cytotoxic effectors including production of reactive oxygen species (ROS) and reactive nitrogen species (RNS), via activation purinergic signalling pathways (Bours et al., 2006).

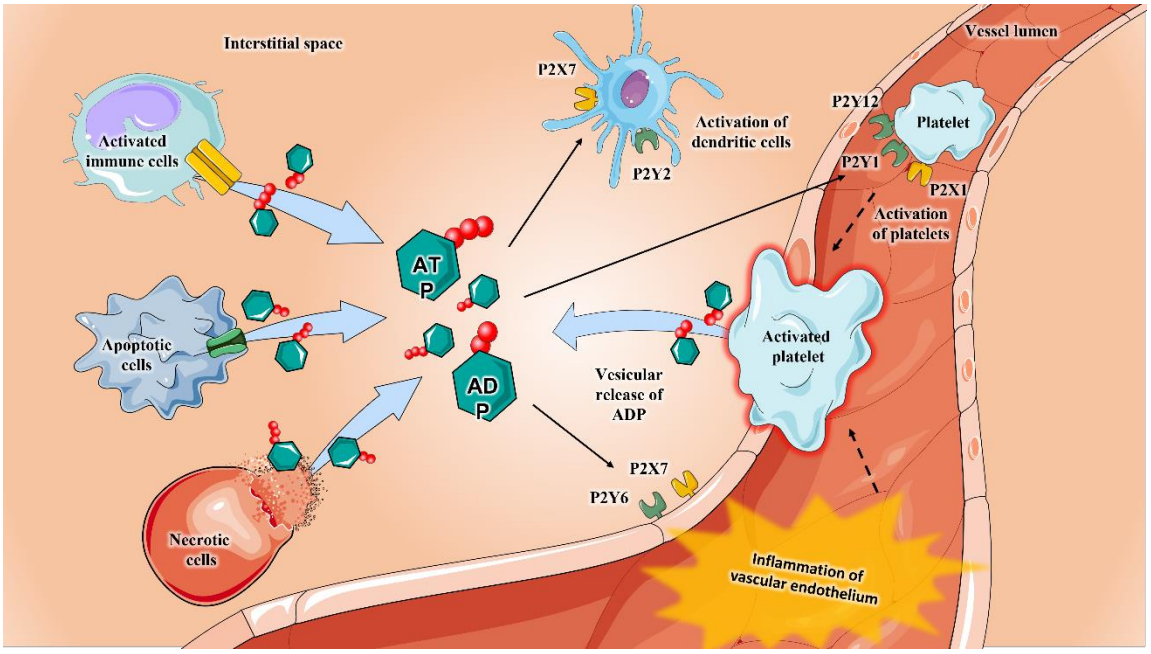

Figure 1.2: Effects of ATP on immune cells function.
Several mechanisms have been implicated in the release of ATP during inflammatory conditions including vascular thrombosis, lung injury, inflammatory bowel condition, and hypoxia. Particularly, ATP can be released from apoptotic either through pannexin or connexin hemichannels present on activated immune cells, or by necrotic cells. Upon release, ATP acts as a potent signalling molecule activating different types of purinergic receptors. (Image source: T.-T. T. Le, Berg, et al., 2019).

Extracellular ATP also induces maturation of dendritic cells (DCs), representing the most efficient antigen-presenting cells (APCs), which activate naïve T cells for the induction of primary immune responses (Banchereau & Steinman, 1998). Immature DCs mainly reside in unperturbed tissues, monitoring the environment for danger signals. Following differentiation or maturation, DCs migrate from peripheral tissues to T cell

areas, releasing both antigen and DC-derived cytokines, thus defining specific lymphocyte-effector mechanisms (e.g., cytotoxic T cells). In particular, la Sala et al., study on the implications of ATP on DCs' maturation found that chronic 24 h incubation of immature purified peripheral blood monocytes-derived DCs with 250 μM ATP doses led to an upregulation of membrane maturation markers (CD54, CD86, CD80, and CD83) as well as augmented their ability to induce proliferation of naïve allogenic T cells (la Sala et al., 2001). The effect of ATP on DCs' differentiation was also described to be in synergy with that of locally assorted pro-inflammatory mediators, including TNFα, bacterial lipopolysaccharide (LPS) and CD40 ligand, perhaps by simulation of different classes of purinergic receptors, such as P2X7 and P2Y11(Cella et al., 1996; la Sala et al., 2001; Schnurr et al., 2000, 2004).

1.1.1.5 The biology of adenosine

ATP's breakdown product, the nucleotide adenosine (Ado), also exerts an important function in physiology as well as pathophysiology, acting as a crossroads between different metabolic signalling pathways (Fredholm, 2007). When compared to ATP, Ado concentrations in the plasma are considerably lower (about 10-fold lower, 40-80 nM; Ontyd & Schrader, 1984). Nonetheless, levels of Ado may rise markedly in response to cellular damage or stress, such as hypoxia, inflammation, and ischemia (Bours et al., 2006). As previously discussed, nucleotides are usually hydrolysed by a cascade of extracellular hydrolysis enzymes, resulting in the formation of their respective nucleotides and free phosphates. For adenine nucleotides, the hydrolysis product Ado initiates additional receptor-mediated function, acting as a ligand for the P1 receptor family (Fredholm, 1997, 2007; Zimmermann, 2000). Together with ATP, Ado is central to the proper functioning of cells, serving as a component for energy production, and precursor to a component of RNA and DNA molecules. Furthermore, an intracellular increase of adenosine production in response to cellular workload, especially at the synapse, mediates excitatory transmitter release (Fredholm, 2007; Jonzon & Fredholm, 1985). For insights into Ado production, regulation, and immunomodulation, an overview of Ado catabolising enzymes, and effects on major immune cell type including a wealth of

publications on the immunologic impact of ATP and Ado extracellular balance are outlined in this section.

Similarly to ATP, extracellular levels of Ado are tightly governed by so-called ecto-enzymes catalysing their conversion and may be found on cell surfaces or in body fluids (Zimmermann, 2000) (Figure 1.3). The currently known ectonucleotidases include members of the ecto-nucleoside triphosphate diphosphohydrolase (E-NTPDase) family, ecto-nucleotide pyrophosphatase-phosphodiesterase (E-NPP) family, alkaline phosphatase, and the key enzyme for the formation of extracellular adenosine, ecto-5'-nucleotidase, also known as lymphocyte surface protein CD73 – all partially sharing tissue distribution and substrate specificity (Zimmermann, 2000). The E-NTPDase family catalyses the sequential degradation of extracellular nucleotide tri- and diphosphates albeit with differing affinity for the individual type of nucleotide. These enzymes share five highly conserved motifs known as apyrase regions, which are of major interest for their catalytic activity (Zimmermann, 2000). Eight different ENTPD genes encode members of this protein family, of which NTPDase1, 2, 3, and -8 are cell surface-located enzymes containing an extracellularly facing catalytic site involved in the breakdown of ATP to adenosine 5'-monophosphate (AMP) with the transient production of free adenosine 5'-diphosphate (ADP) (Robson et al., 2006). Secondly, the E-NPP family consists of three members, including the murine plasma cell differentiation antigen NPP1 (PD-1a; PC-1), NPP2 (autotaxin) and NPP3 (PD-1b), which are capable of hydrolysing cAMP to AMP, ATP to AMP and ADP to AMP (Zimmermann, 2000). Interestingly, a splice variant of NPP2, autotaxin, which is a tumour cell motility-stimulating factor, is also involved in the conversion of AMP to Ado (Bours et al., 2006).

The third ectonucleotidase family comprises non-specific ecto-phosphomonoesterases enzymes mediating the degradation of nucleotide 5'-tri-, -di-, and –monophosphate. Lastly, the fourth family is characterised by the glycosyl phosphatidylinositol (GP1) CD73 protein, which also represents a maturation marker for T- and B-lymphocytes. Surface-bound CD73 is central to the formation and interconversion of extracellular Ado from released adenine nucleotides, and subsequent

signalling through P1 receptors (Zimmermann, 1992). Importantly, CD73-induced adenosine formation has been associated with tumour growth and metastasis (Zhang, 2012). In addition to CD73, two other enzymes are involved in the regulation and catabolism of extracellular Ado including adenosine deaminase (ADA) and adenosine kinase (ADK) (Fredholm, 2007). ADA is a ubiquitously expressed cytosolic enzyme but may also be found on the cell surface in a complex with CD26, which is thought to be an integral component of several cellular processes. Enzymatically, EctoADA functions as a part of the purine metabolism pathways, catalysing the irreversible deamination of Ado and deoxyadenosine, forming inosine and deoxyionosine, respectively. Thus, they contribute to the removal of Ado from the extracellular milieu (Bours et al., 2006; Sauer et al., 2012). Targeted deletions leading to impaired ADA activity may result in accumulation of Ado, deoxyadenosine and dATP, hence excessive purinergic receptors activation (Hönig et al., 2007).

Due to their profound effects on lymphocyte maturation and function, deficiency of ADA leads to severe combined immunodeficiency (SCID) increasing the risk of infection because of generalised immune suppression (Sauer et al., 2012). ADK is also critically involved in the regulation of extracellular Ado by rapid phosphorylation of Ado into AMP. Thus, maintaining the physiological levels of Ado at a low concentration (Fredholm, 2007). Importantly, upon deletion and/or inhibition of ADA, the capacity of ADK is exceeded, resulting in increasing extracellular Ado levels, perhaps contributing to SCID observed in ADA deficient individuals (Fredholm, 2007; Hershfield, 2005). Taken together, a broad range of enzymes participate in the regulation of extracellular nucleotides and nucleoside levels in cells and tissue fluids – critical to purinergic signalling functioning by ATP and Ado (Figure 1.3). Furthermore, such coexistence of ATP and Ado-interconverting pathways on the surface of immune and non-immune cells is central to determining the duration, magnitude, and nature of purinergic receptors-induced signalling.

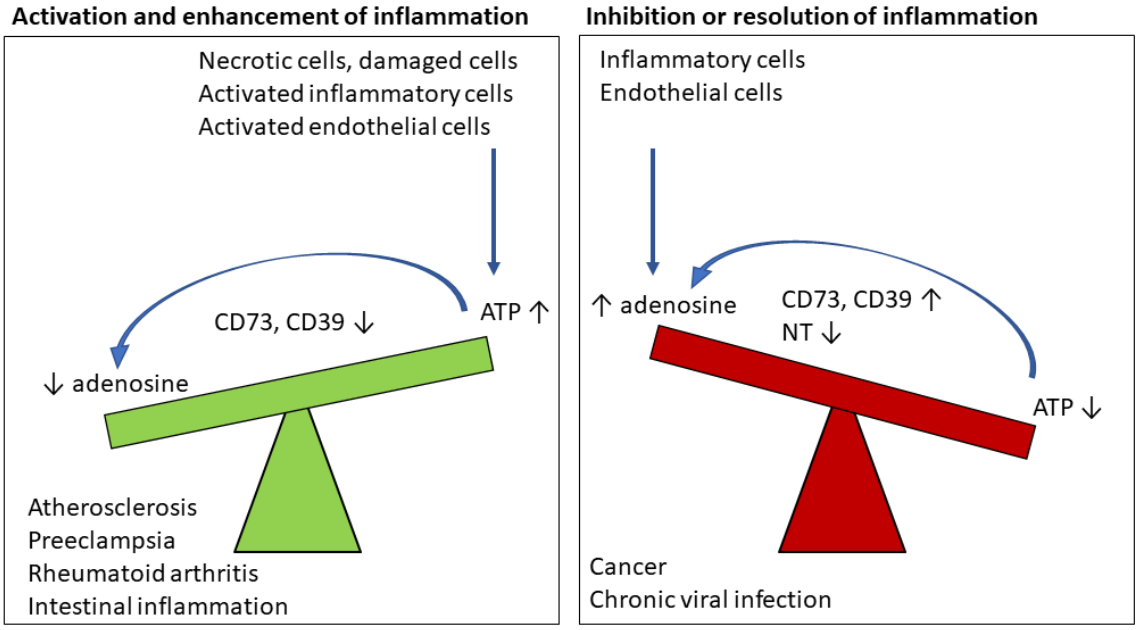

Figure 1.3: Regulation of ATP and Ado balance during inflammation.
High ATP levels at inflammatory sites enhance the production of pro-inflammatory factors, such as ROS and cytokines inhibiting ATP phosphorylating enzymes CD73, and CD39, which together prolong inflammation as observed in conditions including atherosclerosis and rheumatoid arthritis. On the other hand, as cells undergo apoptosis ATP levels at the inflammatory sites significantly diminish by the dephosphorylation of ATP to Ado facilitated by hypoxia increasing the activity of phosphorylating enzymes facilitating the resolution of inflammation (Image source Faas et al., 2017).

1.1.1.6 The role of Ado in the immune system

Ado levels increase in response to conditions of pathology and/or stress in order to diminish the risk of developing adverse events by decreasing cellular work and enhancing energy supply influencing multiple components on immune cells. The clearest example may be attributed to the nervous system. As a neuromodulator, the adenosine A1 receptor affects synaptic transmission via two major mechanisms: inhibition of excitatory neurotransmitters release by limiting calcium entry at the nerve terminals, and secondly by hyperpolarisation of nerves leading to reduced rates of firing, due to increased potassium conductance in the cell body and dendrites (Fredholm, 2007; Fredholm et al., 2005; Prasad, 2011). Furthermore, adenosine acting on A1 receptors have been shown to limit seizure-dependent cell death (Fedele et al., 2006), whereas in astrocytes, ADK may be involved in decreasing Ado levels, thus promoting cell death (Boison, 2006; Fedele et

al., 2006; Kochanek et al., 2006). Additionally, cells of the immune system also express abundant adenosine receptors regulating a plethora of immune functions (Fredholm, 2007). Ado-mediated neutrophils activation appear to bi-directionally regulate neutrophil adhesion to the vascular endothelium (Bours et al., 2006). Increased expression of endothelial P-selectin and neutrophil Mac-1 in response to stimulation of A1 receptors on both neutrophils and endothelial cells have been found to enhance adhesion (Cronstein et al., 1992). Contrarily, Ado inhibits neutrophil adherence to vascular endothelial cells via acting on A2B receptors (Cronstein et al., 1992; D. Yang, 2006). However, it is very likely that Ado-driven inhibitory effects predominate under inflammatory and/or hypoxic conditions, in which extracellular Ado levels are markedly increased. Indeed, studies by Eltzschig et al., (2004; 2005) provided supporting arguments on the implications of extracellular Ado in the regulation of neutrophil leukocytes recruitment to inflamed site. Using wild-type and CD39- and CD73-null mice, they showed that hypoxia-induced neutrophil activation led to ATP release and elevated CD37 and CD39 expression on the vascular endothelium. Together, these factors accelerated the production of Ado from the released ATP4S breakdown, altering the neutrophil adhesion pathway by activating A2 receptors on neutrophils (Eltzschig et al., 2004).

Furthermore, under hypoxic conditions elevated extracellular Ado concentration may be a result of the equilibrative nucleoside transporter (ENT; described in 1.1.2.2) inhibition on the endothelial cells (Eltzschig et al., 2005). Therefore, given A2 receptors expression on endothelial cells providing a barrier to leukocyte migration, it is believed that endogenous adenosine-mediated signalling limits the number of inflammatory neutrophils within a tissue via A2 receptors activation resulting in barrier closing (Fredholm, 2007). Following extravasation (or diapedesis) leukocytes migrate away from the vascular endothelium against a chemoattractants gradient present in inflamed tissues. Chen et al., findings have shown that human neutrophils migration is depended on ATP release amplifying chemotactic signals and direct cell orientation by feedback via ATP receptor and adenosine A3 receptors (Y. Chen et al., 2006). Indeed, following ATP hydrolysis to Ado, A3 receptors were found to be trafficked to the leading edge of the stimulated cell from the intracellular milieu providing signal amplification, and

subsequent neutrophils migration by coupling to $P2Y_2$ receptors (Y. Chen et al., 2006). On the other hand, A2 receptor activation elsewhere on neutrophils was shown to promote membrane retraction at the receding end (Fredholm, 2007). Hence, such antagonist function observed in adenosine receptor may, actually, work in concert to minimise neutrophil-induced collateral damage to healthy tissues – essential to bactericidal function of neutrophils such as phagocytosis, ROS and degranulation (Akkari et al., 2006; Bours et al., 2006; Cronstein, 1994; Fredholm, 1997, 2007).

Other major immune regulators of extracellular Ado are macrophages and monocytes. Indeed, these cells express all four adenosine receptors, albeit the expression level and function vary with the phenotype (Bours et al., 2006). Ectoenzymes regulate mononuclear phagocyte trafficking (Salmi & Jalkanen, 2005), with CD39 and CD37 expression increasing following differentiation by feedback through, for example, Toll-like receptors (TLR), which in turn regulate adenosine production (Fredholm, 2007). Recruitment, adhesion, and migration of these cells to inflammatory foci are critical mechanisms dictating the course of inflammation in tissues. Conflicting studies have been described in the literature concerning the implication of Ado in monocytes, macrophages, and/or microglia function, especially across different species – not surprising given the difficulty of studying tissue-resident cells in a well-defined active state. Indeed, some studies described that in human M1 macrophages, exhibiting a pro-inflammatory phenotype, the expression levels of CD39 and CD73 were considerably lower when compared to anti-inflammatory macrophages (i.e., M2). Thus, indicating lower Ado production (Zanin et al., 2012). While others indicated no changes in macrophage's polarisation following exogenous CD73 or AMP inhibition (Eichin et al., 2015). However, it does seem clear that endothelial A2 receptor activation limits monocytes' migration and adherence to the human endothelial cells by inhibiting cytokines release, mediated by down-regulation of nuclear factor Kappa B (NF-kB)-dependent E-selectin expression (Bouma et al., 1996; Bours et al., 2006; Morandini et al., 1996; Zernecke et al., 2006). Moreover, Zernecke et al., work on CD73 knockout ($CD73^{-/-}$) mice epitomised the role of CD73 in impairing monocytes functioning through A2 receptors. Indeed, they demonstrated that carotid arteries of CD73-deficient mice showed upregulation of

vascular cell adhesion molecule-1 (VCAM-1; CD106) lumina and mRNA levels but reduced intracellular adhesion molecule 1 (ICAM-1; CD54), than do wild-type mice (Zernecke et al., 2006). Interestingly, following wire injury, $CD73^{-/-}$ mice exhibited an even more pronounced increased of endothelial adhesion molecule VCAM-1 then uninjured $CD73^{-/-}$ mice (Zernecke et al., 2006). In agreement with elevated VCAM-1 levels, monocytes' arrest were conspicuously increased in CD73-deficient mice and attributed to the counteraction of Ado binding through A2 receptor limiting very late antigen (VLA)-4 binding to VCAM-1 (Zernecke et al., 2006). The latter is required for monocytes recruitment to $CD73^{-/-}$ carotid arteries (Zernecke et al., 2006). Together, these findings provide crucial insights on the constitutive regulation of adenosine (as the active metabolite produced by CD73) and inflammatory homeostasis.

Lastly, contrarily to ATP, far less is known about the implications of extracellular Ado regulation processes on antigen-presenting cells such as DCs (Fredholm, 2007). P1 receptor expression on dendritic cells appears to be expressed in a phenotype-dependent manner, as in macrophages (Bours et al., 2006; Schnurr et al., 2004). Since defined lymphocyte populations, expressing A2 receptors, employ extracellular Ado to convey immunosuppressant functions, as described for regulatory T cells, acting as a guidance signal for DCs' migration following Treg-derived Ado activation (Ring et al., 2015; Silva-Vilches et al., 2019). First promising evidence for adenosine effects on antigen-presenting cell system were generated from monocyte-derived DCs, in which Ado driven chemotaxis markedly reduced T helper (Th)-1 immune mechanisms by inhibiting TNFα and interleukin (IL)-12 (Panther et al., 2003). Additionally, Schnurr et al., study on P1 receptors in human plasmacytoid DCs (PDCs) indicated a dual adenosine-dependent maturation role: Ado acting on A1 receptors regulates immature PDCs recruitment to inflammatory foci, whereas Ado-mediated A2A receptors expressed on matured PDCs downregulates the pool of cytokines attenuating adverse events of improperly sustained cell signaling activation (Schnurr et al., 2004). Given that Ado is an immunosuppressive metabolite generated by the tumour to promote immune evasion and metastasis (Leone & Emens, 2018) it will be interesting to investigate its effects on the novel type of DCs

termed interferon-producing killer DC (IKDC) exhibiting properties of both natural killer (NK) cells and DC (C. W. Chan et al., 2006; Pletneva et al., 2009).

The extensive available literature on the immunomodulatory signalling of the purinergic system mediated by extracellular ATP and Ado, as detailed in these paragraphs, provides strong quality data, encompassing these endogenous signalling molecules and their purinergic receptor counterparts. Altogether, these regulate extremely complex and interdependent inflammatory, and immune processes. In vitro studies have revealed numerous molecular aspects underlying "the purinergic signaling framework," which connects all types of cell behaviors such as proliferation, migration, differentiation, and death. Thus, the following paragraph will address the importance of purine metabolism – the purinosome – and its components providing exciting evidence on the molecular mechanisms and treatment of human diseases.

1.1.2 Regulators of purinosome

Purinergic signalling is a sophisticated system of regulatory elements that has long been recognised as a fundamental functional unit allowing cells to adopt specific behaviours under dynamically changing conditions. For instance, activation of metabotropic P2Y receptors through ATP contributes to cell proliferation, whereas ATP acting on ionotropic P2X7 receptor may induce cell growth arrest via the recruitment of different protein kinases (Neary et al., 2008). Thus, deregulation or malfunctioning of purinergic transmission can lead to profound pathophysiological conditions including neurological disease, diabetes, and cancer, to mention but just a few. Given the importance of the purinergic system several drugs have already been developed (including A317491 and AF-219 antagonists for P2X2/3 receptors, JNJ-54175446 unlicensed antagonist for P2X7, tecadenoson agonist for A1 Ado receptor, among others) targeting different purinergic receptors, whilst others are currently undergoing clinical trials (Huang et al., 2021). Therefore, the generation of specific cell morphologies is an active process requiring a broad range of scaffold proteins and cellular regulators that together form the purinosome.

The purinosome is composed of four fundamental units: The omnipresent second messenger cAMP, equilibrative nucleoside transporter (ENT) and concentrative nucleoside transport (CNT), the salvage & de novo pathways generating cellular purine pools, and the mammalian target of rapamycin (mTOR)-microtubule-purinosome-mitochondria axis that is central to spatial regulation of the purinosome (Huang et al., 2021). These four building blocks differ in their function and range of cellular effects that govern purine biogenesis and metabolism. Often this means dynamically influencing the outcome of purinergic signalling in tissues microenvironment.

1.1.2.1 Cyclic AMP

First described in 1957, the cyclic adenosine monophosphate is now the universal second messenger regulator of extracellular ligands, fundamental to cellular physiological responses to hormones, neurotransmitters, cytokines, and lipid mediator – i.e., first messengers (Sutherland & Rall, 1958). The expression and activity of cAMP homeostasis are tightly regulated by two families of enzymes called adenylyl cyclase (AC) and cyclic nucleotide phosphodiesterase (PDE), whose balance is critical for normal metabolism and gene expression in all living organisms (Raker et al., 2016; Sassone-Corsi, 2012). AC is comprised of nine membrane-bound isoforms and one soluble isoform (Raker et al., 2016) catalysing the conversion of ATP into cAMP (Taussig & Gilman, 1995), and differing in their expression patterns as well as stimulus-specific responses (Sassone-Corsi, 2012; McKnight, 1991). Additionally, PDE consisting of 11 different subfamilies serves as the sole route for degradation of intracellular cyclic nucleotides, occuring in isoforms- and splice variants-dependent manners (Bender & Beavo, 2006). For instance, it has been described that certain cAMP phosphodiesterase enzymes, such as PDE4, increase in response to adenylate cyclase in human Jurkat T-cells, eliciting changes in cAMP expression, which in turn stimulates the mRNA synthesis of new PDEs (Erdogan & Houslay, 1997). Thus, resulting in a cAMP/ PDE-specific feedback loop, contributing to the complexity of this pathway. Furthermore, spatial compartmentalisation of both ACs and PDEs within the cell further regulates the evanescent presence of cAMP at a more subcellular level (Serezani et al., 2008). The recognition mechanism occurring between

intracellular second messengers and extracellular receptors is what engender unique biochemical reactions involved in a series of physiological effects.

Second messengers are intended to convert and amplify extracellular signals either through the activation of protein kinases or by acting on intracellular ligand-gated channels altering membrane potentials and their degradations, as in the case of PDE in cAMP lead to signal termination (Yan et al., 2016). Most prominently, AC-derived cAMP production stimulates activation of cAMP-dependent protein kinase A (PKA), a symmetrical complex consisting of a regulatory (R) subunit dimer and two catalytic (C) subunits (Brown et al., 2012; Walsh et al., 1968). Binding of cAMP to the R subunit leads to conformational changes in the PKA holoenzyme, resulting in dissociation of its catalytic subunits, which is now available to phosphorylate with specific Ser and Thr residues on numerous downstream targets, such as the transcription factor cAMP response element-binding protein (CREB) (Serezani et al., 2008; Turnham & Scott, 2016). Thus, propagating the cAMP responsive cell signalling cascade events. PKA-induced stimulation from a high level of cytosolic cAMP also leads to phosphorylation of other cAMP response element members including cAMP-responsive modulator (CREM), activation of transcription factor-1 (ATF-1), nuclear factor-κB (NF- κB), and other nuclear receptors (Raker et al., 2016); thus strengthening the concept of cAMP as a regulator of immunity. Particularly important is the phosphorylation event occurring as a result of PKA activation allowing the aforementioned proteins to interact with the transcriptional coactivators CREB-binding protein (CBP) and p300 upon binding to cAMP-response elements (CREs) in target genes (Mayr & Montminy, 2001; Sassone-Corsi, 2012). Notably, in IPC-81 leukaemia cells the CREM was shown to induce transcripts corresponding to the powerful repressor ICER (Inducible cAMP Early Repressor), which levels remain elevated until cell death (Sassone-Corsi, 1995). This generates a negative feedback loop that regulates cAMP-induced transcription (Sassone-Corsi, 1995). cAMP is uniformly distributed all through the cytoplasm of the cell (Iancu et al., 2008), forming submembranous pools compartmentalised in microdomains, containing AC and PDE localised next to PKA signalling to A-kinase anchoring proteins (AKAPs) (Edwards & Scott, 2000). Note, however, that the activity of PKA can also be counterbalanced by

many other transcription factors, i.e., nuclear receptors (Sassone-Corsi, 2012), or by specific protein phosphatases (Raker et al., 2016). Importantly is the cAMP effector EPAC, a guanine nucleotide exchanger (or GEF), promoting activation of small GTPases, such as Rap1, that results in the increase of integrin-mediated cell adhesion (Bos, 2003, 2006). Thus, making such system much more complex, and together influence the specificity and selectivity of cAMP signalling, tailoring distinct forms of cell or tissue-specific regulation.

Transmitted cAMP directly augments cytosolic cAMP levels, which shortly after excretion is converged to Ado and AMP by the sequential actions of cell-surface bound PDE and the ectoenzymes CD73 and CD39 (Gödecke, 2008; Raker et al., 2016). Notably, the effect of extracellular cAMP conversion to Ado is dependent on the P1 receptors expressed on neighbouring cells. For instance, Ado-mediated A2A and A2B receptors activation stimulates AC increasing intracellular cAMP levels, whereas by signalling through A1 and A3 receptors, extracellular Ado downregulates AC stimulation, attenuating cAMP generation (Gödecke, 2008; Mazziotta et al., 2022). Furthermore, due to the ability of cAMP effectors to fuel cellular function, cyclic AMP also exerts modulatory effects on many immune cells (Figure 1.4). Markedly, in the innate immunity, where the functional state of macrophages and polymorphonuclear leukocytes (PMNs) orchestrate the inflammatory phases of the immune response, appears to be accompanied by alterations in intracellular cAMP levels, leading to changes in inflammatory effectors (Aronoff et al., 2006; Raker et al., 2016; Serezani et al., 2008). Two major phenotypes of monocytes can be found in mice: $LyC6^{high}$ exhibiting proinflammatory behaviour and $LyC6^{low}$ displaying, on the other hand, anti-inflammatory activity (Raker et al., 2016). Elevated cAMP levels appear to upregulate murine orphan nuclear receptor Nr4a1 (Nur77), whose expression represses inflammatory genes. Thus, preferentially transitioning from an inflammatory $LyC6^{high}$ phenotype to $LyC6^{low}$ reparatory state in the presence of inflammatory stimuli that would otherwise inhibit the Nur77 expression (Raker et al., 2016). In regard to immunosuppressive functions, elevations in intracellular

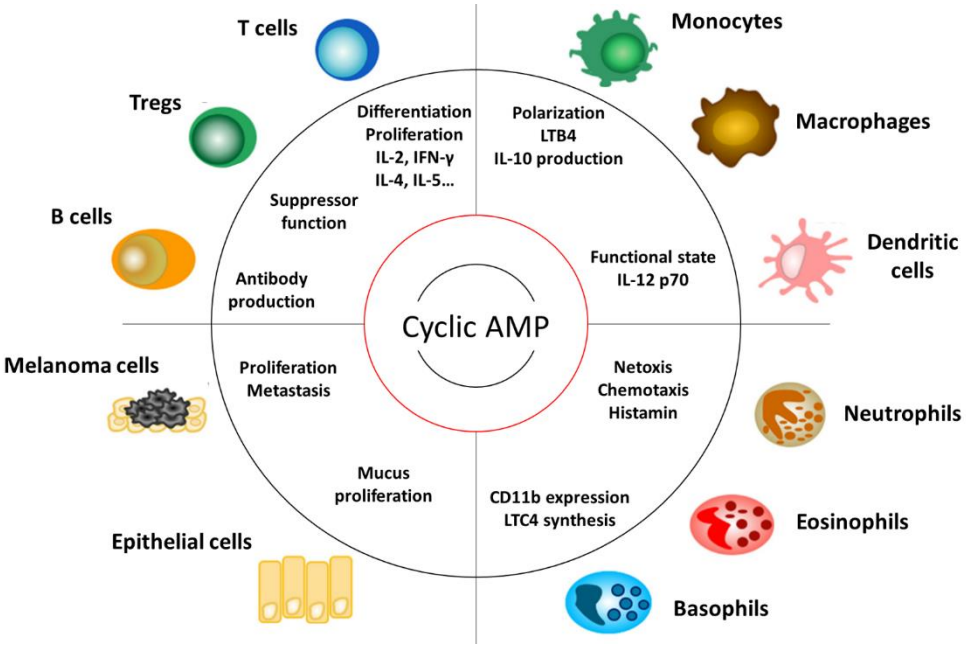

Figure 1.4: Effects of cyclic AMP on cell physiology.
Evaluation of cyclic adenosine monophosphate (cAMP) function on different cell types including immune (T and B lymphocytes, monocytes, macrophages, granulocytes, and dendritic cells), tumour, (melanoma cells) and epithelial cells (Image source: Raker et al., 2016).

cAMP levels depress proinflammatory cytokines including TNF-α, IL-1β and IL-12, among others, whilst enhancing IL-10 immunosuppressive cytokine production (Aronoff et al., 2006); as it occurs also in DCs, in which cAMP levels in turn modulate T cell adaptive immunity (J. Lee et al., 2015). Notably, the latter cytokines are also known as effectors regulated by purinergic receptors signalling. Therefore, through these effects, cyclic AMP allows myeloid cells to mount an effective immune response against foreign pathogens. In addition to innate cell function, cAMP concentrations also influence NK cell adherence and cytotoxic activity (Raker et al., 2016), in which adenosine stimulation has been shown to inhibit lymphokine-activated killer (LAK) cytotoxic function via cAMP-dependent activation of the regulatory subunits of PKA (Lokshin et al., 2006). Accordingly, since its discovery, cyclic AMP has positioned itself as the archetypal second messenger controlling cellular information processing, further highlighting the importance of purine metabolism for the correct functioning of all organisms.

1.1.2.2 ENT & CNT transporters

Other fundamental regulatory units of the purine metabolism include the adenosine transporters belonging to two gene families encoding equilibrative and concentrative nucleoside transporter proteins (Figure 1.5). In particular, ENT1, in which pharmacology is relatively well understood, has long been recognised as a major component of the purinoceptors signalling system – albeit CNT2 and CNT3 have also been identified as purinergic modulators given their affinity for Ado and concentrative capacity (Pastor-Anglada & Pérez-Torras, 2018b). Together, this further strengthens the relevance of ENT and CNT in purinergic signalling.

As mentioned previously (see subsection 1.1.1.5), oscillations of Ado levels are very likely to be dependent upon the tissue microenvironment and their appearance may be viewed as the result of sequential metabolic signals from various ectonucleotidases as well as other enzymes such as ADA and ADK, which orchestrate this cascade. Adenosine cannot permeate through cellular membranes and, thus, requires selective transport that maintains its homeostatic levels. Both translocation processes involved in the transport of Ado are encoded by genes belonging to the SoLute Carrier (SLC) families – the sodium-dependent, concentrative solute family 28 (SLC28; containing CNT1, CNT2 and CNT3) and the equilibrative solute carrier family 29 (SLC29; containing ENT1, ENT2, ENT3, and ENT4) (Hammond, 2021; Pastor-Anglada & Pérez-Torras, 2018a, 2018b). Although small slicing variants of human CNT3 and ENT2 have been reported in the literature (Grañé-Boladeras et al., 2016; Redzic et al., 2010), appear, nevertheless, to play no significant role in modulating purinergic signalling (Pastor-Anglada & Pérez-Torras, 2018b). CNTs are obligatory inward transports mediating unidirectional uptake of nucleosides in the cells coupled to the sodium gradient, with a translocation stoichiometry ratio of 1:1 for CNT1 and CNT2, whereas a 2:1 coupling ratio for CNT3 (Pastor-Anglada & Pérez-Torras, 2018a, 2018b). Substrate selectivity and specificity differ between subtypes, allowing CNT proteins displaying high-affinity transport for Ado to promote its disposal from the extracellular milieu owing to their “concentrative” capacity (Gray et al., 2004; Pastor-Anglada & Pérez-Torras, 2018b). Accordingly, predominant substrates

specificity for hCNT1 include pyrimidine nucleosides and adenosine, while hCNT2 carries purine nucleosides and uridine, and hCNT3 mediate the uptake for both pyrimidines and purines (Gray et al., 2004). On the other hand, transport through ENTs is bidirectional, exhibiting a broad permeant selectivity driven by a nucleoside concentration gradient across biological membranes, and broad substrate specificity for both purines and pyrimidines (Pastor-Anglada & Pérez-Torras, 2018a). Moreover, ENTs are widely distributed across cell types, displaying a lower nucleoside specificity as compared to their CNT counterparts, with the exception of ENT4, which is evolutionary divergent from the other ENT subtypes (Pastor-Anglada & Pérez-Torras, 2018a). In particular, hCNT2 and hCNT3 display the highest affinity for adenosine among both transporter subtypes (Pastor-Anglada & Pérez-Torras, 2018b). Moreover, due to its unique stoichiometry, hCNT3 is a promising candidate to direct crosstalk regulations between Ado receptors and transporters, considering also the remarkable ability to concentrate nucleosides intracellularly (Pastor-Anglada & Pérez-Torras, 2018b). Accordingly, ENT proteins translocating adenosine equalise its levels on the two sides of the membrane, while CNT proteins transport extracellular adenosine against a concentration gradient, thus maintaining elevated Ado levels in the cells (Huang et al., 2021).

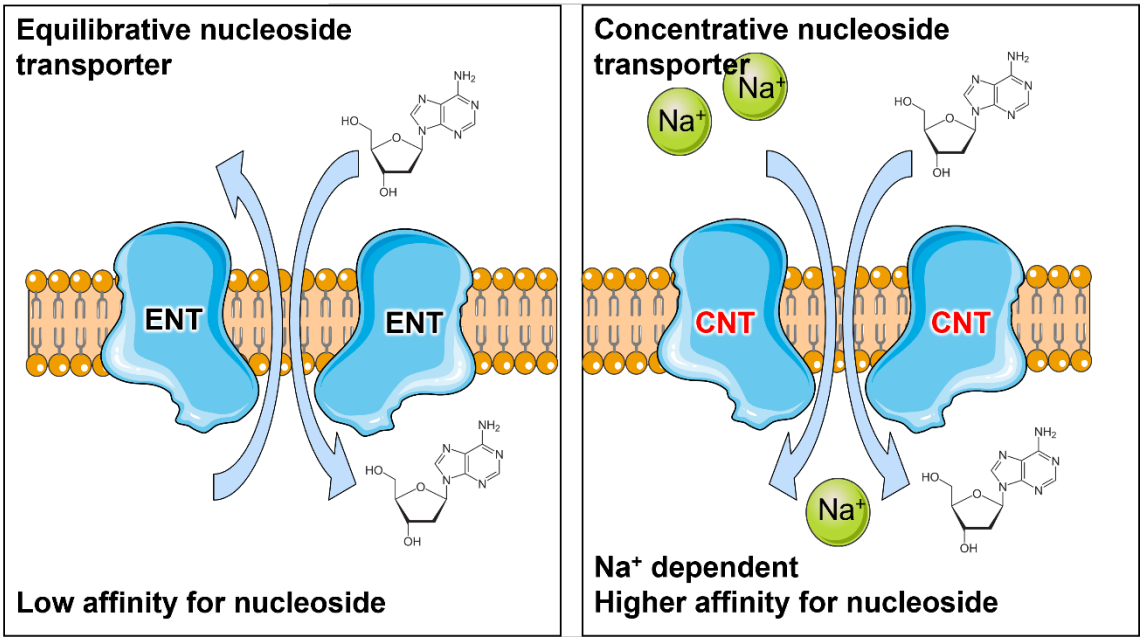

Figure 1.5: Equilibrative nucleoside transporter and concentrative nucleoside transporter activity differences. Concentrative nucleoside transporter (CNT) is an obligatory inward transport orchestrating unidirectional uptakes of nucleosides against a sodium gradient. On the contrary, equilibrative nucleoside transporter (ENT) is

bidirectional owing to its broad permeant selectivity for both purines and pyrimidines (Image source: Dasari et al., 2016).

Evidence supporting the functional link between these plasma membrane transporters and purinergic signalling derives from several pharmacological approaches employing subtype-specific inhibitors targeting ENTs exclusively. This is because no specific inhibitors are currently available for CNTs proteins, with the exception of Cladribine (Mavenclad®), whose absorption, uptake and distribution were recently described to be mediated exclusively by both ENTs proteins and CNT3, but with low affinity (Hermann et al., 2021). In general terms, purinosome mediated NT-stimulation envisages both nucleoside transporters being activated by extracellular Ado acting on P1 receptors, resulting in Ado removal and purinergic signalling termination. Furthermore, functional changes in the expression patterns of some NT proteins (particularly ENT1) in pathophysiological states that are also known to be associated with oscillations in Ado concentrations provide more support to this NT-purinosome cascade (Pastor-Anglada & Pérez-Torras, 2018b). Most of the available literature highlighting the role of ENT function in purinergic-dependent physiology has been developed around Choi's et al., ENT1 knock-out mouse model, which is phenotypically normal compared to the wild-type. It has long been hypothesised that acute ethanol administration activates adenosine receptors, raising extracellular Ado levels by selectively reducing ENT1 activity (Nagy et al., 1989). However, long-term exposure decreases ENT1 expression, which prevents ethanol from increasing extracellular Ado levels (Nagy et al., 1990). Additionally, *in vivo*, ENT1 knock-out mice displayed reduced ethanol-induced acute responses (i.e., hypnosis and ataxia) but increased alcohol consumption (Choi et al., 2004). These findings correlated with a reduction in the activation of adenosine A1 receptors-mediated attenuation of glutamatergic excitatory postsynaptic currents (EPSC) in the nucleus accumbens, that led to a decrease in Ado tone and increased CREB phosphorylation in the striatum (Choi et al., 2004). Ethanol consumption into ENT1 knock-out mice was reversed to a wild-type level upon administration of A1 receptor agonist (Choi et al., 2004). This animal model also provided crucial insights in ENT1-induced purinosome cardio-protection in the cardiovascular system. It is widely accepted that purinergic cardio-protection is orchestrated by several components including NTs, purine nucleoside,

adenosine receptors, adenosine, and their concomitant signalling pathways. Indeed, ENT1 knock-out mice exhibited fewer myocardial infraction associated with increased adenosine plasma lever as well as higher cardio-protection when compared to wild-type littermates (Rose et al., 2010). Overall, the involvement of ENTs in the modulation of purinergic signalling especially in the central nervous system (CNS), but also in other organs, furthered our understanding of NTs implication in modulating flux of adenosine signalling representing an important component of the purinosome.

1.1.2.3 The salvage & de novo pathways

So far, we have highlighted the importance of purine metabolism in meeting energy demands (as enzyme cofactors) and facilitating nucleotide assembly (as components of signal transduction), generating a cellular purine pool that aids in a broad range of cellular processes, allowing for the proper functioning of organisms. This purine pool is determined and maintained through two major pathways, namely de novo synthesis and the salvage cascade (Figure 1.6), each depending on a shared metabolite, phosphoribosylpyrophosphate (PRPP) (Camici et al., 2019). Purines are synthesised de novo in 10 chemical reactions catalysed by 6 enzymes clustering adjacent to microtubules and mitochondria forming a multi-enzyme dynamically purinosome complex (An et al., 2008) – that is activated when purines are in deficit to meet increasing purine synthesis demand.

Biosynthetically, the de novo synthesis begins with the consumption of PRPP, and finishes with the production of ionosine monophosphate (IMP), whose by-products include adenosine and guanosine (An et al., 2008). Briefly, these six enzymes include trifunctional purine biosynthetic protein adenosine-3 (trifGART) containing a glycinamide ribonucleotide (GAR) synthase (GARS) catalysing the conversion of phosphoribosylamine (PRA) to GAR via GARS (Step 2), GAR to formylglycinamide ribonucleotide (FGAR) via GAR transformylase (Step 3), and of formylglycinamide ribonucleotide (FGAM) to aminoimidazole ribonucleotide (AIR) (Step 5) via AIR synthase domain (An et al., 2008). In addition to this, two bifunctional enzymes, the

multifunctional protein ADE2 (PACS) that catalyses carboxyaminoimidazole ribonucleotide synthase (CAIRS) (Step 6), and succinyl-aminoimidazole carboxamide ribonucleotide synthetase (SAICARS) (Step 7); and a purine biosynthesis protein PURH (ATIC) responsible for the last two synthesis steps: aminoimidazole carboxamide ribonucleotide transformylase (AICAR Tfase) (Step 9) and IMP cyclohydrolase (IMPCH) (An et al., 2008). The remaining three enzymes are described as monofunctional including FGAM synthetase (FGAMS), PRPP amidotransferase (PPAT) and adenylosuccinate lyase (ADSL) catalysing only one reaction through the de novo synthesis (Figure 1.6) (Huang et al., 2021). The core of the purinosome, however, is generated through strong binding interactions occurring among PPAT, trifGART and FGAMS (Huang et al., 2021). This highly conserved and energy-intensive pathway also features a higher amino acids consumption (mainly, aspartate, glutamine, and glycine) and metabolites than the salvage pathways (Huang et al., 2021). Interestingly, this metabolic fluctuation is also observed in proliferating cancer cells requiring elevated glutamine consumption and acidic microenvironments, which would suggest a potential synergy effect between overexpressed de novo purine synthesis and oncogenesis.

On the other hand, the salvage pathway ensures that during proliferation and in the absence of the purinosome, purine nucleotides are supplied by recycling degraded bases derived from the de novo pathway. In fact, preformed purine rings can be catalysed into their corresponding nucleoside monophosphate in just one step by reacting via adenine phosphoribosyltransferase (APRT) and hypoxanthine-guanine phosphoribosyltransferase (HPRT) activities utilising PRPP as co-substrate (Camici et al., 2019) (Figure 1.6). For instance, during this cascade, AMP can be produced from adenine through the action of APRT (Silva et al., 2008), and IMP and GMP may also be generated from hypoxanthine and guanine, respectively, by using HPR transferase as donor for the phosphoribosyl moiety (Townsend et al., 2018). Importantly, preformed purine rings were reported to alter purinosome formation ensuring that an appropriate amount of nucleotides is produced in order to sustain metabolic and replicative needs of organisms (Camici et al., 2019). Besides, due to lower energy costs, cells tend to be highly dependent on the salvage pathway, especially in the case of brain and bone marrow cells, which lack the de novo

synthesis pathway (Huang et al., 2021). In addition to purinosome formation, the salvage housekeeping gene, HPRT also serves as a functional regulatory unit to purine production as documented by Lesch-Nyhan patients whose deficits in the latter gene showed significant overproduction of purines (Townsend et al., 2018). Furthermore, individual with partial reduction in HPRT levels, rather than total loss, have been shown to develop gout-like conditions leading to Kelley-Seeg-Miller conditions (Townsend et al., 2018; Zoref-Shani et al., 2000). Interestingly, one of the most widespread purine-related conditions associated with dysregulation of purinoceptors function (mainly, P2Y1, P2Y2, A1, A2, P2X2,P2X3, P2X4, P2X6 and P2X7) is indeed gout disease (Huang et al., 2021). Accordingly, the regulatory role of the HPRT gene establishes important connections with other purine-related enzymes, further shaping the complexity of this system. It has been suggested that a negative feedback loop may be responsible for directing purines production within the cells, which upon sustained productions have been achieved, cells utilise HPRT to block further synthesis (Townsend et al., 2018). Similarly, in the de novo pathway the six enzymes generating the purinosome tend to form numerous metabolic complexes, termed metabolon, with other purine-derived enzymes in order to meet nutrient demand (Huang et al., 2021).

In this regard, the purinosome cannot be described and/or associated as single functional entity to de novo pathways, but as a driving force contributing to the whole purine metabolic system that also control cell homeostasis and movement. Additional components associated with the purinosome include adenylsuccinate synthase (ADSS) catalysing the conversion of IMP to AMP, inosine monophosphate dehydrogenase (IMPDH) regulator of intracellular guanine pool catalysing IMP to xanthosine (X) MP, and also non-enzyme proteins including chaperons HSP70 and HSP90 (Huang et al., 2021; Zhao et al., 2015). Collectively, this further confirms the idea that cells are capable of perceiving extracellular purine concentrations by dynamically controlling formation, signalling initiation and turnover of purinosome leading to undefined molecular cascades that underly many physiological and pathophysiological processes. Furthermore, its formation has been described to be cell-cycle dependent and regulated also by numerous GPCR agonists and kinase (as casein kinase 2; CK2) (French et al., 2016).

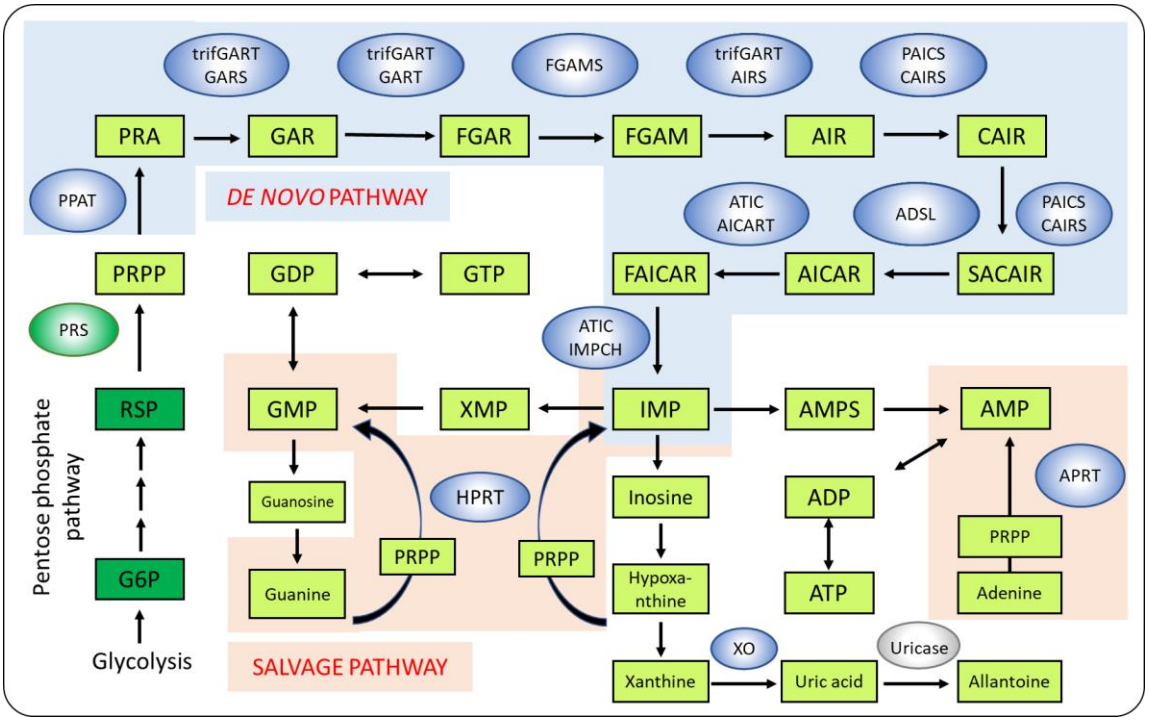

Figure 1.6: The salvage cascade and de novo synthesis pathways.
The de novo synthesis (blue) composed of six enzymes catalysing implicated in 10-step reactions using as a substrate phosphoribosylpyrophosphate (PRPP) produced by glycolysis and pentose phosphate pathways (green). The salvage pathway (orange) generates purine nucleotides characterised by the activity of two enzymes, termed hypoxanthine-guanine phosphoribosyl transferase (HPRT) and adenine phosphoribosyl transferase (APRT) (Image source: Huang et al., 2021).

1.1.2.4 mTOR-microtubule-purinosome-mitochondria axis

Increasing number of purinosome-modulating components were reported to undergo phosphorylation, further implying that certain kinase pathways play important signalling roles in this process (Huang et al., 2021). To examine the implications of intracellular signalling in the purinosme, French et al., (2016) carried out a high-throughput kinome screening, which showed that mTOR influences not only purinosome assembly with mitochondria, but it is also critical for proper functioning of the purinosome itself (French et al., 2016). Accordingly, considering the high-energy supply demand required for de novo purine biosynthesis, spatiotemporal colocalisation with the mitochondria generates elevated concentrations of ATP, allowing for efficient purinosome-linked enzymatic reactions. Thus, providing purines that can be concurrently used for the production of ATP

(French et al., 2016). This synergy poses a greater risk in cells that preferentially utilise oxidative phosphorylation for ATP including numerous cancerous tumours, for instance breast cancer, glioblastoma, hepatocellular carcinoma, among others (French et al., 2016). In addition to mTOR association, cytoskeletal structures have also been proposed to participate in the organisation of purinosome formation (An et al., 2010) – not surprising given important cellular structural elements associated with the cytoskeleton as previously discussed. Considering also long proposed roles of cytoskeletal structures in the organisation of sequential metabolic enzymes (Srere, 1987). For instance, aldolase, a glycolytic enzyme, that has been identified in the actin cytoskeleton. Importantly, to satisfy increases in energy demands, glycolysis rapidly augments ATP availability production, which appears to be correlated with dynamic conformational changes in actin structures taking place in the cell cycle (Bereiter-Hahn et al., 1995). In this regard, work by An's et al. group identified, using fluorescent live cell imaging, that functionally active purinosomes colocalised with a network of microtubule, which govern their spatial distributions in the cytoplasm upon purine production is demanded (An et al., 2010). Furthermore, nocodazole treatment directly interfering with microtubule formation in cells impeding the rate of de novo synthesis (An et al., 2010) as well as abrogating physical interaction between mitochondria and purinosome (C. Y. Chan et al., 2018). Collectively, these findings point towards a microtubule-assisted transport mechanism contributing to purinosome-mitochondria colocalization, in which mTOR facilitates microtubule-based protein transport. Thus, generating this newly termed mTOR-microtubule-purinosome-mitochondria axis (Huang et al., 2021) that is central to purinosome regulation required for proper functioning of organisms.

1.2 Purinoceptors structure & function

So far, we have introduced all the fundamental players orchestrating the regulation and production of purines. The latter in turn exert essential physiological effects by acting on purinergic receptor (or purinoceptors) initiating complex signal transduction cascades referred to as the purinergic signalling system, pivotal factor in cell proliferation,

differentiation, and death occurring during development and regeneration (Burnstock, 1990, 2018a; Burnstock & Verkhratsky, 2010). Cells may express different subclassifications of purinoceptors, such as P2 recognising ATP or P1 for adenosine (Burnstock, 1990). In this section we shall briefly summarise key concepts in purinoceptor family classification, structure, and transduction mechanisms with a focus on P2X7 receptors.

1.2.1 A brief history of purinoceptors

The purinergic signalling system employing purines and pyrimidines as cellular effectors was initially proposed in the early 1970s, when ATP was recognised as a chemical transmitter in the autonomic nervous system (Burnstock & Verkhratsky, 2010). Particularly, the term "purinergic system" was first coined by Burnstock et al., following direct evidence for ATP release from non-adrenergic, non-cholinergic inhibitory nerves of the guineapig taenia coli and bladder (Burnstock et al., 1970, 1978). Importantly, after considerable discontent and resistance in the scientific community, purinergic signalling is now widely recognised and its interaction with other signal molecules makes it an attractive target for therapeutics (Burnstock & Verkhratsky, 2010). This initial refusal was partly due to the fact that, at the time, ATP was only viewed as an ubiquitous intracellular molecule rather than a neurotransmitter, despite strong evidence surrounding the existence of a powerful ectoenzyme involved in the breakdown of ATP (Burnstock, 2006). Today, the purinergic signalling machinery comprises a diverse range of eco-, soluble, and intracellular enzymes, nucleoside transporters, ion channels, and GPCRs (as examined so far) that are ubiquitously expressed in every organ and/or system of the human body.

1.2.2 Adenosine: P1 receptors

P1 receptor (P1R) subtypes are a class of purinergic GPCRs recognising Ado as endogenous ligand. Briefly, P1 family members were cloned and characterised in the early 1990s, including A1, A2A, A2B and A3 owing to their distinct affinity for Ado and tissue-specific expression (Burnstock, 2018a; Fredholm et al., 2001). These four subtypes exhibit

a similar molecular architecture made of a 7-transmembrane (TM) α-helical structure with an extracellular N-terminus and an intracellular C-terminus, three extracellular loops (ECL1-3) and three intracellular loops (ICL1-3). All subtypes have an *N*-glycosylation site located on the amino-terminal domain contributing to receptors trafficking to the plasma membrane (Sheth et al., 2014). Located on the C-terminus are serine and threonine residues acting as phosphorylation sites for kinases, enabling receptor desensitisation (Sheth et al., 2014). Contrary to Ado A2A, all other receptor subtypes display palmitoylation sites at the end of a short membrane associated helix (termed helix 8), which mutations were shown to have no particular effect on the binding to G proteins or receptor down-regulation (Piirainen et al., 2011). Coupling of P1 receptors to G proteins occurs through the C-terminus and the third intracellular loop (Sheth et al., 2014).

P1 receptors A1, A2A and A3 are activated by physiological levels of extracellular Ado that are in the nanomolar range, whereas A2B requires elevated micromolar levels of extracellular Ado (Fredholm et al., 2001). Similar levels have been observed in pathological conditions including hypoxia (Huang et al., 2021). Notably, low extracellular concentration of Ado preferentially activates A1 receptor subtype. Functionally, Ado receptors can also be classified depending on their differential coupling to AC affecting cytoplasmic cAMP, as previously described. The A1 and A3 receptors couple to $G_{i/o}$ proteins supressing AC and thus, negatively regulating cAMP production leading to a reduction in both PKA activity and CREB phosphorylation (Sheth et al., 2014). On the other hand, the A2A and A2B receptors couple to $G_{s/olf}$ proteins, which stimulate AC augmenting cAMP production resulting in PKA activation and CREB phosphorylation (Sheth et al., 2014). Physiologically speaking, this positive and negative feedback mechanism is of paramount importance. For instance, activation of A1R in cardiac monocytes and of A2R in cardiac fibroblast by extracellular Ado, resulted in reduction of cAMP levels in cardiac monocytes, but increased cAMP production in cardiac fibroblast, thereby preventing fibrosis and myocardial hypertrophy (Huang et al., 2021). Furthermore, in some cases, the A1R may also regulate other effectors, apart from AC, such as phospholipase C (PLC) via a pertussis toxin-sensitive G protein or by direct coupling to G_q protein, and mitogen-activated protein kinase (MAPK) (Sheth et al., 2014).

Importantly, PLC mediates diacyl glycerol (DAG) production, which endogenously stimulates protein kinase C activation and inositol triphosphate (IP3), which leads to calcium release from the endoplasmic reticulum (ER) calcium stores (Huang et al., 2021). Moreover, different P1 receptors can form functional heteromeric structures with each other, altering the binding properties of receptors present in the complex, as demonstrated for A1-A2A receptors heterometric complex (Ciruela et al., 2006; Cristóvão-Ferreira et al., 2013; Sheth et al., 2014). Thus, coupling to both G_i and G_s proteins, which display opposite cAMP signal regulation as described above. Together, Ado receptors modulate numerous pathophysiological functions with greater implications, mostly in the cardiovascular, immune and CNS systems (Figure 1.7) (Burnstock, 2018a). Furthermore, the formation of Ado has been viewed as a "protective" signal effector, occurring in different conditions of stress and distress (Fredholm, 2007). This is because Ado reduces energy-rich activities while promoting nutrient supply, thus making Ado receptors important therapeutic targets (Huang et al., 2021).

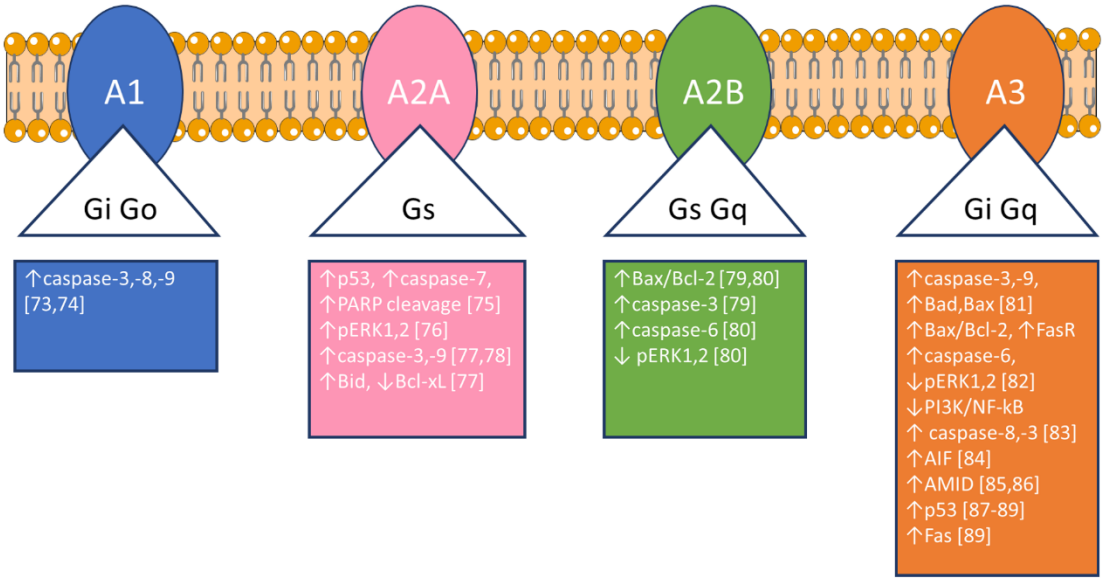

Figure 1.7: Classification of P1 adenosine receptor subtypes.
Four different P1 receptors are depicted in the figure differing from one another according to their association to G-proteins including Gi/Go for A1; Gs for A2A; Gs/Gq for A2B; and Gi/Gq for A3 (Image source: Camici et al., 2019).

P1 receptors are also widely distributed in the CNS, acting as "go-between", regulating the release of neurotransmitters as well as neuromodulators (Sebastião & Ribeiro, 2009). The A1 receptors are more abundant in synaptic regions of the cortex, hippocampus, and cerebellum, but may also be present on oligodendrocytes, astrocytes, and microglia, thereby modulating synaptic transmission (i.e., release of glutamate, serotonin, GABA etc…) in most brain areas (Sheth et al., 2014). On the contrary, A2A receptors are mainly localised to the striatum and olfactory bulb, but also to presynaptic sites in the hippocampus, modulating as well the release of neurotransmitters including noradrenaline (Sheth et al., 2014). Low levels of both A2B and A3 receptors have been detected in neuronal, glial cells and in the cortex, hippocampus and stratum, respectively (Sheth et al., 2014). Important functional effects of genetic deletion targeting P1 receptors have been described in the literature including increased aggression and anxiety, no inhibition of synaptic transmission, decreased long-term potentiation and increased insulin and glucagon secretion associated with A1 receptors (Burnstock & Verkhratsky, 2010); A2A receptors deletion reported decreased motor activity, reduced alcohol sensitivity and withdrawal, increased platelet aggregation and inflammatory responses, and decreased pain threshold (Burnstock & Verkhratsky, 2010); $A2_B$ deletion increased histamine level whilst reducing IL-13 secretion from mast cells (Burnstock & Verkhratsky, 2010); lastly, deletions impairing A3 receptors resulted in increased in motor activity, reduced TNFα production from mast cells, attenuated local inflammatory response and increased tolerance to ischaemia (Burnstock & Verkhratsky, 2010), to name but just a few.

1.2.3 ATP: P2Y receptors

P2Y receptors (P2Y-Rs) belonging to the metabotropic GPCRs subfamily group of the P2 nucleotide receptor family are subdivided into eight receptor subtypes including $P2Y_1$, $P2Y_2$, $P2Y_4$, $P2Y_6$, $P2Y_{11}$, $P2Y_{12}$, $P2Y_{13}$, and $P2Y_{14}$. The missing subtype numbers were reported as non-mammalian receptors having no functional responsiveness to nucleotides (Burnstock, 2018a). Generally, all P2YRs are classed within the δ-branch of rhodopsin-like GPCRs containing two structurally different subgroups owing to high levels of

sequence divergence: $P2Y_1$, $P2Y_2$, $P2Y_4$, $P2Y_6$, $P2Y_{11}$, and $P2Y_{12\text{-}14}$ (Jacobson et al., 2020). Indeed, human $P2Y_1$ and $P2Y_{12}$ have a reported sequence homology of just 19%, yet sharing similar pharmacological profiles (von Kügelgen & Hoffmann, 2016; Figue 1.8). P2YRs are activated not only by ATP but also through other exogenous nucleotides, such as uridine triphosphate (UTP), uridine diphosphate (UDP) and ADP, with varying efficacy (Figure 1.8). By analogy to Ado receptors, crystal structures of $P2Y_{\text{-}1}$ and $_{\text{-}12}$ receptors confirmed general GPCRs features, including 7TM hydrophobic regions flanked by three ECLs and three ICLs (von Kügelgen & Hoffmann, 2016). All P2YRs contain four cysteine residues localised at their extracellular domains forming two disulfide bonds between the amino-terminal region and ECL-3, and between ECL-1 and ECL-2 as described for $P2Y_{\text{-}1}$, $_{\text{-}2}$ and $_{\text{-}12}$ (von Kügelgen & Hoffmann, 2016). Furthermore, mutagenesis and modelling studies have identified TM-3, -6 and -7 as ligand recognition sites for P2YRs (von Kügelgen & Hoffmann, 2016). Structurally, P2Y receptors may also form homo- and heterodimers complex as described for P1 receptors. Interestingly, Yoshioka at al., showed a dimer consisting of $P2Y_1$ and A1 receptors, which differed markedly in their pharmacological profiles as to the respective monomers (Yoshioka et al., 2001). They also reported a reduced ADPβS (P2Y1R agonist) dependent forskolin-evoked cAMP regulation in HEK293T A1R/$P2Y_1$R co-transfected cells affected by A1 receptor antagonist (Yoshioka et al., 2001). Thus, collectively, indicating that binding of ADPβS to the complex inhibits AC via A1R coupled $G_{i/o}$ protein (Yoshioka et al., 2001), further highlighting the diversity and complexity of purine signalling.

Functionally, P2Y receptors couple to G proteins, differentially modulating similar downstream effectors as to those previously describe for P1 receptors including AC and PLC (Huang et al., 2021) as well as stimulation of MAPK (Burnstock, 2018a). The G_q-coupled P2Y receptors including $P2Y_1$, $P2Y_2$, $P2Y_4$, and $P2Y_6$ regulate PLC activation leading to increases in inositol phosphate and calcium release from the ER stores, whereas the G_i-coupled $P2Y_{12}$, $P2Y_{13}$, and $P2Y_{14}$ attenuate AC reducing cAMP accumulation and control of ion channel activity (Figure 1.8) (von Kügelgen & Hoffmann, 2016). In contrast, $P2Y_{11}$ receptors couple to both G_q and G_s resulting in the activation of cAMP and calcium signalling with implications in cancer cell motility and invasion (Di Virgilio,

Sarti, Falzoni, et al., 2018). As previously discussed, nucleotide affinity of P2YRs varies among subtypes, but is generally in the lower micromolar range (Jacobson et al., 2020), indicating a high reactivity of these receptors to very small variations in the local nucleotide concentration. Briefly, $P2Y_1$ G_q-coupled receptors are activated by ADP and 2-methylthio-ADP analogue, which is even more potent (Jacobson et al., 2020). On the contrary, ATP acts as an antagonist or partial agonist at the $P2Y_1$Rs (Jacobson et al., 2020). $P2Y_1$ mRNA expression has been shown to be expressed in the brain, prostate, and placentas (Burnstock, 2018a), as well as in post-mortem individuals diagnosed with Alzheimer's disease (Moore et al., 2000). Here, a strong $P2Y_1$-like immunoreactivity in the hippocampal pyramidal cells and adjacent interneurons is strikingly localised to neurofibrillary tangles, neuritic plaques, and neuropil threads (Moore et al., 2000).

$P2Y_2$Rs are activated by equivalent concentrations of ATP and UTP but also by dinucleoside polyphosphates, such as diquafosol that is currently used as medication for dry eye syndrome in East Asia (Jacobson et al., 2020). $P2Y_2$ mRNA has been observed in olfactory bulb, basilar artery, and other tissues (Burnstock & Knight, 2004). For instance, in smooth muscle cells, key pro-inflammatory cytokines (i.e., TNFα, IL-β and interferon, IFNγ) were shown to upregulate $P2Y_2$ receptors expression, whereas $P2Y_2$R activation in epithelial cells augments Cl^- secretion and promotes inhibition of sodium (Na^+) absorption (Burnstock, 2018a). The most potent agonist for human $P2Y_4$ is UTP, albeit contradictory evidence is also reported equipotent activation by ATP in rat and mouse $P2Y_4$ (Burnstock, 2018a; Jacobson et al., 2020). $P2Y_4$ receptors are mainly distributed in the endothelial cells but have been described also in other organs (Burnstock & Knight, 2004). $P2Y_6$ receptors are activated by UDP displaying high levels of expression primarily in epithelial cells, placenta, T cells and thymus (Burnstock & Knight, 2004). $P2Y_{11}$R gene exhibits a unique profile as compared to P2Y subtypes containing within the coding sequence a 1.9kb intron separating two exons encoding the first six amino acid residues and the remaining part of the protein, respectively (Abbracchio et al., 2006). ATP is a potent physiological activator of human $P2Y_{11}$ receptors sharing 70% homology with the canine P2Y11 receptors, which, however, display a higher efficacy for ADP than ATP (Jacobson et al., 2020) – not found in the mouse or rat genome (von Kügelgen &

Hoffmann, 2016). They exhibit a wide tissue distribution, including the human brain, pituitary gland, spleen, liver and intestine (Abbracchio et al., 2006). A naturally occurring agonist for both P2Y-$_{12}$ and -$_{13}$ is ADP located in subregions of the brain, but also abundant in smooth muscle cells, heart and monocytes, among others (Burnstock, 2018a). Importantly, $P2Y_{12}$ antagonists are commercially used for the treatment of cardiovascular events including myocardial infraction or stroke by reducing platelet aggregation (von Kügelgen & Hoffmann, 2016). Lastly, $P2Y_{14}$ receptors are about 47% identical to the $P2Y_{12}$ and $P2Y_{13}$ counterparts, activated by UDP and sugar derivatives, and show potential chemoattractant and neuroimmune function (Burnstock, 2018a). Gene deletion targeting P2Y receptors has also been described in the literature with reported implications in haemostatic, metabolic, epithelial, immunological and cardiovascular phenotypes (Burnstock & Verkhratsky, 2010).

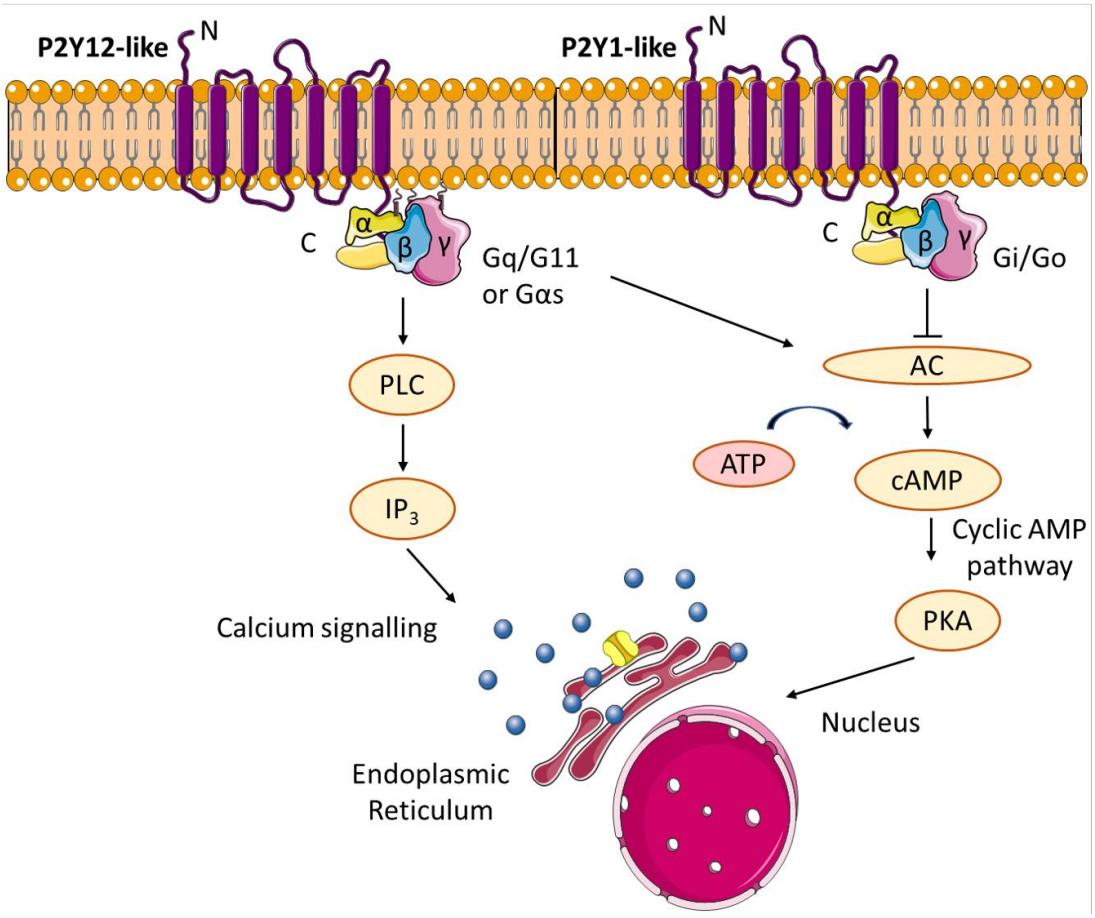

Figure 1.8: P2Y purinoceptors structure and signalling pathways initiation. Structural characteristics of P2Y receptors include and extracellular N-terminus, an intracellular C-terminus containing the protein kinase interacting motif influencing the degree of the receptor to couple to G-proteins (particularly Gq/G11, Gαs, Gi/Go), and

seven-transmembrane domains generating the ligand interacting motif. G proteins stimulation initiates a downstream signalling cascade implicated in Ca^{2+} signalling and cyclic AMP pathways. PLC: Phospholipase C; IP_3: Inositol triphosphate; AC: Adenylyl cyclase (AC) and PKA (protein kinase A). (Image source: Zhou et al., 2021).

1.2.4 ATP: P2X receptors

Contrary to P2Y receptors, P2X receptors (P2XRs) are archetypical ATP-gated non-selective cation channels enabling transmembrane fluxes of small ions including Na^+, potassium (K^+), Ca^{2+} and Cl^- (R. Jiang et al., 2013). The P2XRs are plasma membrane receptors with ATP being the solely known endogenous agonist to date (Huang et al., 2021), mediating a myriad of physiological and pathophysiological responses (Di Virgilio, Sarti, Falzoni, et al., 2018). The P2X family comprises seven receptor subtypes P2X1, P2X2, P2X3, P2X4, P2X5, P2X6 and of greater focus P2X7, ubiquitously expressed in all tissues in humans as well as other eukaryotic organisms, but not present in *Drosophila*, yeast and/or bacteria (R. Jiang et al., 2013). P2XRs can be further subdivided into fast desensitizing, including P2X1R and P2X3R, slowly-desensitising, including P2X2R, P2X4R, and P2X5, non-desensitising unique to P2X7R, and non-functional P2X6R (North, 2002) (Figure 1.9b). Structurally, P2XR stoichiometry consists of three subunits, forming a stretched trimer and/or a hexamer of conjoined trimers (Figure 1.9a) (Burnstock, 2018a; Nicke et al., 1998). Furthermore, Nicke et al., work provided further evidence for heteromultimers assembly (i.e., P2X1/4 receptors) but also homomultimers involved in the functional formation of the trimer ion pore (Nicke et al., 1998, 2005). These also included heteromerics receptor association with other subunits such as P2X1/2, P2X1/5, P2X2/3, P2X2/6 and P2X4/6 (Burnstock, 2018a).

Affinity for ATP varies among homotrimeric P2XRs, with P2X1 receptor being activated at the lowest ATP concentration (<1 μM; thus, highest affinity for ATP), whereas P2X7 receptor exhibits a remarkably high ATP activation threshold in the millimolar range (0.5-1 mM; lowest affinity to ATP) (North, 2002). Importantly, ATP sensitivity dictates P2X receptors desensitisation rate – lower the ATP sensitivity, slower is the desensitisation, except for P2X7 receptors, which do not desensitise as described

above. P2X receptor proteins are 384 (P2X4) to 595 (P2X7) amino acid long (North, 2002), having a subunit topology consisting of intracellular amino and carboxy termini processing consensus binding motifs for kinases, and two hydrophobic transmembrane-spanning segments (TM1 and TM2) separated by a large ectodomain (R. Jiang et al., 2013). Sequence homology between P2XRs is present throughout the extracellular domain containing the ATP binding sites and 10 conserved cysteine residues engaged in disulfide bonds (North, 2002). TM1 has been described to gate channel ions permeation with TM2 lining the ion pore (Burnstock, 2018a). In addition to TMs, they exhibit an intracellular domain of variable size according to the subtype, with P2X7R having a unique 120 amino acids intracellular region termed "ballast" (McCarthy et al., 2019; see section below 1.2.3.1), implicated in the functional regulation and trafficking of the receptor (R. Jiang et al., 2013).

Very little was known about the structural role of cytoplasmic termini due to truncated constructs that precluded visualisation of cytoplasmic residues – with the exception of a minimally truncated version of the human P2X3 receptor (Li et al., 2019), and very recently published cryoelectronic microscopy (cryo-EM) structures of full-length rat P2X7R (McCarthy et al., 2019) (Figure 1.9a). These structures revealed how cytoplasmic element provides stability to the receptor dictating the lifetime of the open pore conformation, and thus, the rate of desensitisation /non-desensitisation. Intriguingly, no sequence similarity among P2XRs and other proteins have been identified to date, albeit a structural homology was proposed in our lab between P2X receptors and truncated mechanoreceptor (Δ) Piezo-1, recently awarded Nobel Price for its essential role in mechanosensory transduction in organisms.

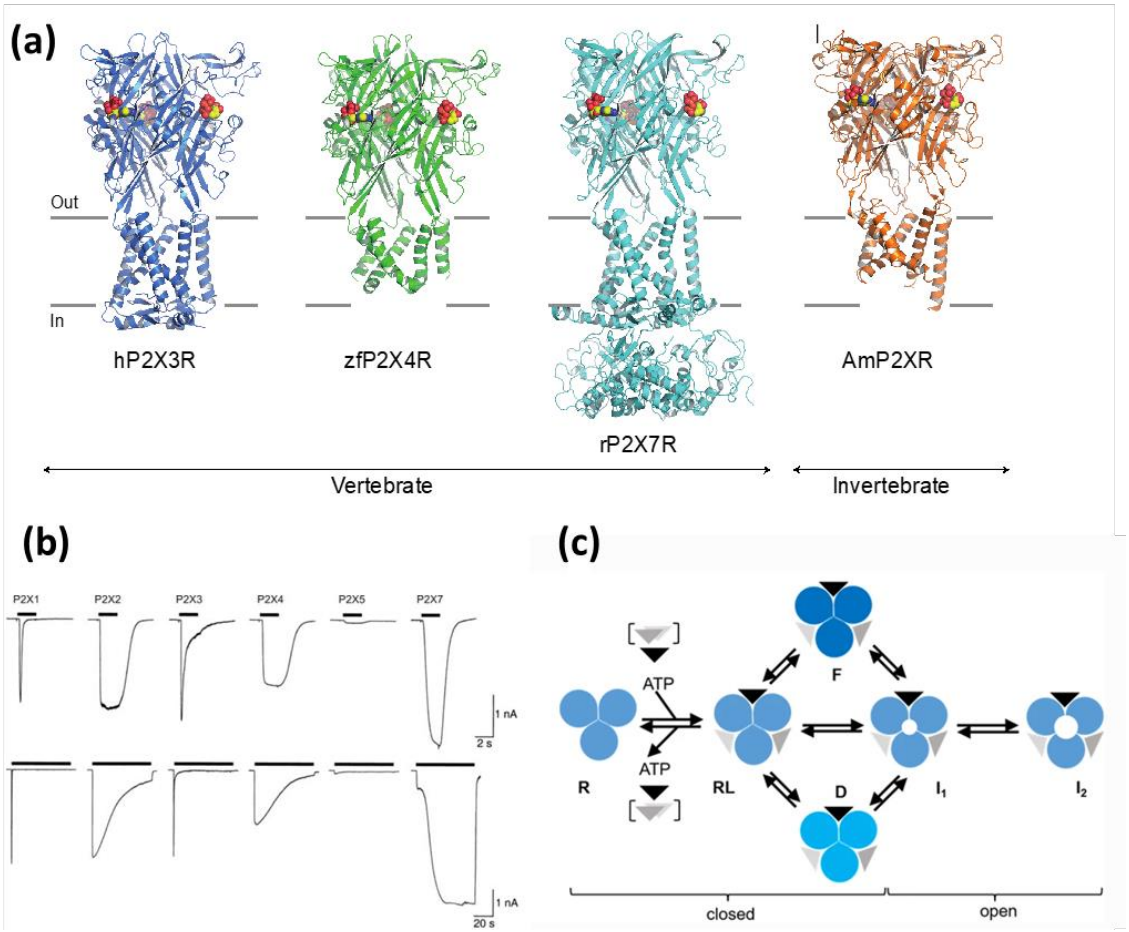

Figure 1.9: Structural and functional properties of P2X receptor subtypes.
(**a**) Evaluation of P2X subtypes structure in vertebrate, human (h) P2X3, zebrafish (zf) P2X4, and rat (r) P2X7 and invertebrate, *Amblyomma maculate* (Am) P2X receptors, in the *apo* resting state, consisting of three subunits forming trimer and ATP binding motif located at the extracellular (out) part. (**b**)Examples of whole-cell recordings from rP2X subtypes transfected HEK293 cells at saturating ATP concentrations. Top panel exhibits short (2 s) ATP applications, whereas, bottom panel shows prolonged (20 s) ATP applications, consisting of 100 µM ATP for P2X1-5 and 1 mM for P2X7. (**c**) Semplified kinetic scheme illustrating resting state form (**R**) in the absence of ATP molecule, a receptor ligand complex (**RL**) occurring upon binding of ATP. According to the P2X subtypes different isomerisation are possible, such as flipped (**F**) closed state, desensitised (**D**) closed state, and $\mathbf{I_1}$ and $\mathbf{1_2}$ depicting open states. (Image source: Kasuya et al., 2016; Kawate et al., 2009; Mansoor et al., 2016; McCarthy et al., 2019; Sattler & Benndorf, 2022).

A functional P2X receptor must be therefore co-/assembled in ether homotrimeric and/or heterotrimeric configurations (Figure 1.9c). For instance, homomeric P2X1 receptors exhibit a remarkable feature that is the mimicry of the agonist activity of ATP by α, β-methylene ATP (α,β-meATP) differentiating P2X1 and P2X3 subunits from other homomeric forms (Burnstock, 2018; North, 2002). Particularly, meATP resembles ATP - evoked maximal currents, activating P2X1Rs at reported concentrations of 10 μM, which are estimated to be about 30-fold lower than to those required for the homomeric P2X3R activation (North, 2002). Several antagonists have also been developed that selectively target P2X1 receptors, for example, NF 279 and MRS 2179, which were described to inhibit HIV p24 viral protein reducing HIV-1 infection in primary human macrophages to over 90% (Hazleton et al., 2012). Using an adenovirus-based fluorescent P2X1 construct reporter approach, clusters of the P2X1 receptor were found, in the vas deferens and in significant numbers close to the nerve varicosities (Burnstock, 2018). Platelets and smooth muscle cells both express P2X1 receptors.

A cDNA encoding human P2X2 receptor was produced from pituitary gland, whereas rat P2X2R cDNA was amplified from PC12 cells (North, 2002). No selective agonists have been found for homomeric P2X2 receptors (Burnstock, 2018). ATP-elicited currents differ notably from P2X1Rs as the ATP action cannot be mimicked by α,β-meATP. Moreover, low concentrations of certain ions including zinc and copper, as well as protons have been shown to potentiate these receptors (North, 2002). P2X2 receptors can form functional and stable heterotrimers with P2X-1, -3 and -5, albeit no cryo-EM or X-ray structures are currently available (Illes et al., 2021). Therefore, most of the literature is based on X-ray templates derived from zebrafish (zf)-P2X4 receptors, which aided in building reliable P2X2R homology structures (Illes et al., 2021). This has than allowed for the characterisation (through electrophysiology) of homotrimeric P2X2 receptor-specific signatures including also rapid activation by external ATP application inducing a stable steady-state current through prolonged ATP exposure generating defined slow-desensitisation rates. P2X2 receptors are distributed abundantly throughout the body on both non-/neuronal cells. For instance, taste stimuli acting on oral taste receptor cells were shown to induce release of ATP co-activating P2X2 and P2X3 receptors expressed in the

taste buds innervating the tongue (Illes et al., 2021). Additionally, single-KO either of the aforementioned receptor subtypes led to reduced taste responses in mice, while double-KO resulted in a complete taste blindness (Illes et al., 2021).

Complementary DNAs encoding homemeric P2X3 receptors were made from rat dorsal root ganglion, human heart and zebrafish libraries (North, 2002), predominantly expressed on nociceptive nerve terminals and other sensory neurons (Burnstock, 2018). Similarly to the P2X1 subtype, P2X3 can also be inhibited by NF023 but with a lower affinity (Burnstock, 2018). Heteromeric assembly of P2X3/2 yielded a sustained ATP- and α,β-meATP -activated currents characterised by a slow desensitisation rate, and potentiated by low pH as observed for homomeric P2X2 receptors (Burnstock, 2018; Illes et al., 2021). Regulatory pathophysiological mechanisms concerning both P2X3 and P2X3/2 have been addressed in the literature with implications in sympathetic and sensory neurons' function (Illes et al., 2021).

Homomeric P2X4 receptors, first isolated from superior cervical ganglia, hippocampus and whole rat brain cDNA libraries are activated by ATP, but not by α,β-meATP (North, 2002). P2X4R elicited ATP currents can be potentiated by invermectin, which is in striking contrast to homomeric P2X2, P2X3 or P2X7 receptors and heteromeric P2X2/3 complex (North, 2002). P2X4R subtype forms functional heterotrimers with P2X- 1 and -6 receptors (Illes et al., 2021). P2X4/1 assembly exhibited similar kinetic profile as to homomeric P2X4Rs, with pharmacological properties that are characteristic of homomeric P2X1Rs (Nicke et al., 2005). Furthermore, homotrimeric and heterotrimerc P2X4 receptors have been described to undergo rapid constitutive and agonist-evoked clathrin- and dynamin-dependent internalisation from the plasma membrane into endosomes and lysosomes (Illes et al., 2021). Internalisation is driven by the C-terminal interaction with adaptor protein 2 (AP2). Indeed, mutations impairing either AP2 or the endocytic motif result in accumulation of P2X4 receptors to the membrane (Illes et al., 2021). This P2X4R-related feature is particularly important when carrying out experiments of co-localisation or FRET with other proteins, as quantification of receptors trafficking to the plasma membrane may be misleading. So far, P2X4

receptors intracellular functions remain elusive and hardly addressed (Kaczmarek-Hájek et al., 2012).

Homomeric P2X5 subtype was first cloned from rat celiac ganglion and heart and later, also from embryonic chick skeletal muscle and bullfrogs (North, 2002). P2X2R is abundantly expressed in developing skeletal muscle and other proliferating cells (Burnstock, 2018). They display a rather small ATP-evoked maximal current ranging between 50-200 pA in HEK293 cells, as compared to currents observed in other P2R subtypes such as P2X2 receptors, which in similar conditions elicit currents of several nanoamperes in amplitude (North, 2002). Interestingly, the defining phenotypes of P2X1/5 heteromer include a maintained α,β-meATP-induced current and higher sensitivity to ATP – features that are not observed for either the homomers, when expressed separately (Burnstock, 2018; North, 2002).

The rat P2X6 receptor cDNA was first isolated from rat brain and superior cervical ganglia, whereas the human cDNA equivalent derived from peripheral lymphocytes (North, 2002). P2X6 subtypes have been identified in skeletal muscle, adult midbrain, kidney, thymocytes, urinary tract and atrium (Illes et al., 2021). They are only functional when expressed in a heteromultimer with P2X2 and P2X4 receptors (North, 2002). P2X2/6 heteromeric receptors are particularly expressed in respiratory neurons in the brain stem, whereas, P2X4/6 heteromultimer localise prominently in hippocampus CA1 and trigeminal mesencephalic nucleus (Burnstock, 2018). Interestingly, glycosylation motifs at asparagine (N) position N157, N187 and N202, present in the extracellular domain of P2X6 receptors, may perhaps determine whether P2X6Rs express a functional phenotype (Illes et al., 2021).

Lastly, contrary to all other six members of the P2X family, P2X7 subtype displays unique properties (detailed below in 1.2.3.1). It requires millimolar concentrations of extracellular ATP for activation (Figure 1.10), similarly to those observed near sites of inflammation or in cancer (Di Virgilio, Sarti, Falzoni, et al., 2018); progressive permeation of large cationic dyes, for example Yo-Pro1, NMDG, ethidium or

propidium iodine (Di Virgilio, Schmalzing, et al., 2018). Interpretation of "macropore" formation induced mechanisms has long brought up conflicting arguments in the literature. In this regard, my PhD work provided convincing evidence of a physical and functional P2X7 and TMEM16F channel complex facilitating high molecular weight (MW) cationic dyes permeation and other pathophysiological mechanisms. This, however, does not exclude the possibility that P2X7 may have itself also the ability to form a large-conductance pore, as previously suggested (Di Virgilio, Sarti, Falzoni, et al., 2018; Peverini et al., 2018). Accordingly, a denoted section (i.e., 1.3.1 P2X7 macropore formation) has been provided in this manuscript highlighting major breakthroughs in this field.

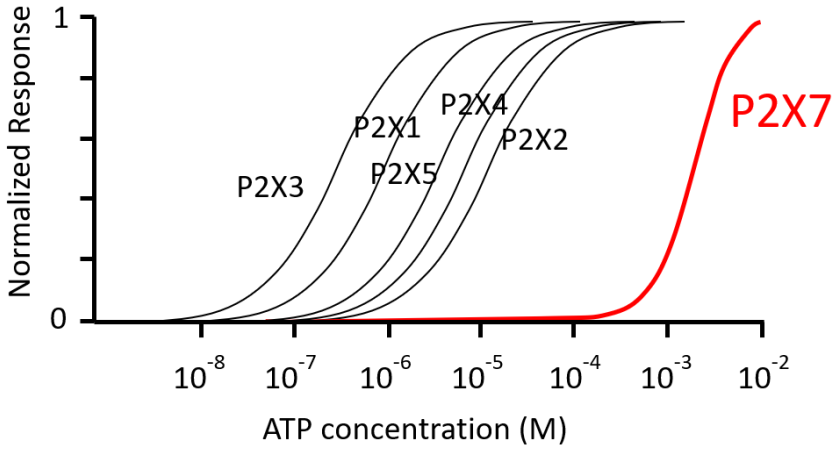

Figure 1.10: ATP dose-response curve for P2X receptor subtypes.
Evaluation of P2X receptors to ATP activation displaying the range of extracellular ATP concentration (M) required for each subtype. Notably, highlighted in red is the unique normalised response of P2X7 activation to high ATP concentrations.

1.2.4.1 P2X7 receptors: structure, function & physiology

As research investigations continue to progress and novel findings that implicate P2X7 receptors in key signalling pathways are still being characterised; this section shall provide an update on recent structural aspects of this receptor, and great focus will be placed on enigmatic P2X7-evoked signal transduction modules involved in the immune system.

P2X7R gene is located on chromosome 12, at 12q24.31, in the proximity of P2X4R genes in humans (Illes et al., 2021). Several different naturally occurring P2X7R splice

variants have been identified in human including P2X7R-A through -J (Giuliani et al., 2014), with $P2X7R_A$ being the well-characterised and cryo-EM validated full-length receptor. Among these splice variants, $P2X7R_B$, $P2X7R_E$, $P2X7R_G$ and $P2X7R_J$, lack the lengthy cytoplasmic ballast typical of $P2X7R_A$ (Giuliani et al., 2014). Notably, $P2X7R_B$ truncated variant displays a unique functionally ion channel that is, however, unable to induce cytotoxic macropore formation. Interestingly, $P2X7R_B$ protein structure is characterised by a retained intron placed between exons 10-11, generating an additional 18 amino acids insertion after residues 346 terminating in a stop codon (Giuliani et al., 2014). Furthermore, $P2X7R_A$ and $P2X7R_B$ exhibit a shared agonist and antagonist profile, and susceptibility to promote tumour growth, metastasis and resistance (Pegoraro et al., 2020; Zanoni et al., 2022).

The overall architecture of the rat P2X7 receptor has been recently elucidated (McCarthy et al., 2019) (Figure 1.11). Briefly, the apo-state configuration of the P2X7 receptor features a narrowed channel pore as compared to hP2X3, in which ATP must access to occupy the orthosteric binding pocket, representative of the agonist-bound open conformation. TM2 resides in the pore lumen with residue S339 and S342 underlying the extracellular and cytoplasmic boundaries of the TM gate, respectively (McCarthy et al., 2019). S342 residue has also been suggested to act as ion selectivity filter through the TM gate, which in the apo state has a maximal radius of just 0.1 Å. Thus, shielding P2X7 receptors from solvents and ligands (McCarthy et al., 2019). The latter residue also defines the narrowest region of this receptor in the ATP-bound open state conformation, which in hP2X3 is characterised by the amino acid threonine (T) at the analogous position (McCarthy et al., 2019).

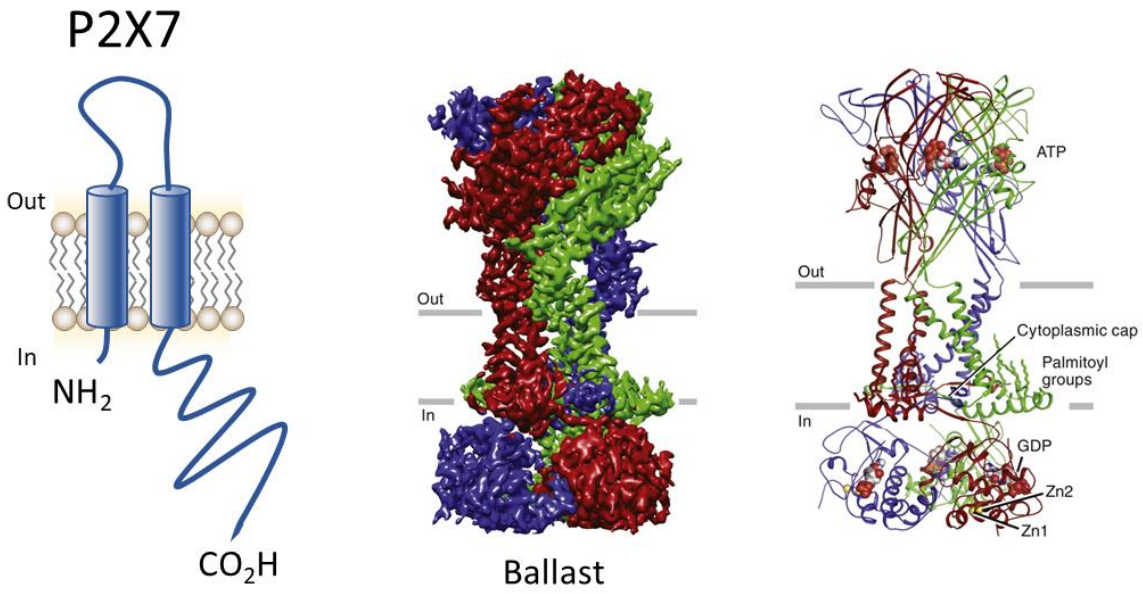

Figure 1.11: P2X7 receptor structure.
Illustration of P2X7 cryo-EM full-length architecture in the *apo* state configuration revealing a lengthy cytoplasmic C-terminus (acknowledged as: cytoplasmic ballast); a cytoplasmic cysteines cap or anchor containing palmitoyl groups required for receptor stabilisation to the membrane; presence of two zincs (Zn) binding sites and one GDP binding site located in the ballast, whose functions are currently unknown. All these features are unique to P2X7 exclusively (Image source: McCarthy et al., 2019).

Cryo-EM structures further revealed two P2X7-specific cytoplasmic domains termed the C-cysteines (C-cys) anchor and ballast. The C-cys anchor (Figure 1.12) consists of six cysteines residues (C362, C363, C377, C374 C371 and C373) pointing toward the TM region and one serine (S) 360 residues. It originates as TM2 appears from the plasma membrane and enters the cytoplasm forming a loop that serves as a molecular hinge, physically connecting TM2 and cytoplasmic cap to the membrane (McCarthy et al., 2019). Importantly, these two domains have been described to play a role in hP2X3 receptor desensitisation. In this regard, refinements of apo conformation reconstruction revealed that at least four cysteines (i.e., C362, C363, C374 and C377) and S360 are palmitoylated, thus securing the aliphatic chains in to the plasma membrane and preventing desensitisation of the receptor (McCarthy et al., 2019).

It was also demonstrated that deletion of the C-cys anchor or mutation of cysteine residues into alanine prevented their palmitoylation, resulting in complete desensitisation following 30s application of 100 μM ATP (McCarthy et al., 2019). Importantly, most

amino acid residues located in the C-cys anchor are essential for full receptor expression at the membrane, making mutagenesis experiments hard to carry out due to receptor retention in the endoplasmic reticulum and degradation. Therefore, cell-surface labelling is advised prior to study any physiological implications of a particular amino acid residue. In addition to the cytoplasmic domains, a putative phospholipid binding site was also identified near the middle of the plasma membrane, perhaps employed for PS redistribution across the membrane (McCarthy et al., 2019). Another unique feature of P2X7 receptors is the additional 120 amino acids residues in the C-terminus domain termed "the ballast" as previously mentioned. The cytoplasmic ballast also contains cysteine residues that are not, however, palmitoylated, but are essential for proper trafficking of the receptor to the membrane (McCarthy et al., 2019). Moreover, the ballast displays a dinuclear zinc ion complex coordinated by seven cysteine residues and a high-affinity guanosine nucleotide binding site that is occupied by a GDP molecule (McCarthy et al., 2019). Collectively, these cytoplasmic domains may hold the key to unlock modulatory P2X7 signal transduction mechanisms perhaps responsible for many pathophysiological conditions. Our laboratory has provided for the first-time insights into the role of the C-cys anchor domain as a novel immunoregulatory target as documented later in this manuscript.

Homomeric P2X7 receptors are widely expressed in immune cells including myeloid leukocytes circulating in the blood and lymphatic system, epithelial cells, but also in oligodendrocytes and schwann cells of the CNS and peripheral nervous system (PNS), respectively (Di Virgilio, Sarti, & Grassi, 2018; Kaczmarek-Hajek et al., 2018; Kopp et al., 2019). Unlike immune cells, in which P2X7 "signature" expression has been long studied, its presence and function in neurons remain rather controversial. For instance, cellular neuronal localisation of P2X7 mRNA was described in the rat brain (Y. Yu et al., 2008). However, this does not necessarily correlate with the expression of the respective protein. Furthermore, differentiation between P2X7-specific neuronal activation and eATP-evoked neurotransmitter release has been somewhat questionable and more prone to be dependent on specificity of model systems being investigated (Illes et al., 2017). Hereof, Nicke's lab generated P2X7-EGFP BAC transgenic mice providing a

comprehensive evaluation of P2X7 subcellular localisation, but also interaction with other proteins (for details see Kaczmarek-Hajek et al., 2018). Briefly, thorough characterisation of P2X7 BAC transgenic mice showed a dominant expression of the receptor in microglia, oligodendrocytes and Bergmann glia (consistent with previous published data), but surprisingly not in neurons (Kaczmarek-Hajek et al., 2018). A more recent study from the same lab further characterised interaction partners of P2X7 employing *in-situ* cross-linked transgenic mice by nano-HPLC/nanoESI-Orbitrap-MS/MS identifying as a likely candidate TMEM16F channels among others (work by Prof. Dr. Nicke's lab; refer to Kopp, 2020). Thus, providing additional evidence in support of P2X7-TMEM16F forming complex interaction, which will be later introduced in section 1.3 below.

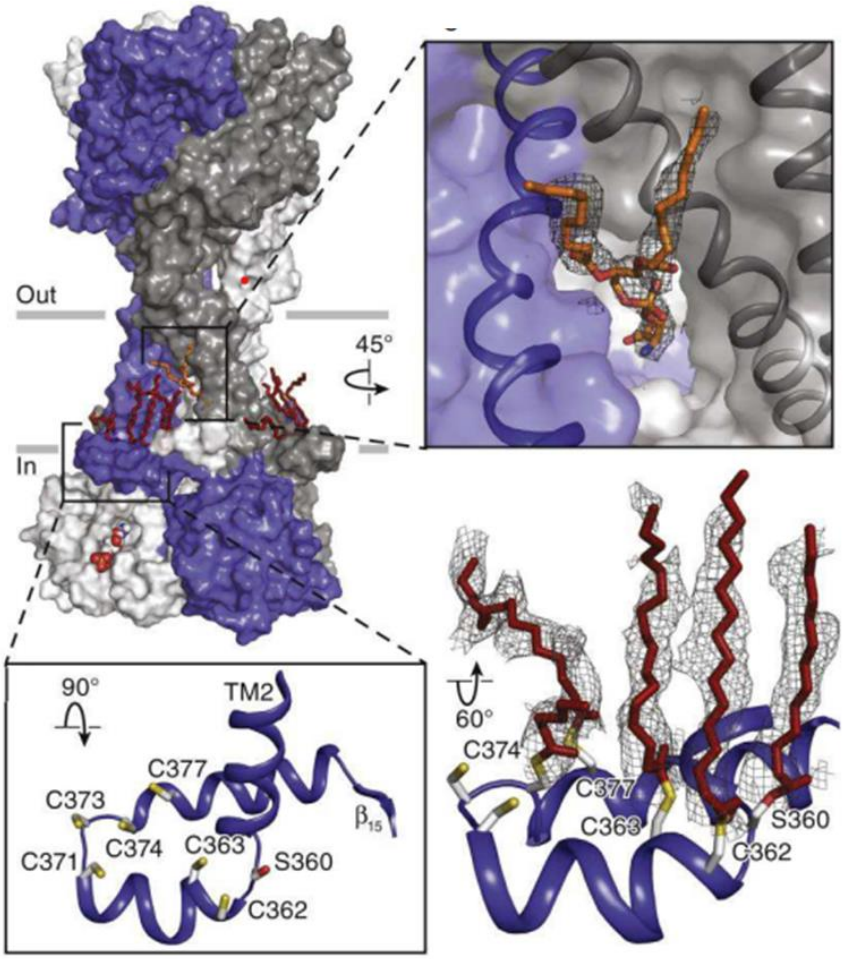

Figure 1.12: Structure of rP2X7 cytoplasmic anchor and lipid binding site.
Key zoomed features providing detailed insights into C-cys region showing the four palmitoylated cysteine residues (C362, C363, C374 and C377) as well as one serine residue (S360; as illustrated in the 90° orientation), these palmityl groups are essential for

an effective anchoring of the receptor to the bilayer membrane (as illustrated in the 60° orientation), and the putative phospholipid binding site located near the middle of the membrane (as illustrated in the 45° orientation) (Image source: McCarthy et al., 2019).

1.2.4.2 P2X7 as "danger-sensing" receptor

The most studied functions of P2X7 receptors are attributed to their roles as effector regulators of inflammation and immune signalling. Injured or dying cells induced by invading microorganisms release intrinsic host molecules such as endogenous pro-inflammatory factors and ATP acting as natural adjuvants. Thus, stimulating innate immunity response through conserved determinants, known as pathogen-associated molecular patterns (PAMPs), acting as "exogenous danger signals", and adaptive immunity via antigens secretion (Janeway & Medzhitov, 2002). Because host-triggering danger signals occur following cell damage, these effectors are also referred to as damage-associated molecular patterns (DAMPs), among which extracellular ATP (eATP) is perhaps the best-investigated DAMP member. Accordingly, P2X7 receptor may be described as "danger sensing receptor" activating in the presence of elevated ATP concentration and mediating pro-inflammatory cytokine release (i.e., IL-1β and IL-18 tightly controlled by P2X7) and death arising from the ATP-stimulated cell.

Accumulation of eATP at inflammatory sites gates P2X7 receptors to a multiplicity of pathophysiological responses, with the most important being the activation of the NOD-, LPR- and pyrin domain-containing protein 3 (NLRP3) inflammasome in the cytoplasm of mononuclear and polymorphonuclear phagocytes (Di Virgilio, Sarti, & Grassi, 2018) (Figure 1.13). The inflammasome (more detailed in section 1.5) is a multi-protein complex, consisting of a central scaffold protein, coordinating assembly with inflammatory caspases. The inflammasome is central to innate immunity and is involved in many pathologies, ranging from autoinflammatory conditions to cancer. ATP-primed P2X7-induced NLRP3 inflammasome activation drives pro-caspase-1 cleavage via ASC (the adaptor molecule apoptosis-associated protein containing CARD) into caspase-1 (CASP1), and proceeding to maturation of cytokine precursors pro-IL-1β and pro-IL-18 into IL-1β and IL-18, which are ultimately secreted (Di Virgilio, Sarti, & Grassi, 2018; Y.

Yang et al., 2019a). Moreover, gating of T cells P2X7 receptor by eATP leads to activation of proteinases A-disintegrin and metalloproteinase family members (ADAM-10 and -17)-mediated shedding of IL-6 receptor (IL-6R), CD62L and CD27 (Di Virgilio, Sarti, & Grassi, 2018). Collectively, these factors aid in T cell polarisation, clonal expansion of antigen-specific B cells, and homing of naïve T cells into secondary lymphoid tissues (Di Virgilio, Sarti, & Grassi, 2018).

Interestingly, TMEM16F activation by elevated intracellular Ca^{2+} (similarly to those observed following P2X7 activation) also results in rapid PS translocation triggering ADAM10 and -17 shedding functions (Seidel et al., 2021), initiation of cell shrinkage and activation of caspase-3/7. Together, these studies provide evidence for an intriguing scenario, in which coupling of P2X7 and TMEM16F generate the foundation for optimal initiation of innate immune responses. Intriguingly, elevated pro-thrombotic responses have been observed following P2X7 receptor stimulation that were associated to increase expression of macrovesicle-associated tissue factors (Di Virgilio et al., 2017). This peculiar function has been proposed to bridge inflammation response to coagulation. TMEM16F channels are key effectors of the clotting system, which further strengthen the P2X7R and TMEM16F channel interaction hypothesis.

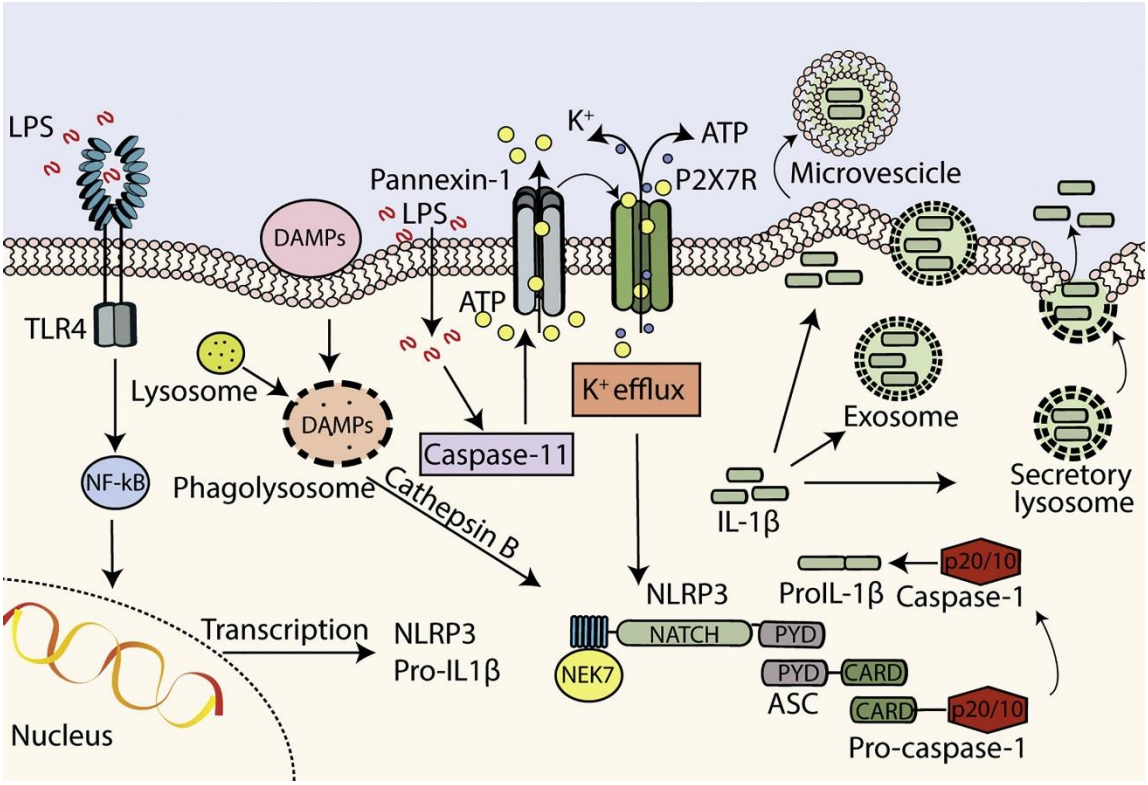

Figure 1.13: Overview of P2X7 in the NLRP3 inflammasome activation.
Evaluation of key steps involving P2X7 activation and NLRP3 inflammasome culminating with maturation of the pro-inflammatory cytokine IL-1β. (Image source: Di Virgilio et al., 2017).

1.2.4.3 P2X7 Receptors: ATP sensitisation

The lack of desensitisation, as discussed above, represents another unique functional property of P2X7 receptors – that is in sharp contrast to other P2X subtypes. In this regard, rather than desensitise, P2X7 receptors exhibit a strikingly inverse behaviour, that of facilitation occurring following prolonged agonist (such as ATP) stimulation, accompanied by a 2.5-fold leftwards shift in the EC_{50} value (Roger et al., 2008). This phenomenon is usually acknowledged as ATP sensitisation, whereby an increase in the current responses is initiated upon repetitive or prolonged ATP-stimulation, as illustrated in Figure 1.14. Importantly, ATP sensitisation is also unique to P2X7, and it has been shown to be associated with cholesterol-rich lipid rafts in both recombinant and naïve systems (Robinson et al., 2014; Roger et al., 2008). The time course of ATP sensitisation is concomitant to several cellular alterations such as PS translocation, mitochondrial

swelling, and membrane blebbing underlying, important cytotoxic features associated with P2X7 stimulation as evaluated in Chapter 4 (section 4.1.3.2).

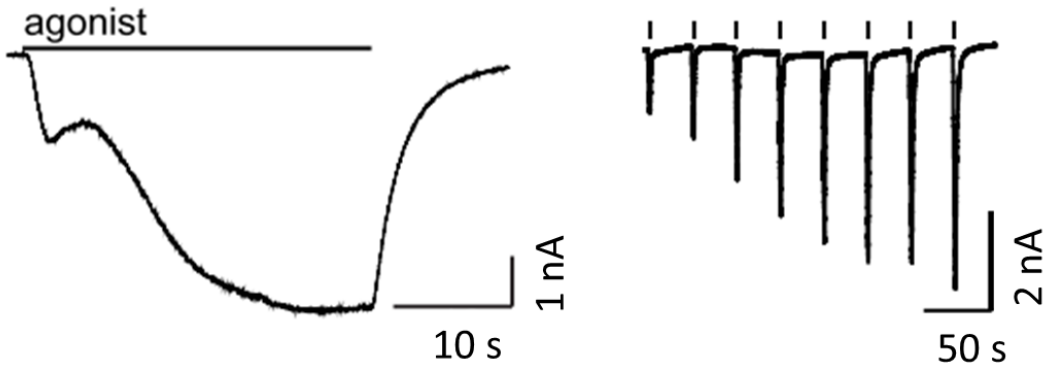

Figure 1.14: ATP sensitisation of P2X7.
Sensitisation of rP2X7 currents following BzATP (agonist) stimulation. On the left is depicted a prolonged agonist application, whereas on the right are repetitive applications. (Image source: Roger et al., 2008).

1.3 Introduction to channel-forming complex interaction

Plasma membrane receptors are proteins that convey outside signals into the cell, activating signalling pathways, affecting cytosolic or nuclear transcriptional machineries. Thus, representing the starting point for signal transduction initiation. Identifying precise signalling cascades are of outmost importance in order to guide novel treatment-specific therapeutics. In this regard, knowing the direct molecular interaction partners of P2X7 may represent potential pharmacological targets, especially in cancer research. Discovery of the P2X7 macropore (reaching an astonishing diameter of 8.5 Å) engaged the whole purinergic scientific community in a hunt for potential recognition of molecular-forming channel complexes, which might be responsible for such phenomenon.

1.3.1 Macropore formation: An overview of key research findings

The peculiar macropore formation or permeability hallmark of P2X7 receptors was initially observed over 40 years ago in mast cells (Cockcroft & Gomperts, 1979), and fibroblasts (Di Virgilio, Sarti, & Grassi, 2018). It was noticed that as the eATP concentration increased, conformational changes must have occurred, affecting the permeation properties of cation channels (P2X2, P2X4 and P2X7), which would allow the passage of nanometer-sized molecules (<900Da) across the membrane. This was thereafter confirmed in other cell types, such as macrophages (both mouse RAW264.7 and human), microglia, HEK293, and in both recombinant and endogenous system (Dunning et al., 2021). The macropore activity is usually measured through cellular uptake of fluorescent dyes (as in Yo-Pro-1, enthidium, or propidium iodine, as previously mentioned) – that is often referred to as dye-uptake experiments. This progressive permeabilisation feature during long-lasting ATP stimulation has led to several interpretations, which we shell discuss in this section. These include (i) “pore dilation” theory, (ii) participation of associated channel-forming proteins, such as pannexin-1 or connexin-43 hemichannel and (iii) Intrinsic permeability of P2X7R to larger cation

molecules: the reconstitution of panda P2X7 into liposome. Furthermore, P2X7 receptor activation initiates numerous signalling cascades that similarly correlate with the activity of TMEM16F, as for instance, caspase activation, plasma membrane reorganisation, cell death, eco-domain shedding and cytokine release. Together, these findings led our lab and others to a potential speculation of (iv) P2X7-TMEM16F proteins complex. This, however, does not exclude that perhaps P2X7 receptor itself may also form long-conductance pores in the absence of any significant dilatation (see review Illes et al., 2021) resulting eventually to cell death.

1.3.1.1 Putative pore dilation

Appealing in its very simplicity, an early work by Virginio et al., argued that prolonged and progressive ATP applications (10-60 s) induce the P2X ion channels (P2X2 or P2X4) to become gradually permeable to larger cations such as N-methyl-D-glucamine ($NMDG^+$) and Yo-Pro-1. Thus, resulting in time-dependent expansion of the pore, which led to the so-called "pore dilation" theory (Virginio et al., 1999). Briefly, it was observed that sustained 40-s ATP application of P2X2 and P2X4 receptors in native neurons, but also in heterologous expressed conditions, led to an increase in both current and large molecule permeability, as to those observed at the cytolytic P2X7 receptor level. Furthermore, no cell lysis was detected throughout this highly reversible permeability-configuration state (Virginio et al., 1999). Hence, it was concluded that because P2X4 receptors are particularly expressed in the presynaptic transmitter-release termini in the brain; the latter may be involved in the transfer of high MW molecules into or out of the nerve terminals, thereby regulating, therefore, synaptic transmission (Virginio et al., 1999). This interpretation of the data was later challenged by other studies (as reviewed by Illes et al., 2021) including first ion depletion study (Li et al., 2015). Hereof, it was suggested that the entry of these large molecules through the "assumed" pore dilation of P2X7 was rather caused as a result of either calmodium-dependent current facilitation through P2X7Rs (Roger et al., 2010), or by secondary activation of chloride channels as demonstrated in macrophages (Janks et al., 2019). Accordingly, a new permeation mechanism was later introduced, in which passage of $NMDG^+$ and other small cationic

molecules, such as spermidine occurs, immediately after ATP gating as demonstrated by our lab through electrophysiological, photochemical, and modelling data (Harkat et al., 2017). Particularly, the permeation rate of $NMDG^+$ ion was however reduced when compared to that of Na^{2+} (Harkat et al., 2017). Nonetheless, many questions remain, as of today, still unanswered. For instance, how does Yo-Pro-1 (376 Da) or YoYo-1 (763 Da) directly permeate the P2X7 receptors itself? An increasing number of conflicting data appear in the literature, as to those in support of the pore dilation theory, whereas others, as in McCarthy's et al., cry-EM P2X7 structure, demonstrating no evidence of dilated state. Given the important pathophysiological role of P2X7 receptors, understanding the molecular foundations of macropore formation would undoubtedly provide novel insights into potential therapeutics.

1.3.1.2 Intrinsic permeability property of P2X receptor: The reconstitution of P2X7 into liposomes

Reconstitution of the engineered panda P2X7 receptor into artificial liposomes by Kawate's lab provided important pharmacological properties concerning both the channel activity and permeability. Briefly, Karasawa et al., presented a truncated panda P2X7 construct lacking the N- and C-termini (termed P2X7-ΔNC) and consequently reconstituted into liposomes. It is worth mentioning that this *in vitro* system is particularly advantageous as it would allow to freely control all components of the liposome including lipid composition and ratio. They observed that panda P2X7-ΔNC was sufficient to form a dye-permeable pore independently of its unique ballast and displayed a channel activity predominantly dependent on the lipid composition (i.e., phosphatidylglycerol and sphingomyelin). The latter was inhibited by cholesterol via interaction with the TM domain (Karasawa et al., 2017). Collectively, these findings indicate that N- and C-terminal domains are indispensable for dye-uptake itself, whose opening is mediated by palmitoylated cysteine residues located close to the pore helix. Given, however, new findings demonstrating the presence of a zinc ion complex and a guanosine nucleotide binding site on the P2X7 cytoplasmic ballast; these features may as such be crucial to P2X7's signalling properties. It appears, therefore, more and more likely that perhaps

P2X7-ΔNC construct may have rendered the receptor itself unfunctional or in an open-state configuration.

1.3.1.3 Channel recruitment: Pannexin-1 hypothesis

The other hypothesis constituting the dye-permeable pore arises from studies showing that P2X7 itself is unable to permeate dyes, cells expressing P2X7R exhibit two distinct pores for small and large ions (L.-H. Jiang et al., 2005; Virginio et al., 1997), and the absence of pannexin-1 (Panx1) in heterologous systems failed to induce a P2X7-dye permeable pore (Pelegrin & Surprenant, 2006). Participation of an associated hemichannel-forming protein identified as Panx1 was first described by Surprenant's lab, in order to provide evidence in support of inflammasome formation and processing of IL-1β maturation. As previously mentioned, elevated eATP concentrations gating P2X7Rs in macrophages and other immune cells lead to fast opening of the membrane-permeable pore, but also to downstream release of proinflammatory cytokines. In brief, they observed that when ectopically expressed Panx1 hemichannels co-immunoprecipitated with P2X7 receptors in macrophages, generating the so-called "dye-uptake pathway", whose signals were also described to be essential for P2X7-evoked caspase-1 processing and of IL-1β maturation (for more details see Pelegrin & Surprenant, 2006). This hypothesis was later challenged by other studies demonstrating that Panx1-knockout, -knockdown or -inhibition in murine macrophages resulted in a normal of Yo-Pro-1 uptake phenotype expression (Alberto et al., 2013; Qu et al., 2011; Xu et al., 2012), and that ATP surprisingly antagonised Panx1 activity (Qiu & Dahl, 2009). Today, a new hypothesis has been postulated, whereby immediately after activation, P2X7 receptor channel simply allows the passage of large cationic molecules, in the absence of a pore-dilation mechanism (Di Virgilio, Sarti, Falzoni, et al., 2018).

1.3.1.4 Novel candidate: TMEM16F

As an ion channel the P2X7R features large Na^+, K^+ and Ca^{2+} dependent conductances as documented in the literature (Di Virgilio, Schmalzing, et al., 2018). Released ATP from

injured or dying cells, activates the central pore of the P2X7R (but also other P2 subtypes) causing Na^+ uptake-associated swelling, and fast and long lasting Ca^{2+} permeation. This permeability to cations, especially Ca^{2+} leads to a marked cell depolarisation and generation of downstream calcium signalling. The increase in intracellular Ca^{2+} is essential for cell survival and proliferation but if prolonged may result in mitochondrial damage and cell death (Di Virgilio et al., 2017). Accordingly, Ca^{2+}-activated Cl^- channels have been recently suggested to constitute new promising candidates.

In mouse peritoneal macrophages TMEM16F was first identified as interacting partner of P2X7R proposed to meditate effects essential for the innate immune response downstream of P2X7 (Ousingsawat et al., 2015). It was postulated that carbohydrate-binding of bacteria proteins to macrophage membranes induce ATP release (from a currently unknown mechanism) activating the P2X7 receptor in an autocrine manner. As a result, increased intracellular Ca^{2+} causes activation of Cl^- currents, among which TMEM16F, leading to rapid cell shrinkage. Furthermore, given the dual role of TMEM16F, acting as CaCCs and phospholipid scramblase, its activation enhanced macrophages migration, and thus, phagocytosis of pathogens, and scrambling, leading to plasma membrane blebbing and apoptosis. These findings were supported by TMEM16F knockout macrophages data, in which P2X7R stimulation largely attenuated essential functions, including caspase3/7 activation and dye-uptake pore formation (Ousingsawat et al., 2015). Although this work has proven that this complex is fundamental to innate immune response, major questions as to whether P2X7R and TMEM16F channel physically or functionally couple, remain yet to be addressed. Furthermore, the constant use of tannic acid, a potent non-selective inhibitor, and importantly a fluorophore quencher (Dunning et al., 2021), has left this study to some extend doubtful.

Our recent work, also provided further insights in support of this P2X7-TMEM16F regulatory complex mechanisms essential for P2X7 current facilitation and macropore formation (Dunning et al., 2021). We previously showed that brief agonist application activates complex-embedded P2X7 open probability to a low level of channel activity, which is presumably regulated by cholesterol; whereas prolonged agonist stimulation

transitions P2X7 channels to a higher open probability that is recapitulated by plasma membrane cholesterol depletion (Dunning et al., 2021). Meanwhile, activated P2X7 receptors induce permeation of large molecules through two distinct components: one requiring TMEM16F binding, while the other is most likely to occur through the P2X7 pore itself as previously discussed. Importantly, molecular mechanisms underlying macropore formation, and other P2X7-dependent processes (i.e., inflammasome) remain, so far, rather inconclusive. It is also strongly believed that P2X7R targeting may present novel perspectives for anti-inflammatory therapy. In this regard, compelling evidence have been proposed throughout this manuscript directed at specific P2X7-TMEM16F amino acid residues that can serve as targetable immunoregulatory components.

1.3.2 TMEM16 channel family

Over 20,000 genes contained in the human genome encode for membrane proteins of unknown function (Almén et al., 2009). Among these orphan proteins, the transmembrane (TMEM) protein 16A (or anoctamin-1) was the first form of plasma membrane localised Ca^{2+}-activated Cl^- channel to be identified back in 2008 (Pedemonte & Galietta, 2014). The family of anoctamins includes a vast group of transmembrane proteins characterised by a high level of functional divergence attributed to roles as CaCCs, Ca^{2+}-dependent phospholipid scramblase, and dual function non-selective ion channel/ scramblase. So far, 10 isoforms belonging to the TMEM16/anoctamins have been identified in human, including TMEM16A-K (ANO1-10) except for TMEM16I/ANO9. The two family-founding members TMEM16A and TMEM16B exert voltage- and calcium-dependent gating exclusively, whereas TMEM16F has been described as a dual function component displaying, however, a poorly selective ion channel activity. The remaining members have been recently suggested to function mainly as Ca^{2+}-dependent phospholipid scramblase mediating also non-selective ion transport (B.-C. Lee et al., 2018). Intriguingly, there is increasing evidence that TMEM16E may be exhibiting similar due function properties as to TMEM16F in HEK293.

Crystal structures of the dual function channel/ scramblase fungus *Nectria haemotococca* (nh)-TMEM16 (Brunner et al., 2014), as well as cryo-EM structures of CaCCs TMEM16A (Dang et al., 2017), uncovered crucial features of the dimeric TMEM16 architecture, and calcium-dependent mechanism. Briefly, each anoctamin consists of ten TM helices, intracellular amino group and COOH-end termini, and a pore-containing p-loop formed by fifth and sixth TM helices, which plunge back into the membrane. Furthermore, each TMEM16 monomer is characterised by a hydrophobic groove-like cavity exposed to the membrane lined by TM3-7, with helices 6 and 7 directing the formation of two calcium binding sites (B.-C. Lee et al., 2018). In nhTMEM16 the intracellular end of the cavity appears to be wider, about 35 Å, as it approaches the inner leaflet, but it gradually narrows to 5 Å towards the extracellular end.

It is currently believed that the groove-like cavity acts as lipid pathway, whereby phospholipid scrambling occurs through the so-called “credic-card” mechanism (B.-C. Lee et al., 2018). The latter postulates that the headgroup of the phospholipid permeate into the cavity, whereas the hydrophobic tail is retained in a more stable position in the hydrocarbon core of the membrane. Thus, upon activation phospholipids scrambling translocate from the inner to the outer leaflet, and vice versa. High-impact mutations also provided evidence in support of a shared route between the lipid and ion pathways (B.-C. Lee et al., 2018). They were initially termed anoctamin as believed to be strictly chloride channels consisting of eight TMs. Nevertheless, it was later shown that this was not always the case, and it was later introduced the TMEM16 family having ten TM domains (Figure 1.15), with a high degree of functional divergence. Accordingly, we will use the term TMEM16 going forward.

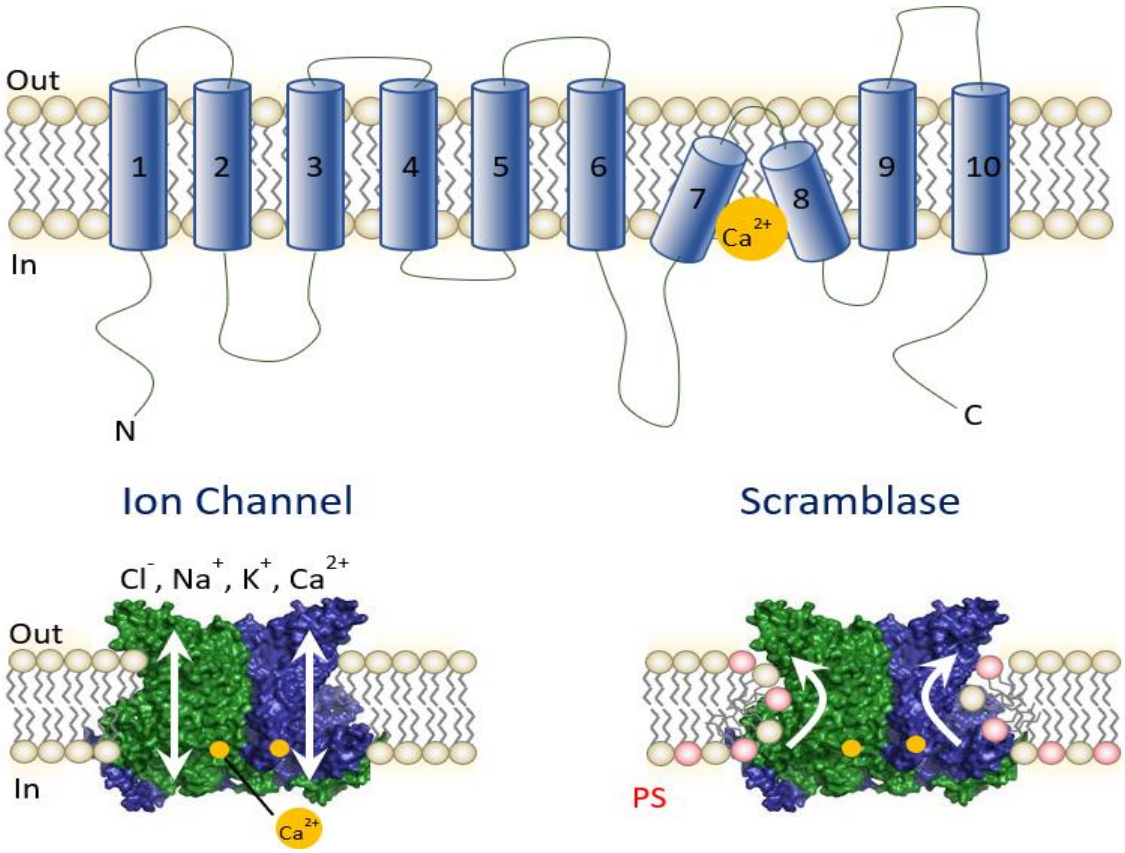

Figure 1.15: Structure and function of TMEM16 channels.
Structural representation of the 10 transmembrane domains illustrating Ca^{2+} binding site, ion channel function and scramblase activity involved in PS externalisation.

Biological membrane bilayers delimit the boundaries of all living cells and their sub-compartmentalisation sites. In eukaryotes, lipid biogenesis occurring in the ER is responsible for the lipid composition and asymmetrical distribution across the leaflets of the plasma membrane (Falzone et al., 2018). Particularly, membranes asymmetry occurs as lipids transit from the ER to the membrane via the Golgi apparatus mediated by the catalysis of two classes of ATP-dependent enzymes, including flippase and floppase, which establish their chemical compositions (Falzone et al., 2018). For instance, phosphatidylcholine and sphingolipids are abundantly present in the outer leaflet, whereas negatively charged PS, and phosphatidylethanolamine reside in the inner leaflet. Maintenance of membrane asymmetry is essential for proper cellular homeostasis. In fact, rapid collapse in lipid asymmetry occurring during the phospholipid scrambling process, resulting in uncontrolled exposure of PS, disrupts cellular homeostasis with reported implications for blood coagulation, and phagocytosis clearance of apoptotic cells (Falzone

et al., 2018; B.-C. Lee et al., 2018). Another family of regulated scramblases is the Xk-related (Xkr) proteins, which unlike TMEM16s, are caspase-activated scramblases activated during apoptosis (as reviewed in Williamson, 2015) but, however, will not be covered in this manuscript. Early increases in cytosolic calcium, as evoked by P2X7Rs, trigger TMEM16s activation resulting in blood coagulation and membrane repair. Identifying molecular and cellular signalling network by which these protein functions remain fundamentally important given their effects on several genetic disorders.

1.3.2.1 TMEM16F structure, function & physiology

TMEM16F is widely expressed in many tissues and cell types – a characteristic that is often observed in housekeeping proteins (Pedemonte & Galietta, 2014). Phylogenetically, TMEM16F is a close relative of TMEM16E, as compared to TMEM16A and TMEM16A, which remain relatively distant. The Ca^{2+}-gated ion channel and scramblase features of TMEM16F are required for exposing PS, as well as for the generation and release of extracellular vesicles (EVs) by the platelets (Feng et al., 2019). Indeed, in humans, the main phenotype attributed to TMEM16F mutations is a bleeding disorder known as Scott Syndrome characterised also by defects in Ca^{2+}-dependent phospholipid scrambling in B lymphocyte and erythrocytes cell types (H. Yang et al., 2012). Notably, ANO6 Knockdown in B cells decreased markedly the rate of Ca^{2+} ionophore-evoked PS externalisation, whereas TMEM16F overexpression firmly increased PS exposure rates (Suzuki et al., 2010). As a Ca^{2+}-activated channel, TMEM16F generates a small single-channel conductance, dynamically shifting its ion selectivity with increasing Ca^{2+} levels (H. Yang et al., 2012). Thus, indicative of a positive feedback mechanism kept in check, preventing excess of intracellular calcium.

Functionally different from its homologues CaCCs TMEM16A and TMEM16B, TMEM16F is to some extent similar to fungal scramblase nhTMEM16 and *Aspergillus fumigato* (af)-TMEM16. The latter exhibit a hydrophilic groove half-open cavity, projecting toward the interior of the lipid bilayer, resembling the lipid-scrambling configuration model (i.e., “credit-card” mechanism), observed in TMEM16F (Feng et al.,

2019). This theory has been further strengthened by recent findings showing that in a calcium-free conformation of the scramblase hydrophobic disparity induced membrane distortion that reduced the energy barrier for lipid movement through the hydrophilic groove-like cavities (Falzone et al., 2019). Recent cryo-EM studies added an additional level of complexity in the lipid scrambling model demonstrating that membrane distortion and lipid motion do not require an open groove, but also arguing that lipid scrambling and ion permeation feature distinct pathways (Feng et al., 2019). In apparent contrast to current view, in which (i) lipid movement requires an open groove cavity (Falzone et al., 2018), (ii) lipid scrambling engages in an "out-of-the-groove" configuration without tight contact with the protein (Alvadia et al., 2019) and (iii) both ions and lipids permeate alternatively through the same protein-forming pore (Alvadia et al., 2019). In Feng's et al. study, structural TMEM16F data revealed that the channel retains an intact ion permeation function, whilst employing a conformation leading to plasma membrane distortion and lipid movement facilitation (Feng et al., 2019). Importantly, amino acid mutations, such as N621A and K706A significantly reduced onset of calcium influx and N621A also PS exposure. On the contrary, mutation R542A increased both Ca^{2+} ions and PS externalisation (Feng et al., 2019). This further confirms the importance of calcium binding in both aforementioned mechanisms.

Another enigmatic question concerns the plasma membrane repair ability to prevent death initiated by pore-forming agents. A variety of bacterial toxins, including listeriolysin O (LLO), can trigger cell death via a pore-forming mechanism initiated in the outer leaflet of the membrane (N. Wu et al., 2020). This process differs from other forms of cell death (i.e., pyroptosis and necroptosis) in that it does not require secondary intracellular effectors activation by the death cascades (N. Wu et al., 2020). Maintenance of cell integrity is governed by the intrinsic repair capacity of the plasma membrane by removing damaged membranes through a multitude of processes including EVs, endocytosis and releasing (N. Wu et al., 2020). It has long been known that pore-forming agents induce PS externalisation from the inner leaflet to the outer leaflet of the plasma membrane – perhaps reflecting the movement from plasma membrane injury to full cell-death. Alternatively, this may be demonstrative of a repair-evoked mechanism that

requires PS exposure aimed at resisting cell death (N. Wu et al., 2020). Intriguingly, because PS externalisation occurs as a result of lipid scrambling, a recent study implicated TMEM16F as key in triggering repair mechanisms induced by pore-forming agents. Briefly, TMEM16F-mediated activity facilitated blebbing, release of EVs, decreased pore-formation that led to a significant improvement in cell survival as compared to TMEM16F knockout mice (N. Wu et al., 2020). Collectively, these features have attracted significant interest in recent years pertaining to developmental biology and cancer research fields.

1.3.2.2 Insights into regulatory mechanisms of other TMEM16 members

Among anoctamins, TMEM16H and TMEM16K are highly expressed in many tissues, as is their homologous member TMEM16F. On the other hand, TMEM16B expression is retained in neuronal tissues and the eyes, whereas TMEM16C and TMEM16D are localised mainly in the spinal cord, brain stem, and cerebellum (Pedemonte & Galietta, 2014). TMEM16A is one of the most studied members beside TMEM16F, and is highly overexpressed in cancer, especially amplified in prostate tumours similarly to TMEM16G (Hartzell et al., 2009). Developmental defects of the trachea and lethality were observed in TMEM16A deletion in mice, while conditional KO experiments indicated that the TMEM16A channel Cl^- transport is implicated in smooth muscle contraction and epithelial secretion (Falzone et al., 2018). Homologies associated with scramblase function have also been described for TMEM16C, TMEM16D, TMEM16J, and TMEM16G, albeit it remains unclear whether they exhibit a channel function (Falzone et al., 2018). Additional effects attributed to TMEM16F deletion included also skeletogenosis defects (Ehlen et al., 2013), spinal microglial function to injury (Batti et al., 2016), downregulation of innate immunity in macrophages (Ousingsawat et al., 2015), and termination of T-cell receptor signalling (Hu et al., 2016), to only name a few. In addition, a similar panoply of developmental disorders has been noticed in TMEM16E deletion, with the most known disorders being the limb-girdle muscular dystrophy and Miyoshi myopathy type 3 (Falzone et al., 2018) – indicative of a role in vesicle fusion and membrane repair. Various CaCCs and scramblase members of the anoctamins family have

also been reported to modulate neural activity, as for example TMEM16A, and -B CaCCs, which allow for thermosensory signal in nociception and proper axonal action potential firing across different brain regions, respectively; or as TMEM16C, in which scramblase activity was found to control neurosensory transmissions in pain perception in rat primary sensory neurons by activating sodium-activated potassium currents (Falzone et al., 2018). Furthermore, calcium signalling defects associated with mutations in the uncharacterised TMEM16K channel resulted in several neurological disorders, such as epilepsy, porencephaly, and ataxia (Falzone et al., 2018).

Collectively, the underlying cellular and molecular pathophysiological mechanisms involved in the anoctamin family remain still a work in progress, as new functions are being characterised for known homologues aiding in the profiling of poorly studied members. It is worth noting that despite huge advances in recent years, no major breakthroughs have been reported in the literature – with TMEM16A, B, and F representing the most studied members of the whole group.

1.3.3 Biophysical & molecular approaches to the study of complex system

Protein-protein complex interactions (PPIs) are crucial for the correct upkeep of biological systems because of their implications for the emergence and progression of disease conditions. Particularly, different classes of proteins allow for proper functioning of most biological processes in a cell, such as gene expression, cell growth, proliferation, morphology, and metabolism, as well as intracellular signalling and apoptosis. Moreover, due to a cell response to a plethora of extracellular and intracellular cues, stimulus-specificity within a biological system may be hard to define. Thus, generating a much higher level of complexity and dynamism when trying to investigate complex interaction networks. It has been proposed that over 80% of known proteins operate in complexes (Berggård et al., 2007). Identifying the basis for PPIs is becoming a major objective in drug discovery and delivery, aiding in the identification of novel potential therapeutical targets. Critical investigations into certain aspects of protein function are required in order

to deliver a successful protein-protein interaction study. These include understanding of protein sequence motifs and structure; thorough analysis into the evolutionary history of the proteins that may be used to predict conserved residues or regions implicated in the interactions; extensive profiling of the proteins cell or tissue-types expression, post-translational modifications, and literature on interactions with other already known binding partners. Once all the above criteria are met, a myriad of methods for the detection of PPIs have been developed and categorised into three classes, including *in vivo*, *in vitro,* and *in silico* techniques. Some of the most common *in vitro* methods include co-immunoprecipitation, chemical cross-linkers, fusion protein tags, and tandem affinity purification-mass spectroscopy (TAP-MS), whereas *in vivo* methods may include synthetic lethality and yeast 2 hybrid (Y2H) and lastly *in silico* techniques involve sequence-based approaches, gene fusion, and phylogenetic profile (Rao et al., 2014), to only name a few. Different PPI approaches were employed throughout my Ph.D. research, including chemical cross-linkers, Co-PI, CrisprCas9-KO, modelling, amino acid residues screening, and interfering peptides, which will be later discussed. This section, however, particularly emphasises the use of two-photon microscopy to better address the dynamic properties of PPIs in living cells in real-time.

1.3.3.1 Two-photon or multiphoton microscopy

In vitro FRET-based techniques combining both widefield and confocal microscopes and fluorescence-activated cell sorting (FACS) present several drawbacks when describing protein-protein interactions in which light-activated donor molecules may also excite the acceptor, and/or the donor emission can leak into the detection channel of the acceptor, respectively. Furthermore, both approaches may also be affected by autofluorescence and photobleaching, which further convolute measurement acquisition. A more robust approach has been developed to monitor FRET by using FLIM, as discussed in Chapter 3. This is because the fluorescence lifetime is an intrinsic parameter of the fluorophore, independent of its total concentration. Therefore, in conditions in which interacting parameters cannot be controlled, as those previously mentioned, results are more prone to errors, requiring a higher number of image acquisitions of the same sample in various

combinational settings. Two-photon microscopy also allows for live-cell imaging of biological samples, characterisation of molecules within the specimen of up to 1 mm depth, and 3D imaging of various tissues as well as organoids.

The two-photon fluorescence scanning microscopy concept was initially introduced by Sheppard et al. in 1977 (refer to Sheppard et al., 1977), and in 1990 was applied to biological specimens (refer to Denk & Webb, 1990). In general principal, in single photon absorption, the fluorophore-emitted electrons are excited by a wavelength that has higher energy than their ground state. In striking contrast, two-photon excitation refers to the ability of two photons having a much longer wavelength to excite one electron of a given fluorophore in the ground state, as illustrated by the Jablonski diagram (Figure 1.16a). Importantly, the light used to generate the excitation has a lower wavelength than the resulting fluorescence emission. As a result, low energy produced photons are capable of exciting commercially available fluorophores allowing for a deeper light penetration into tissues than standard fluorescence microscopy. Owing to its low-energy production fewer photobleaching is observed with less tissue or cell damage – particularly advantageous when working in living cells. High-intensity lasers are, however, required to increase the probability of the two photons to hit the fluorophore at the very same time. Moreover, the two-photons laser scanning microscope only allows the infrared light to excite the fluorophore in the focus of the objective, as it is the only area in which the proper number of photons per time and space is reached (Benninger & Piston, 2013).

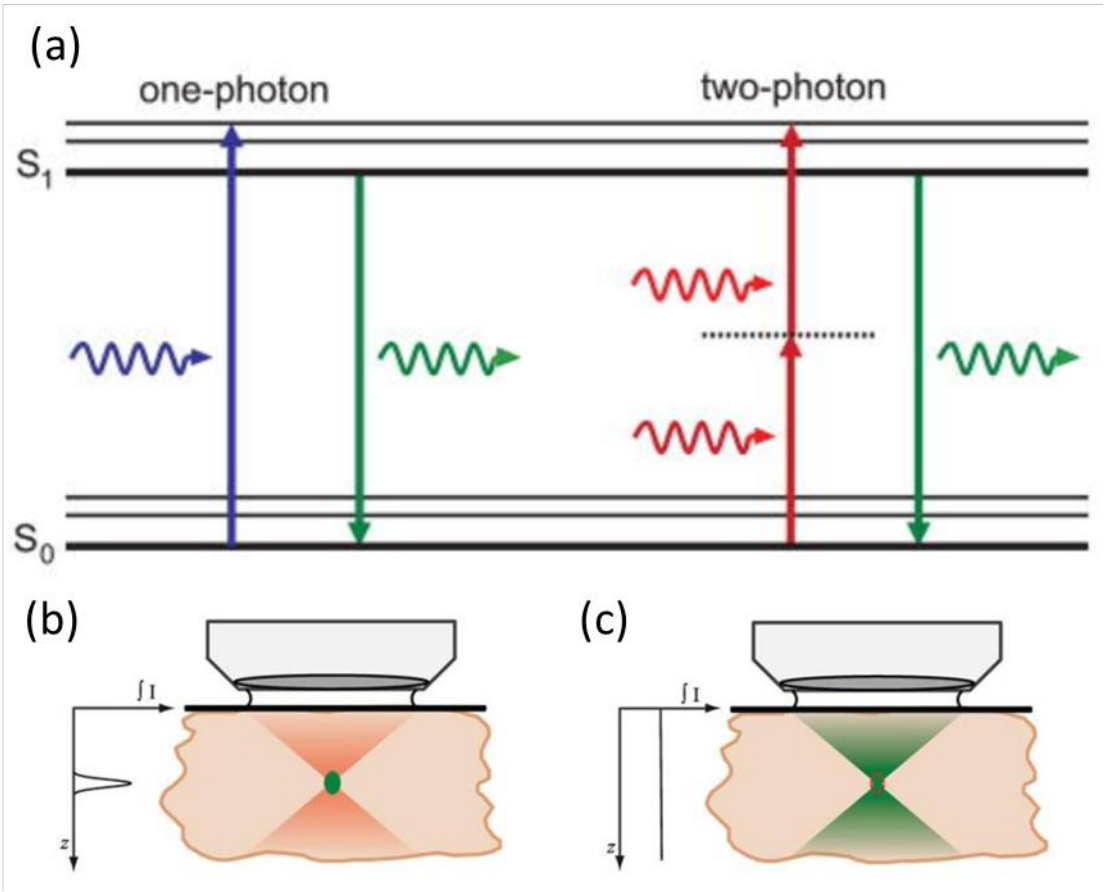

Figure 1.16. Differences between one-photon and two-photon microscopy.
(**a**) Jablonski diagram illustrating differences in conventional one-photon excitation and two-photon excitation of fluorescence. (**b**) two-photon absorption at the focal plane. (**c**) Single-photon absorption displaying confocal pinhole (red dotted line) for proper optical sectioning. (Image source: (Benninger & Piston, 2013)

In photophysics, the energy carried out by a single photon is inversely proportional to its wavelength (λ). Thus, the photon wavelength (λ_{2p}) in two-photon excitation microscopy should correspond to twice that of the photons observed under one-photon excitation. For instance, let's imagine that under a conventional microscope, a given fluorophore reaches its optimal absorption at 400 nm; consequently, the latter may be excited by two co-occurring photons at 800 nm. This is particularly important as it implies that fluorescence can be excited by infra-red illumination rather than UV (Benninger & Piston, 2013). The emission intensity of fluorescence is therefore contingent on the square of the excitation intensity. This quadratic relationship generates the enhanced pulsed laser excitation source and the intrinsic signal optical imaging of the two-photon microscope

(Benninger & Piston, 2013). Collectively, conventional one-photon and two-photon absorptions share the same singlet state resulting from the emission of the excited state.

In two-photon microscopy, the high numerical aperture (NA) objective lens pulses the infra-red source converging the illumination to a diffraction-limited beam spot on the focal plane. Photon density becomes grater at the focal plane due to temporal confinement of photons (Papagiakoumou et al., 2020) (Figure 1.16b,c), enhancing, therefore, the probability of simultaneous interactions between the two photons and the fluorophore. Accordingly, based on the quadratic dependence of two photon absorption on excitation intensity, as previously discussed, the absorption only occurs at the focus of the beam (Benninger & Piston, 2013). This means that the probability of absorption increases by the square of the excitation intensity under a given focus. Importantly, this indicates that objects outside of the focal plane are not excited achieving an intrinsic optical sectioning (Benninger & Piston, 2013).This represents a major difference between conventional confocal microscopy and two photon absorption. Another crucial characteristic is the absence of a pinhole to obtain 3D resolution, as opposed to confocal microscopy, allowing a higher photon detection efficiency as well as flexible recognition geometries (Benninger & Piston, 2013).

A nondescanned two-photon detection approach (used for this manuscript) containing a dichroic mirror reflecting the objective-collected fluorescence emission, transferring the light from the back aperture of the objective to an internal photomultiplier tube (PMTs) (Benninger & Piston, 2013). This approach allows for a more efficient deep sectioning mechanism providing superior imaging resolution into thick samples. In particular, in heterogeneous biological specimens excitation light scatter as the imaging depth is increased in order that un-scattered “ballistic” photons reduce in intensity exponentially to tissue depth (Benninger & Piston, 2013). Importantly, in the presence of a turbid/thick object scattered light originating from the focal plane can still be collected because of the absence of the confocal pinhole. Furthermore, no out-of-focus fluorescence excitation light is generated, the amount of scattering is also enhanced, whereas the background noise reduced. Collectively, two-photon excitation microscopy is a powerful

alternative to conventional confocal microscopy allowing for deep tissue imaging and determination of physical distance between two or more proteins, among others.

1.4 Purinoceptors & TMEM16 in health & disease

1.4.1 Molecular mechanisms of cell death

Many immune and inflammatory events are initiated mostly in response to the activation of purinoceptors as well as TMEM16 members. Particularly important is their implications in cell death regulation – hallmarks of numerous cancers and neurological disorders. Cell death has been recently characterised as a set of genetically encoded mechanisms allowing for targeted removal of redundant, irreversibly injured and potentially harmful cells (Galluzzi et al., 2018). Contrary to accidental cell death (ACD), resulting due to the exposure to severe physical, chemical, and mechanical insults, regulated cell death (RCD) depends on a much more sophisticated molecular machinery that may be influenced by pharmacological and genetic intercessions. Intriguingly, RCD displays two diametrically opposed events: it can operate as an integral effector or programmed cell death (PCD) of physiological homeostasis, directing development or tissue turnover. On the other hand, RCD originating from prolonged perturbations acts as modulators of the adaptive stress response mechanism for the preservation of a biological equilibrium (Galluzzi et al., 2018).

According to morphological alterations associated with cell death, three morphotypes identifying mechanisms of cell and fragment disposal have been used to classify cell death forms. Type 1 cell death, referring to apoptosis, manifests cell shrinkage, plasma membrane blebbing, pyknosis (irreversible condensation of chromatin), karyorrhexis (nucleus fragmentation), and terminating with the formation of apoptotic bodies (Galluzzi et al., 2018). Type 2 cell death or autophagy, exhibiting large-scale autophagic vacuolisation of the cytoplasm (Galluzzi et al., 2018). Type 3 cell death known

as necrosis defined by irreversible mechanism culminating with cell corpse disposal in the absence of phagocytosis or lysosome (Galluzzi et al., 2018).

A major focused will be placed on type 1 cell death, on the two forms of apoptosis (i.e., intrinsic and extrinsic) because of its implications in caspase3-7 activation, and regulation by P2X7 receptor and TMEM16F channel complex interactions (refer to Chapter 5). RCD intrinsic apoptosis is activated by several microenvironmental stimuli, such as DNA damage, ischemia, ER stress, reactive oxygen species (ROS) overload, and microtubular defects, to name only a few. The critical irreversible step for intrinsic apoptosis is demarcated by the extensive mitochondrial outer membrane permeabilization (MOMP) regulated through pro-apoptotic and anti-apoptotic members of the BCL2 protein family (Galluzzi et al., 2018). Together with other apoptosis regulator, intrinsic apoptosis culminates in the activation of executioner caspases, mainly caspase-3 (Galluzzi et al., 2018). Contrarily, extrinsic apoptosis, as described by the nomenclature committee on cell death (NCCD), is initiated by extracellular stimuli acting on plasma membrane receptors, propagated by caspase-8 cleavage and activation, and culminated by caspase-3 activation (Galluzzi et al., 2018). Together, discovering protein complexes that disrupt this system will greatly help in developing tailored therapies that could be used to treat a variety of pathophysiological disorders.

1.4.2 P2X7 & NLRP3 inflammasome

P2X7 receptors are a major trigger of NLPR3 inflammasome activation, demarcated by caspase-1 cleavage and precipitated by IL-1β release (Di Virgilio et al., 2017). Briefly, pathogen-associated molecular patterns (PAMPs), as LPS, may be used to stimulate transcription factor NF-kB production, among others, promoting the activation of genes encoding pro-IL-1β, NLRP3 and other inflammasome components. DAMPs acting at the cytosol or plasma membrane activate the NLPR3 inflammasome, resulting in the release of several effectors including cathepsin B. An Increase in extracellular ATP concentrations from DAMPs and PAMPs signalling interactions feeds back on P2X7 receptors, allowing for potassium efflux, leading to the formation of NEK7, NLRP3, ASC

and caspase-1 complex assembly. The activated inflammasome catalyses the maturation of IL-1β, which is then liberated through membrane-formed micro-vesicles and secretory lysosomes. Activation of P2X7 macropore conductance by aforementioned effectors further allows ATP efflux, augmenting the activation signal (Di Virgilio et al., 2017). It is worth noting that this process is intertwined with extrinsic and intrinsic apoptotic machinery. In other words, LPS-priming indirectly activates P2X7 receptors, culminating by executioner caspases, mainly caspase-3. Mitochondrial permeability transition (MPT) resulting from these processes can also induce type-3 cell death or necrosis. This, however, may vary depending on the experimental systems (i.e., type of cell line or tissue) employed. The P2X7-NLRP3 inflammasome regulation has been associated to many form of cancers, such head and neck cancer (Bae et al., 2017), chronic lymphocytic leukemia (Salaro et al., 2016), breast cancer (Xia et al., 2015) and gastritis cancer (P. Yu et al., 2021), but also to depression and diabetes (D. Wang et al., 2020).

1.4.3 CNS implications

Extracellular ATP can act synergistically as a growth and potent long-term tropic factor, influencing neuronal and glial development through cytoplasmic Ca^{2+} and cAMP (Burnstock, 2008). ATP release from neural activity assists in functional neural circuitry signalling, growth, and differentiation of different cells in the CNS. In a healthy system, the functional state of glial cells, receptor subtypes, and ectoenzyme expression regulate ATP and Ado availability, inducing proper mitogenesis or apoptosis (Burnstock, 2008). ATP and glutamate release as neurotransmitters from presynaptic primary afferent nerve terminals on the spinal cord dorsal horn neurons can postsynaptically activate purinergic receptors including P2X2, P2X4, P2X7, P2Y subtypes, and AMPARs, or NMDARs, respectively (Burnstock, 2008). The byproducts of the breakdown of ATP via ectonucleotidase result in the production of Ado exhibiting inhibitory presynaptic function through stimulation of A1 receptors. However, presynaptic ATP itself may also either inhibit transmitter release through P2Y receptor signalling or augment glutamate secretion via P2X3 receptors. Furthermore, ATP release from astrocytes along with glutamate also participates in complex glial-neuronal interactions (Burnstock, 2008). Given the

complexity of purines signalling in neurotransmission and neuromodulation, it is not surprising that dysregulation of such a system has been associated with severe neurodegenerative and neuropsychiatric diseases. CaCCs also play a manifold role in neural physiology, controlling nociception and neuronal excitability (Duran & Hartzell, 2011). Some TMEM16 members were indeed reported to regulate membrane exocytosis via adjusting intracellular Ca^{2+} or Cl^{-} concentrations near the plasma membrane (Kunzelmann et al., 2019). TMEM16F-induced exocytosis increases chloride channel trafficking to the membrane, including CFTR, known for cystic fibrosis and congenital absence of the vas deferens (CAVD) conditions. Due to its dual function, TMEM16F-activated scramblase is pivotal to the sheddases (or cleavage) function of the ADAM family, as discussed previously. Thus, promoting IL-6 trans-signalling activation enhancing cell death and tumorigenic activity (Kunzelmann et al., 2019). Importantly, some anoctamin members have also been associated with head and neck cancer, breast cancer, glioblastoma, and myoblast proliferation to name but just a few (Kunzelmann et al., 2019). These overlapping functions between purinoceptors and anoctamins may potentially uncover novel therapeutical targets.

1.4.3.1 Multiple sclerosis

Multiple sclerosis (MS) is a disabling disorder in which the body's immune system attacks the protective insulating layer of the nerve cells referred to as the myelin sheath of the CNS – brain and spinal cord. Following neural damage, the nerve fiber is exposed impairing the signal being transmitted within, resulting in multiple lesions or scars (Litin & Nanda, 2018). There different types of MS have been identified, with the most frequent or common being the relapsing-remitting MS, whereas the other two forms include primary progressive MS and secondary progressive MS. Symptoms differ greatly from patient to patient based on the area of nerve fibers affected, often leading to movement defects. For instance, tremors, lack of coordination, numbness and/or weakness of the limbs, and Lhermitte-like signs (i.e., electric-shock sensations) are common manifestations (Litin & Nanda, 2018). There is no specific diagnostic test currently available (Hermann et al., 2021). However, one treatment option include Cladribine

(Mevenclad®), whose absorption, uptake and distribution were recently described to be entirely mediated by both ENTs proteins and CNT3, but with low affinity (Hermann et al., 2021), as previously mentioned (refer to section 1.1.2.2). Intriguingly, MS pathophysiology is defined by macrophage accumulation and inflammatory cells infiltrating into the CNS leading to demyelinating. P2X7 receptors and TMEM16F channels are abundantly expressed on myeloid lineage cells. Furthermore, reported increased immunoreactivities of P2X7 receptors in activated macrophages/microglia have been identified in the literature, along with elevated ATP levels contributing to MS lesion induced IL-1β release (Amadio et al., 2017; C.-C. Lin & Edelson, 2017). Thus, these receptors represent pivotal candidates aiding perhaps in the identification of new molecular pathways that may lead to novel therapeutic development.

1.4.3.2 Glioblastoma

A grade IV astrocytoma, often known as glioblastoma (GBM), is an aggressive, fast-growing CNS tumour that develops in the brain or spinal cord but does not metastasise to distant organs. GBM, originating from astrocytes, has a median survival time of about 14 months (Stupp et al., 2005). It may arise either form *de novo* or from a lower-grade astrocytoma (Litin & Nanda, 2018). GMB most frequently develops in the cerebral hemispheres, mainly in the frontal (40%), temporal (29%), parietal (14%) and occipital (3%) lobes of the brain (Larjavaara et al., 2007). GBM treatment includes surgical resection, followed by radiation therapy and chemotherapy, albeit relapse occurs in almost all cases. This is due to GBM complex tumor heterogeneity (Stupp et al., 2005). Interestingly, essential pathophysiological processes associated with GBM have been attributed to purinergic signalling (Zanoni et al., 2022). Briefly, following radiotherapy extracellular ATP is released into the tumour microenvironments activating purinergic P2 receptors (mostly P2X7 subtypes). As a result, a significant shift in P2X7 isoform expression was observed in GBM cells, defined by a downregulation of the $P2X7_A$ isoform and up-modulation of the $P2X7_B$ isoform associated also with extensive cell death and senescence-associated stemness markers (Zanoni et al., 2022). This post irradiation-evoked $P2X7_B$ isoform upregulation was further potentiated upon application of P2X7

inhibitors enhancing trophic/growth stimuli (Zanoni et al., 2022). TMEM16 channels expression also seems to be increased in several distinctive types of cancer including GBM, although the signalling mechanisms employed remain as of today elusive (Y.-S. Lee et al., 2016).

1.4.3.3 Cystic Fibrosis

Cystic Fibrosis (CF) is an autosomal recessive condition occurring in epithelial organs resulting also in severe peripheral nervous system abnormalities, such as neuropathy (Reznikov et al., 2013). Intriguingly, it has been suggested that the CFTR gene directly interfere with the CNS function of CFTR-deficient pigs, resulting in severe ultrastructural changes of myelin sheath, as to those observed in peripheral neuropathy (Reznikov et al., 2013). Recent improvement diagnosis and treatment has allowed a better prognosis with some patients living into their 50s (Litin & Nanda, 2018). CFTR is an essential chloride channel, whose activation is enhanced by TMEM16F activation, perhaps due to signalling proteins translocation to the plasma membrane (Simões et al., 2018). Other members of the anoctamins, such as TMEM16A have also been reported as indispensable for regulation of CFTR (Benedetto et al., 2019). CF monocytes exhibit an unusual, elevated level of IL-1β attributed to mucopurulent discharge in CF airway (Cantin, 2022). Together with the accumulation of neutrophil elastase, extensive bronchial damage or bronchiectasis is induced – that is the hallmark of cystic fibrosis in the lungs. Emerging evidence suggest that CF monocyte signalling pathways involves P2X7-driven NLRP3 inflammasome complex activation (Cantin, 2022).

1.4.4 Therapeutics development

As has been mentioned thus far, a wealth of research exists that demonstrates the involvement of several TMEM16 family members and purinergic system in various diseases, including cancer, psychiatric, and neurological disorders, to only name a few. Research on the expression and activity patterns of these proteins throughout the processes of proliferation, migration, and differentiation in various disease states has been carried

out over the past several years. Altogether, this highlights the significance potential of novel therapeutics (Burnstock, 2008, 2008, 2017; Cheffer et al., 2018; Duran & Hartzell, 2011; Pedemonte & Galietta, 2014). There is, however, no drug nor therapy currently available on the market targeting P2X7 receptors, albeit a very recent clinical trial has started in the UK using JNJ-54175446, a P2X7 antagonist, for treatment of depression and depression-related symptoms (refer to identifier: NCT04116606). Nevertheless, several other treatments have been developed for other P2 receptors subtypes. For instance, clopidogrel a $P2Y_{12}$ antagonist acting as antiplatelet and commonly employed as medication for thrombosis and stroke (Burnstock, 2017); Diquafosol, on the contrary, is an agonist for $P2Y_2$ receptors used for keratoconjunctivitis sicca (KCS; i.e. dry eye syndrome) (Burnstock, 2017). Other investigations include P2X3 antagonists for potential use as medication for chronic cough, urinary incontinence, visceral pain, and hypertension (Burnstock, 2017). On the other hand, no selective inhibitors are currently available for TMEM16s, albeit screening of a chemical library recognised benzbromarone as TMEM16A inhibitor (Pedemonte & Galietta, 2014). Intriguingly, the latter is commercially used for the treatment of gout conditions for the past 30 years (Azevedo et al., 2019) – an inflammatory arthritis condition known as the archetypal purine-related disease. No drug nor clinical trial are currently being developed for TMEM16F or other TMEM16 members, perhaps because their pharmacology is still in its very infancy. The overwhelmingly overlapping molecular physiology as well as pathophysiology between purinoceptors and TMEM16 family, further suggest an intertwined activity that may aid in tailoring better and much more specific therapeutics.

1.5 Theoretical approach

1.5.1 Aims & objectives

P2X7 non-selective ligand-gated cation channels activate upon elevated concentrations of extracellular ATP, similarly to those observed in tissues injury, chronic inflammation, T-cell activation, and in the scrambling of phospholipids triggering membrane shrinkage, swelling, lysis, bleb, and apoptosis. Owing to its unique macropore and cytoplasmic domains P2X7 receptors present promising therapeutical targets for drug development. In the last few years, different screening approaches identified over 50 potential protein partners that may physically interact with P2X7R, as determined by the P2X7 interactome database. Furthermore, the ability of P2X7Rs to permeate large organic cations (≤900 Da) further strengthened the hypothesis that these receptors may be, indeed, engaged in channel-forming complexes with other proteins. There have been several proposed mechanisms to the macropore formation including (i) pore dilation, (ii) channel recruitment – pannexin-1, (iii) liposome reconstitution, and (iv) very recently a major family of regulated scramblases – TMEM16/anoctamin channels were proposed as promising interacting patterns to P2X7 receptors. The TMEM16 family includes 10 isoforms TMEM16A-J, with some exhibiting Ca^{2+}-activated Cl^- channels and Ca^{2+}-dependent phospholipid scramblase dual function. TMEM16F is a transmembrane protein, which remarkably display similar cell/tissues expression patterns as P2X7 receptors, with significant implications in blood coagulation, membrane blebs and apoptosis. Interestingly, it has been proposed that P2X7R stimulation potentiates influx of calcium resulting in downstream activation of TMEM16F channels responsible for translocation of PS, initiation of cell shrinkage culminating with activation of caspases-3 and -7. Accordingly, it is worth noting that such downstream modulation may also influence inflammasome activation and cell death signalling mechanisms. So far, only preliminary loss-of-function studies highlighted the potential interaction between TMEM16F channels and P2X7 receptors in macrophages – yet physical coupling and functional modulation and amino acids profiling between these two proteins remain

uncharacterised. Therefore, the aim of my Ph.D. research is to experimentally demonstrate the physical coupling, and to identify regulatory components or regions critical to complex stability and interaction. Contributing as such to the biophysical and molecular characterisation of the proteins-forming complex, but also exploring its implications in the immune response. Thus, providing insights into novel pharmacological and immunoregulatory targets. A broad range of techniques were employed to carry out this research work including two-photons microscopy, molecular modelling, interfering peptides, patch-clamp electrophysiology, qRT-PCR, CrisprCas9-knockout, mutagenesis studies, video- and confocal-microscopy, contributing, therefore, to proper understanding of developmental aspects in molecular neuroscience. In this manuscript, data acquisition and interpretation have been structured in three chapters: Chapter 3 illustrating the biophysical interaction, Chapter 4 delineating the molecular interaction and Chapter 5 the immunological interaction.

Chapter 2

Materials and Methods

2.1 Animals

Four C57B16 male mice were used in the study aged between 6 and 12 weeks. All animals were maintained in a controlled environment (temperature 20 ± 2 °C; 12-hour light-dark cycle). Food and water were supplied ad libitum. All procedures for the care and treatment of animals were performed in compliance with the institutional animal welfare guidelines and had full approval by the local board.

2.1.1 Peritoneal macrophages extraction and culture

Mice were euthanised via rapid cervical dislocation. A small incision was carried out along the abdomen midline to expose the peritoneal wall. Extraction of resident peritoneal cells was then performed by delivering 10 mL of ice-cold (4°C) harvest medium (PBS,) into the peritoneal cavity using the bevelled end of a 20-gauge needle. Cells were centrifuged at 1500 rpm for 5 min and counted on an automated cell counter using a trypan blue exclusion. The total yield obtained ranged between 1-3 x 10^6 cells/mL per mouse.

The macrophages were seeded into 96-well plates at 0.5 x 10^5 cells/wells (100μL of medium per well). Cells were allowed to adhere for 2h at 37 °C and non-adherent cells were removed by washing three times with PBS. Peritoneal macrophages were cultured in DMEM media supplemented with 10% fetal bovine serum, 1× GlutaMax, 100 units/mL penicillin and 100 μg/mL streptomycin prior to experiments.

2.2 Cell culture and Biochemistry

2.2.1 Cell culture and Transfection.

Human embryonic kidney (HEK293; ATCC) cells and murine RAW264.7 (ATCC; TIB-7 – kindly provided by 3BIO's lab) macrophages were maintained in Dulbecco's modified Eagle's medium containing L-GlutaMax, supplemented with 100 units/mL penicillin and 100 μg/mL streptomycin (Gibco Life Technology). For HEK293 TMEM16F-KO cell line, the media were further supplemented with 1 μg/mL puromycin dihydrochloride (Gibco Life Technology). Cells were incubated at 37 °C in a humidified incubator in 5 % CO_2. Trypsin-treated cells were cultured in 6, 8, and 96-wells plates as detailed in the legends to the figures. For patch-clamp and video fluorescent microscopy experiments cells were seeded onto poly-l-lysin (Sigma Aldrich, USA) pre-treated 9 and/or 12 mm glass coverslips (Marienfeld), or in P100 dishes for biochemical experiments. Cells were transfected using the calcium phosphate precipitation approach. Rat P2x7 (rP2X7) and enhanced Green Fluorescent Protein construct (eGFP) cDNA' constructs were contained within pcDNA3.1(+) vectors (Invitrogen), whereas the cDNA encoding rat ANO6/TMEM16F was contained within a pCMV6 plasmid including a myc-tag (OriGene) located in the C-terminus. Cells transfection efficiency was measured by eGFP construct expression. For video microscopy experiments cells were either co- or triple-transfected with rP2X7 (2 μg), TMEM16F (0.1 μg) and eGFP (0.3-0.05 μg) as illustrated in the text. For whole-cell experiments rP2X7 cDNA was decreased to 0.8 μg, whilst for biochemical experiments cells were either transfected with each construct alone i.e., myc tagged rP2X7 (5 μg) and myc tagged rANO6/TMEM16F (5 μg) or together at a 1:0.05

ratio as indicated. Cells were washed 3 times in PBS solution 24-48h post-transfection prior to all experiments. For RAW264.7 cell line, macrophages were studied under endogenous conditions and seeded into 96-well plates at 0.3-0.5 x 10^5 cells/wells (100µL of medium per well) as described in section 2.4.

2.2.2 Surface biotinylation, Co-immunoprecipitation, Cross-linkers, and Western-blot

For cell surface biotinylation assay, 24 h-post transfection with rP2X7- and/or rTMEM16F-myc tagged plasmids at a ratio of 1:0.05, respectively, HEK293 and TMEM16F-KO cell lines were washed three times in ice-cold PBS+ solution (PBS; 1 mM $MgCl_2$, 0.4 mM $CaCl_2$ and adjusted to pH 8.0 at 4 °C) and incubated with 2 Mm sNHS-SS-Biotin or sNHS-LC-Biotin (Thermo Fisher) in PBS+ for 30 min under gentle agitation. Cells were washed one time in PBS+ and excess of sNHS-SS-Biotin and sNHS-LC-Biotin quenched with 20-mM Tris in PBS+. Cells were further washed three times in ice-cold PBS and lysed by gentle incubation for 60 min at 4 °C in lysis buffer containing: HEPES, 100mM NaCl, 5mM EDTA, 1% Triton-X, pierce protease inhibitor tablets (Thermo Fisher, Waltham, USA). Samples were centrifuged at 14000 rpm at 4 °C, and input collected at this stage. Following this, NeutrAvidin-agarose (Thermo Fisher) resin was added to lysis samples prior to a pre-cleaning step with lysis buffer. The resin was then washed three in washing buffer (WB; 20 mM Hepes, 500 mM NaCl, 5mM EDTA, 1% Triton X-100, pierce protease inhibitor tablets) and two times in lysis buffer. Samples were then resuspanded in 70 mM DTT and NuPage LDS sample buffer (Thermo Fisher) and boiled for 10 min at 95 °C. The supernatant was loaded and run onto NuPage Novex Bis-Tris 4%-12% gel (Thermo Fisher) using MOPS running buffer for 30 min at 110V and consequently increased to 150V for 60 min. Mini-PROTEAN TGX 7.5% gels were also employed, based on the molecular weight of interest (as described in the text) using TGS running buffer (BioRad). The proteins were then transferred onto nitrocellulose membrane using the TransBlot Turbo system (BioRad) and ran at 1.3A or 2.5A at 25V for 10-20 min for one or two gels, respectively. Membranes were blocked for 1 h in TBST (PBS; 1% non-fat milk, 0.5% BSA and 0.05% Tween-20) and incubated in primary

antibody diluted in TBST overnight at 4 °C. Detailed list of primary and secondary antibodies is illustrated in Table 2.1. Membranes were then washed three times in PBST before and after incubation with an appropriate HRP secondary antibody for 2 hours at ambient temperature. Revelation was done by Amersham ECL select western blotting detection reagent (GE Life Sciences) and chemiluminescence was assesed using the Amersham Imager 600.

For co-immunoprecipitation, tranfected and non-transfected cells were washed in ice-cold 4°C PBS+ and lysed as described above. Following this, the cell lysate was incubated with 5 µg anti-FLAG mouse antibody under gentle agitation for 2 h at 4 °C. Protein G sepharose fast flow resin (Sigma Aldrich) was then added to the sample and further incubated for 1 h at 4 °C. Sample preparation and western blot procedures were carried out as described for cell surface biotinylation assay. For cross-linkers assay, transfected cells were washed three times in ice-cold 4°C PBS+ and incubated with bis(NHS)PEG5 (Thermo Fisher), bis(NHS)PEG9 (Thermo Fisher) and BS3 (Thermo Fisher) diluted in PBS+ at a different concentrations as detailed in the text for 30 min under gentle agitation. Cells were then washed one time in PBS+ and cross-linkers reaction was quenched with 20-mM Tris in PBS+. At this step, samples were lysed, centrifuged and the total lysate was run on SDS-pages as described above.

Table 2.1: List of primary and secondary antibodies

Type	Antigen	Speceis	Manufacturer	Catalogue code #	Western Blot
Primary Antibody	Actin	Mouse	Sigma Aldrich	A5441	1:1000
	Ano6	Rabbit	Sigma Aldrich	HPA038958	1:500
	P2X7	Rabbit	Alamone	ARP008	1:500
	Ano5	Rabbit	Biorbyt	ORB39268	1:500
	C-myc	Mouse	Invitrogen	13–2500	1:500
	Anti-FLAG	Mouse	Sigma Aldrich	F1804	5 µg
Secondary Antibody	Goat Anti-Mouse IgG HRP		Thermo Fisher	31430	1:10000
	Goat Anti-Rabbit IgG HRP		Thermo Fisher	31460	1:10000

2.3 Molecular biology

2.3.1 Fusion proteins and Site-directed mutagenesis

Fusion protein constructs were generated by cloning the coding region of the proteins of interest along with the linker and the fusion GFP tag in the C-terminus of vectors using specific restriction enzymes by PCR reaction. rP2X7-GFP expression construct was created by amplifying of rP2X7 fragment (Fgt rP2x7) within its pcDNA3.1(+) vectors using personally designed primers 5'-GTCGCCAAGCTTATGCCGGCTTGCTGCAGCTGGAAC-3' and 3'-GCATTTGCGGCCGCGTAGGGATACTTGAAGCCACTGTA-5' that targeted the cleavage of HindIII and NotI restriction enzymes, respectively. For rANO6/TMEM16F fusion GFP tag fragment was produced by amplifying the GFP fragment (Fgt GFP) within the cDNA encoding rP2X2-GFP contained in pcDNA3.1(+) plasmid using specific primers 5'-ATTCATCTCGAGGTCTCAAAGGGAGAAGAGCTGTTCACTGG-3' and 3'-ATGTAACCGCGGTTACTTGTACAGTTCGTCCATACCCAGGGTGATACC-5' that corresponded to restriction enzymes XhoI and SacII. Fgt rP2x7 and Fgt GFP were carried out using standard PCR reaction parameters (Table 2.2), to a final volume of 50 µL per reaction containing: 2.5 µL (or 0.5 µM) forward and reverse primers, 1 µL (or 30 ng) of cDNA plasmids, 25 µL Q5 Hot Start fidelity master mix (2x) and 19 µL ddH_2O.

Table 2.2: Fgts PCR reaction cycle

Step	Temperature (°C)	Time	
Initial denaturation	98 °C	30 sec	
Denaturation	98 °C	10 sec	
Annealing	72 °C	40 sec	30 cycles
Extension	72 °C	40 sec	
Final extension	72 °C	05 min	
Hold	04 °C	∞	

The fragment constructs were then cleaved by Dpn1 following 1h incubation at 37 °C and dialysed on 0.025 µM filters (Millipore; VSWP02500) for 30 min. Prior to directional cloning, the cDNAs encoding rP2X2-GFP and rANO6/TMEM16F contained within pcDNA3.1(+) and pCMV6 vectors, respectively and fragments were double digested with their corresponding restriction enzymes as detailed in Table 2.3 and 2.4 for 1h at 37 °C. The vectors were then dephosphorylated using alkaline phosphatase, calf intestinal (CIP) for 1h at 37 °C. 10 µL of the vector and fragment product was ran on a 1% agarose gel (1g Agarose, 100mL TAE) to verify that had undergone correct cleavage before ligation with T4 DNA ligase for 2h at 25 °C (Table 2.5). rP2X7-mScarlet, instead, was achieved by tagging mScarlet (from gene synthesis) in the C-terminus of rP2X7 within a pcDNA3.1(+) vector.

Table 2.3: Digestion of insert and vector

	Insert	**Vector**
	Fgt GFP	pCMV rANO6
DNA	50 µL (PCR DpnI-dialised)	0.5 µL (1 µg)
CutSmart	10 µL	
XhoI	1 µL	
SacII	1 µL	
ddH₂O	38 µL	87.5 µL

Table 2.4: Digestion of insert and vector

	Insert	**Vector**
	Fgt rP2X7 myc	pcDNA3.1 rP2X2 GFP
DNA	50 µL (PCR DpnI-dialised)	0.5 µL (1 µg)
CutSmart	10 µL	
XhoI	1 µL	
SacII	1 µL	
ddH₂O	38 µL	87.5 µL

Table 2.5: Ligation of vector and insert

	pCMV ANO6 GFP	**pCDNA3.1 rP2X7 GFP**
Insert	2µL Fgt GFP (35 ng)	2µL Fgt rP2X7 (35 ng)
Vector	4µL pCMV rANO6 XhoI-SacII (64 ng)	2µL pcDNA3.1 rP2X2 GFP HindIII-NotI (64 ng)
T4 buffer	2 µL	
T4 DNA ligase	1 µL	
ddH₂O	11µL	13µL

For site-directed mutagenesis, primers were designed introducing appropriate single amino acid mutation (Table 2.6) and PCR was carried out using Q5 High-Fidelity DNA polymerase to a final volume of 25 µL per reaction, containing: 0.5 µM of forward and reverse primers, 1-25 ng of template DNA, Q5 Hot Start master mix (1x) and nuclease-free water. The annealing temperature was adjusted for each mutagenic primer. Phosphorylation, intramolecular ligation and circularization of PCR products were achieved by using KLD enzyme mix (NEB). Transformation was performed using *E. cloni* 10G chemically competent cells (Lucigen) or NEB 5-alpha competent *E. coli* (NEB). For pcDNA3.1 rP2X7 mutants, transformation mix was plated on pre-poured LB agar plate supplemented with 100 µg/mL ampicillin or with kanamycin for pCMV6 rANO6/TMEM16F mutants. Mini- and max-scale purification of DNA was carried out using NucleoSpin plasmid kit (Macherey-Nagel) and mutations were confirmed by sequencing (Eurofin).

Table 2.6: PCR site-directed mutagenesis primers

Residue	Amino acid sequence (5'-3')	Annealing Temperature (°C)
rP2X7 E375R	CCTCCTGTAAGTGCTGCCGGCCCTGCGCAGTGAATGAGTAC	82 °C
rP2X7 E375A	CCCCTCCTGTAAGTGCTGCGCACCCTGTGCAGTGAATGAG	84 °C
rP2X7 E375C	CCTCCTGTAAGTGCTGCTGTCCCTGCGCAGTGAATGAGTAC	82 °C
rANO6 R495E	GATCACCAACTTCGAACTCCCAGAGACCCAGACTG	76 °C
rANO6 R495A	GATCACCAACTTTGAGCTCCCAGCGACCCAGACTG	77 °C
rANO6 R495C	GATCACCAACTTTGAGCTCCCATGTACCCAGACTG	70 °C
rANO6 R117E	GAAACAGAAGGAGAAAAGGCAAGC	57 °C
rANO6 R137E	GGAAGCCACAGAATCTGTTTCTGATGACAAGCTTGTGTTC	71 °C
rANO6 R589E	TCTAATTGGAGAATATAAAAGAGTCTCGGGATC	61 °C

2.3.2 Quantitative reverse transcription PCR

Total RNA was isolated from wild-type HEK293T and HEK239-ANO6 knock-out cell lines using NucleoSpin RNA Plus kit (Macherey-Nagel). Briefly, cells were lysed, and RNases inactivated in chaotropic ion lysis buffer. Contaminating gDNA was then removed by centrifugation in NucleoSpin gDNA removal column. Binding solution was then applied to the flowthrough, and the RNA washed, dried in silica membrane, and eluted in 30 µL RNase-free water. RNA integrity was verified on 1 % TBE polyacrylamide gel containing: 1 g agarose-D5, 20 mL TBE (5x), 10 µL BET and 80 mL RNase-free water and samples were ran at 90V. 1 µg of total RNA per sample was then reverse transcribed in10 µL RT master mix (2 µL RT buffer 10x, 0.8 µL or 100 mM dNTP mix 25x, 2 µL RT random primers 10x, 1 µL reverse transcriptase, 1 µL RNase inhibitor and 3.2 µL RNase-free water) using standard PCR procedures (Table 2.7). qPCR was performed using Taqman probe primers specific for hANO1/TMEM16A to hANO10/TMEM16K (Table 2.8). Following this, qPCR reaction was carried out in 10 µL mixture (qPCR Master Mix 2X, cDNA 2.5 ng, 0.5 µM primers and probes) and programmed as followed: (i) enzyme activation at 95 °C for 30 s (1 cycle); (ii) denaturation at 95 °C 0.3 s and (iii) annealing, extension, acquisition at 60 °C for 30 s. These last two points were ran for 40 cycles. The relative ratio and relative expression values for hANO6/TMEM16 and GDPDH calculated from equations and standard curves (Figure 2.1). Samples were analysed in duplicates and normalised to the corresponding GDPDH.

Table 2.7: Reverse transcription PCR parameters

	Step 1	**Step 2**	**Step 3**	**Step 4**
Temperature °C	25 °C	37 °C	85 °C	4 °C
Time	10 min	120 min	5 min	∞

Table 2.8: FAM- labelled MGB TaqMan probes

Gene	Probes	Amplicon length
ANO1	Hs00216121_m1	75
ANO2	Hs01021384_g1	69
ANO3	Hs01119680_m1	73
ANO4	Hs01128244_m1	80
ANO5	Hs01381106_m1	116
ANO6	Hs03805835_m1	63
ANO7	Hs00417639_m1	60
ANO8	Hs00394261_m1	79
ANO9	Hs00947743_g1	62
ANO10	Hs01106643_m1	116

RT − qPCR Efficiency: $\mathbf{E} = 10^{\left(-\frac{1}{\text{slope}}\right)}$

Relative expression ratio: $\mathbf{R} = \frac{\left(\mathrm{E}_{target}\right)^{\wedge \Delta CP\ target\ (\ control-sample)}}{\left(\mathrm{E}_{ref}\right)^{\wedge \Delta CP\ ref\ (\ control-sample)}}$

Under the condition:

$\mathrm{E}_{target} = \mathrm{E}_{ref} = 2$

Relative expression ratio: $\mathbf{R} = 2^{(\Delta CP\ sample - \Delta CP\ control)}$

Relative expression ratio: $\mathbf{R = 2^{(-\Delta\Delta CP)}}$

Figure 2.1: Mathematical model for relative quantification of target genes in RT-qPCR. Representative equations for quantification of qPCR data.

2.3.3 Generation of Crispr-Cas9 knock out

CRISPR-Cas9 single- and double-knock out methods were carried out as described in (Zhang *et al*., 2013). CRISPOR (Concordet and Haeussler, 2018) and CHOPCHOP (Labun *et al*., 2019; Labun *et al*., 2016; Montague *et al*., 2014) were used to design sgRNA sequences targeting exon 15 of hANO5/TMEM16E gene and exon 2 of hANO6/TMEM16F gene (Table 2.9). The oligonucleotides encoding the sgRNA sequences containing BbsI overhangs were then cloned into BbsI sites in pSpCas9(BB)-2A-Puro (Addgene plasmid ID:48139). The plasmids obtained were verified by sequencing (Eurofins Genomics) and transfected into HEK293T by calcium phosphate precipitation method (see section 1.2). Transfection of each sgRNA was performed in triplicates in P100 plates. After 24-48 h transfection, 1 μg/mL puromycin was applied to select cells for 48-72 h. Monoclonal selection of transfected cells was carried out by dilution in 96-well plates at a final concentration of 0.5 cells per 100 μL to reduce multiple-cell colonies per well. Single-cell colonies were allowed to expand for 15-20 days. Genomic DNA was then harvested from cells and deletions of hANO6/TMEM16F gene confirmed by sequencing (Eurofins Genomics), western blot and in vitro pharmacology.

2.4 Immunology and *In vitro* pharmacology

2.4.1 Interfering HIV-1 TAT peptide

Membrane-permeant fusion peptides were manufactured by GenScript and comprised 18-amino acid residues corresponding to specific regions of mP2X7R and mANO6/TMEM16F (Table 2.12) fused together to 11-amino-acid protein transduction domain of HIV-1 TAT by a linker. Among these, two TAT-peptides denoted as random sequence were used as control. Cell treatment was carried out using 50 μM TAT-peptides incubated overnight at 37 °C in DMEM 10 % FBS, or in DMEM FBS-free medium 6 hours before experiments.

Table 2.9: HIV-1 TAT peptide sequence

Peptide	Sequence	Target
mP2X7	FCRSGVYPYCKCCEPCTVGGGYGRKKRRQRRR	C-cys anchor
mP2X7-E375R	FCRSGVYPYCKCCRPCTVGGGYGRKKRRQRRR	C-cys anchor
mP2X7-random	FVCKYESCPRCPCVTGYCGGGYGRKKRRQRRR	N/A
mANO6	KKKEKVAIMITNFELPRTQTDGGGYGRKKRRQRRR	
mANO6-R520E	KKKEKVAIMITNFELPETQTDGGGYGRKKRRQRRR	
mANO6-random	NREVDTLKTPAITEMQFIGGGYGRKKRRQRRR	N/A

2.4.2 ELISA

RAW247.6 macrophages were seeded in 96-well plates at 3 x 10^5 cells/well and incubated overnight with membrane-permeant HIV-1 TAT-peptides at 37 °C as described in section 2.4.1. ELISA analysis for TNF-α release was carried out in cell-free supernatant primed with LPS 1 µg/mL for 4 h followed by stimulation or non-stimulation with ATP 3 Mm for 20 min at 37 °C. When indicated, cells were treated with 25 µM of selective P2X7 receptor antagonists AZ10606120 (Bio-Techne) and A740003 (Bio-Techne) before and during LPS/ATP stimulation. ELISA plate was coated in anti-mouse TNF-α antibody 1 µg / mL (clone 1F3F3D4) in a 0.05 M coating buffer (Na_2CO_3 15 mM, $NaHCO_3$ 35 mM and adjusted to pH 9.6) and left overnight at 4 °C. The plate was washed three time in washing buffer (PBS supplemented with 0.05 % Tween 20) and incubated in blocking solution (PBS, 0.05 % Tween 20 and 1 % BSA) for 1 h at 37 °C. Three further washing steps were carried out between and after incubation with cell-free supernatant samples for 2 h at 37 °C. This was followed by incubation with 0.5 µg/mL anti-mouse TNF-α biotinylated detection antibody (clone XT3/XT22) for 1 h at 37 °C. Avidin-HRP was then added to the plate, before revelation using 1.25 mM tetramethylbenzidine and 13.05 mM H202 in 0.1 M pH 5 citrate buffer, which was stopped by 1 M HCl. The absorbance was measured at 450 nm using a microliter plate photometer (Safas SP2000, Xenius, Monaco) and TNF-α

concentration was estimated using a mouse TNF-α recombinant protein solution as standard curve.

2.4.3 Griess assay

Nitrate (NO_2) production was measured in 40 µL cell-free supernatant using Griess method. Equal volumes of Griess reagents consisting of p-aminobenzene-sulfonamide (58.1 mM; Sigma) in 30 % acetic acid and N-1-Naphtylethylene diamine dihydrochloride (3.9 mM; Sigma) in 60 % acetic acid, were added into individual wells of 96-well plates. The absorbance was measured at 543 nm using a microliter plate photometer (Safas SP2000, Xenius, Monaco). Total nitrate concentration was determined using a sodium nitrate (Sigma) standard curve.

2.4.4 Caspase-3/7 activation

Caspase-3/7 activation in cells was carried out using Caspase-Glo 3/7 Assay (Promega, G8091). In brief, this assay kit provides a luminogenic substrate coupled to the caspase 3/7 DEVD tetrapeptide sequence. When Caspase-Glo 3/7 Reagent is added pro-luciferin DEVD is cleaved and aminoluciferin released resulting in the production of light, in the presence of ATP and luciferase. Mouse peritoneal macrophages were plated at 5 x 10^5 cells/well and left for 24 h under normal growth condition in DMEM 10 % FBS. TAT-peptides were added to the cells 6 h prior to treatment in DMEM-free FBS medium. Cells were then treated with 5 mM ATP for 5 min at ambient temperature. Culture medium was changed, and cells were allowed to rest for 12 h at 37 °C. Following this, the Caspase-Glo 3/7 Reagent was added to the cells at an equal ratio and incubated for 30 min at ambient temperature protected from light. Luminescence was recorded using Safas (SP2000, Xenius, Monaco) at 15 min time intervals for 2 h. Data was collected, and 1 h-post treatment was selected as luminescent signal of choice across all replicates, which was consistent with manufacturer's instruction.

2.4.5 Phospholipid scrambling assay

HEK293T and ANO6-KO cells were seeded on poly-l-lysin coated glass coverslips and transfected using plasmids DNA shown in Table 2.6. 24 h-post transfection cells were washed three times in PBS and examined for their scramblase activity using CF-594 tagged annexin V (Biotium) at 50 μg/mL diluted in annexin V-binding solution (NaCl 140 mM, HEPES 10Mm, and $CaCl_2$ 2.5 mM, adjusted to pH 7.3). Annexin V-binding solution was added to coverslips imaging chamber prior to time-lapse video fluorescence microscopy measurements using FW4000 and 40X objective. Imaging acquisition of PS labelled annexin V- CF 594 cells was carried out at 5-s intervals and recorded by MetaMorph software (Molecular Devices). PS assay was divided into two acquisition intervals. Cells were imaged for 2 min in annexin V- CF 594-binding solution followed by a gentle exchange of solution for a second acquisition period of 13 min in annexin V-CF 594-binding solution containing BzATP (10 μM), ionomycin (5 μM) and/or co-application of 9-AC (1 mM) with agonists. The inhibitor solution was prepared immediately prior to acquisition. Cells were maintained at 37 °C throughout the measurements. For Ca^{2+} influx experiments, cells were pre- or co-incubated with 10 μM BAPTA-AM and 10 μM EGTA-AM for 15 min at ambient temperature before measurements started.

2.4.6 YO-PRO-1 dye-uptake assay

HEK293T and ANO6-KO cells treatment and video fluorescence microscopy measurements were carried out as described in section 2.4.5. Cells were incubated in NES solution (NaCl 140 mM, KCl 2.8 mM, CaCl2 1 mM, MgCl2 0.1 mM, HEPES 10 mM, Glucose 10 mM and pH adjusted to 7.32) for an initial 2 min acquisition. The solution was then gently exchanged, and 10 μM YO-PRO-1 (Thermo Fischer) in NES solution added to the microscopy chamber for a second acquisition time of 15 min.

2.5 Biophysics

2.5.1 FLIM-FRET Two-photon microscopy

HEK293T ANO6-KO cells were seeded into 8 chambered coverglass system (Cellvis; C8-1.5H-N) at 15-30 x 10^4 cells/wells (300 µL medium per well). Cells were transfected or co-transfected with rP2X7-scarlet or rANO6 -GFP plasmids at a 1:0.05 ratio, respectively. In the presence of TAT-peptides, transfected cells were imaged 48 h post-transfection allowing sufficient time for the peptides to exert their activity. The experiment was performed in live-cell condition.

Time-correlated single-photon microscopy (FLIM) coupled to fluorescence resonance energy transfer (FRET) counting was carried out as described in Richert *et al*., 2015. FLIM-FRET Measurements were performed on a home-made two-photon excitation laser scanning microscope ("Plateforme d'imagerie quatitative", PIQ, University of Strasbourg) constructed on an Olympus IX70 inverted microscope using an Olympus 60 x 1.2 NA water immersion objective collecting fluorescent photons in the descanned mode. Two-photon excitation wavelength at 930 nm was achieved by a Spectra Physics Tsunami Ti: sapphire laser. Photons were collected through two filters featuring a short pass filter with a cut-off wavelength at 680 nm (F75-680; AHF) and a band-pass filter of 520 $\pm$ 17 nm (f37-520, AHF). The fluorescence was directed to a fiber-coupled detector APD (SPCM-AQR-14-FC) connected to a time-correlated single photon counting module (TCSPC; SPC830, Beker & Hickl). FLIM-FRET data was continuously scanned for 60 s per condition achieving accurate photon statistics for fluorescence lifetime estimates analysed by SPCImage FLIM software (Becker & Hickl). When co-transfected ANO6-GFP plasmid acted as a FRET donor, whereas, rP2X7-scarlet acted as an acceptor. The FRET efficiency (E) was expressed as a function of distance between the two fluorophores according to:

$$E = \frac{R_0^6}{R_0^6 + R^6} = 1 - \frac{\tau DA}{\tau D} \quad (1)$$

where, R is the distance between the donor and the acceptor, R_0 known as the Förster radius, τDA is the lifetime of the donor in the presence of the acceptor, and τD is the lifetime of the donor in the absence of the acceptor.

2.5.2 Electrophysiology

Patch pipettes were pulled using borosilicate glass capillaries (Harvard Apparatus) yielding a resistance between 3–5 MW. Transfected HEK293T cells were continuously bathed and perfused in NES as in YO-PRO-1 protocol (refer to section 2.4.6). Intracellular solution contained 140 mM KCl, 5 mM EGTA, mM MgCl2, 10 mM HEPES, 10 mM glucose, adjusted to pH 7.32 – 7.33 with NaOH. All solutions were maintained at 300 mOsm. For BzATP-evoked response solutions of 10 μM BzATP were prepared in NES. Cells were voltage clamped at -60 mV using the EPC10 amplifier (HEKA) using PATCHMASTER (HEKA) software.

2.6 Image and Analysis

2.6.1 CaPLSase and dye-uptake imaging quantification

Microscopy images were loaded into Image-J for screening of Annexin-V CaPLase-mediated PS positive cells. Background noise was subtracted to each individual cell by manually selecting region of interest (ROI) close to the scrambling cells. ROI Annexin-V fluorescent intensity values were then generated for each cell/noise at each time-point through 15 min sample acquisition. A customised R-studio script was then programmed to quantify CaPLase change overtime of each cell. I_{max} and $t_{1/2(Imax)}$ values were calculated using basic straight line equation on Excel:

$$y = mx + b \quad (1)$$

Where, m is the slope of the line and b is the y-intercept. $t_{1/2(Imax)}$ refers to the time reaching half of I_{max}. Graphs with R^2 >0.85 were discarded. Only cells that were Annexin-V positive and expressed GFP-tag were selected for imaging analysis. Importantly, any cell expressing Annexin-V tag prior to agonist stimulation was discarded.

For YO-PRO-1 dye-uptake experiments, imaging processing was carried out as for CaPLase assay. However, after R-studio data acquisition, the results were further assessed to determine the area under the curve at each time-point following agonist application. Furthermore, due to green-fluorescent stain of YO-PRO-1, no GFP-tag was used when assessing dye-uptake across different conditions and relied on agonist selectivity as well as on control conditions.

2.6.2 FLIM-FRET image reconstruction

Image processing and analysis were carried out using costumised algorithms on MATLAB and FLIMfit software designed by Dr. Richert UMR7213 CNRS University of Strasbourg. All acquired images were bulk processed recovering their individual lifetimes, intensity and fluorescence decays.

2.6.3 Statistics

All data were obtained using at least three independent experimental replicates and indicated in the figure legend as ‘N’ unless otherwise stated. All data was subjected to a thorough analysis using Shapiro-Wilko test in order to assess data distribution, Skewness and Kurtosis shapes. All statistical analysis was then performed on GraphPad (GraphPad Software, CA, USA) and tested for statistical test accordingly as detailed in the text. All data are presented as mean ± standard error of the mean (SEM).

Chapter 3

Results: Biophysics

3.1 Biophysical Characterisation of P2X7-TMEM16F Proteins Complex

3.1.1 FLIM-FRET: The principle

A much more robust and direct method to monitor FRET is Fluorescence Lifetime Imaging Microscopy (FLIM) (Richert et al., 2015). In FRET technology, the excitation energy stored in a donor fluorophore or molecule is non-radiatively transfer to a neighbouring non-exited fluorescent molecule termed, the acceptor (Forster, 1946). Due to its high affinity, the FRET method requires that the donor and acceptor dipoles' emission and excitation spectra overlap, that their distances do not exceed 10^{-9} m, and that they have the proper relative orientation (Figure 3.1). Unlike intensity-based FRET, FLIM-FRET measures the nanosecond-scale fluorescence decay function of the FRET donor fluorophore, known as fluorescence lifetime (τ), at each pixel of a FLIM image

(Richert et al., 2015). FLIM probes changes in fluorophores' microenvironment using a pulsed laser that periodically excites the fluorophores in the sample, which is then relaxed into their ground-state emitting photon through a non-radiative pathway. The τ can be then calculated as the average time a fluorophore remains in the excited state after excitation. Importantly, fluorescence decay functions deriving from the average fluorescence lifetime and amplitude of many decay parameters do not depend on variations in excitation intensity, probe concentrations, inner filtering, detector sensitivity and donor photobleaching (Richert et al., 2015). Thus, it unambiguously monitors the amount of FRET as a function of the decrease of the donor lifetime allowing for live cell imaging using low photostable probes and high tissue scattering (Bajar et al., 2016). Other advantages include no need for detector calibration, which, on the contrary, is required in intensity-based FRET due to spectral sensitivity cross-talk overlaps, and only the lifetime of the donor is measured in FLIM-FRET approach (Bajar et al., 2016). Moreover, regardless of single or double exponential decay different donor fractions involved in FRET can be identified in FLIM through a multiexponential analysis of the decay functions recorded at high temporal resolution, whilst avoiding also photoconversion or photobleaching (Richert et al., 2015). This high signal-to-noise ratio acquisition can be achieved by the Time-Correlated Single-Photon Counting (TCSPC) FLIM.

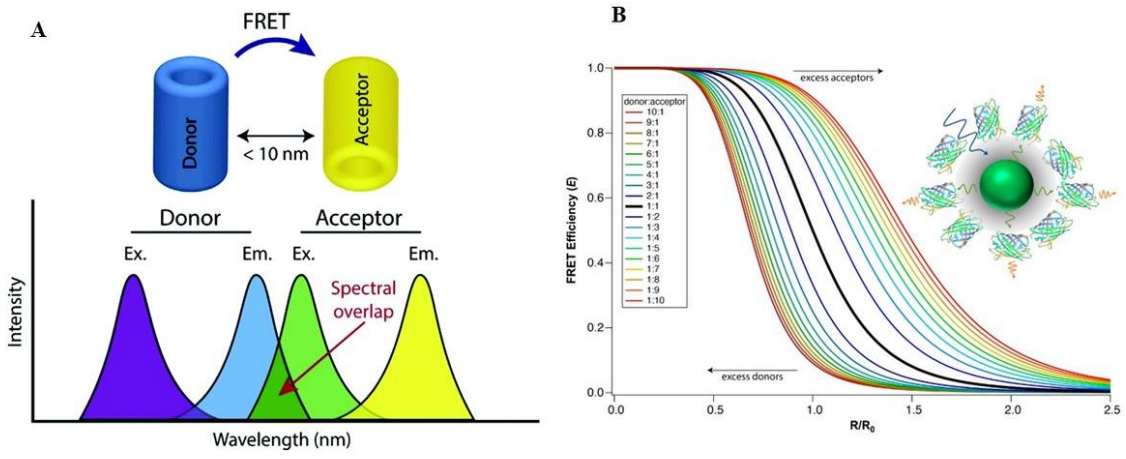

Figure 3.1: Förster resonance energy transfer (FRET) principles.
Panel (**A**) illustrates the required parameters for an accurate FRET showing donor (blue) and acceptor (yellow) fluorophore spectral overlapping regions, and distance (<10 nm). (**B**) evaluates the efficiency and accuracy of FRET at a specific distance as the number of

acceptors per donor molecules augments. (Images adapted from Chou & Dennis, 2015; Singh et al., 2020).

Experimentally, TCSPC FLIM result is a photon distribution (Becker & Hickl, 2021). A high-frequency pulsed laser beam (as shown in Figure 3.2) scanning a given sample detects single photons emitted by the fluorescence light. The TCSPC system determines the arrival time, t, of each photon within the pulsed laser period, and the spatial coordinates of the beam (i.e., x,y) upon photon detection has occurred. Thus, providing a precise photon distribution representing the sample lifetime image, consisting of an array of x × y pixels data indicating the spatial coordinates, each containing a fluorescence decay function, which builds up the times of the photons (see Figure 3.2) (Becker & Hickl, 2021). However, the fluorescence decay in the individual pixel is markedly "noisy" because of the photon statistics effect and the large number of pixels within which the photons are distributed (Becker & Hickl, 2021). Therefore, to establish clearer fluorescence decay curves in the individual pixels more photons need to be recorded.

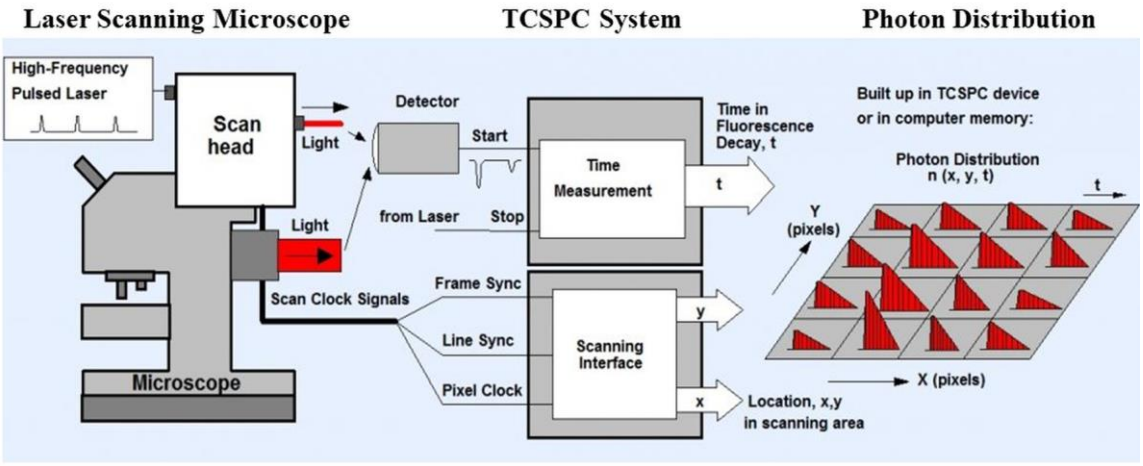

Figure 3.2: Description of recording processes in a TCSPC FILM system.
A (i) laser scanning microscope with a high-frequency pulsed laser detects single photons generated from the fluorescence signal returning from the sample. The (ii) TCSPC system characterises each photon based on its time spent in the laser pulsed period (i.e., time management) providing the coordinates (location, x, y) of the laser in the scanning interface upon detection. The recording steps culminates with a build-up of a (iii) photon distribution map n (x, y, t). (Image adapted from Becker & Hickl, 2021).

When the FLIM apparatus has detected many photons a build-up of the arrival time of such photons after excitation is generated correlating to the average time or fluorescence lifetime the molecule was in the excited state generating an exponential

function (see Figure 3.3) (Becker & Hickl, 2021). This is an essential property of FLIM as it implies that the standard deviation, $\sigma_{\tau,}$ of each individual photon arrival times is the same as the lifetime of the fluorescence itself (Becker & Hickl, 2021). In other words, the σ_{τ} is simply the square root of the photons in the decay curve. This allowed to convey several concepts, for example, the pixel intensity corresponds to the pixel lifetime signal-to-noise ratio, which in turn is depended only on the number of photons (N) (Becker & Hickl, 2021). Collectively, this suggests that by simply increasing N a robust lifetime accuracy can be achieved.

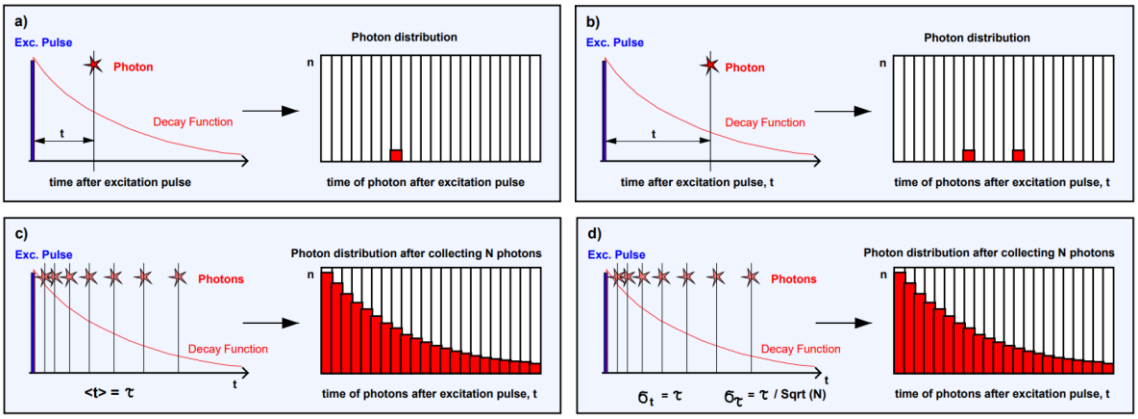

Figure 3.3: Evaluation of photon build-up and distribution.
Top panels (**a** and **b**) display the detection of the photon following the time after the excitation pulse, *t*. Panel (**c**) shows the photon distribution after collecting *N* photons averaging photons based on their arrival time after excitation, <*t*>, corresponding to the fluorescence lifetime, τ, thus, <*t*> = τ. Because this yields an exponential function the standard deviation (**d**) of individual photons equals to the lifetime itself depending on the square root (sqrt) of the number of photons; hence: $\sigma_{\tau} = \tau$ / Sqrt (N). The standard deviation therefore dictates the signal-to-noise ratio of the average arrival time i.e., pixel intensity. (Image adapted from Becker & Hickl, 2021).

In addition to this the first-moment (M1) of photon distribution represent another essential experimental parameter in the FLIM system. It allows for the determination of a full photon distribution of a single-exponential decay at an ideal signal-to-noise ratio, if the photon-specific arrival time cannot be calculated (Becker & Hickl, 2021) (see Figure 3.4). Importantly, FLIM is technically challenging and requires experience users with deep understanding of the physics of fluorescence lifetime dynamics, TCSPC FLIM data acquisition and instrumentation. When designing a FLIM-FRET experiment it is paramount that the FLIM system instrumentation is calibrated with fluorescence lifetime

standards and FLIM set-up specified (for further information regarding the physics of measurement technique, visit: Sun et al., 2011; Becker & Hickl, 2021). Importantly, the acquisition time is trivial to the lifetime accuracy and, thus, the number of photons, as such a Single Photon Counting Module (SPCM) detector is employed to determine whether enough photons have been recorded (see Figure 3.5). In this chapter, FLIM-FRET measurements were performed on a home-made two-photon excitation laser scanning microscope constructed on an Olympus IX70 inverted microscope, a Spectra Physics Tsunami Ti: sapphire laser, a short pass filter with a cut-off wavelength at 680 nm (F75-680; AHF) and a band-pass filter of 520 $\pm$ 17 nm (f37-520, AHF). The fluorescence was directed to a fiber-coupled detector APD (SPCM-AQR-14-FC) connected to a time-correlated single photon counting module (TCSPC; SPC830, Beker & Hickl) (for more details refer to section 2.5.2 above).

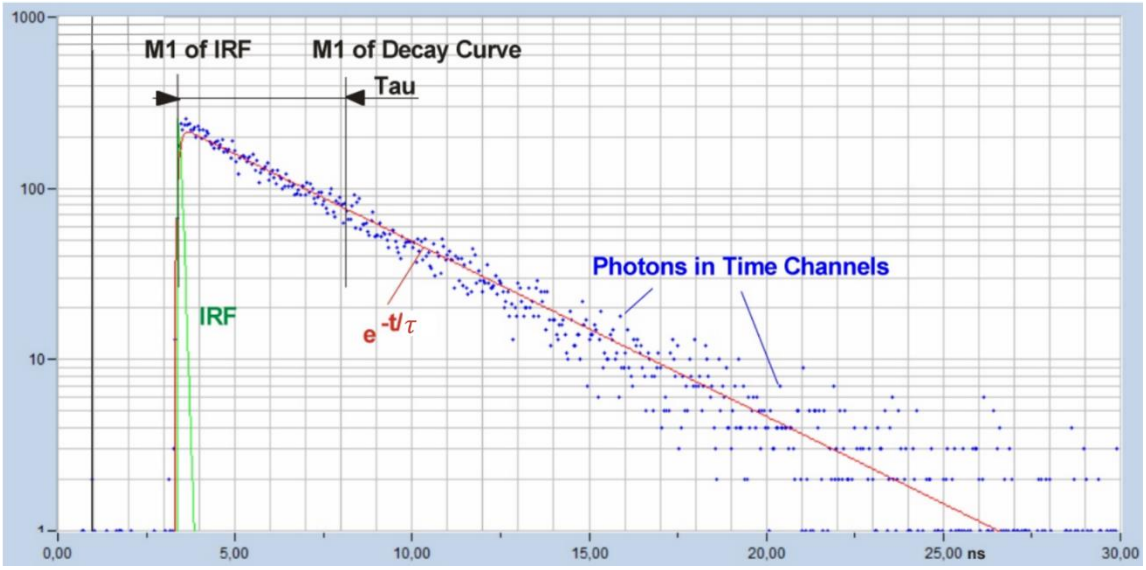

Figure 3.4: First-momentum (M1) of fluorescence lifetime.
M1 is generally set up prior to data acquisition. The blue spots represent the photon arrival in each individual channel; the instrument response function or IRF is illustrated by the green curve; the exponential function given by $e^{-t/\tau}$. The τ corresponds to the lifetime generated by convoluting the difference of fluorescence M1 with the M1 of the IRF. (Image adapted from Becker & Hickl, 2021).

3.1.2 FLIM-FRET: Aims & Objectives

As discussed in Chapter 1, protein-protein interactions regulate essential aspects of cell homeostasis. As the fluorescence lifetime of a molecule is susceptible to local changes in cellular or tissue microenvironment including ion concentrations, pH and temperature, FLIM provides accurate measurements of PPIs signalling events dynamics occurring in living cells (Sun et al., 2011). Indeed, FLIM applications aided in several facets of clinical research, such as oncology, study of dental diseases, steam cell studies, and Alzheimer's disease diagnostics (Sun et al., 2011). When combined with FRET, FLIM reveals subcellular spatial distribution maps of multiple probe lifetimes, accurately measuring the "shorter" donor lifetime resulting from FRET. Significant progress has been made in recent years on the understanding of the structures and properties of P2X7 receptors and TMEM16F channels, yet no well-suited real-time characterisation of these proteins in living cells has ever been reported. Identifying physical complexes in which P2X7 and/or TMEM16F functions are co-regulated within a living cell constitutes a fundamental functional unit of major biological processes. Today, only one study provided promising data on the intertwined cellular regulation activity between P2X7 receptors and TMEM16F channels (Ousingsawat et al., 2015). As a result, we monitored for the first time the formation of a physically interacting complex occurring between full-length P2X7_Scarlet I and TMEM16F-fused eGFP reporter using advanced imaging techniques, FLIM-FRET.

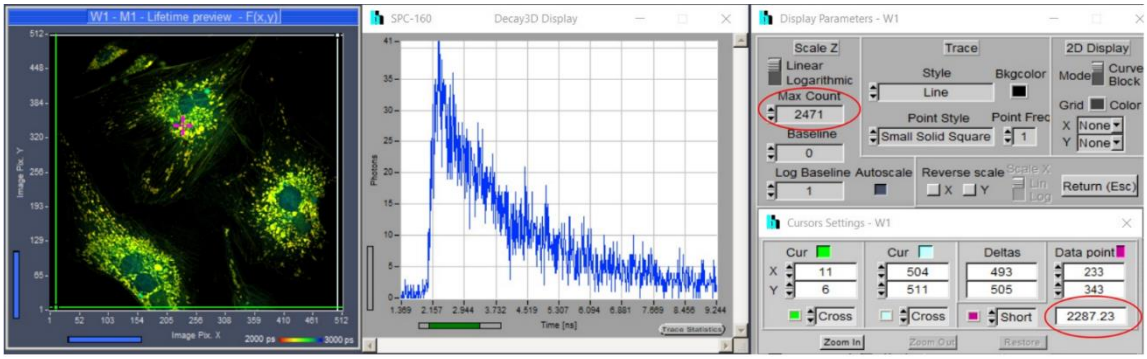

Figure 3.5: Single Photon Counting Module (SPCM) detector by bh's FLIM system for proper experimental set-up. SPCM functions illustrating (left to right) lifetime preview image, the decay 3D display curve yielded by a particular position selected from the online preview, and the amount of max photon number at a given position of data point (Image adapted from Becker & Hickl, 202).

3.1.3 P2X7 & TMEM16F form a 71.9 Å interaction complex

To study the interaction between TMEM16F and P2X7, fusion protein constructs were produced by expressing eGFP fragment into the C-terminus of vectors employing home-made primers targeting for XhoI and SacII restriction enzyme cleavage in TMEM16F contained pCMV vector (see Figure 3.6a). For rP2X7, instead, fusion construct was achieved by tagging mScarlet-I (from gene synthesis) in the C-terminus of rP2X7 within a pcDNA3.1(+) vector (see Figure 3.6b). Both fluorescence constructs were designed with an appropriate short linker sequence. This allowed for the generation of two fully functionally fluorescent-tagged proteins that can now be applied to the study of PPI as well as other biological processes, such as proteins conformational changes in living cells. Furthermore, the eGFP-Scarlet-I pair establishes the proper suitability for accurate monitoring of FRET measurements owing to their well-studied photophysics, good spectral overlap, and low channel crosstalk. To investigate the formation of a channel-forming P2X7-TMEM16F complex, FLIM-FRET technology was used as it is independent of fluorophore concentration and brightness. This is crucial when operating on overexpressed system (as in this experiment), thus no fluorophore bleed-through adjustment is required. Collectively, these features make FLIM the most accurate apparatus for FRET occurring events as of today.

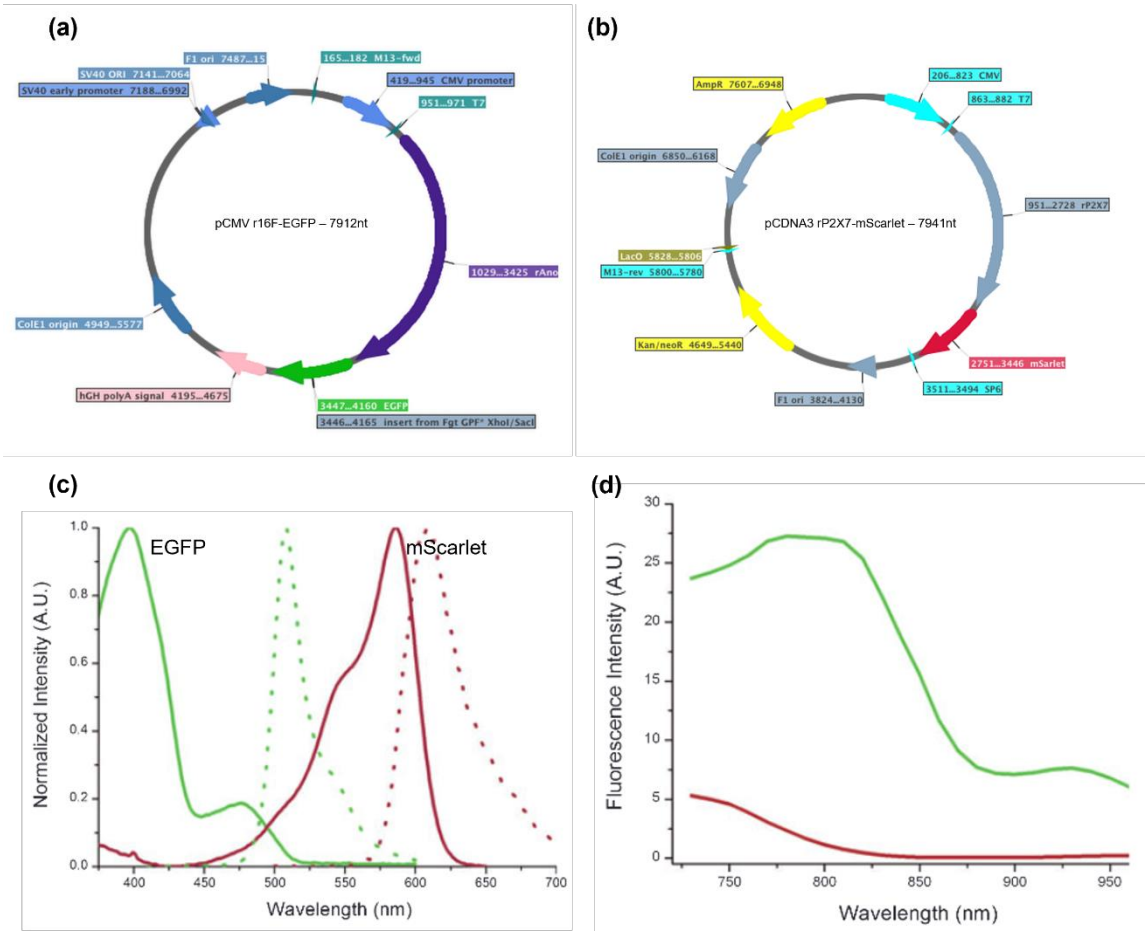

Figure 3.6: Illustration of fusion protein generation and spectroscopic properties. (**a**) Shows the characteristic features of the pCMV rTMEM16F (16F)-fused eGFP cDNA, representing the donor molecule, along with restriction enzymes XhoI and SacII that were used to insert the eGFP fragment. (**b**) Displays the rP2X7-tagged mScarlet-I from gene synthesis used as an acceptor molecule. Fluorescence probes were fused to the C-termini of their respective proteins. (**c**) Solid and dashed lines exhibit the normalised absorption and emission, respectively of eGFP (showed in green) and mCherry/mScarlet-I (showed in red). (**d**) The two-photon excitation spectra of eGFP and and mCherry/mScarlet-I. (image partially adapted from Albertazzi et al., 2009).

FLIM-FRET experiments were performed under living cell conditions. HEK293T-KO TMEM16F cells (termed HEK293TΔ) were co-transfected with plasmid encoding P2X7-mScarelt-I and TMEM16F-eGFP at a specific 1:0.05 ratio, respectively. This is because we previously found that this cDNA ratio was critical for optimal P2X7 expression (Dunning et al., 2021). Additionally, control conditions included single-transfection of eGFP and TMEM16F-fused eGFP plasmids, which allowed the determination of the lifetime of eGFP plasmid constructs in the absence of P2X7-mScarlet-I. Time correlated single photon counting FLIM was carried out by a home-made two photons inverted microscope with an eGFP excitation wavelength set at 930 nm and a two-photon laser pulsing femtosecond at an 80 MHz frequency. For each condition at least 8 independent images were acquired, unless otherwise stated, as detailed in the Figure 3.7 legend below. The lifetime of eGFP in all conditions was measured for approximately 90s in order to obtain a suitable photon count (see Figure 3.7b). The lifetimes for eGFP plasmid alone and TMEM16F-fused eGFP construct in HEK293TΔ did not significantly differ yielding 2325 $\pm$ 20 ps (SD) and 2285 $\pm$ 20 ps (SD), respectively – values that are consistent with the literature (see Figure 3.7c). On the contrary, a significant difference in the eGFP lifetime was observed following co-transfection of TMEM16F-fused eGFP (i.e., donor molecule) with P2X7-mScarelt-I (acceptor molecule) plasmids exhibiting a marked lifetime reduction of 1993 $\pm$ 20 ps (SD) (see Figure 3.7c). Thus, indicating for the very first time the possibility of a TMEM16F-P2X7 interaction complex in living cells. A FRET event, generally speaking, occurs if the lifetime of the donor is reduced by at least 5%. Based on our data, therefore, different FRET parameters were calculated that together resulted with a proposed Föster distance value of 71.9 Å:

FRET efficiency termed E_{FRET}:

$$E_{FRET} = 1 - \left(\frac{\tau_{FRET}}{\tau}\right) \quad \text{(i)}$$

Where, τ_{FRET} refers to the lifetime of the donor (i.e., TMEM16F-fused eGFP plasmid) in the presence of the acceptor (i.e., P2X7-tagged mScarlet-I plasmid) and τ refers to the lifetime of TMEM16F-eGFP in the absence of the P2X7-mScarlet-I.

Therefore:

$$E_{FRET} = 1 - \left(\frac{1.99\ ns}{2.29\ ns}\right) = 0.131 = 13.1\% \quad \text{(i.i)}$$

Thus, indicating that under the above conditions the efficiency of FRET events occurring between TMEM16F channels and P2X7 receptors is 13%, which is more than double the E_{FRET} general average. In addition to this, another important value is the distance *(r)*, provided by the following equation:

$$r = \mathrm{R_0}\ \mathrm{x}\ \left[\left(\frac{1}{\mathrm{E_{FRET}}}\right) - 1\right]^{1/6} \quad \text{(ii)}$$

Where, $\mathrm{R_0}$, represents the Föster distance. As previously discussed, the eGFP-mCherry/mScarlet-I fluorophore pair is well-studied in the literature, therefore, information concerning the Föster distance have already been provided. Particularly, for the EGFP-mCherry the $\mathrm{R_0}$ was calculated as 4.7 nm (Tramier et al., 2006) or more commonly used 5.25 nm (Akrap et al., 2010).

Hence, $r = 5.24\ \mathrm{nm}\ \mathrm{x}\ \left[\left(\frac{1}{0.131}\right) - 1\right]^{1/6}$, which resulted in 7.19 nm or 71.9 Å.

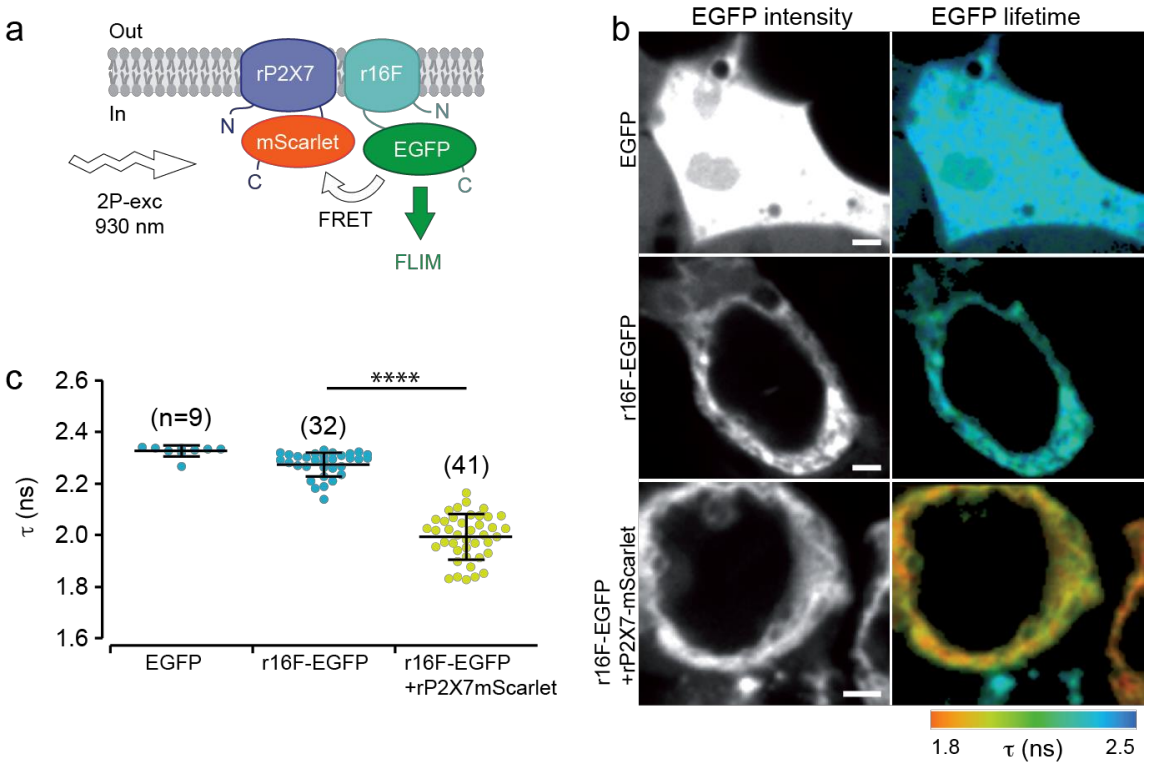

Figure 3.7: FLIM-FRET experimental results in living cells.
(**a**) Schematic illustration of FLIM-FRET method. Representative image of each condition illustrated in panel (**b**): HEK293TΔ cells were either transfected with eGFP (0.3 µg) and rANO6-eGFP (0.1 µg) plasmids or co-transfected with rP2X7-mScarlet-I and rANO6-eGFP at a 1:0.05 ratio. Cells were imaged under serum-starved conditions and changed approximately every 3-4 hours. The donor fluorescence decay was measured by FLIM with a home-build two-photon microscope and an excitation wavelength set at 930 nm. Each cell was continuously scanned for about 90s through SPCImage software (v4.9; Becker & Hickl) to obtain suitable photon statistics to achieve high signal-to-noise-ratio for accurate fluorescence lifetime recovery. (**b**) left panel shows the normalised fluorescence intensity for each condition, whereas the right panel displays the donor lifetime distribution in ns ranging from 2.5 ns to 1.8 ns. (**c**) quantification of donor lifetime. At least 8 images per condition were carried out for each FLIM measurement with four different transfection – except for eGFP plasmid alone for which only 1-2 images per transfection were acquired. A Mann-Whitney test was performed **** = P<0.0001; n.s. = non-significant.

However, it is worth noting that because the stoichiometry between the two proteins remains uncharacterised and the orientation of the fluorophore molecules is unknown, the Föster distance calculated above may only be viewed as a hypothetical estimation. To overcome this issue, Fluorescence Correlation Spectroscopy (FCS) method can be employed to determine fluctuations occurring through the diffusion of fluorescence probes via the two-photon excitation volume used in FLIM measurements. FCS provides data on diffusion time and mode of different fluorophore species as the diffusion time of the probe species is inversely proportional to the cubic root of their molecular weight (Meseth et al., 1999). Accordingly, this allows to characterise specific distribution of monomers and dimers population in any given microenvironment and hence the stoichiometry. Several attempts to FCS measurements were made, but without any success. One major concern emerged from the fact that TMEM16F-eGFP and P2X7-mScarlet-I resulted in a very efficient FRET meaning that the lifetime of the donor was reduced significantly. Using proteins known to FRET it is greatly discouraged in FCS technique, as the lifetime reduction observed in the latter may be producing misleading diffusion time results.

3.1.4 Biochemical approaches: Cross-linkers

Additional techniques to further characterise the physical interactions between P2X7 receptors and TMEM16F channels were used in this section, albeit data remained somehow inconclusive. Given the availability of many chemical reactive groups in proteins, cross-linker rapidly became an attractive tool to capture and stabilise PPIs owing to their reactivity with several functional groups, such as primary amines and sulfhydryls. Cross-linkers have also assisted for many years in the determination of molecular interactions on cell membrane, three-dimensional protein structures, near-neighbouring relationships. Importantly, using chemical cross-linkers of known arm lengths allows for the characterisation of distances between two interacting molecules. It is worth noting that cross-linkers are strictly depended on the experimental model or system under investigation. As a result, complex heterologous system severely impairs the specificity of commercially available crosslinkers. This section provides an overview of methods

utilised to biochemically determine rP2X7-rTMEM16F complex including a broad range of co-immunoprecipitation and cell-surface labelling assays containing cross-linkers of different nature and length.

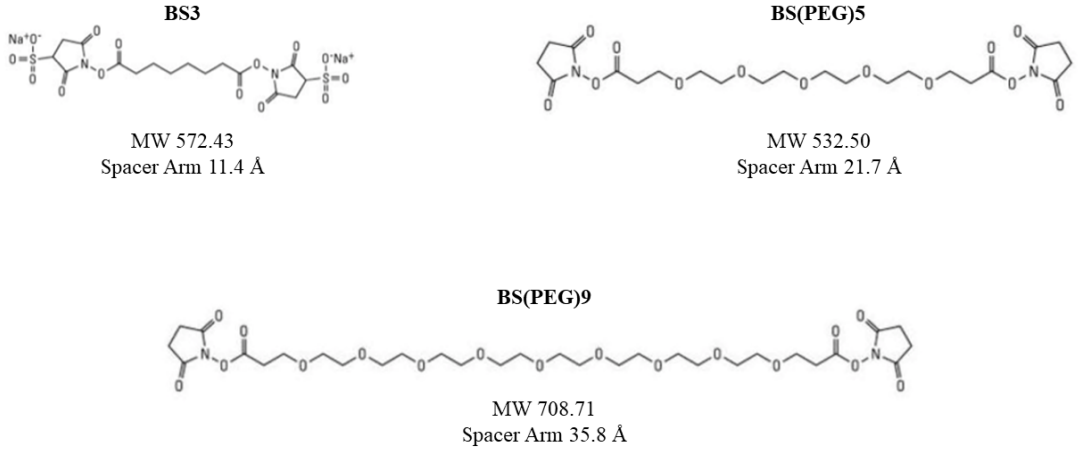

Figure 3.8: Homobifunctional cross-linkers structures
Illustration of chemical compositions of cross-linkers used in this unit. BS3 containing two sulfo-NHS-esters at the extremities separated by a 11.4 Å arm. PEGylated bis(sulfosuccinimidyl)suberates BS(PEG)5 and BS(PEG)9 consisting of two N-hydroxysuccinimide ester groups separated by 21.7 Å and 35.8 Å spacer armes, respectively.

All cross-linkers employed in this study are illustrated in Figure 3.8. Because of the trimeric nature of purinergic receptors and the dimeric form of TMEM16 family, different molecular sizes can be detected on western blot depending on cross-linkers applied. For instance, 70 kDa, 140 kDa, and 210 kDa represent the monomeric, dimeric, and trimeric structures of P2X7R, respectively, whereas 140 kDa and 210 kDa correspond to the monomeric and dimeric forms of TMEM16F channels, respectively (Figure 3.9a). This results in five potential different combinations according to their monomer, dimer, or trimer association. Co-immunoprecipitation between these two proteins has been already demonstrated by our lab (Dunning et al., 2021) as well as others (Ousingsawat et al., 2015). Therefore, the aim of cross-linkers in this section was chiefly to provide insights into the distance of this complex. HEK293TΔ were either transfected with 5 µg of rP2X7 and 0.25 µg of rTMEM16F plasmids, or co-transfected at 1:0.05 ratio, respectively.

Importantly, our lab assayed different ratios and found that higher concentrations of TMEM16F than those stated above, result in a downregulation of P2X7 signal on western blot (Dunning et al., 2021). Some attempts included the use of cell surface labelling assays by membrane impermeable sulfo-NHS-biotin, reactive to cell surface primary amines to label both proteins at the membrane. To prevent spontaneous receptors endocytosis, cells were washed several times in ice-cold PBS^{+} prior to incubation with sulfo-NHS-biotin, as detailed in the methods (see section 2.2.2). Following this, several conditions were tested including monitoring of rP2X7- rTMEM16F complex formation under the presence or not of reducing agents such as dithiothreitol (DTT) and iodoacetamide (see Figure 3.9b). The latter is particularly useful when working in the absence of DTT, as it prevents the formation of "technical" disulphide bonds formed during solubilisation. In addition, homobifunctional crosslinkers including bis(sulfosuccinimidyl)suberate, BS3 (space arm 11.4 Å), PEGylated bis(sulfosuccinimidyl)suberates, BS(PEG)9 and BS(PEG)5, characterised by a space arm of 35.8 Å and 21.7 Å, respectively (see Figure 3.8). These chemical linkers act similarly to the sulfo-NHS-biotin, thereby selectively reacting to primary amine such as lysine. Mini-Protean TGX precast 7.5% polyacrylamide gels were used to detect expected high molecular size proteins. Although a myriad of concentrations was assayed for each cross-linker, ranging from 0-μM to 2 mM, as illustrated in Figure 3.9b, no clear MW band was observed on any polyacrylamide gels used. Hence, at the extracellular level, the physical distance of the rP2X7-TMEM16F complex remains uncharacterised.

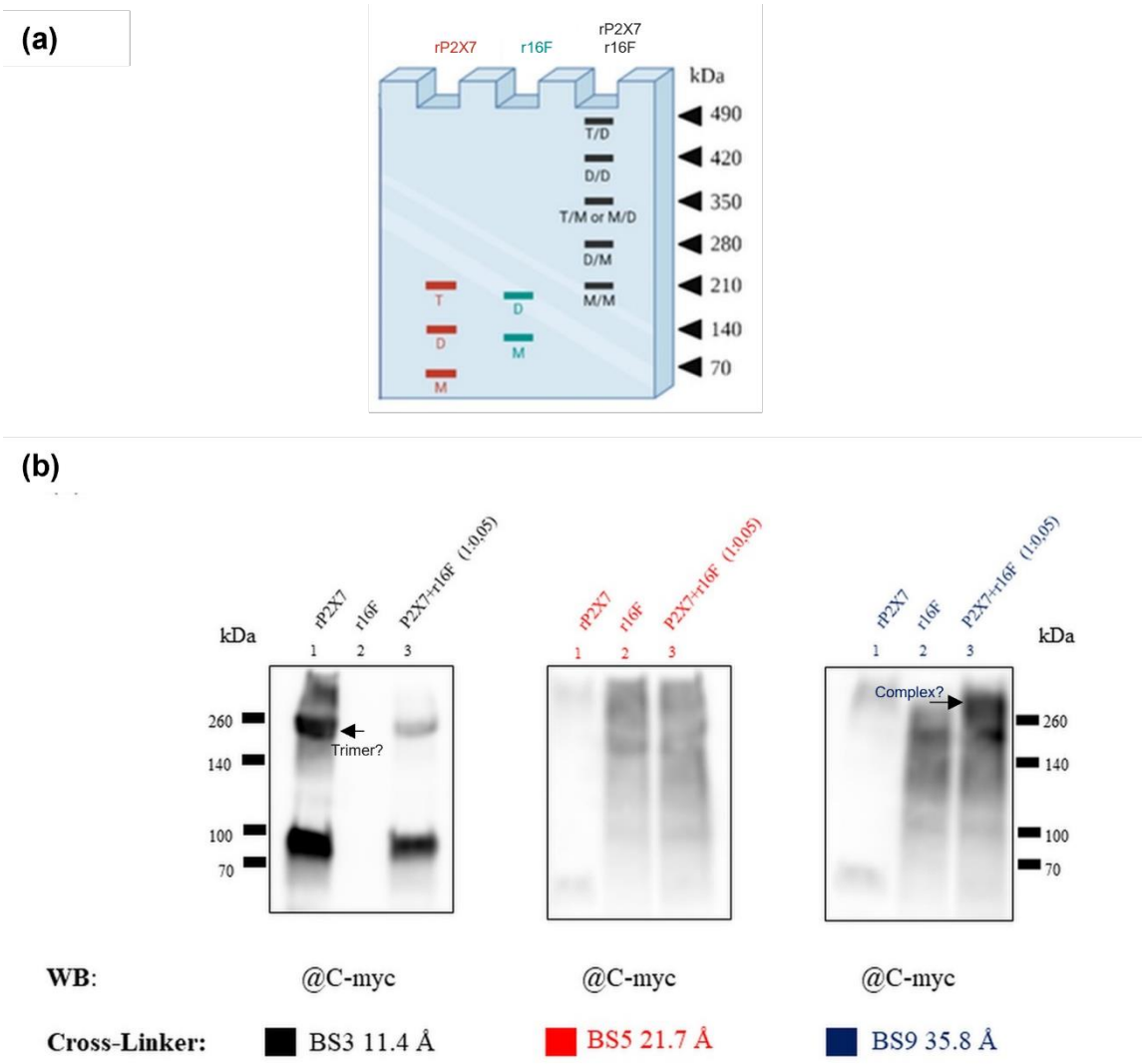

Figure 3.9: Evaluation of cross-linkers formation in HEK293TΔ-transfected cells. (**a**) Illustrates individual as well as five possible combinations that may take place if a cross-linking between rP2X7 and rTMEM16F occurs: M = monomer, D = dimer, T = trimer. (**b**) Shows the experimental results in the presence of different cross-linkers – black: BS3, red: BS5, and blue: BS9. Final concentration used for all conditions was 2 mM with triplicates were carried out for each cross-linker. All western blots were performed with anti-c-myc antibody recognising c-myc tagged rP2X7 and rTMEM16F transfected plasmids.

3.1.5 Overall Discussion

In this section, we employed an independent fluorescence-based method, namely FLIM-FRET to assess the overall P2X7 receptors and TMEM16F channels complex formation. A major breakthrough occurred following the discovery that this protein complex formed an estimated 71 Å in size in living cell conditions, characterised by a measured FRET efficiency of about 13.1%. A considerably high range value in FRET for two interacting proteins (Koschut et al., 2016). As the fluorescence lifetime is an intrinsic parameter of the fluorophore, independently of its concentration, FLIM-FRET provides a more robust approach to intensity-based methods for measurements of FRET when concentrations of interacting fluorophore molecules cannot be controlled. To co-localised both proteins at the plasma membrane, fusion tags were constructed using mScarlet-I and eGFP and inserted into the C-terminus of P2X7 and TMEM16F, respectively. FLIM probes changes occurring in the fluorophore microenvironment via a pulsed laser that periodically excites fluorophores in a given sample. The latter is then relaxed from its ground-state emitting photons, which in the case of FRET, it occurs through a non-radiative pathway. In this way, the fluorescence lifetime can now be calculated as the average time a fluorophore remains in the excited state after excitation. Accordingly, in our experimental conditions the presence of the acceptor (P2X7-mScarlet-I) in the very close proximity of the donor (TMEM16F-eGFP) increased the non-radiative de-excitation rates of the donor molecule, which led to a decrease of its fluorescence lifetime resulting in FRET. Together, this implies that a physical interaction between the labelled fluorescence proteins has indeed occurred. Limitations due to proteins orientations and fluorescence construct probes prevented, however, P2X7-mScarlet-I and TMEM16F-eGFP complex size determination. To assess stochiometric ratio between the labelled proteins, cellular FCS measurements were carried out to resolve this aforementioned ambiguity. FCS analyses the brightness distribution or fluctuation allowing to characterise specific populations of monomers and dimers in any given microenvironment. Unfortunately, FCS measurements failed to provide concrete results of P2X7-mScarlet-I and TMEM16F-eGFP stochiometric ratio due to technical issues associated with transfection efficiency, complex data acquisition, and analysis software. Nevertheless, we successfully demonstrated for the first time that

P2X7-mScarlet-I and TMEM16F-eGFP are engaged in a protein-forming complex, which molecular as well as immunological implications will be addressed in the next few chapters (see Chapter 4/5).

To further evaluate the distance between the two proteins, several cell surface labelling approaches including cross-linkers with varying arm lengths were assayed. By examining BS3, BS5 and BS9 reagents efficacy on selected HEK293TΔ-transfected conditions, we failed to reach conclusive data. It is worth noting, however, that the calculated 11.4 Å arm length of BS3 corresponds approximately to two nearest lysine residues on P2X7R alone, which has a molecular weight of 70 kDa (McCarthy et al., 2019). In fact, this resulted in either 140 kDa or 210 kDa bands on western blots representing dimer and trimer formation, respectively, specific to P2X7R. This suggests that BS3 arm length is insufficiently long to assess the distance between P2X7 and TMEM16F at the extracellular level and as such, it was ruled-out from the study. Moreover, application of BS5 with an arm length of 21.7 Å led to smear bands on western blots across all conditions. Interestingly, however, BS9 cross-linkers characterised by an arm length of 35.8 Å generated an intense molecular band at 280 kDa, which was absent from the TMEM16F-single transfected condition. Nevertheless, a low intensity molecular band was detected at the same size in P2X7-single transfected sample. Collectively, this might be representative of either an TMEM16F monomer (140 kDa) associated with a P2X7 dimer (140 kDa) complex setting-up a 1:2 ratio, respectively; alternatively, it might be just a technical issue due to protein accumulation and aggregation at the top of the gel. Furthermore, the complex heterogeneity of the HEK293TΔ system containing a high-protein density microenvironment leading to experimental bias against protein-protein interactions involving membrane-associated proteins – such as, in the case of P2X7 receptors and TMEM16F channels.

Chapter 4

Results: *In-vitro* Pharmacology

4.1 Molecular characterisation of P2X7-TMEM16F proteins complex

Characterising molecular interactions between proteins requires selective experimental methods for depicting large-scale interaction networks, molecular mechanisms, and cellular pathways in virtually all systems biology. In this Chapter, we established a rigorous model to evaluate P2X7 receptors induced TMEM16F channels activation elucidating for the first time the signalling machinery responsible for the hallmark processes of cell death. Using selective pharmacological agonists, we shifted current understandings of TMEM16F and P2X7 signalling to a more specific form. Thus, eliminating experimental bias occurring upon application of unselective ionophore drugs (for instance, ionomycin). This Chapter begins with the identification of a proper experimental system, in which molecular modelling strategies aided in the final determination of important amino acids residues, paramount to P2X7-TMEM16F complex functionality.

4.1.1 P2X7-mediated phosphatidylserine externalisation

Phospholipids residing in the plasma membrane are asymmetrical with PS exclusively enriched in the inner leaflet. PS-mediated scramblases exposure represents an essential physiological signal underlying several cellular processes, such as blood coagulation, phagocytosis, cell-cell fusion, bone mineralisation and regulation of a variety of cell-to-cell interactions (Bevers & Williamson, 2016). TMEM16F is a major lipid transporter within the TMEM16 family catalysing PS exposure in response to elevated intracellular Ca^{2+}. This often results in rapid collapse of phospholipids asymmetry in an energy-independent mechanism as compared to flippases and floppases, as previously discussed in Chapter 1, section 1.3.2. In platelets, TMEM16F Ca^{2+}-activated lipid scrambling activity has been shown to prompt the recruitment and activation of blood clotting factors led by PS externalisation. Furthermore, deficiency in PS exposure, due to loss-of-function mutations in TMEM16F in platelets, has been associated with a rare bleeding disorder known as Scott syndrome. A latest structure-guided mutagenesis study suggests that phospholipid translocation is governed by an inner activation gate, located in the middle of the channel lipid permeation pathway, form by residues F518, Y563 and I612 (T. Le, Jia, et al., 2019). Strikingly, TMEM16F-F518K analogous TMEM16A-L543K mutant conferred the latter the capacity of permeating phospholipid (T. Le, Jia, et al., 2019). It is worth noting, however, that most studies use unspecific Ca^{2+} ionophore representing a major experimental bias, especially in HEK293T cell-line model.

Considering TMEM16F activation in response to increase concentrations of cytosolic Ca^{2+}, P2X7 receptors represent, therefore, a perfect candidate for co-regulation of transport mechanisms inducing phospholipid scrambling, membrane blebbing and apoptosis. A comprehensive understanding of the molecular machinery governing P2X7R-induced TMEM16F activation would certainly aid drug discovery for these therapeutic targets. First, we established a selective experimental model for the quantification of scramblase activity using Annexin-V-induced imaging assay (Figure 4.1). Defining a system, in which to study, exclusively, the functional interaction between P2X7 and TMEM16F – that is pharmacologically driven by BzATP and not ionomycin.

A microscopy-based assay using fluorescently conjugated Annexin-V, a PS apoptotic marker, to monitor scramblase-driven PS plasma membrane externalisation allows for an effective quantification of lipid scrambling at a single-cell resolution. Studies investigating TMEM16F scramblase interference in HEK293T cells have already been optimised in recent years (T. Le, Jia, et al., 2019; T. Le, Le, et al., 2019) highlighting important implications of TMEM16F as scramblase effector. Here, we characterised the scrambling activities of rTMEM16F in association with rP2X7 in both HEK293TΔ and HEK293T-wild type (WT), such to detect Annexin-V labelled PS translocation through activation of P2X7 receptors using BzATP. In this regard, experimental bias, as in the case of ionomycin-induced PS scrambling, was predominantly reduced. For all Annexin-V-based imaging microscopy assay, we used BzATP at 10 μM, unless otherwise stated. Heterologous expression of rTMEM16F into the HEK293TΔ cells and rP2X7 into HEK293TΔ or HEK293T-WT cells was achieved by calcium-phosphate transfection allowing about 24-h prior to carry out measurements. Time-lapse imaging was limited to 15 min with 5-s intervals in between images acquisition in the presence or absence of BzATP, ionomycin, or co-stimulation with 9AC as shown by Figure 4.1 and Figure 4.2. All Annexin-V labelled cells detected pending agonists stimulation during the first 2 min of the assay were neglected. Interestingly, stable expression of rP2X7 and treatment with non-specific CaCC inhibitor 9AC resulted in a full inhibition of Annexin-V fluorescence signal, as compared to that of rP2X7-induced BzATP scramblase (Figure 4.1a, c). To circumvent potential fluorophore quenching activities deriving from 9AC application and Annexin-V detection, co-stimulation with 10μM BzATP were assayed in rP2X7 transfected cells, which resulted in a 40% reduction in the scrambling activity (Figure 4.1a, b). Thus, ruling out any quenching issues associated with the inhibitor, as well as rP2X7-dependent PS externalisation. Furthermore, an additional 35% reduction in Annexin-V signal was also observed in TMEM16F-KO cells following rP2X7-induced BzATP scramblase (Figure 4.1a, c), similarly to that measured in untransfected HEK293TΔ cells upon ionomycin treatment (Figure 4.2a, b). A partial 80% rescue was also detected following rP2X7 and rTMEM16F co-transfection in HEK293TΔ cells.

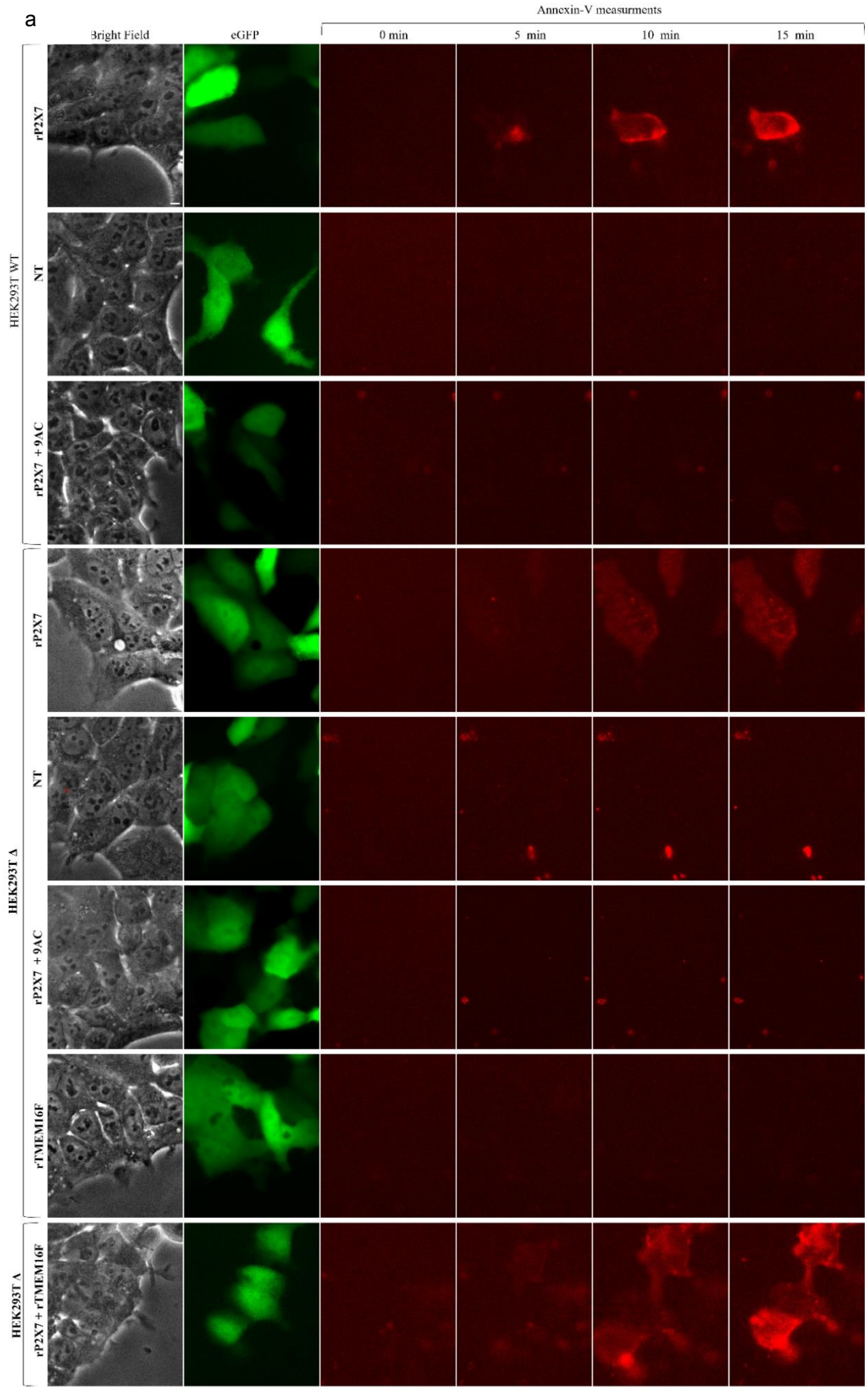
a
Annexin-V measurments
Bright Field
eGFP
0 min
5 min
10 min
15 min
HEK293T WT
rP2X7
NT
rP2X7 + 9AC
HEK293T Δ
rP2X7
NT
rP2X7 + 9AC
rTMEM16F
HEK293T Δ
rP2X7 + rTMEM16F

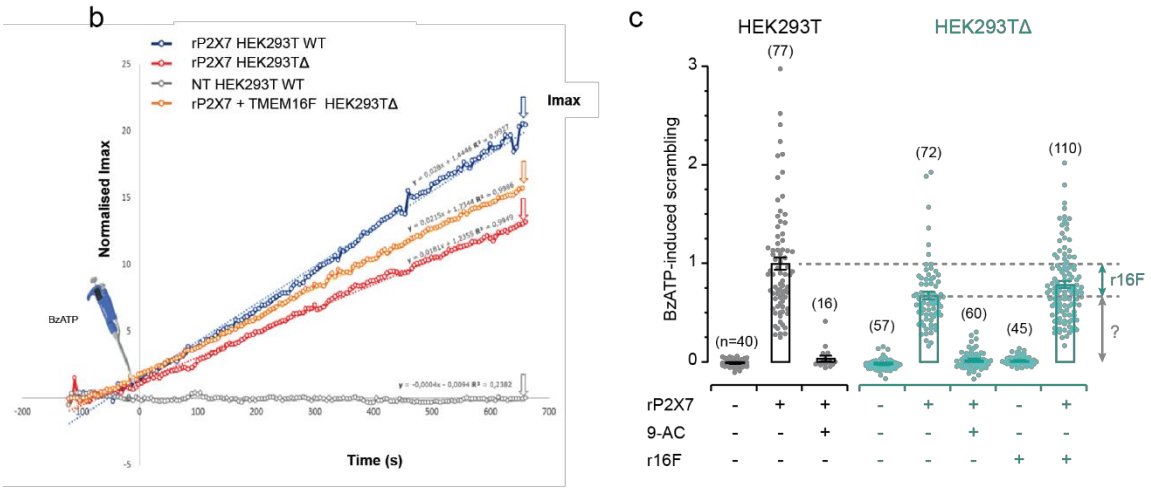

Figure 4.1: Optimisation of scramblase imaging-based assay activity for BzATP-induced Annexin-V PS-binding. (**a**) Representative images for each illustrated condition of BzATP-evoked scrambling activity in both HEK293T WT (top panels) and HEK293TΔ (bottom panels) cells co-expressing eGFP reporter rP2X7, NT (eGFP-only), rP2X7 + 9AC co-application, rTMEM16F and rescue condition rP2X7-rTMEM16F. CF594-tagged Annexin-V indicating PS exposure and binding recorded by video-microscopy 15 min time-laps imaging with 5 s intervals. Scale bar 5 µm. (**b**) Quantification of maximum intensity (Imax) Annexin-V fluorescence intensity values, as function of time 181 s total for control conditions including rP2X7-HEK293T WT (blue), rP2X7-HEK293T Δ (red), NT-HEK293T WT (grey) and rP2X7-rTMEM16F-HEK293T Δ (orange) conditions. Linear equation coordinates showed per condition and the arrows indicate the average Imax values. The pipette depicted at time "0" represents the time in which 200 µL of 10 µM BzATP was applied. (**c**) Quantified Bz-ATP-induced scramblase activity for both HEK293T WT and HEK293TΔ conditions expressed as normalised Imax values. Statistical analysis was carried out using Mann Whitney test (mean ± SEM): rP2X7-HEK293T WT/ rP2X7 HEK293TΔ (1.000 ± 0.064 N=77; 0.674 ± 0.040 N=72, respectively) ***p< 0.0001; rP2X7-HEK293T WT/rP2X7-rTMEM16F- HEK293TΔ (1.000 ± 0.064 N=77; 0.785 ± 0.0346 N=110, respectively) * p=0.014; rP2X7-rTMEM16F- HEK293TΔ/ rP2X7 HEK293TΔ (0.785 ± 0.0346 N=110; 0.674 ± 0.040 N=72, respectively) * p=0.021. At least three different transfections were carried out per each sample. All remaining conditions including rP2X7 + 9AC or NT in both HEK293T WT or HEK293T Δ transfected cells and rTMEM16F transfected HEK293T Δ cells exhibited p <0.0001.

Because of the high selectivity of the BzATP in activating rP2X7 receptors, we use mathematically derived maximum intensity (Imax) values, as demonstrated in Figure 4.1b, for assessment of the scramblase activities across all conditions. We achieved so, by calculating the highest fluorescence intensity value after 15 min BzATP stimulation, through an in-house programme in R-studios. On the contrary, due to elevated variations, resulting from ionophore-mobilised intracellular Ca^{2+} concentrations, most studies in the literature utilise $t_{1/2}$ Imax corresponding to the time at which a cell reaches 50% of its Imax. Collectively, in this assay, we confirmed previous published data showing reduced apoptosis-dependent PS scrambling following TMEM16F KO in HEK293T further implicating TMEM16F as an important effector in cell death. Secondly, our data provides a proper, unbiased model in which to study TMEM16F activities led by downstream effector signals initiated by rP2X7-induced BzATP stimulation. Thirdly, we added further evidence suggesting that P2X7 receptors do not independently engage in PS externalisation in HEK293T system as demonstrated by 9AC data but require full functional TMEM16F channels.

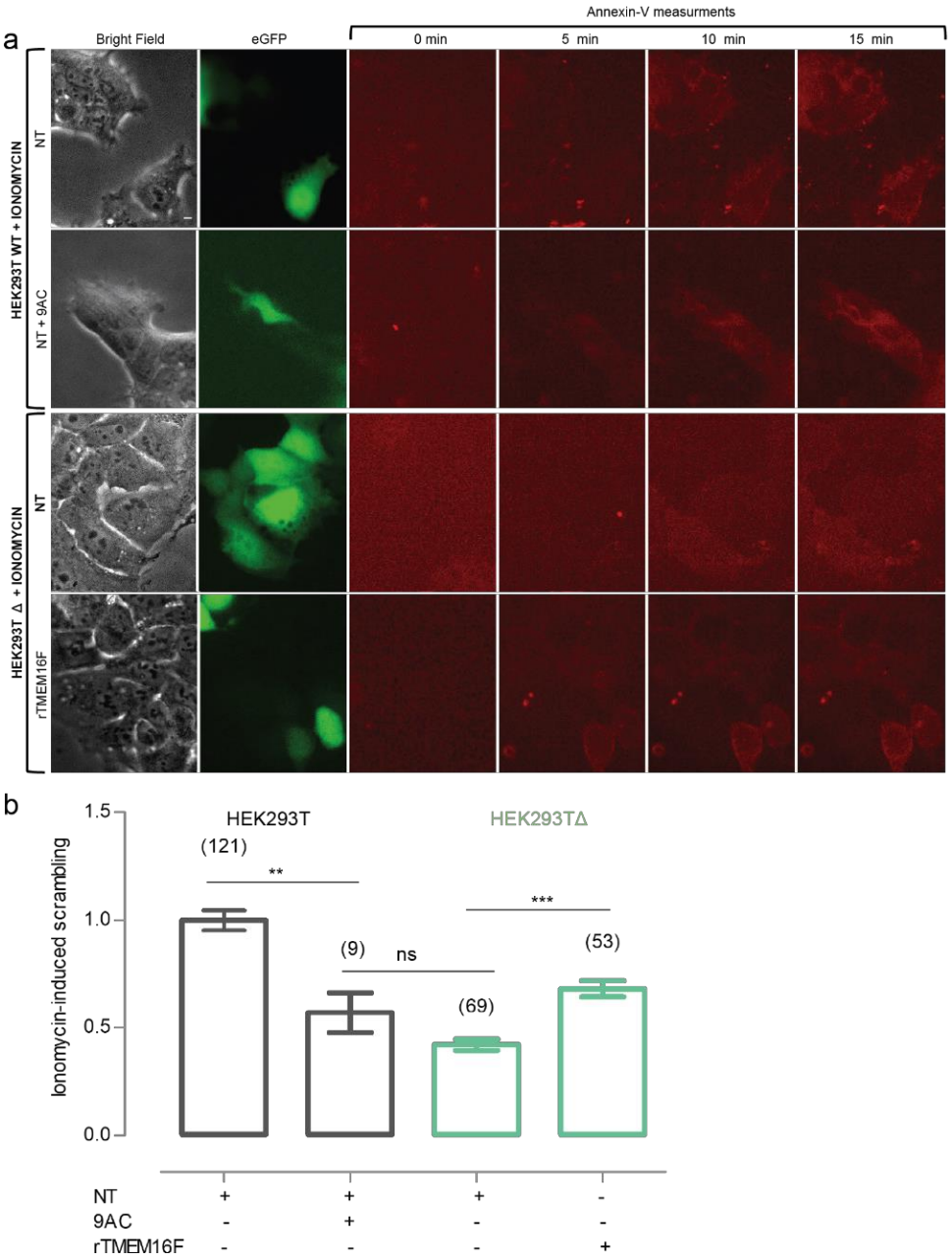

Figure 4.2: Ionomycin-induced scramblase activity assay as a control for Annexin-V-based imaging assay. (**a**) Representative Annexin-V fluorescent intensity images of ionomycin-evoked lipid scrambling in HEK293T WT (top panel) cells expressing either eGFP reporter (NT) or co-incubated with 9AC, and in HEK293T Δ (bottom panel) cells expressing NT or rTMEM16F conditions. Annexin-V binding monitored by video-microscopy over 15 min time-laps imaging period with 5 s intervals Scale bar 5 µm. (**b**) quantified Imax values for each condition expressed as mean ± SEM. Statistical analysis was carried out using Mann Whitney test (mean ± SEM): NT-HEK293T WT/NT-HEK293TΔ (1.000 ± 0.0467 N=121; 0.421 ± 0.026 N=69, respectively) ***p< 0.0001; NT-HEK293T WT/ NT-9AC-HEK293T WT (1.000 ± 0.0467 N=121; 0.571 ± 0.0934 N=9, respectively) ** p=0.0074; NT-HEK293T/ rTMEM16F-HEK293TΔ (1.000 ± 0.0467 N=121; 0.683 ± 0.366 N= 53, respectively) ***p<0.0001. /NT-HEK293TΔ/

rTMEM16F-HEK293TΔ (0.421 ± 0.026 N=69; 0.683 ± 0.366 N= 53, respectively) *** $p<0.0001$. Non-significant data is denoted by "ns". At least three independent transfections were carried out per each condition.

Because the interaction between P2X7 receptors and TMEM16F channels can be attributed to only 40% of the overall scrambling activity, quantitative RT-PCR was then carried out to identify additional components contributing to the complex. Particularly, it was hypothesised that given numerous reported members of the TMEM16 family endogenously expressed in HEK239T, perhaps some other may be indeed participating in P2X7 and TMEM16F complex interactions. The relative gene expression of TMEM16A, TMEM16B, TMEM16C, TMEM16D, TMEM16E, TMEM16F, TMEM16H and TMEM16K in HEK293T was quantitatively assayed by qPCR conducted in duplicates and a cut-off set at <40 cycles. Thus, cycles closer to 40 cycles represent a lower gene expression. Data normalisation was performed against glyceraldehyde-3-phosphate dehydrogenase GAPDH housekeeping gene with determined cycles of 21.86. The calculated relative expressions (Figure 4.3) for the aforementioned members were $4.6 \times 10^{-5} \pm 0.16$ for TMEM16A with 36.27 cycles, $8.2 \times 10^{-6} \pm 0.32$ for TMEM16B with 38.76 cycles, $7.8 \times 10^{-6} \pm 1.06$ for TMEM16C with 38.92 cycles, $1.8 \times 10^{-3} \pm 0.22$ for TMEM16D with 30.96 cycles, $6.8 \times 10^{-3} \pm 0.26$ for TMEM16E with 29.07 cycles, $8.9 \times 10^{-3} \pm 0.01$ for TMEM16F with 28.67 cycles, , $7.2 \times 10^{-4} \pm 0.24$ TMEM16H with 32.3 cycles, and $1.5 \times 10^{-2} \pm 0.05$ for TMEM16K with 27.91 cycles (Figure 4.3). Based on the data grater mRNA contents were found in TMEM16E, TMEM16F and TMEM16K as compared to TMEM16D and TMEM16H, which exhibited very low mRNA level, as well as TMEM16A, TMEM16B and TMEM16C, which showed neglectable values. Although the literature is very minimal, TMEM16E represents a very promising candidate as it the only member that displays both calcium-activated chloride channel activity and calcium-dependent phospholipid scrambling in HEK293T (Di Zanni et al., 2018; Whitlock et al., 2018). It is worth noting, however, that the remaining scrambling activity discussed above may also be due to a calcium-independent mechanism – as such, we next investigated the role of intracellular calcium in the P2X7 and TMEM16F complex formation (see section 4.1.2).

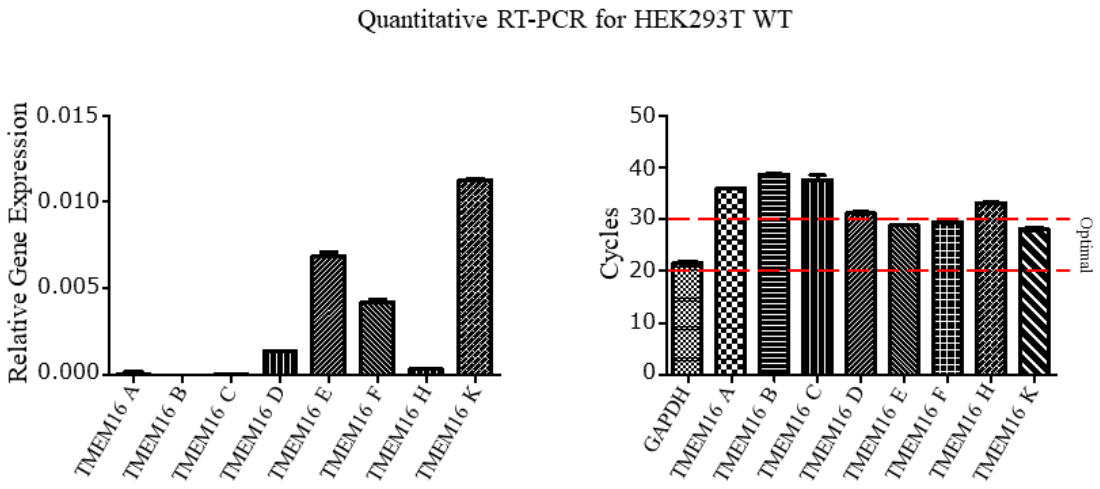

Figure 4.3:mRNAs quantification of human TMEM16 family by quantitative RT-PCR in HEK293T WT. The (left) chart indicates the relative gene expression calculated for each TMEM16 member using GAPDH as reference gene. The (right) chart illustrate the cycles for each individual member carried out by setting a threshold (T) at T300. The cycles closer to 40 and/or above represent low mRNA contents, whereas cycles varying from 20 to 30 indicates optimal amount of mRNA level. The red dotted line shows the optimal range for mRNA expression. All conditions were carried out in duplicates with at least a N=2 per sample.

4.1.2 The effects of intracellular Ca^{2+} in P2X7 & TMEM16F complex formation

Intracellular calcium represents an important effector signal for TMEM16 channels activation. As previously discussed, stimulation of P2X7 receptors by BzATP induces elevated influx of Ca^{2+} required for full functional activation of TMEM16F triggering as a result, a massive TMEM16F-dependent membrane blebbing (see section 4.1.2). Together, this demonstrates an essential cooperative mechanism between P2X7 and TMEM16F that is central to numerous deleterious cellular effects. Therefore, in this section we shall further elucidate the specific function of intracellular Ca^{2+} in the complex formation and functionality using membrane-permeable calcium chelators BAPTA-AM and EGTA-AM but also mutations known to impair TMEM16F Ca^{2+}-binding and PS externalisation. Cells grown onto microscope coverslips were incubated or co-incubated for 15-20 min at ambient temperature with 10 μM of either BAPTA-AM or EGTA-AM (as detailed in the methods; section 2.4.5) prior to Annexin-V imaging assay

measurements with 10 μM BzATP. To avoid significant technical variations in the scrambling activity due to long waiting times among chelators incubation, each experimental condition was performed with their respective control and the overall measurement limited to a maximum of 2 hours. Importantly, Annexin-V conjugated fluorophore requires Ca^{2+} for binding to externalised PS, thus effects of total calcium chelation remain currently uncharacterised. Interestingly, although it has long been reported that BAPTA-AM buffers display a higher selectivity toward Ca^{2+} than EGTA-AM buffers (Tsien, 1980), treatments with either the membrane-permeable calcium chelators resulted in a similar Annexin-V signal reduction in both HEK293T-WT and HEK293TΔ (Figure 4.4, 4.5, and 4.6). Specifically, 10μM BzATP-stimulated HEK293T-WT transfected rP2X7 cells incubated with either BAPTA-AM or EGTA-AM showed a ~35% and ~40% reduction, respectively (Figure 4.4a), whereas co-application of both intracellular Ca^{2+} chelators led to a more marked inhibition of the overall scrambling activity to about ~60% (Figure 4.4b). On the other hand, HEK293TΔ transfected rP2X7 cells recorded a low ~20% inhibition rate in the scrambling activity upon either application or co-application of both membrane-permeable calcium chelators (Figure 4.5a, b). Intriguingly, treatment with BAPTA-AM and EGTAM-AM induced a similar scramblase reduction to that previously observed in HEK293TΔ rP2X7-transfected conditions.

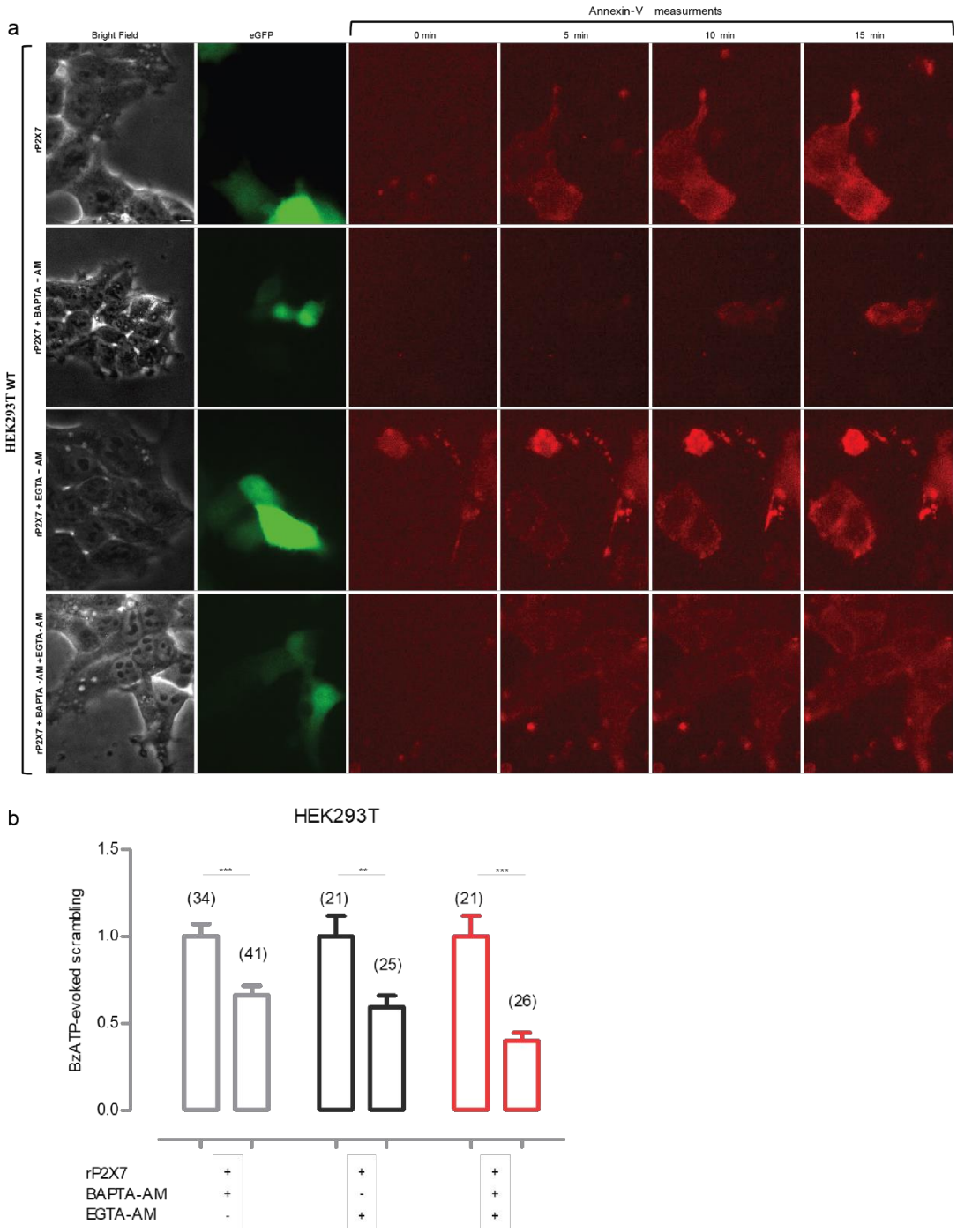

Figure 4.4: Effects of intracellular Ca2+ chelator buffers on BzATP-evoked PS scrambling in HEK293T WT. (**a**) Representative Annexin-V fluorescence intensity images of HEK293T-WT cells expressing rP2X7 in the presence or absence of BAPTA-AM, EGTA-AM, and co-application of BAPTA-AM/EGTA-AM. (**b**) grouped Imax quantification against control condition to limit variations in chelator buffers variabilities expressed as mean ± SEM: rP2X7/rP2X7 + BAPTA-AM (1.000 ± 0.0723 N=34; 0.659 ± 0.0533 N=41, respectively) *** p=0.0002; rP2X7/rP2X7 + EGTA-AM (1.000 ± 0.118 N=21; 0.594 ± 0.0668 N=25, respectively) ** p=0.0033; rP2X7/rP2X7 + BAPTA-AM/EGTA-AM (1.000 ± 0.118 N=21; 0.402 ± 0.046 N=26, respectively) *** p<0.0001.

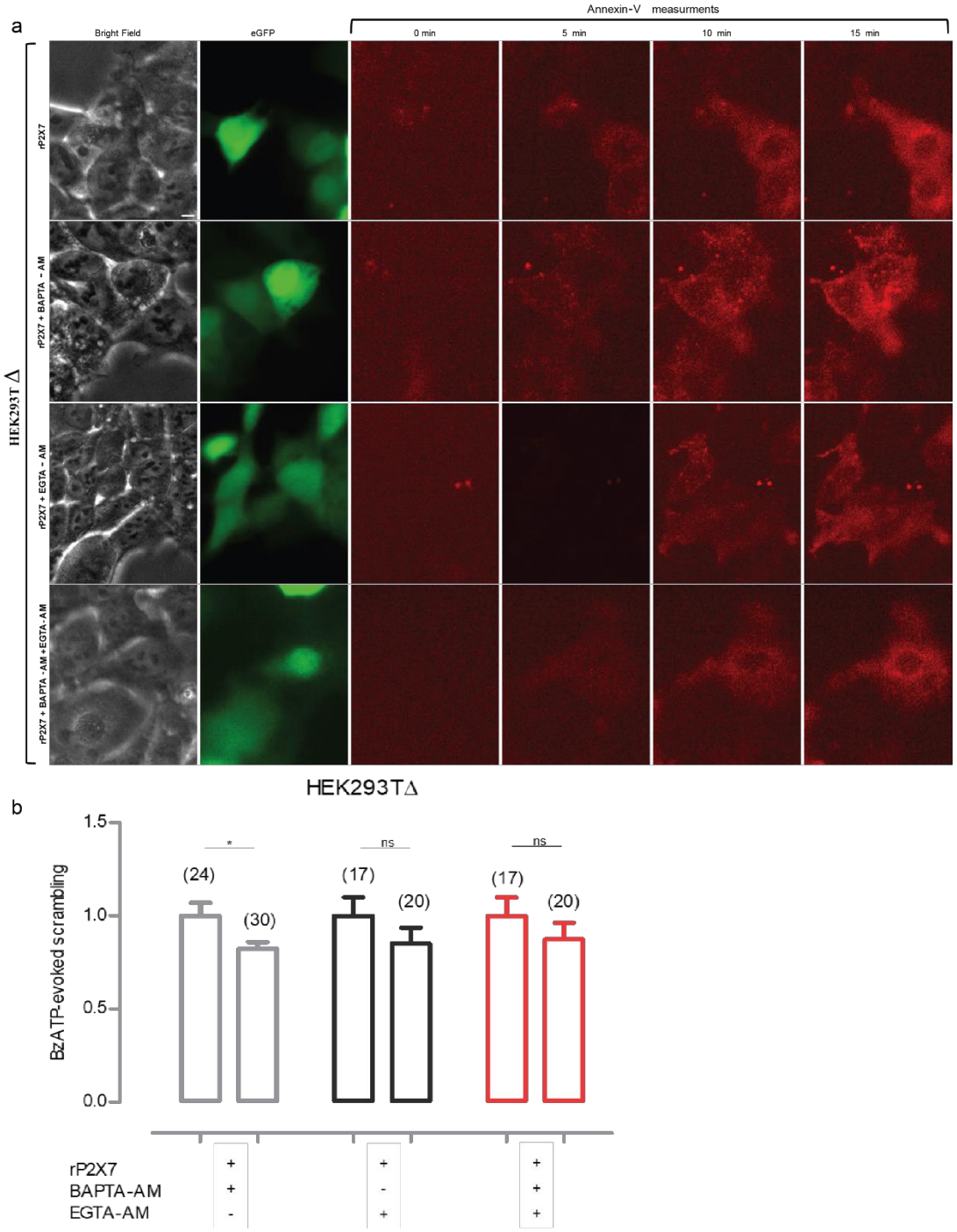

Figure 4.5: Effects of intracellular Ca2+ chelator buffers on BzATP-evoked PS scrambling in HEK293TΔ. (**a**) Representative Annexin-V fluorescence intensity images of HEK293TΔ cells expressing rP2X7 in the presence or absence of intracellular Ca^{2+} chelator buffers as detailed in the text. (**b**) Annexin-V grouped fluorescence intensity changes in HEK293TΔ for each condition against the control expressed as mean ± SEM: rP2X7/rP2X7 + BAPTA-AM (1.000 ± 0.070 N=24; 0.823 ± 0.037 N=30, respectively) *p=0.0217. rP2X7/rP2X7 + EGTA-AM (1.000 ± 0.01 N=17; 0.851 ± 0.084 N=20, respectively) non-significant "ns"; rP2X7/rP2X7 + BAPTA-AM/EGTA-AM (1.000 ± 0.01 N=17; 0.873 ± 0.087 N=20, respectively) ns.

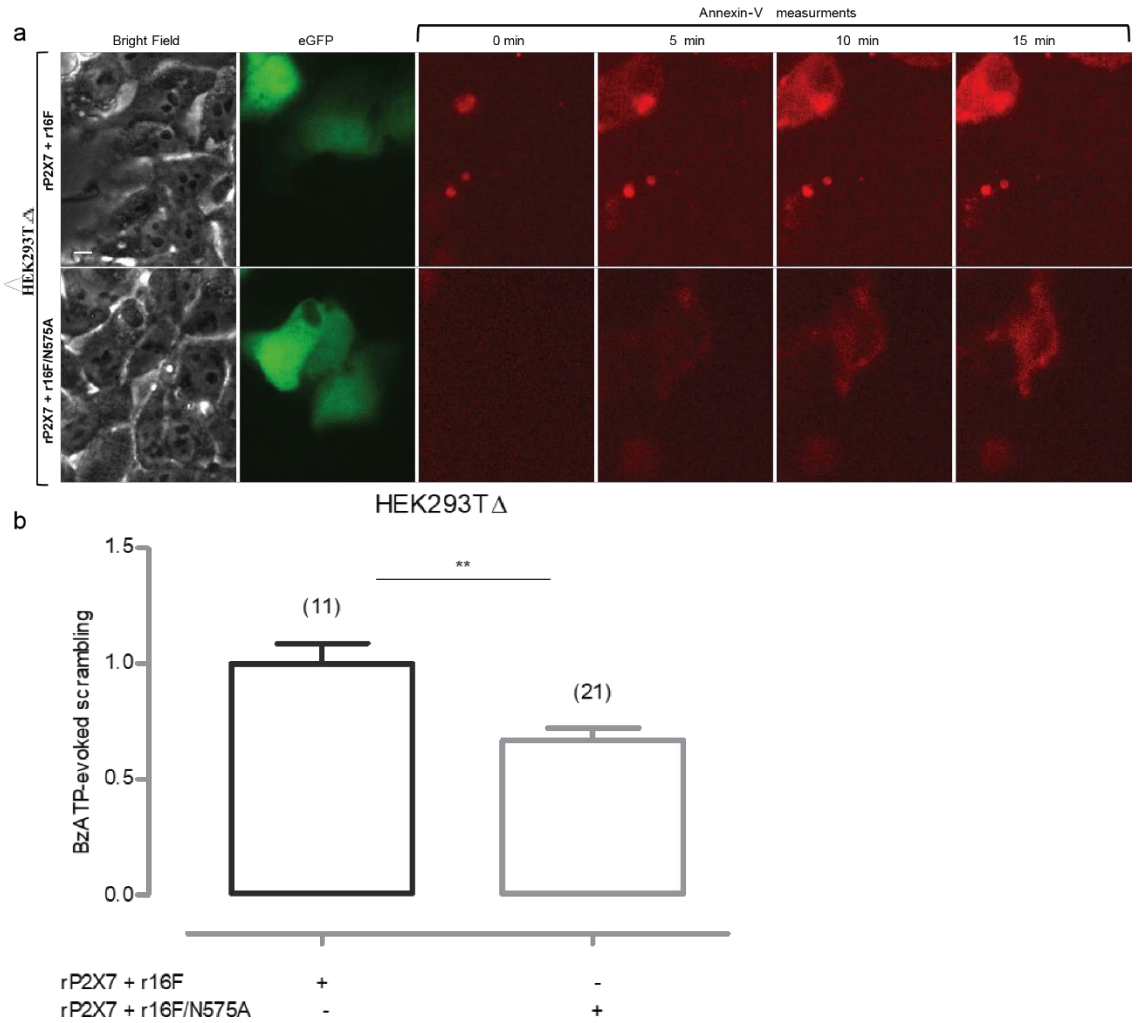

Figure 4.6: Effects of rTMEM16F-N575A mutant on BzATP-induced scrambling activity. (a) representative images of HEK293TΔ co-expressing either rP2X7-rTMEM1F (top panels) or rP2X7-rTMEM1F-N575A mutant (bottom panels). (**b**) BzATP-induced scramblase activity quantified by Imax values and expressed as mean ± SEM: rP2X7-rTMEM1F/rP2X7-rTMEM1F-N575A (1.000 ± 0.088 N=11, 0.667 ± 0.053 N=21, respectively) ** p=0.0016. Scale bars, 5 µm. At least three independent transfections were performed for each condition, and statistical analysis was carried out using Mann Whitney test

To further investigate direct effects of calcium on P2X7-induced TMEM16F activation, mutagenesis experiments were carried out that targeted rTMEM16F amino acid residue asparagine (N) at position 575 into alanine (A) – N575A. This is because the homologous mutation in the mouse (m)TMEM16F (i.e., N621A) was previously described to significantly impair PS exposure, Ca^{2+} influx, and giant plasma membrane vesicle (GPMV) generation in HEK293 cells (Feng et al., 2019). Using the same 10 µM

BzATP application protocol as described above, HEK293TΔ co-transfected rP2X7 and rTMEM16F-N575A mutant reduced PS externalisation levels to about ~35% (Figure Figure 4.6a, b), similarly to those observed in the presence of BAPTA-AM and EGTAM-AM in HEK293T-WT (Figure 4.4 and 4.5), but also in rP2X7-transfected HEK293TΔ (Figure 4.1c). To verify that N575A mutation was indeed responsible for reportedly decreased Ca^{2+} influx, control experiments using 5 μM ionomycin were performed, which confirmed previously published data (Figure 4.7). Collectively, the finding that lipid binding residue N575A and intracellular Ca^{2+} chelators do not fully affect the rTMEM16F-independent scramblase activity, perhaps indicates that P2X7 may be functionally engaged in Ca^{2+}-independent signalling pathway. Furthermore, this may also rule out any interaction with other TMEM16 members having Ca^{2+}-dependent scrambling function. Additionally, these results further support the notion that P2X7-mediated increase in intracellular Ca^{2+} is important for downstream activation of TMEM16F and subsequent lipid scrambling.

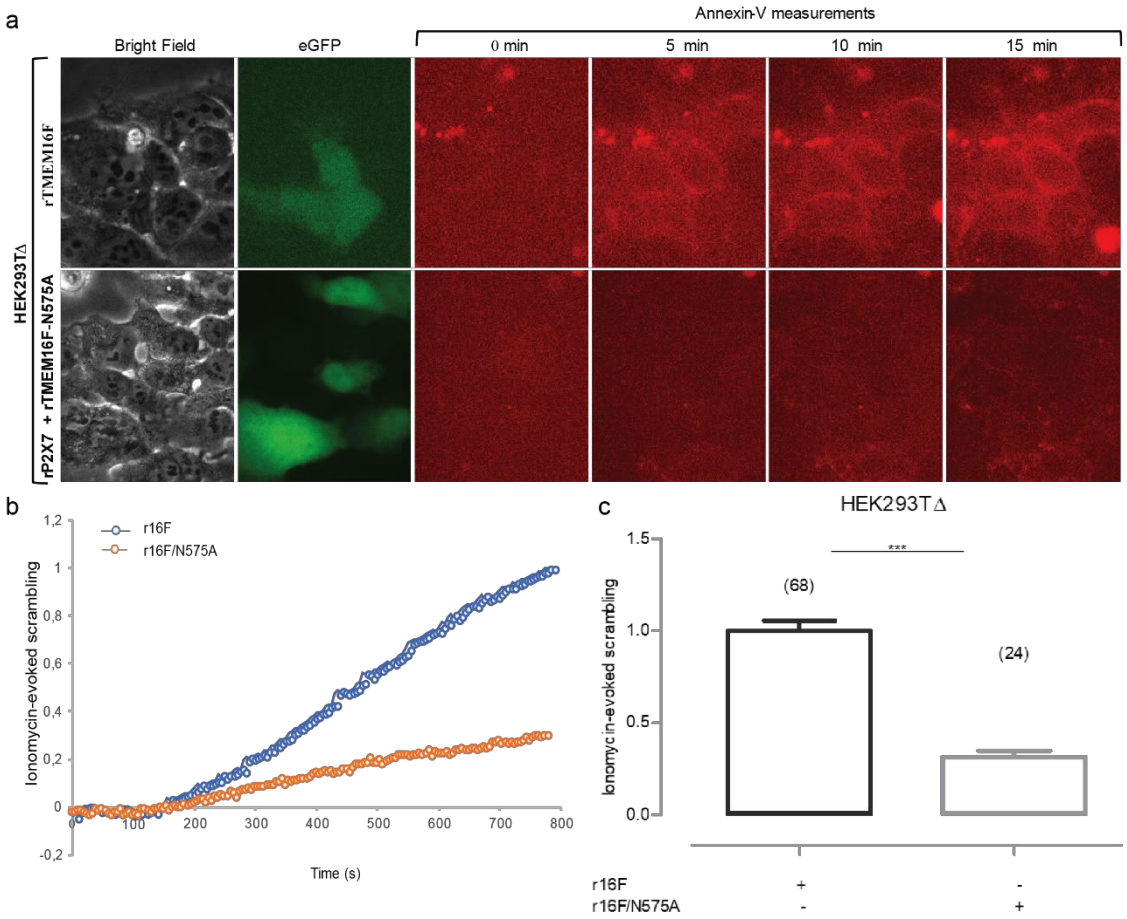

Figure 4.7: Ionomycin-induced rTMEM16F-N575A activation for Ca2+-dependent scramblase activation control. (**a**) Quantification of Annexin-V time-laps images in HEK293TΔ cells expressing eGFP reporter with either rTMEM16F (top panels) or rP2X7- rTMEM16F-N575A mutant conditions (bottom panels) in the presence of ionomycin. Scale bar, 5 µm. (**b**) Normalised Imax values showing difference in PS externalisation as a function of time (s). (**c**) Bar chart illustrating all normalised data points between the WT and mutant conditions. At least three independent transfections were performed for each condition, and statistical analysis was carried out using Mann Whitney test mean ± SEM: rTMEM16F-rP2X7+rTMEM16F-N575A (1.000 ± 0.05626 N=68; 0.3154 ± 0.03373 N=24, respectively) *** p<0.0001.

4.1.3 Functional swapping between P2X7 receptors and TMEM16F channels

Having already demonstrated the existence of a physical and partial functional interaction between P2X7 receptors and TMEM16F channels involved in both scramblase (as discussed above) and dye uptake activities (as illustrated in our previous paper Dunning et al., 2021), we next further dissected this functional coupling at the single amino acid level. Molecular modelling of P2X7-TMEM16F complex was generated by our collaborator (Dr. Taly A., Université Paris Cité) consisting of recent cryo-EM structures of the full-length rP2X7 (McCarthy et al., 2019), and full-length mTMEM16F nanodisc-reconstituted Ca^{2+} state (Alvadia et al., 2019). In this model, one rP2X7 trimer was docked to one mTMEM16F dimer, with no assumption on the stochiometric ratio nor relative orientation. Using a Monte-Carlo (MC) assembly process, the proteins were positioned on the membrane x-y plane allowing for movement along the z-axis designated as the membrane normal. Dockings were carried out by simply determining their initial position on the membrane, and models ranked based on energy-scoring, which led to the generation of a complex model comprising the P2X7 open ATP-bound configuration and Ca2+-bound mTMEM16F model. Based on this modeling data an amino acid residue pair was selected, namely glutamic acid (E) at position 375 located in the C-cys anchor region of rP2X7R (E375) and arginine (R) at position 495 between TM 4-5 on rTMEM16F (R495) – separated by at a calculated distance of 12.4 Å (Figure 4.8). Accordingly, because of the importance of the C-cys anchor in the stability of P2X7 receptors, and its uncharacterised role in physiology, we next examined whether amino acid residues swapping between rP2X7-E375R and rTMEM16F-R495E may be involved in the regulation of both pore formation and lipid scramblase activation. Specifically, we hypothesised whether charge swapping between the two amino acid residues may lead to a salt-bridge formation. Furthermore, we also explored whether a correlation between both protein-associated mechanisms may exist consolidating P2X7-TMEM16F complex interaction. It is worth noting that prior to experiments, all mutations were assessed for proper cell-surface expressions, and sequence verification and validation. Moreover, all experimental

transfections were carried out in HEK293T Δ cell line monitoring exclusively BzATP-induced P2X7 receptors activation.

4.1.3.1 C-cys anchor: the interplay between TMEM16F-dependent functions & pore formation regulation.

As previously reported (section 4.1.1), the activation of P2X7 receptors by 10 μM BzATP induces sufficient Ca^{2+} influx allowing for TMEM16F activation and subsequent PS exposure to the outer leaflet as measured by Annexin-V-binding. We first examined the role of rP2X7-E375R mutant in regulating TMEM16F lipid scrambling activity. For Annexin-V measurements, cells were co-transfected, along with eGFP reporter gene, as follows: control condition including rP2X7-rTMEM16F wild-types, rP2X7-E375R-rTMEM16F, rTMEM16F-R495E-rP2X7, and swapping charge residues rP2X7-E375R-rTMEM16F-R495E. Using the optimised microscopy-based scramblase assay, we found that rP2X7-E375R mutant exhibited a strong ~40% inhibition in the scrambling activities when co-transfected with rTMEM16F WT (Figure 4.8a, c) as compared to the control condition. Additionally, a less marked reduction of about ~25% was also observed following rTMEM16F-R495E co-transfection with rP2X7 WT (Figure 4.8a, c). Accordingly, we tested whether charges amino acid swapping between the two mutants would rescue the pronounced decrease reported in the scramblase activity. Strikingly, a full lipid scrambling rescue, similar to the control condition was found following rP2X7-E375R and rTMEM16F-R495E co-transfection in HEK293T Δ cells (Figure 4.8a, c). Since we monitored BzATP-induced lipid scrambling it was hypothesised that the E375R mutant would perhaps narrow the inner gating mechanisms to constrictively effect the influx of Ca^{2+} through the P2X7R preventing full TMEM16F activation; albeit E375 residue was not previously reported to be involved in $Ca2^{+}$ selectivity (McCarthy et al., 2019). Furthermore, the amino acid swapping data further indicates an intriguing cooperativity between the two proteins further contributing to the molecular complexity of this interaction.

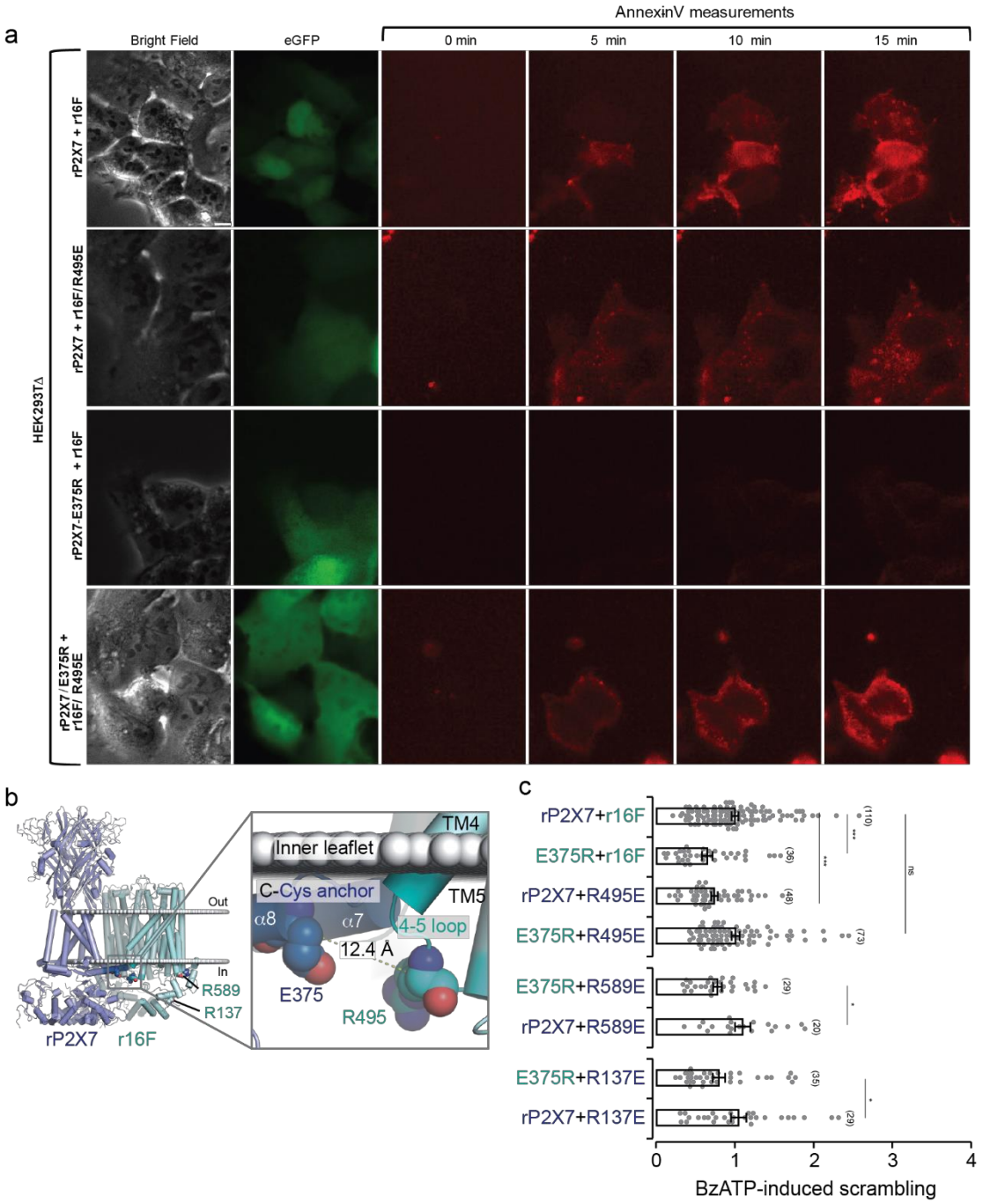

Figure 4.8: Functional rP2X7-rTMEM1F amino acid residues swapping for BzATP-induced scramblase. (**a**) Representative Annexin-V time-laps images following 10 µM BzATP application, recorded using optimised scrambling assay in HEK293TΔ cells expressing eGFP reporter gene along with rP2X7-rTMEM16F, rP2X7-rTMEM16F-R495E, rP2X7-E375R-rTMEM16F, and rP2X7-E375R -rTMEM16F-R495E as indicated per each panel. Scale bar 5 µm. (**b**) Cartoon representation of molecular docking model by Monte Carlo assembly process showing ATP-bound rP2X7 (blue, PDB-6u9W) and mTMEM16F (light blue, PDB-6qpc) used to identify rP2X7 amino acid residue E375 and rTMEM16F amino acid residue R495 at a calculated distance of 12.4 Å as shown by the zoom-in box. E375 resides on the C-cys anchor of rP2X7Rs, whereas R495 is located

between TM4-5 loop of rTMEM16F channels. (**c**) Quantification summary of BzATP-induced scrambling including also mutant control conditions indicated by R137E and R589E. At least three independent transfections were performed for each condition, and statistical analysis was carried out using Mann Whitney test. Data is presented as mean ± SEM: rP2X7-r16F/E375R-r16F (1.000 ± 0.044 N=110; 0.651 ± 0.066 N=36, respectively) ***p<0.0001; rP2X7-r16F/ rP2X7- R495E (1.000 ± 0.044 N=110; 0.7354 ± 0.046 N=48, respectively) ***p=0.0006; rP2X7-r16F/E3754R-R495E (i.e., swapping; 1.000 ± 0.044 N=110; 1.001 ± 0.053 N=73, respectively) ns= non-significant. Control conditions E375R-R589E (control swapping: 1)/rP2X7+R589E (0.78 ± 0.056 N=29; 1.099 ± 0.097 N=20, respectively) *p=0.019; and E375R-R137E (control swapping: 2)/rP2X7+R589E (0.7993 ± 0.076 N=35; 1.052 ± 0.102 N=29, respectively) *p=0.04. No control swapping condition fully rescued the Bz-ATP induced scrambling.

Some reports, including our latest study, also suggested that TMEM16F partially contribute to P2X7R pore formation (Dunning et al., 2021; Ousingsawat et al., 2015). Therefore, we secondly addressed whether the same mutations would also impar the pore formation machinery of P2X7R. We used fluorescent YO-PRO-1 dye of 376 Da, which was shown also by our lab to perform robust dye uptake in HEK293T cells expressing rP2X7 upon 10 μM BzATP stimulation. All optimisation experiments are outlined in Dunning et al., study including no YO-PRO-1 incorporation in the absence of BzATP application or in non-transfected cells. Briefly, we previously found a marked ~40% reduction in BzATP-stimulated YO-PRO-1 uptake in P2X7 transfected HEK293T cells in the presence of 1 mM 9AC applications. A significant ~40% reduction in YO-PRO-1 uptake was also reported in rP2X7-expressing HEK293T Δ cells (for more information regarding assay optimisation refer to Dunning et al., 2021). Having unambiguously demonstrated a statistically significant contribution of rTMEM16F to P2X7R pore formation function, we next tested the effects of aforementioned mutants on dye uptake. Noticeably, we found that rP2X7-E375R-rTMEM16F resulted in a strong ~40% inhibition of BzATP-induced YO-PRO-1 uptake that was fully rescued following amino acids swapping corresponding to the P2X7-E375R-rTMEM16F-R495E condition (4.9a, b). Surprisingly, however, rTMEM16F-R495E mutant caused no reduction in dye-uptake following co-transfection with rP2X7 WT. Collectively, it was speculated that since the pore formation is an inner property of P2X7 receptors initiated exclusively following BzATP application that downstream activation of TMEM16F-R495E mutant was not sufficient in impairing the partially TMEM16F-dependent portion of pore formation.

Together, these data provide evidence for a strong amino acid effector residue, namely E375 on rP2X7, whose mutations severely impair proper functioning of the receptor and rP2X7-rTMEM16F complex itself. To prove the specificity of our mutations and to circumvent the variation bias in both scramblase and dye uptake assays additional mutants targeting different arginine residues on rTMEM16F including R589E and R137E were generated. All control mutants failed to fully rescue both scramblase and dye-uptake activities when co-transfected with rP2X7-E375R (Figure 4.8c and 4.9b). It is also worth noting that despite the use of membrane-permeable Ca^{2+} chelators or specific mutations the resulting calculated reduction in both pharmacological assays was consistent at ~40% similar to that found in BzATP-mediated rP2X7R activation in HEK293T Δ cells. Lastly, we examined whether a correlational association between the proteins' hallmark processes may exist, further highlighting the importance of this interacting complex in physiological and pathophysiological conditions. When analysed all experimental conditions from each of the pharmacological assay including rP2X7-E375R-rTMEM16F, rTMEM16F-R495E-rP2X7, and swapping charge residues rP2X7-E375R-rTMEM16F-R495E exhibited a potential correlation with an $R^2 = 0.86$ (Figure 4.10). Therefore, another question arises to whether a reciprocal relationship between dye-uptake and lipid scrambling drives both processes through a unanimous molecular pathway – perhaps, explaining the consistent, unambiguously demonstrated, ~40% inhibition in each assay.

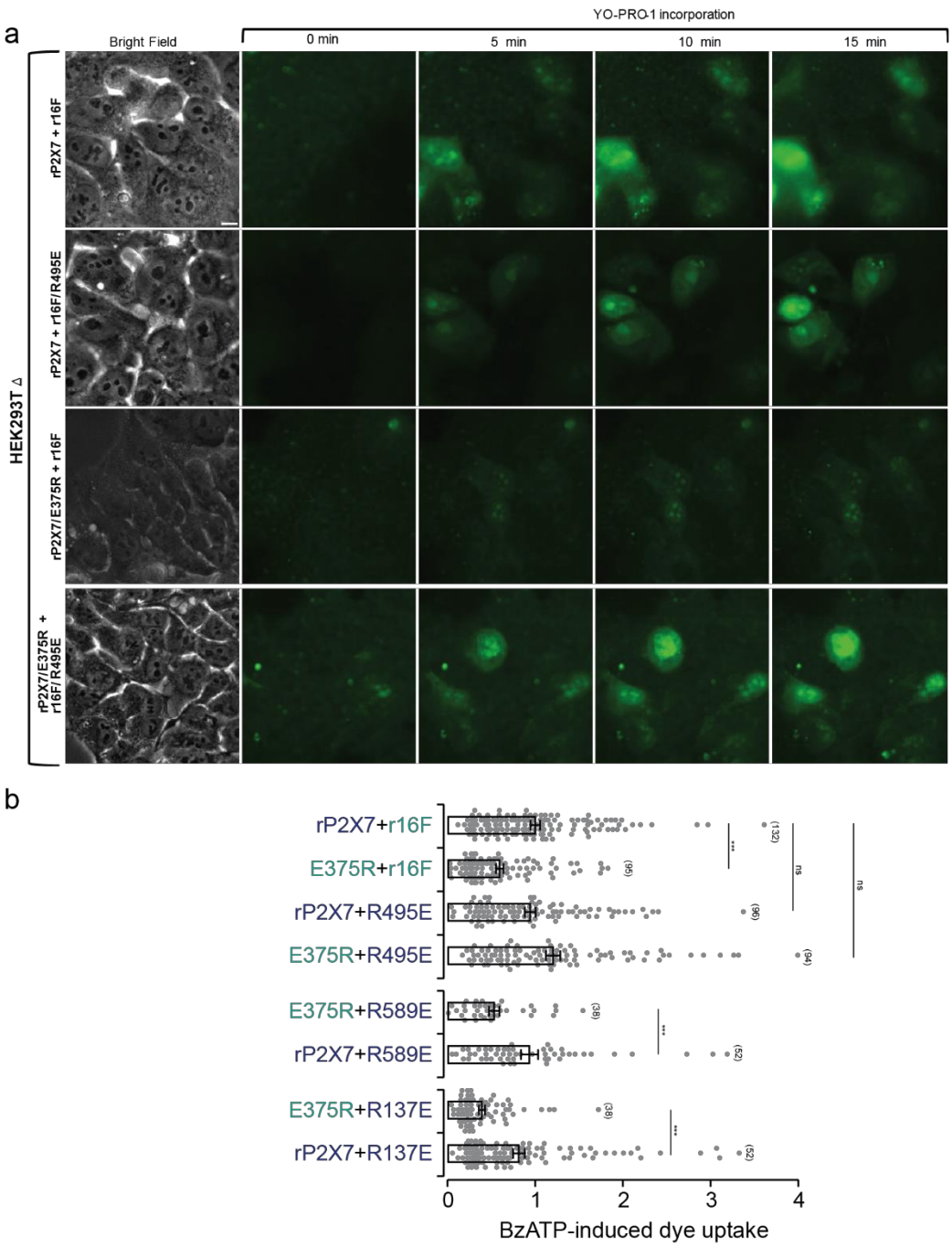

Figure 4.9: Functional rP2X7-rTMEM1F amino acid residues swapping for BzATP-induced YO-PRO-1 dye-uptake. (**a**) Time-laps images illustrating YO-PRO-1 dye-uptake incorporation following 15 min 10 µM BzATP application in HEK293TΔ cells expressing with rP2X7-rTMEM16F, rP2X7-rTMEM16F-R495E, rP2X7-E375R-rTMEM16F, and rP2X7-E375R -rTMEM16F-R495E as indicated per each panel. Scale bar 5 µm. (**b**) Quantification summary of BzATP-induced YO-PRO-1 dye-uptake including also mutant control conditions as indicated by R137E and R589E. At least three independent transfections were performed for each condition, and statistical analysis was carried out using Mann Whitney test. Data is presented as mean ± SEM: rP2X7-r16F/E375R-r16F (1.000 ± 0.054 N=132; 0.592 ± 0.044 N=95, respectively)

***p<0.0001; rP2X7-r16F/ rP2X7- R495E (1.000 ± 0.054 N=132; 0.943 ± 0.07 N=96, respectively) ns non-significant p=0.49; rP2X7-r16F/E3754R-R495E (i.e., swapping; 1.000 ± 0.054 N=132; 1.21 ± 0.082 N=94, respectively) ns= non-significant p=0.09. Control conditions E375R-R589E (control swapping: 1)/rP2X7+R589E (0.531 ± 0.058 N=38; 0.94 ± 0.096 N=52, respectively) ***p=0.0010; and E375R-R137E (control swapping: 2)/rP2X7+R589E (0.393 ± 0.035 N=71; 0.81 ± 0.066 N=109, respectively) ***p<0.0001. No control swapping conditions fully rescued the Bz-ATP induced scrambling**.**

4.1.3.2 E375R mutant exhibits a delayed current facilitation phenotype

The P2X7R ion channel properties are remarkably different from the other P2X receptor subtypes. Among several hallmark features of P2X7R is ATP-evoked current facilitation also acknowledged as ATP sensitisation. This process occurs as a result of repeated or prolonged exposure to ATP simulation yielding an increase in receptor density that leftward shifts agonist affinity curve (i.e., augmentation of the potency). Current facilitation is influenced by an essential component of the cell membrane – that is cholesterol. Interestingly, it has been recently suggested that cholesterol-driven inhibitory mechanism may be counteracted by the activity of palmitoylated cysteine residues, indicating that lipid composition depicts an effective factor that allosterically modulate receptor function (Karasawa et al., 2017). In this regard, we next addressed whether E375R, considering its remarkable location on the C-cys anchor, influenced the receptor response to ATP sensitisation in HEK293T WT cells. The protocol consisted in 8 applications of 10 μM BzATP applications at each 25 s intervals, commonly used to evaluate P2X7 current facilitation. No differences were observed in the current amplitude between rP2X7-WT and rP2X7-E375R mutant. Surprisingly, however, a different behaviour in current facilitation was found, whereby P2X7-WT was facilitated about 2-fold at the 5th application, as compared to rP2X7-E375R mutant, which only reached 1,5-fold facilitation at the 8th Bz-ATP application. Together, this indicates that beside having a similar current amplitude, the current facilitation is either reduced or delayed in the E375R mutant (Figure 4.8). Thus, unambiguously confirming that this mutant incapacitates proper functioning of P2X7R. Consequently, given the profound immunological implications discussed in Chapter 1, we next asked whether this region of the P2X7 may be considered as a novel therapeutic target (See Chapter 5).

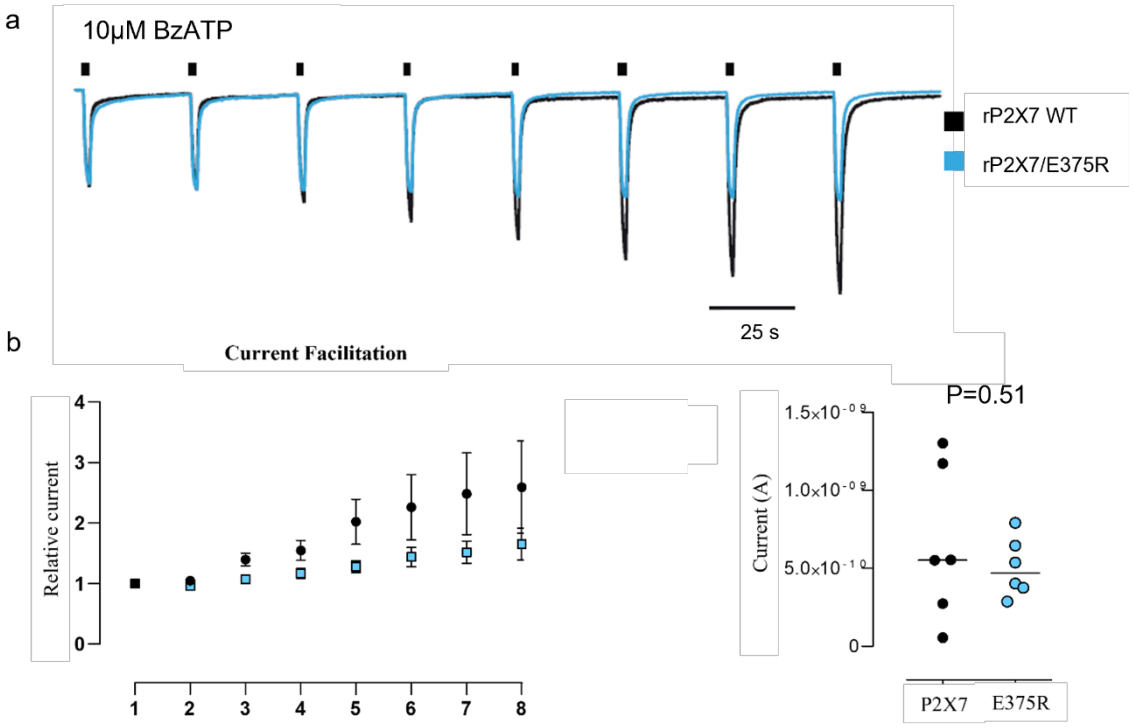

Figure 4.10: Effects of E375R mutant on current facilitation in HEK293T-WT transfected cells. (**a**) Whole-cell currents induced by repeated 2 s 10 µM BzATP application in HEK293T-WT cells expressing rP2X7 (black traces) and E375R mutant (light blue traces). (**b**) Summary of relative currents (left) in function of number of BzATP applications, and total current (A)-evoked (right) per condition rP2X7 (black) and E375R (blue) (n=6 different cells per condition in 2 different transfections).

4.1.4 Overall Discussion

Chapter 4 results provided strong evidence on the molecular mechanisms partially underlying TMEM16F activation by P2X7 receptors-dependent increase in intracellular Ca^{2+} – consistent with previous published work by Ousingsawat et al. We revealed for the first time a potential correlation between macropore formation and membrane lipid scrambling representing the two hallmarks of P2X7 receptors and TMEM16F channels, respectively, that have been enigmatic for several years. Furthermore, we presented a bias-free Annexin-V microscope-based imaging assay, in which to monitor lipid scrambling activities exclusively through activation of P2X7 receptors in HEK293T. Thus, delineating a proper functional assay specific to the complex activation excluding the unspecific Annexin-V signals arising from ionomycin applications – that is very

commonly used for studying scrambling activity in relation to TMEM16F channels. Nonetheless, it remains, as yet, unclear as to what mechanisms operate in the uncharacterised intracellular Ca^{2+}-independent elicited scramblase activity observed in the presence of membrane-permeable Ca^{2+} chelator buffers. As a result, several queries were raised in this regard, including (i) could this activity be attributed to a complex-dependent mechanism operating independently of its intracellular Ca^{2+} concentration? Especially given the very close proximity of the two proteins, as previously determined by FLIM-FRET; (ii) Could there be another TMEM16 member, as illustrated by qPCR data, functioning in a Ca^{2+}-independent PS externalisation manner, whilst contributing to the complex interaction? (iii) Could this be related to another unidentified class of scramblase proteins? It must be noted that due to the use of tannic acid (which we proved in our previous work by Dunning et al., to be a fluorophore quencher) in previously published studies investigating membrane phospholipid scrambling, blebbing and apoptosis in relation to P2X7-TMEM16F complex activation, data addressing this peculiar phenomenon remains poorly discussed in the literature.

Following a thorough investigation, we successfully discovered two set of amino acid residues governing dye uptake and lipid scrambling providing for the very first time a novel potential therapeutic target for P2X7 receptors. Particularly, we discovered that overexpression of E375R in HEK293T and HEK293T Δ cells attenuated P2X7 ability to induce current facilitation, pore formation, and downstream activation of TMEM16F channels, with subsequent reductions in PS externalization, membrane blebbing and cell death. Given the location of the E375R mutants, this further highlights an important new pharmacological role of the cytoplasmic c-cys anchor of the P2X7 that was previously unknown. To provide convincing data on these assertions, we next examined whether the C-cys anchor region of P2X7 receptors can be employed as a novel immunoregulatory region for P2X7-induced inflammation and cell death regulation (discussed in Chapter 5). Collectively, we speculated that TMEM16F channels synergistically operate in several central cellular responses downstream of P2X7 receptors including immediate cell shrinkage caused by K^+ and Cl^- efflux following sustained rise in cytosolic Ca^{2+} by P2X7R activation, PS externalisation, membrane blebbing and culminating in cell death. In this

regard, TMEM16F can be viewed as a fundamental element to a macromolecular complex containing P2X7 receptors characterised by many different molecular and cellular pathways, which we shall attempt to thoroughly explore in the next chapter.

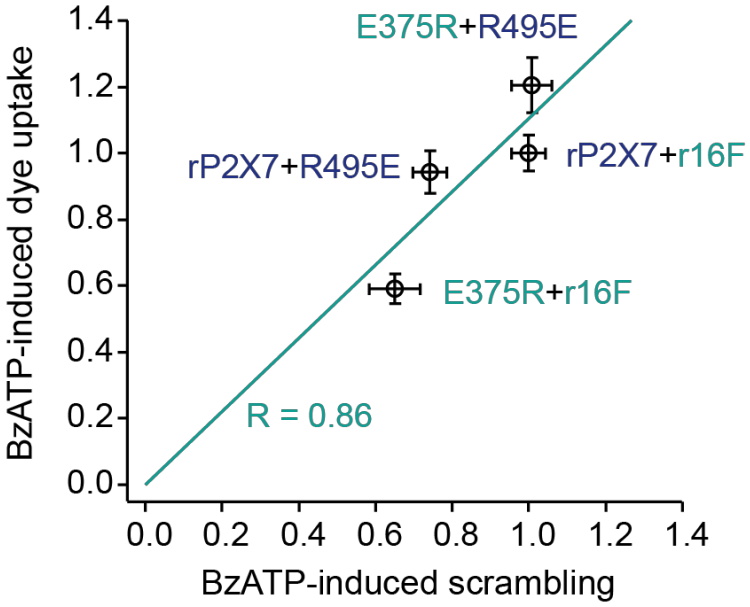

Figure 4.11: Correlation between pore formation and scramblase activity.
Scattered spot curve displaying a direct correlation between mutant conditions expression in BzATP-induced dye-uptake incorporation and phospholipid scrambling in HEK293TΔ-transfected cells. Arrows indicate each mutant combination.

Chapter 5

Results: Immunology

5.1 Introduction to inflammation & cell death

Activation of P2X7 receptors coordinates the innate immune system responses to inflammation by sensing elevated concentrations of extracellular ATP – that is considered a DAMP at site of tissue damage (Ferrari et al., 2016). Physiological P2X7 receptor stimulation in immune cells such as macrophages is a well-known trigger of the NLRP3-caspase-1 inflammasome. Here, it plays a vital role in the release of IL-1β, IL-18 or Annexin-A1, shedding of TM proteins CD23 and CD62L, as we previously discussed, and regulation of numerous cell death pathways, including apoptosis, necrosis, autophagy, and pyroptosis (Di Virgilio et al., 2017). P2X7R's role as a cytotoxic receptor hasn't received much attention to date, making it difficult to predict how it would affect various aspects of the apoptotic machinery, including the assembly of apoptosomes. However, there are scattered studies suggesting that extracellular ATP binding to P2X7R induces cytochrome *c* release resulting in apoptosome formation through caspase-3/8/9 activation (Ferrari et al., 1999; Kong et al., 2005). Given the complex and varied nature of P2X7-dependent inflammasome activation, in this section we proposed a revised NLRP3-caspase-1 inflammasome model from previously published Di Virgilio et al., work, annexing to it an additional plausible mechanism associating P2X7-TMEM16F

interactions underlying cellular basis of the apoptotic machinery (as illustrated in Figure 5.1). Together, this model should serve as an attempt to better understand the following experimental investigations employed in tailoring P2X7-specific interventions addressed below.

Briefly, as the first line of defense against foreign pathogens, the innate immunity is key to infection recognition and clearance. The multiprotein intracellular NLRP3 inflammasome complex is one of the most important components participating in these processes. The NLRP3 protein comprises a pyrin domain (PYD), and the adaptor ASC protein harboring PYD and CARD domains, which upon activation it allows for NLRP3 interaction with ASC through PYD. This enables the recruitment of the CARD domain of pro-caspase-1 via the ASC-CARD domain resulting in the formation of NLRP3-ASC-pro-caspase-1 complex (Schroder et al., 2010), as detailed in Chapter 1 (see section 1.5). In macrophages, the inflammasome can be experimentally induced either by PAMPs such as LPS acting on TLRs (indirect mechanism) or by ATP-dependent stimulation of P2X7 receptors (direct mechanism) (Figure 5.1). In the first instance, LPS priming activates TLR4 inducing NF-κB transcription of proinflammatory cytokines production including pro-IL-1β, pro-TNFα (among others), and NLRP3. The second activation signal step is provided by DAMPs (i.e., including extracellular ATP) either operating at the plasma membrane or in the cytoplasm leading to inflammasome activation and release of additional inflammatory effectors such as cathepsin B (Di Virgilio et al., 2017). At the cytosolic level DAMPs and PAMPs can further increase extracellular ATP via pannexin-1 opening mediated by caspase-11 activation culminating in P2X7R stimulation and pyroptosis. Extracellularly, elevated ATP molecules feedback on P2X7Rs eliciting K^+ efflux – that is an upstream event in the NLRP3 inflammasome activation – required for NIMA-related kinase 7 (NEK7) binding to the NLRP3 protein. The newly formed NLRP3-caspase-1 inflammasome catalyses pro-caspase-1 cleavage to caspase-1 and IL-1β. The latter can now be released by exosomes and secretory lysosomes. For an efficient assembly, NLRP3 inflammasome also requires efflux of Cl^- and ROS production (Y. Yang et al., 2019b). Importantly, K^+ efflux as well as excessive Ca^{2+} resulting from P2X7R activation, cause severe cellular stress in mitochondria and mitochondrial outer membrane

permeabilization (MOMP) triggering the activation of Bcl-2 apoptosis regulator family. MOMP is regulated by apoptosis regulator (BAX) and Bcl-2 antagonist-killer-1 (BAK) oligomers promoting pore formation across the outer mitochondrial membrane (Galluzzi et al., 2018). As a result, various intermembrane space proteins are released into the cytosol including cytochrome *c*, which is now able to activate apoptotic protease activator factor 1 (APAF1), whose oligomerisation induces the formation of the apoptosome. Pro-caspases-9 recruitment by the apoptosome stimulates caspase-9 activation as well as a complex caspase signalling cascade triggering executioner caspase-3 and -7 (Boland et al., 2013). This form of apoptosis is referred to as intrinsic apoptosis. Caspase-1 inflammasome complex also culminates with the activation of caspase-3. Indeed, it has been suggested that both intrinsic and extrinsic apoptosis mechanisms regulate pannexin-1 aiding in NLRP3 inflammasome assembly (K. W. Chen et al., 2019). Therefore, given the complexity of the overall apoptosis machinery and intertwined activities of some apoptotic effector regulator, designing specific pharmacological targets can be sometime very challenging.

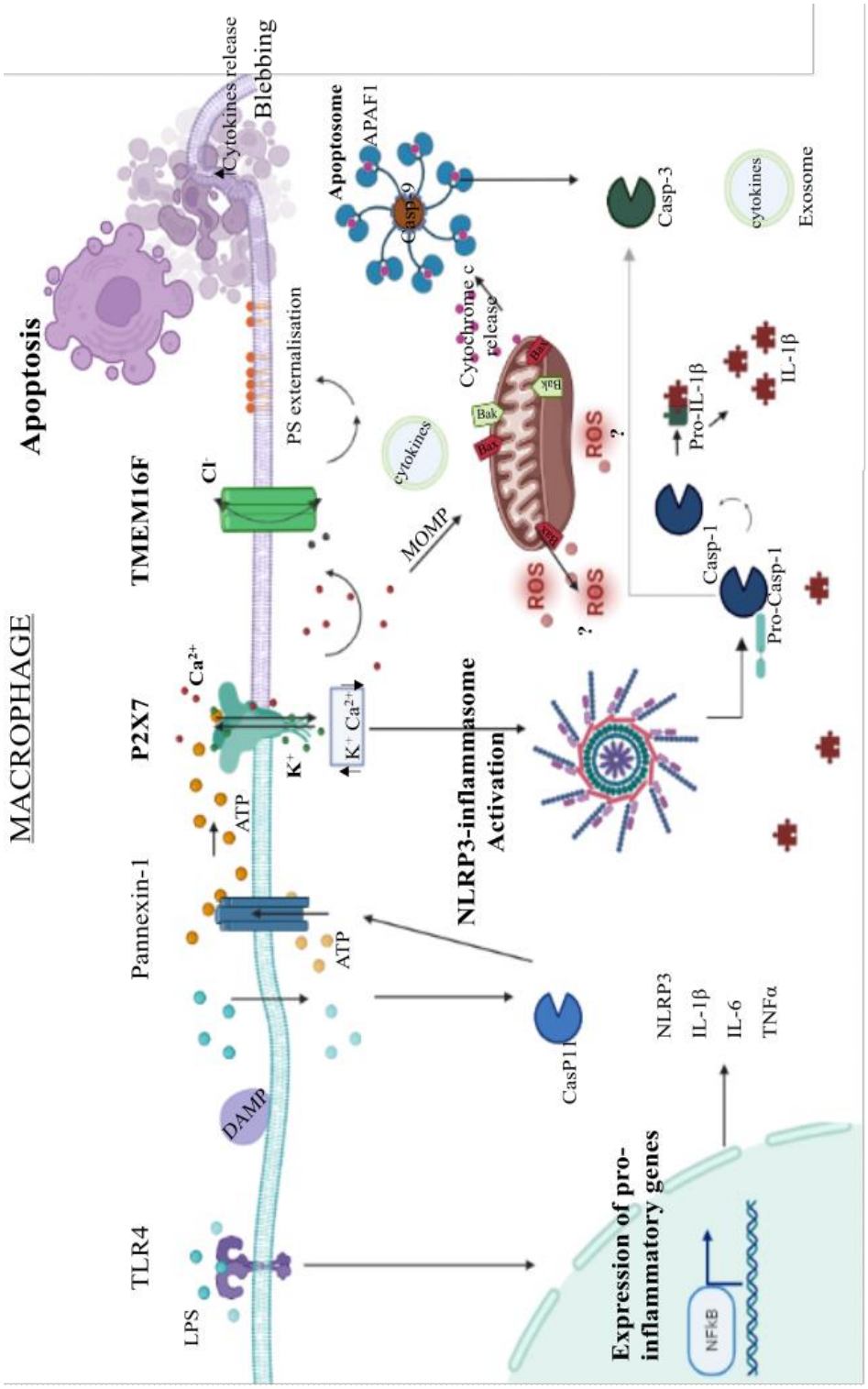

Figure 5.1: P2X7R pathways to inflammation & cell death.
Revised scheme potentially linking P2X7R simulation to downstream TMEM16F activation showing central cellular process involved in cell death regulation as detailed in the main text. The model was made on BioRender using information acquired from the following published work (Boland et al., 2013; DiVirgilio et al., 2017; Galluzzi et al., 2018; Janks et al., 2019; Ousingsawat et al., 2015; Salaro et al., 2016)

5.1.1 Caspase-3 activation is TMEM16F dependent in macrophages

Macrophages endogenously express high levels of P2X7 receptors exerting, in turn, a predominant role in apoptosis. A recent work measured the activation of caspase-3 in primary peritoneal microphages from TMEME16F null mice ($16F^{-/-}$) and TMEME16F WT mice ($16F^{+/+}$) for 12 h post 5 min, 3 mM ATP treatment without previous LPS priming (Ousingsawat et al., 2015). ATP exposure resulted in an immediate proapoptotic morphological effect in peritoneal macrophages leading to a significantly attenuated caspase-3 activation in $16F^{-/-}$ microphages as compared to the $16F^{+/+}$ control conditions (Ousingsawat et al., 2015). Collectively, this data established a new cellular apoptosis effector directly interfering with immunological properties associated to P2X7 receptors. In this regard, given the proposed role of intrinsic and extrinsic apoptosis associated with NLRP3 inflammasome regulation, as discussed above – we next attempted to design tailored specific-P2X7R therapeutics aiming at controlling the receptor ability to initiate downstream effectors signalling contributing to TMEM16F activation.

5.2 The cytoplasmic anchor of P2X7R as a novel immunoregulatory target

Based on our data, as discussed so far (refer to Chapter 4), it appeared that P2X7 mutant E375R mutant severely attenuated the receptor ability to fully engage in signalling generation leading to proper downstream activation of TMEM16F channels in HEK293T system. Therefore, in this chapter, we further addressed the role of P2X7 receptors and TMEM16F channels forming complex in controlling inflammation and cell death regulation in macrophages. To do this, we used engineered HIV-1-TAT peptides that selectively targeted the C-cys anchor region of mP2X7 and TM 4-5 loop of mTMEM16F along with two generated random sequences used as experimental controls (i.e., scramble, Scr-peptides): FCRSGVYPYCKCCEPCTV-, KKKEKVAIMITNFELPRTQTD-, respectively and FVCKYESCPRCPCVTGYC-, NREVDTLKTPAITEMQFI-,

respectively – that collectively represented the specific amino acid residues targeted in this study (Figure 5.2). The HIV-TAT linker region and peptide sequence included GGG-YGRKKRRQRRR as described in Sorge's et al., work. Importantly, due to major sustainability issues related to mTMEM16F peptide synthesis failure, three unrelated lysine residues (K) were added at the beginning of the endogenous amino acid sequence. As a result, given the uncertainty surrounding the specificity of the mTMEM16F the focus of this chapter has been exclusively centred on to the activity of mP2X7 TAT-peptides activity.

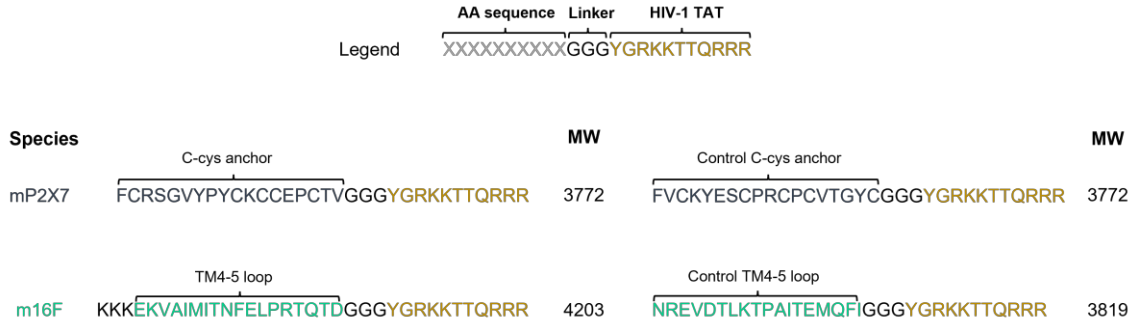

Figure 5.2: Schematic representation of HIV-1 TAT peptides.
Schematic overview of HIV-1 TAT peptides design illustrating specific targeted region of P2X7 C-cys anchor and TMEM16F TM4-5 loop regions along with their respective controls and molecular mass. TAT peptide showing linker (black) and TAT sequence (brownish).

5.2.1 C-cys anchor regulates innate immune functions in macrophages

We investigated whether the cytoplasmic anchor is essential for TMEM16F complex forming interactions as well as its role as an immunoregulatory target. P2X7 is a potent activator of cell death yet its cytotoxic function has been poorly addressed. Considering Ousingsawat's et al., study demonstrating that caspase-3 is dependent on TMEM16F activation, we next exposed mouse peritoneal macrophages to 5 mM ATP for 5 min and assessed caspase-3/7 following 14 h stimulation. No LPS priming was carried out prior to ATP application allowing for a delayed activation of caspase-3/-7 activity. TAT peptides (50 μM) were incubated in FBS-free medium for 6 h prior to ATP stimulation in 10%

FBS medium as detailed in the methods (Chapter 2). Intriguingly, a full inhibition was observed in mP2X7-TAT peptide conditions when compared to either ATP alone, designating the positive control, or to mP2X7 scramble TAT-peptide. On the contrary, no differences were reported in the overall caspase-3/-7 activity between the positive control and scramble TAT-peptide conditions (Figure 5.3b). In addition, mTMEM16F-TAT peptides showed no changes in caspase-3/-7 activation as compared to the ATP conditions. Notably, caspase-3/-7 measurements were performed using a luminescence-based assay providing more robust data interpretation and analysis, as compared to traditional fluorescence-based methods, which has been used by other studies including Ousingsawat's et al. Overall, our results implicate for the first time the P2X7R C-cys anchor in the regulation of cell death mechanisms further dissecting the cytotoxic function of the receptor for novel immunological target.

To further demonstrate the extent to which the unique C-cys anchor of P2X7R governs possibly pore formation and subsequent cell death – we examined whether the mP2X7-TAT peptide also inhibited the release of major pro-inflammatory cytokines, chiefly TNFα in RAW264.7 macrophages. TNFα is produced in response to TLRs stimulation, but its concentration augments following elevated extracellular ATP levels inducing P2X7R activation. We therefore incubated RAW264.7 macrophages overnight with mP2X7 TAT-peptide (50 μM) in 10% FBS medium and exposed them to 3 mM ATP for a minimum of 20 min with previouss priming by 1 μg/mL LPS for 4 h (Figure 5.3c). We assayed different conditions in order to proper optimise the ELISA results including non-treated (NT), ATP, LPS, LPS co-application with ATP, LPS co-application with ATP and AZ (P2X7-specific inhibitor), ATP co-application with LPS and mP2X7 TAT peptide, and ATP co-application with LPS and mP2X7 TAT scramble. TNFα release increased significantly following co-application with ATP as compared to LPS alone, and no to minimal TNFα released was detected in NT as well as ATP conditions alone – that is consistent with the current published literature (Figure 5.3c). Surprisingly, however, the mP2X7 TAT peptide exhibited a similar reduction in TNFα release as to that observed in the AZ condition, as if the peptide itself was inducing an inhibitory effect to P2X7R (Figure 5.3c). Indeed, both conditions evoked statistically fewer TNFα release when

compared to co-application of ATP and LPS, but no differences detected as compared to the LPS primed condition alone. Collectively, these data confirm the previous assertions suggesting a novel essential role for the C-cys anchor of P2X7R in regulation of a macromolecular complex containing TMEM16F channels, which is vital for initiation of different signalling pathways linked with inflammation and apoptosis.

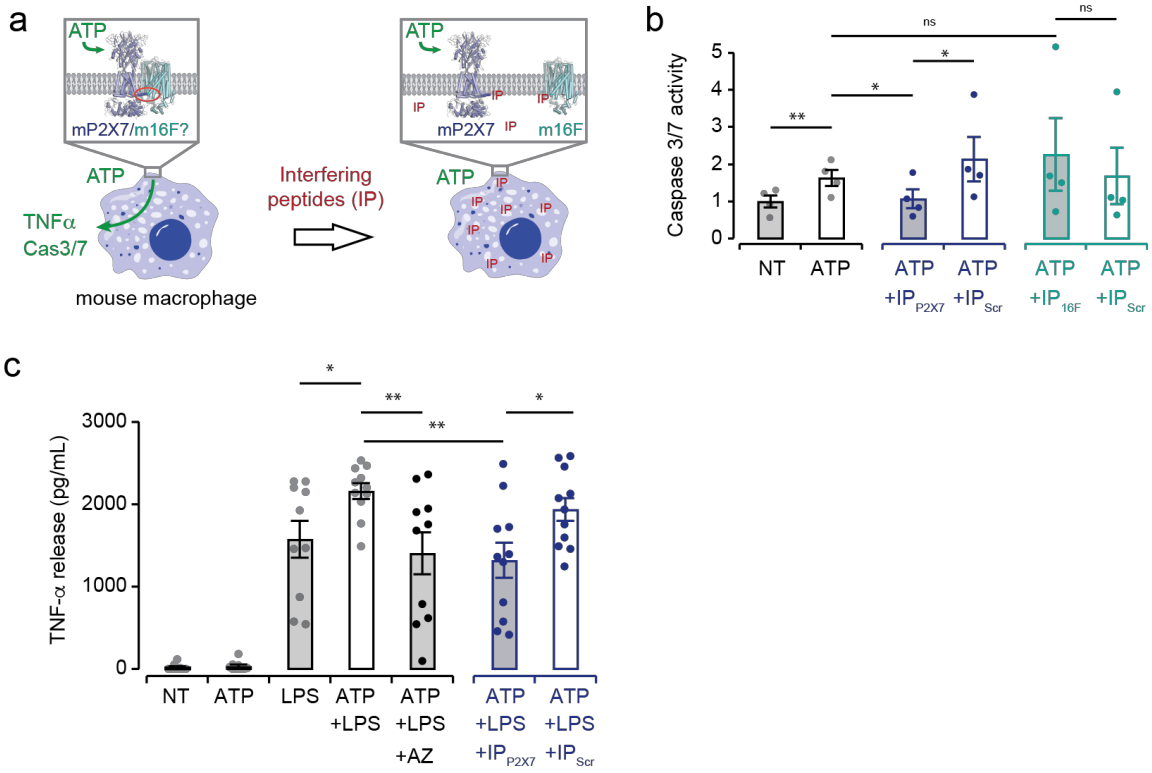

Figure 5.3: Effects of P2X7 C-cys anchor TAT peptide on macrophages function. **(a)** Activation of caspase 3/7 in mouse peritoneal macrophages from four different mice stimulated by 5 mM ATP. Prior incubation with TAT peptides and their respective controls as indicated by TAT_{Scr} conditios was carried out for at least 6 h prior to ATP stimulation. Statistical analysis was performed using unpaired T-test (Mean ± SEM): ATP and non-treated (NT; 1.000 ± 0.1044; 0.6122 ± 0.0707, respectively) **p=0.0082; ATP and P2X7-TAT (1.000 ± 0.1044; 0.654 ± 0.1044, respectively) *p=0.035; ATP and $P2X7_{Scr}$ (1.000 ± 0.1044; 1.53 ± 0.360, respectively) non-significant (ns; p=0.120); P2X7-TAT and $P2X7_{Scr}$ (; 0.654 ± 0.1044; 1.53 ± 0.360, respectively) *p=0.016. **(b)** Quantification of TNFα release (pg/mL) in RAW264.7 macrophages induced by 4 h LPS priming followed by 20 min 3 mM ATP stimulation with overnight TAT peptides incubation or 15 min incubation with P2X7 AZ inhibitor prior to LPS. At least three independent measurements were carried out per condition statistical analysis assessed by Mann Whitney test (Mean ± SEM; expressed as pg/mL): LPS and LPS + ATP (1575 ± 221.0; 2161 ± 94.15, respectively) *p=0.045; LPS + ATP and LPS + ATP + P2X7-TAT

(2161 ± 94.15; 1314 ± 211, respectively) **p=0.0058; LPS + ATP + P2X7-TAT and LPS + ATP + $P2X7_{Scr}$ (1314 ± 211; 1935 ± 141, respectively) *p=0.036; LPS + ATP and LPS + ATP + $P2X7_{Scr}$ (2161 ± 94.15; 1935 ± 141, respectively) ns p=0.23; LPS and LPS + ATP + $P2X7_{Scr}$ (1575 ± 221.0; 1935 ± 141, respectively) ns p=0.34.

5.2.2 Overall Discussion

Undoubtedly, understanding the cellular and molecular mechanisms implicated in the inflammasome activation will certainly improve the development of specific inhibitors tackling several immune-oncology related conditions. Due to a broad diversity of inflammatory stimuli, identification of specific effectors implicated in RCD subroutines mechanisms and inflammasome remain particularly difficult to achieve. In this regard, we have undertaken a preliminary study examining the C-cys anchor region of P2X7R as potential target for drugs development. The present results unambiguously demonstrate for the first time potent inhibitory effects of selective HIV-1 TAT peptides targeting the P2X7 C-cys anchor on proinflammatory cytokines release and cell death regulation. Notably, TMEM16F participates in essential cellular processes downstream of P2X7 receptors (as detailed in the scheme 5.1b), whose activation is liked to marked increases in intracellular Ca^{2+} and decreases in intracellular K^+ concentrations recognised as keys trigger of MOMP and NLRP3 inflammasome activation, respectively. Furthermore, P2X7-induced Ca^{2+} influx activates Cl^- currents resulting in immediate cell shrinkage and TMEM16F- Ca^{2+}-dependent PS scrambling, which together, further contribute to apoptotic machinery processes. Based on our data, we speculate that the unique cytoplasmic anchor of P2X7R mediates essential signalling leading to pore formation and cell death – in striking contrast to current literature attributing these functions to the P2X7R extended C terminus (North, 2002; Ousingsawat et al., 2015; Virginio et al., 1999)– whereas the cytoplasmic C terminus of the receptor might engage in a docking site for TMEM16F-induced proapoptotic stimuli. Nevertheless, due to technical issues related to HIV-1 TAT synthesis, we failed to address the role of TM 4-5 loop of TMEM16F channels in caspase-3/-7 activity and TNF-α production in macrophages. Additional questions as to whether the P2X7 interfering TAT peptide produce therapeutic effects remain, as of now, an intriguing assertion open for debate. Moreover, is there a common

signalling pathway trigger correlating TMEM16F activation to NLRP3-iflammasome formation? And ultimately, is TMEM16F-dependent caspase-3 activity a culminating component of the NLRP3-iflammasome itself.

Chapter 6

Final Discussion

Survival – impossible without a precise regulation machinery within which the immune system, itself, orchestrates the boundaries of death. This thesis has focused on characterising macromolecular complex interactions to better understand the pathophysiological role of P2X7R and the identification of potential P2X7R therapeutic regions implicated in inflammation processes, cell death and autoimmune-related diseases. Following the release of ATP and Ado into the extracellular milieu, cells may display different subclassification of purinergic receptors, according to their ligand affinity and specificity. Ultimately, they engage in a variety of intracellular responses of pathophysiological important. As explored in Chapter 1, at the extracellular level, ATP and Ado balance dictates whether or not tolerance and/or immunity is ensued in human. Among purinoceptor subtypes, P2X7 is unique since it generates caspase activity, cytokine production, and apoptosis (Mehta et al., 2014). Concretely, we used a broad variety of techniques including immunoassays, two-photons microscopy, molecular modelling, patch-clamp electrophysiology, qRT-PCR, CRISPR-Cas9, mutagenesis studies, video- and confocal microscopy, providing for the first time, unambiguous evidence of a P2X7 and TMEM16F complex – that is required for proper innate immune system functioning in macrophages. Our molecular modelling approach has been shown to be useful in overcoming barriers to studying protein-protein interactions, greatly

contributing to enhance developmental aspects in molecular neuroscience. In this work, these advantages have been fully optimised to gain novel insights into immunoregulatory therapeutic targets. Experimentally, a great focus has been primarily placed on the development of P2X7 antagonists for anti-inflammatory therapy and tumour progression (Burnstock & Knight, 2018; Mehta et al., 2014).

In this thesis, Chapter 3 describes our breakthrough in the study of this molecular complex providing robust evidence on the discovery of P2X7 receptor and TMEM16F channel forming an estimated 71Å complex as calculated by FLIM-FRET. To localise both proteins at the membrane fusion tags were constructed using mScarlet and eGFP, which were consequently fused to the C-terminus of P2X7 and TMEM16F, respectively. FLIM-FRET was then carried out to evidence physical coupling, albeit the exact complex stoichiometry remains to be determined. Importantly, as the fluorescence lifetime is an intrinsic parameter of the fluorophore independent of concentration, FRET-FLIM is more robust than intensity-based methods to measure FRET when concentrations of interacting partners cannot be controlled. Briefly, FLIM probes changes in fluorophores' microenvironment, in the presence of a FRET pair, a pulsed laser that periodically excites the fluorophores of the donor in the sample, which is then relaxed into their ground-state emitting photon through a non-radiative pathway. The fluorescence lifetime (τ) can be then calculated as the average time a fluorophore remains in the excited state after excitation. In our experimental conditions the presence of the acceptor P2X7_Sarlet in close proximity of the donor TMEM16F_eGFP, FRET occurred, increasing the nonradiative de-excitation rate of the donor, and thus, decreasing its fluorescence lifetime. Limitations due to proteins orientations and fluorescence construct probes prevented, however, the full determination of the complex size. To overcome this, stochiometric assessments between the labelled proteins remain to be resolved.

Following the existence of this macromolecular complex, in Chapter 4 we established bias-free BzATP-evoked scramblase assay measurements and subsequent assessed though Monte Carlo molecular modelling (carried out by Dr. Taly) amino acids residues, which may be implicated in the modulation of the complex. Thorough

examination of the rP2X7-mTMEM16F MC model identified E375 located in the cytoplasmic anchor of P2X7R, and R495 located on TM-4/5 loop in TMEM16F channel, which appeared to be in a very close proximity (<100 Å). These residues were therefore, mutated via site-directed mutagenesis generating E375R and R495E, in order to observe, if any, charge-dependent activity restoration following transfection. Particularly, we investigated the role of these residues in macropore formation (as measurement of dye-uptake YOPRO-1) and phospholipids scrambling activity (as a function of Annexin-V fluorophore intensity). Thus, addressing both P2X7 and TMEM16F proteins molecular hallmarks. This challenging work was performed on transfected HEK293TΔ and HEK293T wild type cell lineages. Surprisingly, results showed significant reductions in both assays when P2X7_E375R was cotransfected with WT TMEM16F_R495R residue, and rescued following residues swapping (i.e., E375R_R495E). Notably, we successfully demonstrated that E375R, considering its remarkable location, influenced the receptor response to ATP sensitisation in HEK293T WT cells. In addition to this, we also explored the role of intracellular Ca^{2+} in proper complex functioning. We observed that both BAPTA-AM and EGTA-AM resulted in a significant reduction of the scrambling activity in HEK293T-WT but not in HEK239TΔ – as if the physical coupling between the two proteins was sufficient to include PS externalisation. Nevertheless, as of now, we cannot entirely exclude the participation of another TMEM16 member engaging in PS externalisation, as indicated by qRT-PCR mRNA assessments. Furthermore, we presented evidence of a potential correlation between pore formation and lipid scrambling – perhaps, this suggests that P2X7R requires the activation of downstream TMEM16F channel for initiation of innate immune cytotoxic functions.

Ultimately, in Chapter 5, we identified for the first time a potential region within P2X7R that may be used as a pharmacological target given its inhibitory activity. Because of the use of overexpressed system (i.e., HEK293T cell lineages), we explored whether the complex aided in cell death regulation and inflammation in macrophages expressing both proteins endogenously. Using custom-made cell penetrating HIV-1-TAT peptides, we demonstrated for the implications of P2X7 cytoplasmic anchor in the regulation of caspase-3/7 activation and pro-inflammatory cytokines secretion, such as TNFα and IL-

1β (IL-1β; data not shown, currently in progress) in primary macrophages and RAW246.7 macrophages, respectively. Both represent important hallmarks of inflammation. However, mechanisms and physiological significance of this unusual pro-inflammatory activity occurring in inflammatory microenvironments are currently elusive. Together, in this thesis, we also contributed to unravel cytotoxic mechanisms attributed to P2X7 activation, which have remained, for many years, poorly addressed. Although, recent advances have unveiled the potential structural processes of caspase-activating cascade – the inflammasome – specific mechanisms that trigger inflammation are still unclear. Collectively, our findings provide evidence for an intriguing scenario, in which coupling between P2X7R and TMEM16F create the foundation for optimal initiation of innate immune response. Accordingly, this research thesis identified promising pharmacological targets for anti-inflammatory drugs development that may aid in further understanding immune-tumour interactions and immunotherapy.

6.1 Novel therapeutic approaches

Inflammation is part of an intricate immunological complex acting as the body's first response of vascular tissues to foreign stimuli, damaged cells, or irritants (Mehta et al., 2014). The secretion of proinflammatory cytokines is a fundamental aspect of the immune and metabolic responses serving as initial defensive attempt to the injurious stimuli. Indeed, controlled proinflammatory cytokines secretions including ILs and TNFα may promote beneficial inflammatory responses to constrain infection and tissue injury by aiding in local coagulation (Mehta et al., 2014). Termination and/or attenuation of an inflammatory response may also be achieved by in vivo production of inflammatory mediators, such as tissue growth factor-β (TGF-β) and prostaglandins (PGs) from macrophages as well as apoptosis of pro-inflammatory cells (Mehta et al., 2014). Notably, non-steroidal anti-inflammatory drugs (NSAIDs) including COX enzymes inhibitors, which reduce production of prostaglandins are the most widely known and used anti-inflammatory medications (these include ibuprofen, aspirin, and naproxen) (Allaj et al., 2013; Mehta et al., 2014) currently available on the market. Despite their effectiveness in

the management of pain, chronic use of NSAIDs have been associated with severe side effects including kidney impairment, gastrointestinal damage, cardiovascular injuries, and reduced platelet aggregation, to name but just a few (Mehta et al., 2014). In this regard, current anti-inflammatory research has been greatly developed around molecular targets such as receptors or enzymes involved in inflammatory pathways. Several important immunological functions have been attributed to P2X7 receptors and subsequent TMEM16F channels activation, as extensively discussed in this thesis work; yet no clinical review article and/or clinical trial have been discussed in the literature. Conclusively, our efforts to integrate the C-cys anchor of P2X7R as novel therapeutic target for drug development, should certainly provide my jury board readership vital information to further innovate this field of research.

6.2 Future work

In this section, we shall discuss potential applications of P2X7 C-cys anchor HIV-1 TAT peptide for the preclinical development of a mouse model for the treatment of multiple sclerosis. Particularly, we focused on MS because of its pathophysiology defined by macrophage accumulation and inflammatory cells infiltrating into the CNS that are responsible for demyelinating. Given our promising findings in macrophages, and the reported increased immunoreactivity of P2X7 in activated macrophages/microglia exploring the potential implications of the receptor cytoplasmic C-anchor and TMEM16F in MS animal model would perhaps present a new therapeutic path.

6.2.1 Towards novel therapeutics

6.2.1.1 PROJECT TITLE

Adenovirus-mediated P2X7 cytoplasmic anchor targeted TAT-peptide delivery in multiple sclerosis mice brain

6.2.1.2 Summary of proposed research & goals

Multiple sclerosis (MS) is a chronic debilitating disease of the central nervous system (CNS) defined by a severe aggregation of immune cells, demyelination, and axonal injury (Domercq & Matute, 2019). Signs and symptoms vary among MS patients depending on the amount of nerves affected. No cure is currently available for multiple sclerosis and recent treatments include cladribine for relapsing-remitting MS and secondary progressive MS (Deeks, 2018). Due to robust accumulations of macrophages and microgliosis, targeting of myeloid lineages may represent an attractive therapeutic approach. Purinoceptors, mostly P2X7, together with TMEM16 family are potent regulators of immune cell functions as shown by our recent work outlined in this thesis. Thus, being able to interfere with/or regulate the cytotoxicity functions of P2X7 receptor at the cellular level may represent a new therapeutic target to MS, but also other purinergic-related disorders. Accordingly, the key objectives of this research are to implement a preclinical study using experimental autoimmune encephalomyelitis (EAE) mice – widely used as clinical MS murine models – for monocytes assessments of cytokines pool secretions, changes in brain tissues morphology; with the ultimate goal to deliver an adeno-associated virus (AAV)-mediated P2X7 TAT delivery in EAE mice brain for evaluation of immune cells infiltration as compared to wield type (WT) mice.

Importantly, MS an apparent low genetic heritability with monozygotic or identical twins showing a higher clinical concordance rate estimated at 25% as compared to dizygotic or fraternal twins rate of about 3% (Patsopoulos, 2018). Hence, given the poorly understood etiology of this debilitating conditions failure to develop proper diagnosis is often associated to both genetic and environmental influences correlated with MS. Furthermore, MS affects over 2.8 million people globally as for 2020 (Walton et al., 2020) – that corresponds to someone, somewhere in the world, being diagnosed with MS every 5 minutes – as asserted by the national multiple sclerosis society (www.atlasofms.org). The disease often manifests at a highly dynamic stage of life when individuals are building professional careers and/or families. Thus, MS can have significant effects on society. Very little is known about the etiology of the disease and a cure is still lacking. In this

future study, an adenovirus-mediated therapeutic will be constructed directly targeting P2X7 receptors in experimental autoimmune encephalomyelitis mice in order to validate the efficacy of our previously outlined data.

6.2.1.3 Details of research project

At the pathophysiological level, hallmarks of MS include plaques of inflammatory demyelination within the white matter of the CNS (G. F. Wu & Alvarez, 2011) with lesions affecting the brainstem, cerebellum, spinal cord and optic nerve. Lesions comprise an extensive alteration of neural-immunologic effector mechanisms constituting the pathogenicity of MS. In the relapse-remitting phase of MS, for instance, the immune cell response involves an autoreactive infiltration of T- and activated B-cells along with monocytes, natural killer T cells, and dendritic cells mounting aberrant responses against myelin antigens (Domercq & Matute, 2019). Significant research has been done recently to better understand the MS-related axonal damage mechanism process. Notably, macrophages and/or macroglia found in the proximity of damaged neurons have been shown to initiate the release of proinflammatory cytokines such as TNFα, reactive nitrogen species (ROS), and proteases contributing to the disruption of the blood-brain barrier, demyelination, and, ultimately, loss of axonal conduction (G. F. Wu & Alvarez, 2011).

Persistent P2X7R activation induces direct excitotoxicity by Ca^{2+} overload in neurons leading to MS lesions (Domercq & Matute, 2019). Importantly, treatments with P2X7 antagonists have been shown to improve chronic EAE recovery in vivo (Domercq & Matute, 2019). Although promising, it is worth noting that long-term treatments with P2X7 antagonists may lead to deleterious adverse events – especially given its downstream activation of TMEM16F channels, and subsequent immune effector function. Accordingly, based on our recent research data suggesting strong attenuations of inflammatory cytokines and caspases activities in macrophages – here, we propose a first of a kind pre-clinical study using AAV-induced P2X7 C-cys anchor TAT-peptide delivery in EAE mice to further understand the therapeutic effects for novel drug development approaches.

Non-pathogenic AVVs belonging to the Parvoviridae family consist of small non-enveloped viruses and are commonly used in research for expression of exogenous genetic materials. In this research, we will use an AdEeasy adenoviral vector system in which all viral genes are replaced by the P2X7-C-cys anchor TAT-peptide, maintaining only the inverted terminal repeats (ITRs) – that is required for viral replication and vector production. Research objectives include (i) characterisation and confirmation of P2X7R expression in peripheral monocytes deriving from EAE mice; (ii) generation of AdEasy adenoviral vectors carrying P2X7-TAT peptides for subsequent delivery in EAE mice brains; (iii) morphological assessments of oligodendrocytes and/axons damage determining early MS diagnosis preceding immune reactivity by immunohistochemistry and confocal microscopy; (iv) evaluation of potential cytotoxicity deriving from AAV-mediated TAT delivery; (v) identification of inflammation hallmarks including proinflammatory cytokines (IL-1β, TNFα, IL-6 and others), ROS, and proteases using ELISA, ELISpot as well as detection of maturation markers by FACS; (vi) characterisation of extrinsic/ intrinsic apoptosis and subsequent contribution of TMEM16F to caspase 3/7 activation; and (vii) Measurements of locomotor activity behaviours comparing therapeutic efficacy of AVV-injected P2X7-C-cys anchor TAT-peptides against placebo.

6.3 Concluding remarks

The study of P2X7 and TMEM16F complex in relation to immune system function is an intriguing and pertinent matter that bridges essential questions about how purinergic signalling initiate complex network interactions with other molecules, regulating fundamental cellular processes. In this regard, deregulation or malfunctioning of such system underline the origins of several disorders, notably neurodegeneration, inflammation, and cancer. Important progress has been made in this research in characterising P2X7 and TMEM16F complex interaction, and in linking diverse intracellular processes into a common dynamic system, which led to the discovery of a novel immunoregulatory region for drug development. Despite this, important question as to whether TMEM16F downstream activation directly contributes to P2X7 cytotoxic functions still remain largely unknown. Ultimately, this thesis has highlighted the need to translate these new therapeutics into pre-clinical research.

Bibliography

Abbracchio, M. P., Burnstock, G., Boeynaems, J.-M., Barnard, E. A., Boyer, J. L., Kennedy, C., Knight, G. E., Fumagalli, M., Gachet, C., Jacobson, K. A., & Weisman, G. A. (2006). International Union of Pharmacology LVIII : Update on the P2Y G protein-coupled nucleotide receptors: from molecular mechanisms and pathophysiology to therapy. *Pharmacological Reviews*, *58*(3), 281-341. https://doi.org/10.1124/pr.58.3.3

Akkari, R., Burbiel, J., Hockemeyer, J., & Muller, C. (2006). Recent Progress in the Development of Adenosine Receptor Ligands as Antiinflammatory Drugs. *Current Topics in Medicinal Chemistry*, *6*(13), 1375-1399. https://doi.org/10.2174/15680266106061375

Akrap, N., Seidel, T., & Barisas, B. G. (2010). Förster distances for fluorescence resonant energy transfer between mCherry and other visible fluorescent proteins. *Analytical Biochemistry*, *402*(1), 105-106. https://doi.org/10.1016/j.ab.2010.03.026

Albertazzi, L., Arosio, D., Marchetti, L., Ricci, F., & Beltram, F. (2009). Quantitative FRET Analysis With the E ^{0} GFP-mCherry Fluorescent Protein Pair. *Photochemistry and Photobiology*, *85*(1), 287-297. https://doi.org/10.1111/j.1751-1097.2008.00435.x

Alberto, A. V. P., Faria, R. X., Couto, C. G. C., Ferreira, L. G. B., Souza, C. A. M., Teixeira, P. C. N., Fróes, M. M., & Alves, L. A. (2013). Is pannexin the pore associated with the P2X7 receptor? *Naunyn-Schmiedeberg's Archives of Pharmacology*, *386*(9), 775-787. https://doi.org/10.1007/s00210-013-0868-x

Allaj, V., Guo, C., & Nie, D. (2013). Non-steroid anti-inflammatory drugs, prostaglandins, and cancer. *Cell & Bioscience*, *3*(1), 8. https://doi.org/10.1186/2045-3701-3-8

Almén, M. S., Nordström, K. J. V., Fredriksson, R., & Schiöth, H. B. (2009). Mapping the human membrane proteome : A majority of the human membrane proteins can be classified according to function and evolutionary origin. *BMC Biology*, *7*, 50. https://doi.org/10.1186/1741-7007-7-50

Alvadia, C., Lim, N. K., Clerico Mosina, V., Oostergetel, G. T., Dutzler, R., & Paulino, C. (2019). Cryo-EM structures and functional characterization of the murine lipid scramblase TMEM16F. *ELife*, *8*, e44365. https://doi.org/10.7554/eLife.44365

Amadio, S., Parisi, C., Piras, E., Fabbrizio, P., Apolloni, S., Montilli, C., Luchetti, S., Ruggieri, S., Gasperini, C., Laghi-Pasini, F., Battistini, L., & Volonté, C. (2017). Modulation of P2X7 Receptor during Inflammation in Multiple Sclerosis. *Frontiers in Immunology*, *8*, 1529. https://doi.org/10.3389/fimmu.2017.01529

Ambudkar, S. V., Kim, I.-W., Xia, D., & Sauna, Z. E. (2006). The A-loop, a novel conserved aromatic acid subdomain upstream of the Walker A motif in ABC transporters, is critical for ATP binding. *FEBS Letters*, *580*(4), 1049-1055. https://doi.org/10.1016/j.febslet.2005.12.051

Ambudkar, S. V., Kimchi-Sarfaty, C., Sauna, Z. E., & Gottesman, M. M. (2003). P-glycoprotein : From genomics to mechanism. *Oncogene*, *22*(47), 7468-7485. https://doi.org/10.1038/sj.onc.1206948

An, S., Deng, Y., Tomsho, J. W., Kyoung, M., & Benkovic, S. J. (2010). Microtubule-assisted mechanism for functional metabolic macromolecular complex formation. *Proceedings of the National Academy of Sciences of the United States of America*, *107*(29), 12872-12876. https://doi.org/10.1073/pnas.1008451107

An, S., Kumar, R., Sheets, E. D., & Benkovic, S. J. (2008). Reversible Compartmentalization of de Novo Purine Biosynthetic Complexes in Living Cells. *Science*, *320*(5872), 103-106. https://doi.org/10.1126/science.1152241

Annereau, J.-P., Wulbrand, U., Vankeerberghen, A., Cuppens, H., Bontems, F., Tümmler, B., Cassiman, J.-J., & Stoven, V. (1997). A novel model for the first nucleotide binding domain of the cystic fibrosis transmembrane conductance regulator. *FEBS Letters*, *407*(3), 303-308. https://doi.org/10.1016/S0014-5793(97)00363-3

Aronoff, D. M., Carstens, J. K., Chen, G.-H., Toews, G. B., & Peters-Golden, M. (2006). *Short Communication* : Differences Between Macrophages and Dendritic Cells in the Cyclic AMP-Dependent Regulation of Lipopolysaccharide-Induced Cytokine and Chemokine Synthesis. *Journal of Interferon & Cytokine Research*, *26*(11), 827-833. https://doi.org/10.1089/jir.2006.26.827

Askew, K., Li, K., Olmos-Alonso, A., Garcia-Moreno, F., Liang, Y., Richardson, P., Tipton, T., Chapman, M. A., Riecken, K., Beccari, S., Sierra, A., Molnár, Z., Cragg, M. S., Garaschuk, O., Perry, V. H., & Gomez-Nicola, D. (2017). Coupled Proliferation and Apoptosis Maintain the Rapid Turnover of Microglia in the Adult Brain. *Cell Reports*, *18*(2), 391-405. https://doi.org/10.1016/j.celrep.2016.12.041

Azevedo, V. F., Kos, I. A., Vargas-Santos, A. B., da Rocha Castelar Pinheiro, G., & Dos Santos Paiva, E. (2019). Benzbromarone in the treatment of gout. *Advances in*

Rheumatology (London, England), *59*(1), 37. https://doi.org/10.1186/s42358-019-0080-x

Bae, J. Y., Lee, S.-W., Shin, Y.-H., Lee, J.-H., Jahng, J. W., & Park, K. (2017). P2X7 receptor and NLRP3 inflammasome activation in head and neck cancer. *Oncotarget*, *8*(30), 48972-48982. https://doi.org/10.18632/oncotarget.16903

Bai, F., Morimoto, Y. V., Yoshimura, S. D. J., Hara, N., Kami-ike, N., Namba, K., & Minamino, T. (2014). Assembly dynamics and the roles of FliI ATPase of the bacterial flagellar export apparatus. *Scientific Reports*, *4*(1), 6528. https://doi.org/10.1038/srep06528

Bajar, B. T., Wang, E. S., Zhang, S., Lin, M. Z., & Chu, J. (2016). A Guide to Fluorescent Protein FRET Pairs. *Sensors (Basel, Switzerland)*, *16*(9), E1488. https://doi.org/10.3390/s16091488

Bakker, W. W., Donker, R. B., Timmer, A., van Pampus, M. G., van Son, W. J., Aarnoudse, J. G., van Goor, H., Niezen-Koning, K. E., Navis, G., Borghuis, T., Jongman, R. M., & Faas, M. M. (2007). Plasma Hemopexin Activity in Pregnancy and Preeclampsia. *Hypertension in Pregnancy*, *26*(2), 227-239. https://doi.org/10.1080/10641950701274896

Banchereau, J., & Steinman, R. M. (1998). Dendritic cells and the control of immunity. *Nature*, *392*(6673), 245-252. https://doi.org/10.1038/32588

Batti, L., Sundukova, M., Murana, E., Pimpinella, S., De Castro Reis, F., Pagani, F., Wang, H., Pellegrino, E., Perlas, E., Di Angelantonio, S., Ragozzino, D., & Heppenstall, P. A. (2016). TMEM16F Regulates Spinal Microglial Function in Neuropathic Pain States. *Cell Reports*, *15*(12), 2608-2615. https://doi.org/10.1016/j.celrep.2016.05.039

Becker, W., & Hickl (2021). The bh TCSPC handbook. 9th edition. Available on www.becker-hickl.com

Bender, A. T., & Beavo, J. A. (2006). Cyclic nucleotide phosphodiesterases : Molecular regulation to clinical use. *Pharmacological Reviews*, *58*(3), 488-520. https://doi.org/10.1124/pr.58.3.5

Benedetto, R., Ousingsawat, J., Cabrita, I., Pinto, M., Lérias, J. R., Wanitchakool, P., Schreiber, R., & Kunzelmann, K. (2019). Plasma membrane-localized TMEM16 proteins are indispensable for expression of CFTR. *Journal of Molecular Medicine (Berlin, Germany)*, *97*(5), 711-722. https://doi.org/10.1007/s00109-019-01770-4

Benninger, R. K. P., & Piston, D. W. (2013). Two-Photon Excitation Microscopy for the Study of Living Cells and Tissues. *Current Protocols in Cell Biology*, *59*(1). https://doi.org/10.1002/0471143030.cb0411s59

Bereiter-Hahn, J., Stübig, C., & Heymann, V. (1995). Cell cycle-related changes in F-actin distribution are correlated with glycolytic activity. *Experimental Cell Research*, *218*(2), 551-560. https://doi.org/10.1006/excr.1995.1190

Bevers, E. M., & Williamson, P. L. (2016). Getting to the Outer Leaflet : Physiology of Phosphatidylserine Exposure at the Plasma Membrane. *Physiological Reviews*, *96*(2), 605-645. https://doi.org/10.1152/physrev.00020.2015

Bhagavan, N. V., & Ha, C.-E. (2015). Nucleotide Metabolism. In *Essentials of Medical Biochemistry* (p. 465-487). Elsevier. https://doi.org/10.1016/B978-0-12-416687-5.00025-7

Boison, D. (2006). Adenosine kinase, epilepsy and stroke : Mechanisms and therapies. *Trends in Pharmacological Sciences*, *27*(12), 652-658. https://doi.org/10.1016/j.tips.2006.10.008

Boland, K., Flanagan, L., & Prehn, J. H. (2013). Paracrine control of tissue regeneration and cell proliferation by Caspase-3. *Cell Death & Disease*, *4*(7), e725-e725. https://doi.org/10.1038/cddis.2013.250

Bos, J. L. (2003). Epac : A new cAMP target and new avenues in cAMP research. *Nature Reviews Molecular Cell Biology*, *4*(9), 733-738. https://doi.org/10.1038/nrm1197

Bos, J. L. (2006). Epac proteins : Multi-purpose cAMP targets. *Trends in Biochemical Sciences*, *31*(12), 680-686. https://doi.org/10.1016/j.tibs.2006.10.002

Bouma, M. G., van den Wildenberg, F. A., & Buurman, W. A. (1996). Adenosine inhibits cytokine release and expression of adhesion molecules by activated human endothelial cells. *American Journal of Physiology-Cell Physiology*, *270*(2), C522-C529. https://doi.org/10.1152/ajpcell.1996.270.2.C522

Bours, M. J. L., Swennen, E. L. R., Di Virgilio, F., Cronstein, B. N., & Dagnelie, P. C. (2006). Adenosine 5'-triphosphate and adenosine as endogenous signaling molecules in immunity and inflammation. *Pharmacology & Therapeutics*, *112*(2), 358-404. https://doi.org/10.1016/j.pharmthera.2005.04.013

Brenner, B., & Eisenberg, E. (1987). The mechanism of muscle contraction. Biochemical, mechanical, and structural approaches to elucidate cross-bridge action in muscle. *Basic Research in Cardiology*, *82 Suppl 2*, 3-16. https://doi.org/10.1007/978-3-662-11289-2_1

Brown, K. M., Lee, L. C. Y., Findlay, J. E., Day, J. P., & Baillie, G. S. (2012). Cyclic AMP-specific phosphodiesterase, PDE8A1, is activated by protein kinase A-mediated phosphorylation. *FEBS Letters*, *586*(11), 1631-1637. https://doi.org/10.1016/j.febslet.2012.04.033

Brunner, J. D., Lim, N. K., Schenck, S., Duerst, A., & Dutzler, R. (2014). X-ray structure of a calcium-activated TMEM16 lipid scramblase. *Nature*, *516*(7530), 207-212. https://doi.org/10.1038/nature13984

Burnstock, G. (1990). Classification and Characterization of Purinoceptors. In K. A. Jacobson, J. W. Daly, & V. Manganiello (Éds.), *Purines in Cellular Signaling* (p. 241-253). Springer. https://doi.org/10.1007/978-1-4612-3400-5_36

Burnstock, G. (2006). Purinergic signalling. *British Journal of Pharmacology*, *147 Suppl 1*, S172-181. https://doi.org/10.1038/sj.bjp.0706429

Burnstock, G. (2008). Purinergic signalling and disorders of the central nervous system. *Nature Reviews. Drug Discovery*, *7*(7), 575-590. https://doi.org/10.1038/nrd2605

Burnstock, G. (2017). Purinergic Signalling : Therapeutic Developments. *Frontiers in Pharmacology*, *8*, 661. https://doi.org/10.3389/fphar.2017.00661

Burnstock, G. (2018a). Purine and purinergic receptors. *Brain and Neuroscience Advances*, *2*, 2398212818817494. https://doi.org/10.1177/2398212818817494

Burnstock, G. (2018b). Purine and purinergic receptors. *Brain and Neuroscience Advances*, *2*, 2398212818817494. https://doi.org/10.1177/2398212818817494

Burnstock, G., Campbell, G., Satchell, D., & Smythe, A. (1970). Evidence that adenosine triphosphate or a related nucleotide is the transmitter substance released by non-adrenergic inhibitory nerves in the gut. *British Journal of Pharmacology*, *40*(4), 668-688. https://doi.org/10.1111/j.1476-5381.1970.tb10646.x

Burnstock, G., Cocks, T., Kasakov, L., & Wong, H. K. (1978). Direct evidence for ATP release from non-adrenergic, non-cholinergic ("purinergic") nerves in the guinea-pig taenia coli and bladder. *European Journal of Pharmacology*, *49*(2), 145-149. https://doi.org/10.1016/0014-2999(78)90070-5

Burnstock, G., & Knight, G. E. (2004). Cellular distribution and functions of P2 receptor subtypes in different systems. *International Review of Cytology*, *240*, 31-304. https://doi.org/10.1016/S0074-7696(04)40002-3

Burnstock, G., & Knight, G. E. (2018). The potential of P2X7 receptors as a therapeutic target, including inflammation and tumour progression. *Purinergic Signalling*, *14*(1), 1-18. https://doi.org/10.1007/s11302-017-9593-0

Burnstock, G., & Verkhratsky, A. (2010). Long-term (trophic) purinergic signalling : Purinoceptors control cell proliferation, differentiation and death. *Cell Death & Disease*, *1*, e9. https://doi.org/10.1038/cddis.2009.11

Camici, Garcia-Gil, Pesi, Allegrini, & Tozzi. (2019). Purine-Metabolising Enzymes and Apoptosis in Cancer. *Cancers*, *11*(9), 1354. https://doi.org/10.3390/cancers11091354

Cantin, A. M. (2022). The P2X7 Receptor in Cystic Fibrosis Monocytes : Linking CFTR Deficiency to Inflammation. *American Journal of Respiratory and Critical Care Medicine*, *205*(7), 740-742. https://doi.org/10.1164/rccm.202201-0008ED

Cella, M., Scheidegger, D., Palmer-Lehmann, K., Lane, P., Lanzavecchia, A., & Alber, G. (1996). Ligation of CD40 on dendritic cells triggers production of high levels of interleukin-12 and enhances T cell stimulatory capacity : T-T help via APC activation. *The Journal of Experimental Medicine*, *184*(2), 747-752. https://doi.org/10.1084/jem.184.2.747

Chan, C. W., Crafton, E., Fan, H.-N., Flook, J., Yoshimura, K., Skarica, M., Brockstedt, D., Dubensky, T. W., Stins, M. F., Lanier, L. L., Pardoll, D. M., & Housseau, F. (2006). Interferon-producing killer dendritic cells provide a link between innate

and adaptive immunity. *Nature Medicine*, *12*(2), 207-213. https://doi.org/10.1038/nm1352

Chan, C. Y., Pedley, A. M., Kim, D., Xia, C., Zhuang, X., & Benkovic, S. J. (2018). Microtubule-directed transport of purine metabolons drives their cytosolic transit to mitochondria. *Proceedings of the National Academy of Sciences*, *115*(51), 13009-13014. https://doi.org/10.1073/pnas.1814042115

Cheffer, A., Castillo, A. R. G., Corrêa-Velloso, J., Gonçalves, M. C. B., Naaldijk, Y., Nascimento, I. C., Burnstock, G., & Ulrich, H. (2018). Purinergic system in psychiatric diseases. *Molecular Psychiatry*, *23*(1), 94-106. https://doi.org/10.1038/mp.2017.188

Chen, H., & Zhang, Y.-H. P. J. (2021). Enzymatic regeneration and conservation of ATP : Challenges and opportunities. *Critical Reviews in Biotechnology*, *41*(1), 16-33. https://doi.org/10.1080/07388551.2020.1826403

Chen, K. W., Demarco, B., Heilig, R., Shkarina, K., Boettcher, A., Farady, C. J., Pelczar, P., & Broz, P. (2019). Extrinsic and intrinsic apoptosis activate pannexin-1 to drive NLRP3 inflammasome assembly. *The EMBO Journal*, *38*(10), e101638. https://doi.org/10.15252/embj.2019101638

Chen, Y., Corriden, R., Inoue, Y., Yip, L., Hashiguchi, N., Zinkernagel, A., Nizet, V., Insel, P. A., & Junger, W. G. (2006). ATP Release Guides Neutrophil Chemotaxis via P2Y2 and A3 Receptors. *Science*, *314*(5806), 1792-1795. https://doi.org/10.1126/science.1132559

Chhabra, E. S., & Higgs, H. N. (2007). The many faces of actin : Matching assembly factors with cellular structures. *Nature Cell Biology*, *9*(10), 1110-1121. https://doi.org/10.1038/ncb1007-1110

Cho, K. (2004). Advances in chromatin remodeling and human disease. *Current Opinion in Genetics & Development*, *14*(3), 308-315. https://doi.org/10.1016/j.gde.2004.04.015

Choi, D.-S., Cascini, M.-G., Mailliard, W., Young, H., Paredes, P., McMahon, T., Diamond, I., Bonci, A., & Messing, R. O. (2004). The type 1 equilibrative nucleoside transporter regulates ethanol intoxication and preference. *Nature Neuroscience*, *7*(8), 855-861. https://doi.org/10.1038/nn1288

Chou, K., & Dennis, A. (2015). Förster Resonance Energy Transfer between Quantum Dot Donors and Quantum Dot Acceptors. *Sensors*, *15*(6), 13288-13325. https://doi.org/10.3390/s150613288

Ciruela, F., Casadó, V., Rodrigues, R. J., Luján, R., Burgueño, J., Canals, M., Borycz, J., Rebola, N., Goldberg, S. R., Mallol, J., Cortés, A., Canela, E. I., López-Giménez, J. F., Milligan, G., Lluis, C., Cunha, R. A., Ferré, S., & Franco, R. (2006). Presynaptic control of striatal glutamatergic neurotransmission by adenosine A1-A2A receptor heteromers. *The Journal of Neuroscience: The Official Journal of the Society for Neuroscience*, *26*(7), 2080-2087. https://doi.org/10.1523/JNEUROSCI.3574-05.2006

Clapier, C. R., & Cairns, B. R. (2009). The Biology of Chromatin Remodeling Complexes. *Annual Review of Biochemistry*, *78*(1), 273-304. https://doi.org/10.1146/annurev.biochem.77.062706.153223

Cockcroft, S., & Gomperts, B. D. (1979). ATP induces nucleotide permeability in rat mast cells. *Nature*, *279*(5713), 541-542. https://doi.org/10.1038/279541a0

Conaway, R. C., & Conaway, J. W. (1988). ATP activates transcription initiation from promoters by RNA polymerase II in a reversible step prior to RNA synthesis. *The Journal of Biological Chemistry*, *263*(6), 2962-2968.

Conaway, R. C., & Conaway, J. W. (1989). An RNA polymerase II transcription factor has an associated DNA-dependent ATPase (dATPase) activity strongly stimulated by the TATA region of promoters. *Proceedings of the National Academy of Sciences*, *86*(19), 7356-7360. https://doi.org/10.1073/pnas.86.19.7356

Cooper, G. M. (2000). Structure and Organization of Actin Filaments. *The Cell: A Molecular Approach. 2nd Edition*. https://www.ncbi.nlm.nih.gov/books/NBK9908/

Cristóvão-Ferreira, S., Navarro, G., Brugarolas, M., Pérez-Capote, K., Vaz, S. H., Fattorini, G., Conti, F., Lluis, C., Ribeiro, J. A., McCormick, P. J., Casadó, V., Franco, R., & Sebastião, A. M. (2013). A1R-A2AR heteromers coupled to Gs and G i/0 proteins modulate GABA transport into astrocytes. *Purinergic Signalling*, *9*(3), 433-449. https://doi.org/10.1007/s11302-013-9364-5

Cronstein, B. N. (1994). Adenosine, an endogenous anti-inflammatory agent. *Journal of Applied Physiology*, *76*(1), 5-13. https://doi.org/10.1152/jappl.1994.76.1.5

Cronstein, B. N., Levin, R. I., Philips, M., Hirschhorn, R., Abramson, S. B., & Weissmann, G. (1992). Neutrophil adherence to endothelium is enhanced via adenosine A1 receptors and inhibited via adenosine A2 receptors. *Journal of Immunology (Baltimore, Md.: 1950)*, *148*(7), 2201-2206.

Dang, S., Feng, S., Tien, J., Peters, C. J., Bulkley, D., Lolicato, M., Zhao, J., Zuberbühler, K., Ye, W., Qi, L., Chen, T., Craik, C. S., Jan, Y. N., Minor, D. L., Cheng, Y., & Jan, L. Y. (2017). Cryo-EM structures of the TMEM16A calcium-activated

chloride channel. *Nature*, *552*(7685), 426-429. https://doi.org/10.1038/nature25024

Darby, M., Kuzmiski, J. B., Panenka, W., Feighan, D., & MacVicar, B. A. (2003). ATP Released From Astrocytes During Swelling Activates Chloride Channels. *Journal of Neurophysiology*, *89*(4), 1870-1877. https://doi.org/10.1152/jn.00510.2002

Dasari, A., Choi, J.-S., & Berdis, A. J. (2016). Chemotherapeutic intervention by inhibiting DNA polymerases. In *DNA Repair in Cancer Therapy* (p. 179-224). Elsevier. https://doi.org/10.1016/B978-0-12-803582-5.00007-3

Davidson, A. L., & Chen, J. (2004). ATP-Binding Cassette Transporters in Bacteria. *Annual Review of Biochemistry*, *73*(1), 241-268. https://doi.org/10.1146/annurev.biochem.73.011303.073626

Deeks, E. D. (2018). Cladribine Tablets : A Review in Relapsing MS. *CNS Drugs*, *32*(8), 785-796. https://doi.org/10.1007/s40263-018-0562-0

Deeley, R. G., Westlake, C., & Cole, S. P. C. (2006). Transmembrane Transport of Endo- and Xenobiotics by Mammalian ATP-Binding Cassette Multidrug Resistance Proteins. *Physiological Reviews*, *86*(3), 849-899. https://doi.org/10.1152/physrev.00035.2005

Denk, W., & Webb, W. W. (1990). Optical measurement of picometer displacements of transparent microscopic objects. *Applied Optics*, *29*(16), 2382-2391. https://doi.org/10.1364/AO.29.002382

Di Virgilio, F., Dal Ben, D., Sarti, A. C., Giuliani, A. L., & Falzoni, S. (2017). The P2X7 Receptor in Infection and Inflammation. *Immunity*, *47*(1), 15-31. https://doi.org/10.1016/j.immuni.2017.06.020

Di Virgilio, F., Sarti, A. C., Falzoni, S., De Marchi, E., & Adinolfi, E. (2018). Extracellular ATP and P2 purinergic signalling in the tumour microenvironment. *Nature Reviews. Cancer*, *18*(10), 601-618. https://doi.org/10.1038/s41568-018-0037-0

Di Virgilio, F., Sarti, A. C., & Grassi, F. (2018). Modulation of innate and adaptive immunity by P2X ion channels. *Current Opinion in Immunology*, *52*, 51-59. https://doi.org/10.1016/j.coi.2018.03.026

Di Virgilio, F., Schmalzing, G., & Markwardt, F. (2018). The Elusive P2X7 Macropore. *Trends in Cell Biology*, *28*(5), 392-404. https://doi.org/10.1016/j.tcb.2018.01.005

Di Zanni, E., Gradogna, A., Scholz-Starke, J., & Boccaccio, A. (2018). Gain of function of TMEM16E/ANO5 scrambling activity caused by a mutation associated with gnathodiaphyseal dysplasia. *Cellular and Molecular Life Sciences*, *75*(9), 1657-1670. https://doi.org/10.1007/s00018-017-2704-9

Doktorova, M., Symons, J. L., & Levental, I. (2020). Structural and functional consequences of reversible lipid asymmetry in living membranes. *Nature Chemical Biology*, *16*(12), 1321-1330. https://doi.org/10.1038/s41589-020-00688-0

Domercq, M., & Matute, C. (2019). Targeting P2X4 and P2X7 receptors in multiple sclerosis. *Current Opinion in Pharmacology*, *47*, 119-125. https://doi.org/10.1016/j.coph.2019.03.010

Dou, L., Chen, Y.-F., Cowan, P. J., & Chen, X.-P. (2018). Extracellular ATP signaling and clinical relevance. *Clinical Immunology*, *188*, 67-73. https://doi.org/10.1016/j.clim.2017.12.006

Dowhan, W., Vitrac, H., & Bogdanov, M. (2019). Lipid-Assisted Membrane Protein Folding and Topogenesis. *The Protein Journal*, *38*(3), 274-288. https://doi.org/10.1007/s10930-019-09826-7

Dunning, K., Martz, A., Peralta, F. A., Cevoli, F., Boué-Grabot, E., Compan, V., Gautherat, F., Wolf, P., Chataigneau, T., & Grutter, T. (2021). P2X7 Receptors and TMEM16 Channels Are Functionally Coupled with Implications for Macropore Formation and Current Facilitation. *International Journal of Molecular Sciences*, *22*(12), 6542. https://doi.org/10.3390/ijms22126542

Duran, C., & Hartzell, H. C. (2011). Physiological roles and diseases of Tmem16/Anoctamin proteins : Are they all chloride channels? *Acta Pharmacologica Sinica*, *32*(6), 685-692. https://doi.org/10.1038/aps.2011.48

Dürr, H., Körner, C., Müller, M., Hickmann, V., & Hopfner, K.-P. (2005). X-Ray Structures of the Sulfolobus solfataricus SWI2/SNF2 ATPase Core and Its Complex with DNA. *Cell*, *121*(3), 363-373. https://doi.org/10.1016/j.cell.2005.03.026

Edwards, A. S., & Scott, J. D. (2000). A-kinase anchoring proteins : Protein kinase A and beyond. *Current Opinion in Cell Biology*, *12*(2), 217-221. https://doi.org/10.1016/s0955-0674(99)00085-x

Ehlen, H. W. A., Chinenkova, M., Moser, M., Munter, H.-M., Krause, Y., Gross, S., Brachvogel, B., Wuelling, M., Kornak, U., & Vortkamp, A. (2013). Inactivation of anoctamin-6/Tmem16f, a regulator of phosphatidylserine scrambling in osteoblasts, leads to decreased mineral deposition in skeletal tissues. *Journal of Bone and Mineral Research: The Official Journal of the American Society for Bone and Mineral Research*, *28*(2), 246-259. https://doi.org/10.1002/jbmr.1751

Eichin, D., Laurila, J. P., Jalkanen, S., & Salmi, M. (2015). CD73 Activity is Dispensable for the Polarization of M2 Macrophages. *PLOS ONE*, *10*(8), e0134721. https://doi.org/10.1371/journal.pone.0134721

El-Moatassim, C., Dornand, J., & Mani, J.-C. (1992). Extracellular ATP and cell signalling. *Biochimica et Biophysica Acta (BBA) - Molecular Cell Research*, *1134*(1), 31-45. https://doi.org/10.1016/0167-4889(92)90025-7

Eltzschig, H. K., Abdulla, P., Hoffman, E., Hamilton, K. E., Daniels, D., Schönfeld, C., Löffler, M., Reyes, G., Duszenko, M., Karhausen, J., Robinson, A., Westerman, K. A., Coe, I. R., & Colgan, S. P. (2005). HIF-1–dependent repression of equilibrative nucleoside transporter (ENT) in hypoxia. *Journal of Experimental Medicine*, *202*(11), 1493-1505. https://doi.org/10.1084/jem.20050177

Eltzschig, H. K., Thompson, L. F., Karhausen, J., Cotta, R. J., Ibla, J. C., Robson, S. C., & Colgan, S. P. (2004). Endogenous adenosine produced during hypoxia attenuates neutrophil accumulation : Coordination by extracellular nucleotide metabolism. *Blood*, *104*(13), 3986-3992. https://doi.org/10.1182/blood-2004-06-2066

Enomoto, T., Tanuma, S., & Yamada, M. (1981). ATP Requirement for the Processes of DNA Replication in Isolated HeLa Cell Nuclei1. *The Journal of Biochemistry*, *89*(3), 801-807. https://doi.org/10.1093/oxfordjournals.jbchem.a133262

Entova, S., Billod, J.-M., Swiecicki, J.-M., Martín-Santamaría, S., & Imperiali, B. (2018). Insights into the key determinants of membrane protein topology enable the identification of new monotopic folds. *ELife*, *7*, e40889. https://doi.org/10.7554/eLife.40889

Erdogan, S., & Houslay, M. D. (1997). Challenge of human Jurkat T-cells with the adenylate cyclase activator forskolin elicits major changes in cAMP phosphodiesterase (PDE) expression by up-regulating PDE3 and inducing PDE4D1 and PDE4D2 splice variants as well as down-regulating a novel PDE4A splice variant. *Biochemical Journal*, *321*(1), 165-175. https://doi.org/10.1042/bj3210165

Erlinge, D. (2011). Chapter 13—P2Y Receptors in Health and Disease. In K. A. Jacobson & J. Linden (Éds.), *Advances in Pharmacology* (Vol. 61, p. 417-439). Academic Press. https://doi.org/10.1016/B978-0-12-385526-8.00013-8

Faas, M. M., Sáez, T., & de Vos, P. (2017). Extracellular ATP and adenosine : The Yin and Yang in immune responses? *Molecular Aspects of Medicine*, *55*, 9-19. https://doi.org/10.1016/j.mam.2017.01.002

Falzone, M. E., Malvezzi, M., Lee, B.-C., & Accardi, A. (2018). Known structures and unknown mechanisms of TMEM16 scramblases and channels. *The Journal of General Physiology*, *150*(7), 933-947. https://doi.org/10.1085/jgp.201711957

Falzone, M. E., Rheinberger, J., Lee, B.-C., Peyear, T., Sasset, L., Raczkowski, A. M., Eng, E. T., Di Lorenzo, A., Andersen, O. S., Nimigean, C. M., & Accardi, A. (2019). Structural basis of Ca2+-dependent activation and lipid transport by a TMEM16 scramblase. *ELife*, *8*, e43229. https://doi.org/10.7554/eLife.43229

Faulds, D., Chrisp, P., & Buckley, M. M.-T. (1991). Adenosine. *Drugs*, *41*(4), 596-624. https://doi.org/10.2165/00003495-199141040-00007

Faurschou, M., & Borregaard, N. (2003). Neutrophil granules and secretory vesicles in inflammation. *Microbes and Infection*, *5*(14), 1317-1327. https://doi.org/10.1016/j.micinf.2003.09.008

Fedele, D. E., Li, T., Lan, J. Q., Fredholm, B. B., & Boison, D. (2006). Adenosine A1 receptors are crucial in keeping an epileptic focus localized. *Experimental Neurology*, *200*(1), 184-190. https://doi.org/10.1016/j.expneurol.2006.02.133

Feng, S., Dang, S., Han, T. W., Ye, W., Jin, P., Cheng, T., Li, J., Jan, Y. N., Jan, L. Y., & Cheng, Y. (2019). Cryo-EM Studies of TMEM16F Calcium-Activated Ion Channel Suggest Features Important for Lipid Scrambling. *Cell Reports*, *28*(2), 567-579.e4. https://doi.org/10.1016/j.celrep.2019.06.023

Ferrari, D., Los, M., Bauer, M. K. A., Vandenabeele, P., Wesselborg, S., & Schulze-Osthoff, K. (1999). P2Z purinoreceptor ligation induces activation of caspases with distinct roles in apoptotic and necrotic alterations of cell death. *FEBS Letters*, *447*(1), 71-75. https://doi.org/10.1016/S0014-5793(99)00270-7

Ferrari, D., McNamee, E. N., Idzko, M., Gambari, R., & Eltzschig, H. K. (2016). Purinergic Signaling During Immune Cell Trafficking. *Trends in Immunology*, *37*(6), 399-411. https://doi.org/10.1016/j.it.2016.04.004

Flaus, A. (2006). Identification of multiple distinct Snf2 subfamilies with conserved structural motifs. *Nucleic Acids Research*, *34*(10), 2887-2905. https://doi.org/10.1093/nar/gkl295

Forster, Th. (1946). Energiewanderung und Fluoreszenz. *Die Naturwissenschaften*, *33*(6), 166-175. https://doi.org/10.1007/BF00585226

Fredholm, B. B. (1997). Purines and neutrophil leukocytes. *General Pharmacology: The Vascular System*, *28*(3), 345-350. https://doi.org/10.1016/S0306-3623(96)00169-3

Fredholm, B. B. (2007). Adenosine, an endogenous distress signal, modulates tissue damage and repair. *Cell Death and Differentiation*, *14*(7), 1315-1323. https://doi.org/10.1038/sj.cdd.4402132

Fredholm, B. B., Chen, J.-F., Masino, S. A., & Vaugeois, J.-M. (2005). ACTIONS OF ADENOSINE AT ITS RECEPTORS IN THE CNS : Insights from Knockouts and Drugs. *Annual Review of Pharmacology and Toxicology*, *45*(1), 385-412. https://doi.org/10.1146/annurev.pharmtox.45.120403.095731

Fredholm, B. B., IJzerman, A. P., Jacobson, K. A., Klotz, K. N., & Linden, J. (2001). International Union of Pharmacology. XXV. Nomenclature and classification of adenosine receptors. *Pharmacological Reviews*, *53*(4), 527-552.

French, J. B., Jones, S. A., Deng, H., Pedley, A. M., Kim, D., Chan, C. Y., Hu, H., Pugh, R. J., Zhao, H., Zhang, Y., Huang, T. J., Fang, Y., Zhuang, X., & Benkovic, S. J. (2016). Spatial colocalization and functional link of purinosomes with mitochondria. *Science*, *351*(6274), 733-737. https://doi.org/10.1126/science.aac6054

Fujii, T., & Namba, K. (2017). Structure of actomyosin rigour complex at 5.2 Å resolution and insights into the ATPase cycle mechanism. *Nature Communications*, *8*(1), 13969. https://doi.org/10.1038/ncomms13969

Galluzzi, L., Vitale, I., Aaronson, S. A., Abrams, J. M., Adam, D., Agostinis, P., Alnemri, E. S., Altucci, L., Amelio, I., Andrews, D. W., Annicchiarico-Petruzzelli, M., Antonov, A. V., Arama, E., Baehrecke, E. H., Barlev, N. A., Bazan, N. G., Bernassola, F., Bertrand, M. J. M., Bianchi, K., … Kroemer, G. (2018). Molecular mechanisms of cell death : Recommendations of the Nomenclature Committee on

Cell Death 2018. *Cell Death and Differentiation*, *25*(3), 486-541. https://doi.org/10.1038/s41418-017-0012-4

Gasmi, L., McLennan, A., & Edwards, S. (1996). The diadenosine polyphosphates Ap3A and Ap4A and adenosine triphosphate interact with granulocyte-macrophage colony-stimulating factor to delay neutrophil apoptosis : Implications for neutrophil: platelet interactions during inflammation. *Blood*, *87*(8), 3442-3449. https://doi.org/10.1182/blood.V87.8.3442.bloodjournal8783442

Gershowitz, A., Boone, R. F., & Moss, B. (1978). Multiple roles for ATP in the synthesis and processing of mRNA by vaccinia virus : Specific inhibitory effects of adenosine (beta,gamma-imido) triphosphate. *Journal of Virology*, *27*(2), 399-408. https://doi.org/10.1128/JVI.27.2.399-408.1978

Giuliani, A. L., Colognesi, D., Ricco, T., Roncato, C., Capece, M., Amoroso, F., Wang, Q. G., De Marchi, E., Gartland, A., Di Virgilio, F., & Adinolfi, E. (2014). Trophic activity of human P2X7 receptor isoforms A and B in osteosarcoma. *PloS One*, *9*(9), e107224. https://doi.org/10.1371/journal.pone.0107224

Gödecke, A. (2008). cAMP : Fuel for extracellular adenosine formation? *British Journal of Pharmacology*, *153*(6), 1087-1089. https://doi.org/10.1038/bjp.2008.7

Goepfert, C., Imai, M., Brouard, S., Csizmadia, E., Kaczmarek, E., & Robson, S. C. (2000). CD39 modulates endothelial cell activation and apoptosis. *Molecular Medicine (Cambridge, Mass.)*, *6*(7), 591-603.

Goepfert, C., Sundberg, C., Sévigny, J., Enjyoji, K., Hoshi, T., Csizmadia, E., & Robson, S. (2001). Disordered Cellular Migration and Angiogenesis in *cd39*- Null Mice. *Circulation*, *104*(25), 3109-3115. https://doi.org/10.1161/hc5001.100663

González-Jamett, A. M., Bevilacqua, J. A., & Díaz, A. M. C. (2018). Hereditary Myopathies. In *Muscle Cell and Tissue—Current Status of Research Field*. IntechOpen. https://doi.org/10.5772/intechopen.76076

Gordon, J. L. (1986). Extracellular ATP : Effects, sources and fate. *Biochemical Journal*, *233*(2), 309-319. https://doi.org/10.1042/bj2330309

Grañé-Boladeras, N., Spring, C. M., Hanna, W. J. B., Pastor-Anglada, M., & Coe, I. R. (2016). Novel nuclear hENT2 isoforms regulate cell cycle progression via controlling nucleoside transport and nuclear reservoir. *Cellular and Molecular Life Sciences*, *73*(23), 4559-4575. https://doi.org/10.1007/s00018-016-2288-9

Gray, J. H., Owen, R. P., & Giacomini, K. M. (2004). The concentrative nucleoside transporter family, SLC28. *Pfl*[illegible]*gers Archiv European Journal of Physiology*, *447*(5), 728-734. https://doi.org/10.1007/s00424-003-1107-y

Grimwade, J. E., Rozgaja, T. A., Gupta, R., Dyson, K., Rao, P., & Leonard, A. C. (2018). Origin recognition is the predominant role for DnaA-ATP in initiation of chromosome replication. *Nucleic Acids Research*, *46*(12), 6140-6151. https://doi.org/10.1093/nar/gky457

Guilliams, M., Mildner, A., & Yona, S. (2018). Developmental and Functional Heterogeneity of Monocytes. *Immunity*, *49*(4), 595-613. https://doi.org/10.1016/j.immuni.2018.10.005

Hammond, J. R. (2021). SLC28 and SLC29 families of nucleoside transporters in GtoPdb v.2021.3. *IUPHAR/BPS Guide to Pharmacology CITE*, *2021*(3). https://doi.org/10.2218/gtopdb/F149/2021.3

Harkat, M., Peverini, L., Cerdan, A. H., Dunning, K., Beudez, J., Martz, A., Calimet, N., Specht, A., Cecchini, M., Chataigneau, T., & Grutter, T. (2017). On the permeation

of large organic cations through the pore of ATP-gated P2X receptors. *Proceedings of the National Academy of Sciences of the United States of America*, *114*(19), E3786-E3795. https://doi.org/10.1073/pnas.1701379114

Hartzell, H. C., Yu, K., Xiao, Q., Chien, L.-T., & Qu, Z. (2009). Anoctamin/TMEM16 family members are Ca2+-activated Cl- channels. *The Journal of Physiology*, *587*(Pt 10), 2127-2139. https://doi.org/10.1113/jphysiol.2008.163709

Hauk, G., & Berger, J. M. (2016). The role of ATP-dependent machines in regulating genome topology. *Current Opinion in Structural Biology*, *36*, 85-96. https://doi.org/10.1016/j.sbi.2016.01.006

Hazleton, J. E., Berman, J. W., & Eugenin, E. A. (2012). Purinergic Receptors Are Required for HIV-1 Infection of Primary Human Macrophages. *The Journal of Immunology*, *188*(9), 4488-4495. https://doi.org/10.4049/jimmunol.1102482

Hermann, R., Krajcsi, P., Fluck, M., Seithel-Keuth, A., Bytyqi, A., Galazka, A., & Munafo, A. (2021). Review of Transporter Substrate, Inhibitor, and Inducer Characteristics of Cladribine. *Clinical Pharmacokinetics*, *60*(12), 1509-1535. https://doi.org/10.1007/s40262-021-01065-3

Hershfield, M. (2005). New insights into adenosine-receptor-mediated immunosuppression and the role of adenosine in causing the immunodeficiency associated with adenosine deaminase deficiency. *European Journal of Immunology*, *35*(1), 25-30. https://doi.org/10.1002/eji.200425738

Higgins, C. F. (1992). ABC Transporters : From Microorganisms to Man. *Annual Review of Cell Biology*, *8*(1), 67-113. https://doi.org/10.1146/annurev.cb.08.110192.000435

Higgins, C. F., Haag, P. D., Nikaido, K., Ardeshir, F., Garcia, G., & Ames, G. F. (1982). Complete nucleotide sequence and identification of membrane components of the histidine transport operon of S. typhimurium. *Nature*, *298*(5876), 723-727. https://doi.org/10.1038/298723a0

Hogan, C., & Varga-Weisz, P. (2007). The regulation of ATP-dependent nucleosome remodelling factors. *Mutation Research/Fundamental and Molecular Mechanisms of Mutagenesis*, *618*(1-2), 41-51. https://doi.org/10.1016/j.mrfmmm.2006.07.010

Holland, I. B., Cole, S. P. C., Kuchler, K., & Higgins, C. F. (2003). *ABC Proteins : From Bacteria to Man*. Elsevier.

Hollenstein, K., Dawson, R. J., & Locher, K. P. (2007). Structure and mechanism of ABC transporter proteins. *Current Opinion in Structural Biology*, *17*(4), 412-418. https://doi.org/10.1016/j.sbi.2007.07.003

Honda, S., Sasaki, Y., Ohsawa, K., Imai, Y., Nakamura, Y., Inoue, K., & Kohsaka, S. (2001). Extracellular ATP or ADP induce chemotaxis of cultured microglia through Gi/o-coupled P2Y receptors. *The Journal of Neuroscience: The Official Journal of the Society for Neuroscience*, *21*(6), 1975-1982.

Hönig, M., Albert, M. H., Schulz, A., Sparber-Sauer, M., Schütz, C., Belohradsky, B., Güngör, T., Rojewski, M. T., Bode, H., Pannicke, U., Lippold, D., Schwarz, K., Debatin, K.-M., Hershfield, M. S., & Friedrich, W. (2007). Patients with adenosine deaminase deficiency surviving after hematopoietic stem cell transplantation are at high risk of CNS complications. *Blood*, *109*(8), 3595-3602. https://doi.org/10.1182/blood-2006-07-034678

Honigmann, A., Sadeghi, S., Keller, J., Hell, S. W., Eggeling, C., & Vink, R. (2014). A lipid bound actin meshwork organizes liquid phase separation in model membranes. *eLife*, *3*, e01671. https://doi.org/10.7554/eLife.01671

Hu, Y., Kim, J. H., He, K., Wan, Q., Kim, J., Flach, M., Kirchhausen, T., Vortkamp, A., & Winau, F. (2016). Scramblase TMEM16F terminates T cell receptor signaling to restrict T cell exhaustion. *The Journal of Experimental Medicine*, *213*(12), 2759-2772. https://doi.org/10.1084/jem.20160612

Huang, Z., Xie, N., Illes, P., Di Virgilio, F., Ulrich, H., Semyanov, A., Verkhratsky, A., Sperlagh, B., Yu, S.-G., Huang, C., & Tang, Y. (2021). From purines to purinergic signalling : Molecular functions and human diseases. *Signal Transduction and Targeted Therapy*, *6*(1), 162. https://doi.org/10.1038/s41392-021-00553-z

Hume, D. A., Irvine, K. M., & Pridans, C. (2019). The Mononuclear Phagocyte System : The Relationship between Monocytes and Macrophages. *Trends in Immunology*, *40*(2), 98-112. https://doi.org/10.1016/j.it.2018.11.007

Huxley, H. E. (1969). The mechanism of muscular contraction. *Science (New York, N.Y.)*, *164*(3886), 1356-1365. https://doi.org/10.1126/science.164.3886.1356

Iancu, R. V., Ramamurthy, G., Warrier, S., Nikolaev, V. O., Lohse, M. J., Jones, S. W., & Harvey, R. D. (2008). Cytoplasmic cAMP concentrations in intact cardiac myocytes. *American Journal of Physiology. Cell Physiology*, *295*(2), C414-422. https://doi.org/10.1152/ajpcell.00038.2008

Illes, P., Khan, T. M., & Rubini, P. (2017). Neuronal P2X7 Receptors Revisited : Do They Really Exist? *The Journal of Neuroscience: The Official Journal of the Society for Neuroscience*, *37*(30), 7049-7062. https://doi.org/10.1523/JNEUROSCI.3103-16.2017

Illes, P., Müller, C. E., Jacobson, K. A., Grutter, T., Nicke, A., Fountain, S. J., Kennedy, C., Schmalzing, G., Jarvis, M. F., Stojilkovic, S. S., King, B. F., & Di Virgilio, F. (2021). Update of P2X receptor properties and their pharmacology : IUPHAR Review 30. *British Journal of Pharmacology*, *178*(3), 489-514. https://doi.org/10.1111/bph.15299

Jacobson, K. A., Delicado, E. G., Gachet, C., Kennedy, C., Kügelgen, I., Li, B., Miras-Portugal, M. T., Novak, I., Schöneberg, T., Perez-Sen, R., Thor, D., Wu, B., Yang, Z., & Müller, C. E. (2020). Update of P2Y receptor pharmacology : IUPHAR Review 27. *British Journal of Pharmacology*, *177*(11), 2413-2433. https://doi.org/10.1111/bph.15005

Jacobson, K. A., Ivanov, A. A., de Castro, S., Harden, T. K., & Ko, H. (2009). Development of selective agonists and antagonists of P2Y receptors. *Purinergic Signalling*, *5*(1), 75-89. https://doi.org/10.1007/s11302-008-9106-2

Janeway, C. A., & Medzhitov, R. (2002). Innate immune recognition. *Annual Review of Immunology*, *20*, 197-216. https://doi.org/10.1146/annurev.immunol.20.083001.084359

Janks, L., Sprague, R. S., & Egan, T. M. (2019). ATP-Gated P2X7 Receptors Require Chloride Channels To Promote Inflammation in Human Macrophages. *Journal of Immunology (Baltimore, Md.: 1950)*, *202*(3), 883-898. https://doi.org/10.4049/jimmunol.1801101

Jiang, L.-H., Rassendren, F., Mackenzie, A., Zhang, Y.-H., Surprenant, A., & North, R. A. (2005). N-methyl-D-glucamine and propidium dyes utilize different permeation pathways at rat P2X(7) receptors. *American Journal of Physiology. Cell Physiology*, *289*(5), C1295-1302. https://doi.org/10.1152/ajpcell.00253.2005

Jiang, R., Taly, A., & Grutter, T. (2013). Moving through the gate in ATP-activated P2X receptors. *Trends in Biochemical Sciences*, *38*(1), 20-29. https://doi.org/10.1016/j.tibs.2012.10.006

Jonzon, B., & Fredholm, B. B. (1985). Release of Purines, Noradrenaline, and GABA from Rat Hippocampal Slices by Field Stimulation. *Journal of Neurochemistry*, *44*(1), 217-224. https://doi.org/10.1111/j.1471-4159.1985.tb07133.x

Kaczmarek-Hájek, K., Lörinczi, É., Hausmann, R., & Nicke, A. (2012). Molecular and functional properties of P2X receptors—Recent progress and persisting challenges. *Purinergic Signalling*, *8*(3), 375-417. https://doi.org/10.1007/s11302-012-9314-7

Kaczmarek-Hajek, K., Zhang, J., Kopp, R., Grosche, A., Rissiek, B., Saul, A., Bruzzone, S., Engel, T., Jooss, T., Krautloher, A., Schuster, S., Magnus, T., Stadelmann, C., Sirko, S., Koch-Nolte, F., Eulenburg, V., & Nicke, A. (2018). Re-evaluation of neuronal P2X7 expression using novel mouse models and a P2X7-specific nanobody. *ELife*, *7*, e36217. https://doi.org/10.7554/eLife.36217

Kaguni, J. M. (2006). DnaA : Controlling the Initiation of Bacterial DNA Replication and More. *Annual Review of Microbiology*, *60*(1), 351-371. https://doi.org/10.1146/annurev.micro.60.080805.142111

Kannan, S. (2002). Amplification of extracellular nucleotide-induced leukocyte (S) degranulation by contingent autocrine and paracrine mode of leukotriene mediated chemokine receptor activation. *Medical Hypotheses*, *59*(3), 261-265. https://doi.org/10.1016/S0306-9877(02)00213-X

Karasawa, A., Michalski, K., Mikhelzon, P., & Kawate, T. (2017). The P2X7 receptor forms a dye-permeable pore independent of its intracellular domain but dependent

on membrane lipid composition. *ELife*, *6*, e31186. https://doi.org/10.7554/eLife.31186

Kasuya, G., Fujiwara, Y., Takemoto, M., Dohmae, N., Nakada-Nakura, Y., Ishitani, R., Hattori, M., & Nureki, O. (2016). Structural Insights into Divalent Cation Modulations of ATP-Gated P2X Receptor Channels. *Cell Reports*, *14*(4), 932-944. https://doi.org/10.1016/j.celrep.2015.12.087

Katayama, T., Kasho, K., & Kawakami, H. (2017). The DnaA Cycle in Escherichia coli : Activation, Function and Inactivation of the Initiator Protein. *Frontiers in Microbiology*, *8*, 2496. https://doi.org/10.3389/fmicb.2017.02496

Kaufmann, A., Salentin, R., Meyer, R. G., Bussfeld, D., Pauligk, C., Fesq, H., Hofmann, P., Nain, M., Gemsa, D., & Sprenger, H. (2001). Defense against influenza A virus infection : Essential role of the chemokine system. *Immunobiology*, *204*(5), 603-613. https://doi.org/10.1078/0171-2985-00099

Kawate, T., Michel, J. C., Birdsong, W. T., & Gouaux, E. (2009). Crystal structure of the ATP-gated P2X(4) ion channel in the closed state. *Nature*, *460*(7255), 592-598. https://doi.org/10.1038/nature08198

Keller, H. U. (1983). Motility, cell shape, and locomotion of neutrophil granulocytes. *Cell Motility*, *3*(1), 47-60. https://doi.org/10.1002/cm.970030105

Khakh, B. S., & Burnstock, G. (2009). THE DOUBLE LIFE OF ATP. *Scientific American*, *301*(6), 84-92.

Kitao, A., & Hata, H. (2018). Molecular dynamics simulation of bacterial flagella. *Biophysical Reviews*, *10*(2), 617-629. https://doi.org/10.1007/s12551-017-0338-7

Kochanek, P. M., Vagni, V. A., Janesko, K. L., Washington, C. B., Crumrine, P. K., Garman, R. H., Jenkins, L. W., Clark, R. S., Homanics, G. E., Dixon, C. E.,

Schnermann, J., & Jackson, E. K. (2006). Adenosine A1 Receptor Knockout Mice Develop Lethal Status Epilepticus after Experimental Traumatic Brain Injury. *Journal of Cerebral Blood Flow & Metabolism*, *26*(4), 565-575. https://doi.org/10.1038/sj.jcbfm.9600218

Kong, Q., Wang, M., Liao, Z., Camden, J. M., Yu, S., Simonyi, A., Sun, G. Y., Gonzalez, F. A., Erb, L., Seye, C. I., & Weisman, G. A. (2005). P2X(7) nucleotide receptors mediate caspase-8/9/3-dependent apoptosis in rat primary cortical neurons. *Purinergic Signalling*, *1*(4), 337-347. https://doi.org/10.1007/s11302-005-7145-5

Kopp, R. (2020). *Analysis of P2X7 protein complexes in a P2X7-EGFP BAC transgenic mouse model* [Ludwig-Maximilians-Universität München; Application/pdf]. https://doi.org/10.5282/EDOC.25952

Kopp, R., Krautloher, A., Ramírez-Fernández, A., & Nicke, A. (2019). P2X7 Interactions and Signaling – Making Head or Tail of It. *Frontiers in Molecular Neuroscience*, *12*, 183. https://doi.org/10.3389/fnmol.2019.00183

Koschut, D., Richert, L., Pace, G., Niemann, H. H., Mély, Y., & Orian-Rousseau, V. (2016). Live cell imaging shows hepatocyte growth factor-induced Met dimerization. *Biochimica Et Biophysica Acta*, *1863*(7 Pt A), 1552-1558. https://doi.org/10.1016/j.bbamcr.2016.04.015

Kunzelmann, K., Ousingsawat, J., Benedetto, R., Cabrita, I., & Schreiber, R. (2019). Contribution of Anoctamins to Cell Survival and Cell Death. *Cancers*, *11*(3), 382. https://doi.org/10.3390/cancers11030382

Larjavaara, S., Mäntylä, R., Salminen, T., Haapasalo, H., Raitanen, J., Jääskeläinen, J., & Auvinen, A. (2007). Incidence of gliomas by anatomic location. *Neuro-Oncology*, *9*(3), 319-325. https://doi.org/10.1215/15228517-2007-016

la Sala, A., Ferrari, D., Corinti, S., Cavani, A., Di Virgilio, F., & Girolomoni, G. (2001). Extracellular ATP induces a distorted maturation of dendritic cells and inhibits their capacity to initiate Th1 responses. *Journal of Immunology (Baltimore, Md.: 1950)*, *166*(3), 1611-1617. https://doi.org/10.4049/jimmunol.166.3.1611

Le, T., Jia, Z., Le, S. C., Zhang, Y., Chen, J., & Yang, H. (2019). An inner activation gate controls TMEM16F phospholipid scrambling. *Nature Communications*, *10*(1), 1846. https://doi.org/10.1038/s41467-019-09778-7

Le, T., Le, S. C., & Yang, H. (2019). Drosophila Subdued is a moonlighting transmembrane protein 16 (TMEM16) that transports ions and phospholipids. *The Journal of Biological Chemistry*, *294*(12), 4529-4537. https://doi.org/10.1074/jbc.AC118.006530

Le, T.-T. T., Berg, N. K., Harting, M. T., Li, X., Eltzschig, H. K., & Yuan, X. (2019). Purinergic Signaling in Pulmonary Inflammation. *Frontiers in Immunology*, *10*, 1633. https://doi.org/10.3389/fimmu.2019.01633

Lee, B.-C., Khelashvili, G., Falzone, M., Menon, A. K., Weinstein, H., & Accardi, A. (2018). Gating mechanism of the extracellular entry to the lipid pathway in a TMEM16 scramblase. *Nature Communications*, *9*(1), 3251. https://doi.org/10.1038/s41467-018-05724-1

Lee, J., Kim, T. H., Murray, F., Li, X., Choi, S. S., Broide, D. H., Corr, M., Lee, J., Webster, N. J. G., Insel, P. A., & Raz, E. (2015). Cyclic AMP concentrations in dendritic cells induce and regulate Th2 immunity and allergic asthma. *Proceedings of the National Academy of Sciences*, *112*(5), 1529-1534. https://doi.org/10.1073/pnas.1417972112

Lee, Y.-S., Lee, J. K., Bae, Y., Lee, B.-S., Kim, E., Cho, C.-H., Ryoo, K., Yoo, J., Kim, C.-H., Yi, G.-S., Lee, S.-G., Lee, C. J., Kang, S. S., Hwang, E. M., & Park, J.-Y. (2016). Suppression of 14-3-3γ-mediated surface expression of ANO1 inhibits cancer progression of glioblastoma cells. *Scientific Reports*, *6*, 26413. https://doi.org/10.1038/srep26413

Lehninger, A. L., Nelson, D. L., & Cox, M. M. (2008). *Lehninger principles of biochemistry* (5th ed). W.H. Freeman.

Leone, R. D., & Emens, L. A. (2018). Targeting adenosine for cancer immunotherapy. *Journal for ImmunoTherapy of Cancer*, *6*(1), 57. https://doi.org/10.1186/s40425-018-0360-8

Li, M., Toombes, G. E. S., Silberberg, S. D., & Swartz, K. J. (2015). Physical basis of apparent pore dilation of ATP-activated P2X receptor channels. *Nature Neuroscience*, *18*(11), 1577-1583. https://doi.org/10.1038/nn.4120

Li, M., Wang, Y., Banerjee, R., Marinelli, F., Silberberg, S., Faraldo-Gómez, J. D., Hattori, M., & Swartz, K. J. (2019). Molecular mechanisms of human P2X3 receptor channel activation and modulation by divalent cation bound ATP. *ELife*, *8*, e47060. https://doi.org/10.7554/eLife.47060

Lin, A., Du, Y., & Xiao, W. (2020). Yeast chromatin remodeling complexes and their roles in transcription. *Current Genetics*, *66*(4), 657-670. https://doi.org/10.1007/s00294-020-01072-0

Lin, C.-C., & Edelson, B. T. (2017). New Insights into the Role of IL-1β in Experimental Autoimmune Encephalomyelitis and Multiple Sclerosis. *The Journal of Immunology*, *198*(12), 4553-4560. https://doi.org/10.4049/jimmunol.1700263

Litin, S. C., & Nanda, S. (2018). *Mayo Clinic family health book, 2018, 5th Edition.*

Lokshin, A., Raskovalova, T., Huang, X., Zacharia, L. C., Jackson, E. K., & Gorelik, E. (2006). Adenosine-Mediated Inhibition of the Cytotoxic Activity and Cytokine Production by Activated Natural Killer Cells. *Cancer Research*, *66*(15), 7758-7765. https://doi.org/10.1158/0008-5472.CAN-06-0478

Lorent, J., Levental, K., Ganesan, L., Rivera-Longsworth, G., Sezgin, E., Doktorova, M., Lyman, E., & Levental, I. (2020). Plasma membranes are asymmetric in lipid unsaturation, packing, and protein shape. *Nature chemical biology*, *16*(6), 644-652. https://doi.org/10.1038/s41589-020-0529-6

Lymn, R. W., & Taylor, E. W. (1971). Mechanism of adenosine triphosphate hydrolysis by actomyosin. *Biochemistry*, *10*(25), 4617-4624. https://doi.org/10.1021/bi00801a004

Mansoor, S. E., Lü, W., Oosterheert, W., Shekhar, M., Tajkhorshid, E., & Gouaux, E. (2016). X-ray structures define human P2X3 receptor gating cycle and antagonist action. *Nature*, *538*(7623), 66-71. https://doi.org/10.1038/nature19367

Mayr, B., & Montminy, M. (2001). Transcriptional regulation by the phosphorylation-dependent factor CREB. *Nature Reviews. Molecular Cell Biology*, *2*(8), 599-609. https://doi.org/10.1038/35085068

Mazziotta, C., Rotondo, J. C., Lanzillotti, C., Campione, G., Martini, F., & Tognon, M. (2022). Cancer biology and molecular genetics of A3 adenosine receptor. *Oncogene*, *41*(3), 301-308. https://doi.org/10.1038/s41388-021-02090-z

McCarthy, A. E., Yoshioka, C., & Mansoor, S. E. (2019). Full-Length P2X7 Structures Reveal How Palmitoylation Prevents Channel Desensitization. *Cell*, *179*(3), 659-670.e13. https://doi.org/10.1016/j.cell.2019.09.017

Mehta, N., Kaur, M., Singh, M., Chand, S., Vyas, B., Silakari, P., Bahia, M. S., & Silakari, O. (2014). Purinergic receptor $P2X_7$: A novel target for anti-inflammatory therapy. *Bioorganic & Medicinal Chemistry*, *22*(1), 54-88. https://doi.org/10.1016/j.bmc.2013.10.054

Melloni, E., Pontremoli, S., Michetti, M., Sacco, O., Sparatore, B., & Horecker, B. L. (1986). The involvement of calpain in the activation of protein kinase C in neutrophils stimulated by phorbol myristic acid. *The Journal of Biological Chemistry*, *261*(9), 4101-4105.

Meseth, U., Wohland, T., Rigler, R., & Vogel, H. (1999). Resolution of Fluorescence Correlation Measurements. *Biophysical Journal*, *76*(3), 1619-1631. https://doi.org/10.1016/S0006-3495(99)77321-2

Meshki, J., Tuluc, F., Bredetean, O., Ding, Z., & Kunapuli, S. P. (2004). Molecular mechanism of nucleotide-induced primary granule release in human neutrophils : Role for the $P2Y_2$ receptor. *American Journal of Physiology-Cell Physiology*, *286*(2), C264-C271. https://doi.org/10.1152/ajpcell.00287.2003

Miyabe, K., Sakamoto, N., Wu, Y. H., Mori, N., & Sakamoto, H. (2004). Effects of platelet release products on neutrophilic phagocytosis and complement receptors. *Thrombosis Research*, *114*(1), 29-36. https://doi.org/10.1016/j.thromres.2004.04.003

Mizumoto, N., Kumamoto, T., Robson, S. C., Sévigny, J., Matsue, H., Enjyoji, K., & Takashima, A. (2002). CD39 is the dominant Langerhans cell-associated ecto-NTPDase : Modulatory roles in inflammation and immune responsiveness. *Nature Medicine*, *8*(4), 358-365. https://doi.org/10.1038/nm0402-358

Moore, D., Chambers, J., Waldvogel, H., Faull, R., & Emson, P. (2000). Regional and cellular distribution of the P2Y(1) purinergic receptor in the human brain : Striking neuronal localisation. *The Journal of Comparative Neurology*, *421*(3), 374-384. https://doi.org/10.1002/(sici)1096-9861(20000605)421:3<374::aid-cne6>3.0.co;2-z

Morandini, R., Ghanem, G., Portier-Lemarie, A., Robaye, B., Renaud, A., & Boeynaems, J. M. (1996). Action of cAMP on expression and release of adhesion molecules in human endothelial cells. *American Journal of Physiology-Heart and Circulatory Physiology*, *270*(3), H807-H816. https://doi.org/10.1152/ajpheart.1996.270.3.H807

Nagy, L. E., Diamond, I., Casso, D. J., Franklin, C., & Gordon, A. S. (1990). Ethanol increases extracellular adenosine by inhibiting adenosine uptake via the nucleoside transporter. *The Journal of Biological Chemistry*, *265*(4), 1946-1951.

Nagy, L. E., Diamond, I., Collier, K., Lopez, L., Ullman, B., & Gordon, A. S. (1989). Adenosine is required for ethanol-induced heterologous desensitization. *Molecular Pharmacology*, *36*(5), 744-748.

Nakamura, S., & Minamino, T. (2019). Flagella-Driven Motility of Bacteria. *Biomolecules*, *9*(7), 279. https://doi.org/10.3390/biom9070279

Neary, J. T., Shi, Y.-F., Kang, Y., & Tran, M. D. (2008). Opposing effects of P2X(7) and P2Y purine/pyrimidine-preferring receptors on proliferation of astrocytes induced by fibroblast growth factor-2 : Implications for CNS development, injury, and repair. *Journal of Neuroscience Research*, *86*(14), 3096-3105. https://doi.org/10.1002/jnr.21765

Nicke, A., Bäumert, H. G., Rettinger, J., Eichele, A., Lambrecht, G., Mutschler, E., & Schmalzing, G. (1998). P2X1 and P2X3 receptors form stable trimers : A novel structural motif of ligand-gated ion channels. *The EMBO Journal*, *17*(11), 3016-3028. https://doi.org/10.1093/emboj/17.11.3016

Nicke, A., Kerschensteiner, D., & Soto, F. (2005). Biochemical and functional evidence for heteromeric assembly of P2X1 and P2X4 subunits. *Journal of Neurochemistry*, *92*(4), 925-933. https://doi.org/10.1111/j.1471-4159.2004.02939.x

North, R. A. (2002). Molecular Physiology of P2X Receptors. *Physiological Reviews*, *82*(4), 1013-1067. https://doi.org/10.1152/physrev.00015.2002

Odronitz, F., & Kollmar, M. (2007). Drawing the tree of eukaryotic life based on the analysis of 2,269 manually annotated myosins from 328 species. *Genome Biology*, *8*(9), R196. https://doi.org/10.1186/gb-2007-8-9-r196

Ontyd, J., & Schrader, J. (1984). Measurement of adenosine, inosine, and hypoxanthine in human plasma. *Journal of Chromatography B: Biomedical Sciences and Applications*, *307*, 404-409. https://doi.org/10.1016/S0378-4347(00)84113-4

Ousingsawat, J., Wanitchakool, P., Kmit, A., Romao, A. M., Jantarajit, W., Schreiber, R., & Kunzelmann, K. (2015). Anoctamin 6 mediates effects essential for innate immunity downstream of P2X7 receptors in macrophages. *Nature Communications*, *6*, 6245. https://doi.org/10.1038/ncomms7245

Pai, C., & Kearsey, S. (2017). A Critical Balance : DNTPs and the Maintenance of Genome Stability. *Genes*, *8*(2), 57. https://doi.org/10.3390/genes8020057

Panther, E., Corinti, S., Idzko, M., Herouy, Y., Napp, M., la Sala, A., Girolomoni, G., & Norgauer, J. (2003). Adenosine affects expression of membrane molecules, cytokine and chemokine release, and the T-cell stimulatory capacity of human

dendritic cells. *Blood*, *101*(10), 3985-3990. https://doi.org/10.1182/blood-2002-07-2113

Papagiakoumou, E., Ronzitti, E., & Emiliani, V. (2020). Scanless two-photon excitation with temporal focusing. *Nature Methods*, *17*(6), 571-581. https://doi.org/10.1038/s41592-020-0795-y

Parihar, A., Eubank, T. D., & Doseff, A. I. (2010). Monocytes and macrophages regulate immunity through dynamic networks of survival and cell death. *Journal of Innate Immunity*, *2*(3), 204-215. https://doi.org/10.1159/000296507

Pastor-Anglada, M., & Pérez-Torras, S. (2018a). Emerging Roles of Nucleoside Transporters. *Frontiers in Pharmacology*, *9*, 606. https://doi.org/10.3389/fphar.2018.00606

Pastor-Anglada, M., & Pérez-Torras, S. (2018b). Who Is Who in Adenosine Transport. *Frontiers in Pharmacology*, *9*, 627. https://doi.org/10.3389/fphar.2018.00627

Patsopoulos, N. A. (2018). Genetics of Multiple Sclerosis : An Overview and New Directions. *Cold Spring Harbor Perspectives in Medicine*, *8*(7), a028951. https://doi.org/10.1101/cshperspect.a028951

Pedemonte, N., & Galietta, L. J. V. (2014). Structure and function of TMEM16 proteins (anoctamins). *Physiological Reviews*, *94*(2), 419-459. https://doi.org/10.1152/physrev.00039.2011

Pegoraro, A., Orioli, E., De Marchi, E., Salvestrini, V., Milani, A., Di Virgilio, F., Curti, A., & Adinolfi, E. (2020). Differential sensitivity of acute myeloid leukemia cells to daunorubicin depends on P2X7A versus P2X7B receptor expression. *Cell Death & Disease*, *11*(10), 876. https://doi.org/10.1038/s41419-020-03058-9

Pelegrin, P., & Surprenant, A. (2006). Pannexin-1 mediates large pore formation and interleukin-1beta release by the ATP-gated P2X7 receptor. *The EMBO Journal*, *25*(21), 5071-5082. https://doi.org/10.1038/sj.emboj.7601378

Perry, V. H., Hume, D. A., & Gordon, S. (1985). Immunohistochemical localization of macrophages and microglia in the adult and developing mouse brain. *Neuroscience*, *15*(2), 313-326. https://doi.org/10.1016/0306-4522(85)90215-5

Peverini, L., Beudez, J., Dunning, K., Chataigneau, T., & Grutter, T. (2018). New Insights Into Permeation of Large Cations Through ATP-Gated P2X Receptors. *Frontiers in Molecular Neuroscience*, *11*, 265. https://doi.org/10.3389/fnmol.2018.00265

Piirainen, H., Ashok, Y., Nanekar, R. T., & Jaakola, V.-P. (2011). Structural features of adenosine receptors : From crystal to function. *Biochimica Et Biophysica Acta*, *1808*(5), 1233-1244. https://doi.org/10.1016/j.bbamem.2010.05.021

Pletneva, M., Fan, H., Park, J.-J., Radojcic, V., Jie, C., Yu, Y., Chan, C., Redwood, A., Pardoll, D., & Housseau, F. (2009). IFN-producing killer dendritic cells are antigen-presenting cells endowed with T-cell cross-priming capacity. *Cancer Research*, *69*(16), 6607-6614. https://doi.org/10.1158/0008-5472.CAN-09-0508

Prasad, N. K. (2011). *Enzyme technology : Pacemaker of biotechnology*. PHI Learning.

Qiu, F., & Dahl, G. (2009). A permeant regulating its permeation pore : Inhibition of pannexin 1 channels by ATP. *American Journal of Physiology-Cell Physiology*, *296*(2), C250-C255. https://doi.org/10.1152/ajpcell.00433.2008

Qu, Y., Misaghi, S., Newton, K., Gilmour, L. L., Louie, S., Cupp, J. E., Dubyak, G. R., Hackos, D., & Dixit, V. M. (2011). Pannexin-1 Is Required for ATP Release during Apoptosis but Not for Inflammasome Activation. *The Journal of Immunology*, *186*(11), 6553-6561. https://doi.org/10.4049/jimmunol.1100478

Raiden, S., Schettini, J., Salamone, G., Trevani, A., Vermeulen, M., Gamberale, R., Giordano, M., & Geffner, J. (2003). Human Platelets Produce Granulocyte-Macrophage Colony-Stimulating Factor and Delay Eosinophil Apoptosis. *Laboratory Investigation*, *83*(4), 589-598. https://doi.org/10.1097/01.LAB.0000062851.71286.47

Raker, V. K., Becker, C., & Steinbrink, K. (2016). The cAMP Pathway as Therapeutic Target in Autoimmune and Inflammatory Diseases. *Frontiers in Immunology*, *7*. https://doi.org/10.3389/fimmu.2016.00123

Rao, V. S., Srinivas, K., Sujini, G. N., & Kumar, G. N. S. (2014). Protein-Protein Interaction Detection : Methods and Analysis. *International Journal of Proteomics*, *2014*, 1-12. https://doi.org/10.1155/2014/147648

Redzic, Z. B., Malatiali, S. A., Grujicic, D., & Isakovic, A. J. (2010). Expression and functional activity of nucleoside transporters in human choroid plexus. *Cerebrospinal Fluid Research*, *7*(1), 2. https://doi.org/10.1186/1743-8454-7-2

Reznikov, L. R., Dong, Q., Chen, J.-H., Moninger, T. O., Park, J. M., Zhang, Y., Du, J., Hildebrand, M. S., Smith, R. J. H., Randak, C. O., Stoltz, D. A., & Welsh, M. J. (2013). CFTR-deficient pigs display peripheral nervous system defects at birth. *Proceedings of the National Academy of Sciences of the United States of America*, *110*(8), 3083-3088. https://doi.org/10.1073/pnas.1222729110

Richert, L., Didier, P., de Rocquigny, H., & Mély, Y. (2015). Monitoring HIV-1 Protein Oligomerization by FLIM FRET Microscopy. In W. Becker (Éd.), *Advanced Time-Correlated Single Photon Counting Applications* (Vol. 111, p. 277-307). Springer International Publishing. https://doi.org/10.1007/978-3-319-14929-5_8

Riddle, R. C., Taylor, A. F., Rogers, J. R., & Donahue, H. J. (2007). ATP Release Mediates Fluid Flow-Induced Proliferation of Human Bone Marrow Stromal Cells. *Journal of Bone and Mineral Research*, *22*(4), 589-600. https://doi.org/10.1359/jbmr.070113

Ring, S., Pushkarevskaya, A., Schild, H., Probst, H. C., Jendrossek, V., Wirsdörfer, F., Ledent, C., Robson, S. C., Enk, A. H., & Mahnke, K. (2015). Regulatory T cell-derived adenosine induces dendritic cell migration through the Epac-Rap1 pathway. *Journal of Immunology (Baltimore, Md.: 1950)*, *194*(8), 3735-3744. https://doi.org/10.4049/jimmunol.1401434

Riordan, J. R., Rommens, J. M., Kerem, B.-S., Alon, N., Rozmahel, R., Grzelczak, Z., Zielenski, J., Lok, S., Plavsic, N., Chou, J.-L., Drumm, M. L., Iannuzzi, M. C., Collins, F. S., & Tsui, L.-C. (1989). Identification of the Cystic Fibrosis Gene : Cloning and Characterization of Complementary DNA. *Science*, *245*(4922), 1066-1073. https://doi.org/10.1126/science.2475911

Robinson, L. E., Shridar, M., Smith, P., & Murrell-Lagnado, R. D. (2014). Plasma Membrane Cholesterol as a Regulator of Human and Rodent P2X7 Receptor Activation and Sensitization. *Journal of Biological Chemistry*, *289*(46), 31983-31994. https://doi.org/10.1074/jbc.M114.574699

Robson, S. C., Sévigny, J., & Zimmermann, H. (2006). The E-NTPDase family of ectonucleotidases : Structure function relationships and pathophysiological significance. *Purinergic Signalling*, *2*(2), 409-430. https://doi.org/10.1007/s11302-006-9003-5

Roger, S., Gillet, L., Baroja-Mazo, A., Surprenant, A., & Pelegrin, P. (2010). C-terminal calmodulin-binding motif differentially controls human and rat P2X7 receptor

current facilitation. *The Journal of Biological Chemistry*, *285*(23), 17514-17524. https://doi.org/10.1074/jbc.M109.053082

Roger, S., Pelegrin, P., & Surprenant, A. (2008). Facilitation of P2X7 Receptor Currents and Membrane Blebbing via Constitutive and Dynamic Calmodulin Binding. *Journal of Neuroscience*, *28*(25), 6393-6401. https://doi.org/10.1523/JNEUROSCI.0696-08.2008

Rommens, J. M., Iannuzzi, M. C., Kerem, B.-S., Drumm, M. L., Melmer, G., Dean, M., Rozmahel, R., Cole, J. L., Kennedy, D., Hidaka, N., Zsiga, M., Buchwald, M., Tsui, L.-C., Riordan, J. R., & Collins, F. S. (1989). Identification of the Cystic Fibrosis Gene : Chromosome Walking and Jumping. *Science*, *245*(4922), 1059-1065. https://doi.org/10.1126/science.2772657

Rose, J. B., Naydenova, Z., Bang, A., Eguchi, M., Sweeney, G., Choi, D.-S., Hammond, J. R., & Coe, I. R. (2010). Equilibrative nucleoside transporter 1 plays an essential role in cardioprotection. *American Journal of Physiology. Heart and Circulatory Physiology*, *298*(3), H771-777. https://doi.org/10.1152/ajpheart.00711.2009

Ryan, R., Sheldon, K., Kasser, T., & Deci, E. (1996). All goals are not created equal : An organismic perspective on the nature of goals and their regulation. *The Psychology of Action: Linking Cognition and Motivation to Behavior,*.

Salaro, E., Rambaldi, A., Falzoni, S., Amoroso, F. S., Franceschini, A., Sarti, A. C., Bonora, M., Cavazzini, F., Rigolin, G. M., Ciccone, M., Audrito, V., Deaglio, S., Pelegrin, P., Pinton, P., Cuneo, A., & Di Virgilio, F. (2016). Involvement of the P2X7-NLRP3 axis in leukemic cell proliferation and death. *Scientific Reports*, *6*, 26280. https://doi.org/10.1038/srep26280

Salentin, R., Gemsa, D., Sprenger, H., & Kaufmann, A. (2003). Chemokine receptor expression and chemotactic responsiveness of human monocytes after influenza A virus infection. *Journal of Leukocyte Biology*, *74*(2), 252-259. https://doi.org/10.1189/jlb.1102565

Salmi, M., & Jalkanen, S. (2005). Cell-surface enzymes in control of leukocyte trafficking. *Nature Reviews Immunology*, *5*(10), 760-771. https://doi.org/10.1038/nri1705

Sassone-Corsi, P. (1995). Transcription factors responsive to cAMP. *Annual Review of Cell and Developmental Biology*, *11*, 355-377. https://doi.org/10.1146/annurev.cb.11.110195.002035

Sassone-Corsi, P. (2012). The Cyclic AMP Pathway. *Cold Spring Harbor Perspectives in Biology*, *4*(12), a011148-a011148. https://doi.org/10.1101/cshperspect.a011148

Sattler, C., & Benndorf, K. (2022). Enlightening activation gating in P2X receptors. *Purinergic Signalling*, *18*(2), 177-191. https://doi.org/10.1007/s11302-022-09850-w

Sauer, A. V., Brigida, I., Carriglio, N., & Aiuti, A. (2012). Autoimmune Dysregulation and Purine Metabolism in Adenosine Deaminase Deficiency. *Frontiers in Immunology*, *3*. https://doi.org/10.3389/fimmu.2012.00265

Schneider, E., & Hunke, S. (1998). ATP-binding-cassette (ABC) transport systems : Functional and structural aspects of the ATP-hydrolyzing subunits/domains. *FEMS Microbiology Reviews*, *22*(1), 1-20. https://doi.org/10.1111/j.1574-6976.1998.tb00358.x

Schnurr, M., Then, F., Galambos, P., Scholz, C., Siegmund, B., Endres, S., & Eigler, A. (2000). Extracellular ATP and TNF-α Synergize in the Activation and Maturation

of Human Dendritic Cells. *The Journal of Immunology*, *165*(8), 4704-4709. https://doi.org/10.4049/jimmunol.165.8.4704

Schnurr, M., Toy, T., Shin, A., Hartmann, G., Rothenfusser, S., Soellner, J., Davis, I. D., Cebon, J., & Maraskovsky, E. (2004). Role of adenosine receptors in regulating chemotaxis and cytokine production of plasmacytoid dendritic cells. *Blood*, *103*(4), 1391-1397. https://doi.org/10.1182/blood-2003-06-1959

Schroder, K., Zhou, R., & Tschopp, J. (2010). The NLRP3 inflammasome : A sensor for metabolic danger? *Science (New York, N.Y.)*, *327*(5963), 296-300. https://doi.org/10.1126/science.1184003

Sebastião, A. M., & Ribeiro, J. A. (2009). Adenosine receptors and the central nervous system. *Handbook of Experimental Pharmacology*, *193*, 471-534. https://doi.org/10.1007/978-3-540-89615-9_16

Seidel, J., Leitzke, S., Ahrens, B., Sperrhacke, M., Bhakdi, S., & Reiss, K. (2021). Role of ADAM10 and ADAM17 in Regulating CD137 Function. *International Journal of Molecular Sciences*, *22*(5), 2730. https://doi.org/10.3390/ijms22052730

Serezani, C. H., Ballinger, M. N., Aronoff, D. M., & Peters-Golden, M. (2008). Cyclic AMP : Master regulator of innate immune cell function. *American Journal of Respiratory Cell and Molecular Biology*, *39*(2), 127-132. https://doi.org/10.1165/rcmb.2008-0091TR

Sheppard, C., Gannaway, J., Kompfner, R., & Walsh, D. (1977). The scanning harmonic optical microscope. *IEEE Journal of Quantum Electronics*, *13*(9), 912-912. https://doi.org/10.1109/JQE.1977.1069615

Sheshachalam, A., Srivastava, N., Mitchell, T., Lacy, P., & Eitzen, G. (2014). Granule Protein Processing and Regulated Secretion in Neutrophils. *Frontiers in Immunology*, *5*. https://doi.org/10.3389/fimmu.2014.00448

Sheth, S., Brito, R., Mukherjea, D., Rybak, L. P., & Ramkumar, V. (2014). Adenosine receptors : Expression, function and regulation. *International Journal of Molecular Sciences*, *15*(2), 2024-2052. https://doi.org/10.3390/ijms15022024

Silva, C. H. T. P., Silva, M., Iulek, J., & Thiemann, O. H. (2008). Structural complexes of human adenine phosphoribosyltransferase reveal novel features of the APRT catalytic mechanism. *Journal of Biomolecular Structure & Dynamics*, *25*(6), 589-597. https://doi.org/10.1080/07391102.2008.10507205

Silva-Vilches, C., Ring, S., & Mahnke, K. (2018a). ATP and Its Metabolite Adenosine as Regulators of Dendritic Cell Activity. *Frontiers in Immunology*, *9*. https://doi.org/10.3389/fimmu.2018.02581

Silva-Vilches, C., Ring, S., & Mahnke, K. (2018b). ATP and Its Metabolite Adenosine as Regulators of Dendritic Cell Activity. *Frontiers in Immunology*, *9*. https://doi.org/10.3389/fimmu.2018.02581

Silva-Vilches, C., Ring, S., Schrader, J., Clausen, B. E., Probst, H.-C., Melchior, F., Schild, H., Enk, A., & Mahnke, K. (2019). Production of Extracellular Adenosine by CD73+ Dendritic Cells Is Crucial for Induction of Tolerance in Contact Hypersensitivity Reactions. *The Journal of Investigative Dermatology*, *139*(3), 541-551. https://doi.org/10.1016/j.jid.2018.10.016

Simões, F., Ousingsawat, J., Wanitchakool, P., Fonseca, A., Cabrita, I., Benedetto, R., Schreiber, R., & Kunzelmann, K. (2018). CFTR supports cell death through ROS-dependent activation of TMEM16F (anoctamin 6). *Pflugers Archiv: European*

Journal of Physiology, *470*(2), 305-314. https://doi.org/10.1007/s00424-017-2065-0

Simons, K., & Ikonen, E. (1997). Functional rafts in cell membranes. *Nature*, *387*(6633), 569-572. https://doi.org/10.1038/42408

Simons, K., & Sampaio, J. L. (2011). Membrane organization and lipid rafts. *Cold Spring Harbor Perspectives in Biology*, *3*(10), a004697. https://doi.org/10.1101/cshperspect.a004697

Singh, M., Watkinson, M., Scanlan, E. M., & Miller, G. J. (2020). Illuminating glycoscience : Synthetic strategies for FRET-enabled carbohydrate active enzyme probes. *RSC Chemical Biology*, *1*(5), 352-368. https://doi.org/10.1039/D0CB00134A

Skrabanja, A. T. P., Bouman, E. A. C., & Dagnelie, P. C. (2005). Potential value of adenosine 5′-triphosphate (ATP) and adenosine in anaesthesia and intensive care medicine. *British Journal of Anaesthesia*, *94*(5), 556-562. https://doi.org/10.1093/bja/aei093

Smith, S. J. (1988). Neuronal cytomechanics : The actin-based motility of growth cones. *Science (New York, N.Y.)*, *242*(4879), 708-715. https://doi.org/10.1126/science.3055292

Sorge, R. E., Trang, T., Dorfman, R., Smith, S. B., Beggs, S., Ritchie, J., Austin, J.-S., Zaykin, D. V., Vander Meulen, H., Costigan, M., Herbert, T. A., Yarkoni-Abitbul, M., Tichauer, D., Livneh, J., Gershon, E., Zheng, M., Tan, K., John, S. L., Slade, G. D., … Mogil, J. S. (2012). Genetically determined P2X7 receptor pore formation regulates variability in chronic pain sensitivity. *Nature Medicine*, *18*(4), 595-599. https://doi.org/10.1038/nm.2710

Srere, P. A. (1987). Complexes of sequential metabolic enzymes. *Annual Review of Biochemistry*, *56*, 89-124. https://doi.org/10.1146/annurev.bi.56.070187.000513

Stanley McKnight, G. (1991). Cyclic AMP second messenger systems. *Current Opinion in Cell Biology*, *3*(2), 213-217. https://doi.org/10.1016/0955-0674(91)90141-K

Stout, R. D., Jiang, C., Matta, B., Tietzel, I., Watkins, S. K., & Suttles, J. (2005). Macrophages sequentially change their functional phenotype in response to changes in microenvironmental influences. *Journal of Immunology (Baltimore, Md.: 1950)*, *175*(1), 342-349. https://doi.org/10.4049/jimmunol.175.1.342

Stout, R. D., & Suttles, J. (2004). Functional plasticity of macrophages : Reversible adaptation to changing microenvironments. *Journal of Leukocyte Biology*, *76*(3), 509-513. https://doi.org/10.1189/jlb.0504272

Stupp, R., Mason, W. P., van den Bent, M. J., Weller, M., Fisher, B., Taphoorn, M. J. B., Belanger, K., Brandes, A. A., Marosi, C., Bogdahn, U., Curschmann, J., Janzer, R. C., Ludwin, S. K., Gorlia, T., Allgeier, A., Lacombe, D., Cairncross, J. G., Eisenhauer, E., Mirimanoff, R. O., … National Cancer Institute of Canada Clinical Trials Group. (2005). Radiotherapy plus concomitant and adjuvant temozolomide for glioblastoma. *The New England Journal of Medicine*, *352*(10), 987-996. https://doi.org/10.1056/NEJMoa043330

Sun, Y., Day, R. N., & Periasamy, A. (2011). Investigating protein-protein interactions in living cells using fluorescence lifetime imaging microscopy. *Nature Protocols*, *6*(9), 1324-1340. https://doi.org/10.1038/nprot.2011.364

Sutherland, E. W., & Rall, T. W. (1958). Fractionation and characterization of a cyclic adenine ribonucleotide formed by tissue particles. *The Journal of Biological Chemistry*, *232*(2), 1077-1091.

Suzuki, J., Umeda, M., Sims, P. J., & Nagata, S. (2010). Calcium-dependent phospholipid scrambling by TMEM16F. *Nature*, *468*(7325), 834-838. https://doi.org/10.1038/nature09583

Sweeney, H. L., & Houdusse, A. (2010). Structural and Functional Insights into the Myosin Motor Mechanism. *Annual Review of Biophysics*, *39*(1), 539-557. https://doi.org/10.1146/annurev.biophys.050708.133751

Tanaka, N., Kawasaki, K., Nejime, N., Kubota, Y., Nakamura, K., Kunitomo, M., Takahashi, K., Hashimoto, M., & Shinozuka, K. (2004). P2Y receptor-mediated Ca(2+) signaling increases human vascular endothelial cell permeability. *Journal of Pharmacological Sciences*, *95*(2), 174-180. https://doi.org/10.1254/jphs.fpj03036x

Taussig, R., & Gilman, A. G. (1995). Mammalian Membrane-bound Adenylyl Cyclases. *Journal of Biological Chemistry*, *270*(1), 1-4. https://doi.org/10.1074/jbc.270.1.1

Torrents, E. (2014). Ribonucleotide reductases : Essential enzymes for bacterial life. *Frontiers in Cellular and Infection Microbiology*, *4*. https://doi.org/10.3389/fcimb.2014.00052

Townsend, M. H., Robison, R. A., & O'Neill, K. L. (2018). A review of HPRT and its emerging role in cancer. *Medical Oncology (Northwood, London, England)*, *35*(6), 89. https://doi.org/10.1007/s12032-018-1144-1

Tramier, M., Zahid, M., Mevel, J.-C., Masse, M.-J., & Coppey-Moisan, M. (2006). Sensitivity of CFP/YFP and GFP/mCherry pairs to donor photobleaching on FRET determination by fluorescence lifetime imaging microscopy in living cells. *Microscopy Research and Technique*, *69*(11), 933-939. https://doi.org/10.1002/jemt.20370

Traut, T. W. (1994). Physiological concentrations of purines and pyrimidines. *Molecular and Cellular Biochemistry*, *140*(1), 1-22. https://doi.org/10.1007/BF00928361

Tsien, R. Y. (1980). New calcium indicators and buffers with high selectivity against magnesium and protons : Design, synthesis, and properties of prototype structures. *Biochemistry*, *19*(11), 2396-2404. https://doi.org/10.1021/bi00552a018

Tsui, L.-C. (1992). The spectrum of cystic fibrosis mutations. *Trends in Genetics*, *8*(11), 392-398. https://doi.org/10.1016/0168-9525(92)90301-J

Turnham, R. E., & Scott, J. D. (2016). Protein kinase A catalytic subunit isoform PRKACA; History, function and physiology. *Gene*, *577*(2), 101-108. https://doi.org/10.1016/j.gene.2015.11.052

van Horssen, R., Janssen, E., Peters, W., van de Pasch, L., Lindert, M. M. te, van Dommelen, M. M. T., Linssen, P. C., Hagen, T. L. M. ten, Fransen, J. A. M., & Wieringa, B. (2009). Modulation of Cell Motility by Spatial Repositioning of Enzymatic ATP/ADP Exchange Capacity. *Journal of Biological Chemistry*, *284*(3), 1620-1627. https://doi.org/10.1074/jbc.M806974200

Ventura, M. A., & Thomopoulos, P. (1991). Effect of ATP and ADP on U-937 Promonocyte Cell Adhesiveness and Intracellular Ca $^{++}$ Levels. *Nucleosides and Nucleotides*, *10*(5), 1195-1197. https://doi.org/10.1080/07328319108047273

Virginio, C., Church, D., North, R. A., & Surprenant, A. (1997). Effects of divalent cations, protons and calmidazolium at the rat P2X7 receptor. *Neuropharmacology*, *36*(9), 1285-1294. https://doi.org/10.1016/s0028-3908(97)00141-x

Virginio, C., MacKenzie, A., Rassendren, F. A., North, R. A., & Surprenant, A. (1999). Pore dilation of neuronal P2X receptor channels. *Nature Neuroscience*, *2*(4), 315-321. https://doi.org/10.1038/7225

von Albertini, M., Palmetshofer, A., Kaczmarek, E., Koziak, K., Stroka, D., Grey, S. T., Stuhlmeier, K. M., & Robson, S. C. (1998). Extracellular ATP and ADP activate transcription factor NF-kappa B and induce endothelial cell apoptosis. *Biochemical and Biophysical Research Communications*, *248*(3), 822-829. https://doi.org/10.1006/bbrc.1998.9055

von Kügelgen, I., & Hoffmann, K. (2016). Pharmacology and structure of P2Y receptors. *Neuropharmacology*, *104*, 50-61. https://doi.org/10.1016/j.neuropharm.2015.10.030

Walker, J. E., Saraste, M., Runswick, M. J., & Gay, N. J. (1982). Distantly related sequences in the alpha- and beta-subunits of ATP synthase, myosin, kinases and other ATP-requiring enzymes and a common nucleotide binding fold. *The EMBO Journal*, *1*(8), 945-951.

Walsh, D. A., Perkins, J. P., & Krebs, E. G. (1968). An adenosine 3',5'-monophosphate-dependant protein kinase from rabbit skeletal muscle. *The Journal of Biological Chemistry*, *243*(13), 3763-3765.

Walton, C., King, R., Rechtman, L., Kaye, W., Leray, E., Marrie, R. A., Robertson, N., La Rocca, N., Uitdehaag, B., van der Mei, I., Wallin, M., Helme, A., Angood Napier, C., Rijke, N., & Baneke, P. (2020). Rising prevalence of multiple sclerosis worldwide : Insights from the Atlas of MS, third edition. *Multiple Sclerosis (Houndmills, Basingstoke, England)*, *26*(14), 1816-1821. https://doi.org/10.1177/1352458520970841

Wang, D., Wang, H., Gao, H., Zhang, H., Zhang, H., Wang, Q., & Sun, Z. (2020). P2X7 receptor mediates NLRP3 inflammasome activation in depression and diabetes. *Cell & Bioscience*, *10*, 28. https://doi.org/10.1186/s13578-020-00388-1

Wang, X., & Chen, D. (2018). Purinergic Regulation of Neutrophil Function. *Frontiers in Immunology*, *9*, 399. https://doi.org/10.3389/fimmu.2018.00399

Wells, A. L., Lin, A. W., Chen, L. Q., Safer, D., Cain, S. M., Hasson, T., Carragher, B. O., Milligan, R. A., & Sweeney, H. L. (1999). Myosin VI is an actin-based motor that moves backwards. *Nature*, *401*(6752), 505-508. https://doi.org/10.1038/46835

Welsh, M. J., & Smith, A. E. (1993). Molecular mechanisms of CFTR chloride channel dysfunction in cystic fibrosis. *Cell*, *73*(7), 1251-1254. https://doi.org/10.1016/0092-8674(93)90353-R

Whitlock, J. M., Yu, K., Cui, Y. Y., & Hartzell, H. C. (2018). Anoctamin 5/TMEM16E facilitates muscle precursor cell fusion. *Journal of General Physiology*, *150*(11), 1498-1509. https://doi.org/10.1085/jgp.201812097

Williamson, P. (2015). Phospholipid Scramblases. *Lipid Insights*, *8*(Suppl 1), 41-44. https://doi.org/10.4137/LPI.S31785

Wu, G. F., & Alvarez, E. (2011). The immunopathophysiology of multiple sclerosis. *Neurologic Clinics*, *29*(2), 257-278. https://doi.org/10.1016/j.ncl.2010.12.009

Wu, N., Cernysiov, V., Davidson, D., Song, H., Tang, J., Luo, S., Lu, Y., Qian, J., Gyurova, I. E., Waggoner, S. N., Trinh, V. Q.-H., Cayrol, R., Sugiura, A., McBride, H. M., Daudelin, J.-F., Labrecque, N., & Veillette, A. (2020). Critical Role of Lipid Scramblase TMEM16F in Phosphatidylserine Exposure and Repair of Plasma Membrane after Pore Formation. *Cell Reports*, *30*(4), 1129-1140.e5. https://doi.org/10.1016/j.celrep.2019.12.066

Xia, J., Yu, X., Tang, L., Li, G., & He, T. (2015). P2X7 receptor stimulates breast cancer cell invasion and migration via the AKT pathway. *Oncology Reports*, *34*(1), 103-110. https://doi.org/10.3892/or.2015.3979

Xu, X. J., Boumechache, M., Robinson, L. E., Marschall, V., Gorecki, D. C., Masin, M., & Murrell-Lagnado, R. (2012). Splice-variants of the P2X7 receptor reveal differential agonist-dependence and functional coupling with pannexin-1. *Journal of Cell Science*, jcs.099374. https://doi.org/10.1242/jcs.099374

Yan, K., Gao, L.-N., Cui, Y.-L., Zhang, Y., & Zhou, X. (2016). The cyclic AMP signaling pathway : Exploring targets for successful drug discovery (Review). *Molecular Medicine Reports*, *13*(5), 3715-3723. https://doi.org/10.3892/mmr.2016.5005

Yang, D. (2006). The A2B adenosine receptor protects against inflammation and excessive vascular adhesion. *Journal of Clinical Investigation*, *116*(7), 1913-1923. https://doi.org/10.1172/JCI27933

Yang, H., Kim, A., David, T., Palmer, D., Jin, T., Tien, J., Huang, F., Cheng, T., Coughlin, S. R., Jan, Y. N., & Jan, L. Y. (2012). TMEM16F forms a Ca2+-activated cation channel required for lipid scrambling in platelets during blood coagulation. *Cell*, *151*(1), 111-122. https://doi.org/10.1016/j.cell.2012.07.036

Yang, Y., Wang, H., Kouadir, M., Song, H., & Shi, F. (2019a). Recent advances in the mechanisms of NLRP3 inflammasome activation and its inhibitors. *Cell Death & Disease*, *10*(2), 128. https://doi.org/10.1038/s41419-019-1413-8

Yang, Y., Wang, H., Kouadir, M., Song, H., & Shi, F. (2019b). Recent advances in the mechanisms of NLRP3 inflammasome activation and its inhibitors. *Cell Death & Disease*, *10*(2), 128. https://doi.org/10.1038/s41419-019-1413-8

Yegutkin, G. G. (2008). Nucleotide- and nucleoside-converting ectoenzymes : Important modulators of purinergic signalling cascade. *Biochimica et Biophysica Acta (BBA) - Molecular Cell Research*, *1783*(5), 673-694. https://doi.org/10.1016/j.bbamcr.2008.01.024

Yoshioka, K., Saitoh, O., & Nakata, H. (2001). Heteromeric association creates a P2Y-like adenosine receptor. *Proceedings of the National Academy of Sciences*, *98*(13), 7617-7622. https://doi.org/10.1073/pnas.121587098

Yount, R. G., Babcock, D., Ballantyne, W., & Ojala, D. (1971). Adenylyl imidiodiphosphate, an adenosine triphosphate analog containing a P-N-P linkage. *Biochemistry*, *10*(13), 2484-2489. https://doi.org/10.1021/bi00789a009

Yu, P., Zhang, X., Liu, N., Tang, L., Peng, C., & Chen, X. (2021). Pyroptosis : Mechanisms and diseases. *Signal Transduction and Targeted Therapy*, *6*(1), 128. https://doi.org/10.1038/s41392-021-00507-5

Yu, Y., Ugawa, S., Ueda, T., Ishida, Y., Inoue, K., Kyaw Nyunt, A., Umemura, A., Mase, M., Yamada, K., & Shimada, S. (2008). Cellular localization of P2X7 receptor mRNA in the rat brain. *Brain Research*, *1194*, 45-55. https://doi.org/10.1016/j.brainres.2007.11.064

Zaitseva, J., Jenewein, S., Jumpertz, T., Holland, I. B., & Schmitt, L. (2005). H662 is the linchpin of ATP hydrolysis in the nucleotide-binding domain of the ABC transporter HlyB. *The EMBO Journal*, *24*(11), 1901-1910. https://doi.org/10.1038/sj.emboj.7600657

Zanin, R. F., Braganhol, E., Bergamin, L. S., Campesato, L. F. I., Filho, A. Z., Moreira, J. C. F., Morrone, F. B., Sévigny, J., Schetinger, M. R. C., de Souza Wyse, A. T., & Battastini, A. M. O. (2012). Differential Macrophage Activation Alters the

Expression Profile of NTPDase and Ecto-5′-Nucleotidase. *PLoS ONE*, *7*(2), e31205. https://doi.org/10.1371/journal.pone.0031205

Zanoni, M., Sarti, A. C., Zamagni, A., Cortesi, M., Pignatta, S., Arienti, C., Tebaldi, M., Sarnelli, A., Romeo, A., Bartolini, D., Tosatto, L., Adinolfi, E., Tesei, A., & Di Virgilio, F. (2022). Irradiation causes senescence, ATP release, and P2X7 receptor isoform switch in glioblastoma. *Cell Death & Disease*, *13*(1), 80. https://doi.org/10.1038/s41419-022-04526-0

Zarbock, A., & Ley, K. (2009). Neutrophil Adhesion and Activation under Flow. *Microcirculation*, *16*(1), 31-42. https://doi.org/10.1080/10739680802350104

Zeiser, R., Robson, S. C., Vaikunthanathan, T., Dworak, M., & Burnstock, G. (2016). Unlocking the Potential of Purinergic Signaling in Transplantation. *American journal of transplantation : official journal of the American Society of Transplantation and the American Society of Transplant Surgeons*, *16*(10), 2781-2794. https://doi.org/10.1111/ajt.13801

Zernecke, A., Bidzhekov, K., Özüyaman, B., Fraemohs, L., Liehn, E. A., Lüscher-Firzlaff, J. M., Lüscher, B., Schrader, J., & Weber, C. (2006). CD73/Ecto-5′-Nucleotidase Protects Against Vascular Inflammation and Neointima Formation. *Circulation*, *113*(17), 2120-2127. https://doi.org/10.1161/CIRCULATIONAHA.105.595249

Zhang, B. (2012). CD73 promotes tumor growth and metastasis. *OncoImmunology*, *1*(1), 67-70. https://doi.org/10.4161/onci.1.1.18068

Zhao, H., Chiaro, C. R., Zhang, L., Smith, P. B., Chan, C. Y., Pedley, A. M., Pugh, R. J., French, J. B., Patterson, A. D., & Benkovic, S. J. (2015). Quantitative Analysis of Purine Nucleotides Indicates That Purinosomes Increase de Novo Purine

Biosynthesis. *Journal of Biological Chemistry*, *290*(11), 6705-6713. https://doi.org/10.1074/jbc.M114.628701

Zhou, Y., Arredondo, H. M., & Wang, N. (2021). P2Y Receptors in Bone—Anabolic, Catabolic, or Both? *Frontiers in Endocrinology*, *12*, 818499. https://doi.org/10.3389/fendo.2021.818499

Zikánová, M., Wahezi, D., Hay, A., Stibůrková, B., Pitts, C., Mušálková, D., Škopová, V., Barešová, V., Součková, O., Hodaňová, K., Živná, M., Stránecký, V., Hartmannová, H., Hnízda, A., Bleyer, A. J., & Kmoch, S. (2018). Clinical manifestations and molecular aspects of phosphoribosylpyrophosphate synthetase superactivity in females. *Rheumatology*, *57*(7), 1180-1185. https://doi.org/10.1093/rheumatology/key041

Zimmermann, H. (1992). 5′-Nucleotidase : Molecular structure and functional aspects. *Biochemical Journal*, *285*(2), 345-365. https://doi.org/10.1042/bj2850345

Zimmermann, H. (2000). Extracellular metabolism of ATP and other nucleotides. *Naunyn-Schmiedeberg's Archives of Pharmacology*, *362*(4-5), 299-309. https://doi.org/10.1007/s002100000309

Zoref-Shani, E., Feinstein, S., Frishberg, Y., Bromberg, Y., & Sperling, O. (2000). Kelley-Seegmiller syndrome due to a unique variant of hypoxanthine-guanine phosphoribosyltransferase : Reduced affinity for 5-phosphoribosyl-1-pyrophosphate manifested only at low, physiological substrate concentrations. *Biochimica Et Biophysica Acta*, *1500*(2), 197-203. https://doi.org/10.1016/s0925-4439(99)00103-9

Publication List

2021

Dunning, K., Martz, A., Peralta, F. A., **Cevoli, F.,** Boué-Grabot, E., Compan, V., Gautherat, F., Wolf, P., Chataigneau, T., & Grutter, T. (2021). P2X7 Receptors and TMEM16 Channels Are Functionally Coupled with Implications for Macropore Formation and Current Facilitation. *International Journal of Molecular Sciences*, *22*(12), 6542. https://doi.org/10.3390/ijms22126542.

2022: In-progress

(i) Benoit Arnould, Francisco Andrés Peralta, Adeline Martz, **Federico Cevoli**, Eric Hosy, Alexandre Specht, and Thomas Grutter. Affinity-guided labeling of native P2X7 receptor reveals its nanoscale membrane localization in microglia. Status: awaiting final data.

(ii) **Federico Cevoli**, Francisco Andrés Peralta, Ludovic Richert, Adeline Martz, Cendrine Seguin, and Thomas Grutter. P2X7 C-cys Anchor is Implicated in Cell Death Regulation and Inflammation through a physical interaction with TMEM16F. Status: drafting/writing.

CAMB Laboratoire de conception et application de molécules bioactives | UMR 7199 de l'Université de Strasbourg et du cnrs

Biophysical and Molecular Characterisation of the P2X7 Receptors and TMEM16F Channels Complex Unravel Novel Immunoregulatory Targets

PhD candidate: Federico Cevoli

Supervisor: Dr. Grutter, Thomas

Summary

Les récepteurs purinergiques P2X7 (P2X7R) sont des canaux cationiques non sélectifs ligand-dépendants impliqués dans plusieurs conditions physiopathologiques. L'activation de P2X7R est déclenchée par suite de concentrations élevées d'ATP extracellulaire, de la même manière que celles observées dans les lésions tissulaires, l'inflammation chronique et l'activation des lymphocytes T ainsi que dans le brouillage des phospholipides conduisant au saignement membranaire et à l'apoptose. P2X7R présente un domaine cytoplasmique unique contenant un ballast cytoplasmique et une région cytoplasmique riche en cystéine (C-cys) à l'extrémité du deuxième domaine transmembranaire (TM2). Le ballast cytoplasmique comprend 120 résidus supplémentaires dans l'extrémité C-terminale. Une autre caractéristique importante de P2X7 est sa capacité à imprégner de gros cations organiques tels que YO-PRO-1 (900 Da) - ce phénomène est appelé formation de « macropores ». Plusieurs mécanismes ont été proposés pour le macropore, notamment (i) la dilatation des pores, (ii) le recrutement des canaux : pannexine-1, (iii) la reconstitution des liposomes et (iv) la très récemment une grande famille de scramblases régulées: les anoctamines/TMEM16 ont été proposées comme partenaire d'interaction prometteur pour P2X7.

La famille Anoctamin comprend 10 isoformes ANO1-10 (TMEM16A-J) divisées en 2 sous-familles : canaux Cl activés par le Ca2+ (ANO1 et ANO2) et lipides dépendants du Ca^{2+} scramblases (ANO3, ANO4, ANO6, ANO7, ANO10). Anoctamine 6 (ANO6 également appelée TMEM16F) est une protéine transmembranaire exprimée à la surface de nombreux types cellulaires différents et candidat pour le complexe d'interaction P2X7, avec de grandes implications dans la coagulation sanguine,

saignement membranaire et apoptose. En particulier, il a été proposé que l'activation de P2X7R conduit à augmenter l'entrée d'ions Ca2+ entraînant une activation en aval d'ANO6 responsable pour la translocation de la phosphatidylsérine, l'initiation du rétrécissement cellulaire et l'activation des caspases3/7. Jusqu'à présent, les études de perte de fonction ont mis en évidence l'interaction possible entre ANO6 canal et P2X7R dans les macrophages, mais couplage physique et modulation fonctionnelle entre les deux protéines restent indéfinies. Le but de mon projet de recherche doctorale est de démontrer le couplage physique et pour identifier les composants/régions de régulation critiques pour la stabilité complexe et interaction, contribuant ainsi à la caractérisation biophysique et moléculaire des complexe explorant également ses implications dans les réponses immunitaires. Ainsi, donner un aperçu de nouvelles cibles pharmacologiques potentielles. Un large éventail de techniques a été utilisé pour cette these de recherche incluant microscopie à deux photons, modélisation moléculaire, patch-clamp électrophysiologie, qRT-PCR, CRISPR-Cas9, études de mutagenèse, vidéo- et microscopie confocale contribuant ainsi à une bonne compréhension des aspects développementaux chez neurosciences moléculaires.

Une percée majeure dans l'étude de ce complexe moléculaire s'est produite suite à ladécouverte que les canaux P2X7R et ANO6 formaient un complexe 71A estimé tel que calculé par Fluorescence Resonance Energy Transfer (FRET) par Fluorescence Lifetime Imaging Microscopie (FLIM). Pour localiser les deux protéines au niveau de la membrane, des étiquettes de fusion ont été construites en utilisant mScarlet et eGFP, qui ont par conséquent été fusionnés à l'extrémité C-terminale de P2X7 et ANO6, respectivement. FLIM-FRET a ensuite été réalisé pour mettre en évidence le couplage physique, bien que la stoechiométrie complexe exacte reste à déterminer. Surtout, comme la fluorescence la durée de vie est un paramètre intrinsèque du fluorophore indépendant de la concentration, FRET-FLIM est plus robuste que les méthodes basées sur l'intensité pour mesurer le FRET lorsque les concentrations des partenaires en interaction ne peuvent pas être contrôlés. En bref, FLIM sonde les changements dans les fluorophores microenvironnement à l'aide d'un laser pulsé qui excite périodiquement les fluorophores de l'échantillon, qui est ensuite détendu dans leur état fondamental émettant des photons par une voie non radiative. La durée de vie de fluorescence τ peut alors être calculée comme le temps moyen

qu'un fluorophore reste à l'état excité après excitation. Dans nos conditions expérimentales la présence de l'accepteur P2X7_Sarlet à proximité immédiate du donneur ANO6_eGFP, un FRET s'est produit augmentant le taux de désexcitation non radiative du donneur et diminuant ainsi sa durée de vie de fluorescence. Ainsi, impliquant une interaction physique entre les molécules marquées.

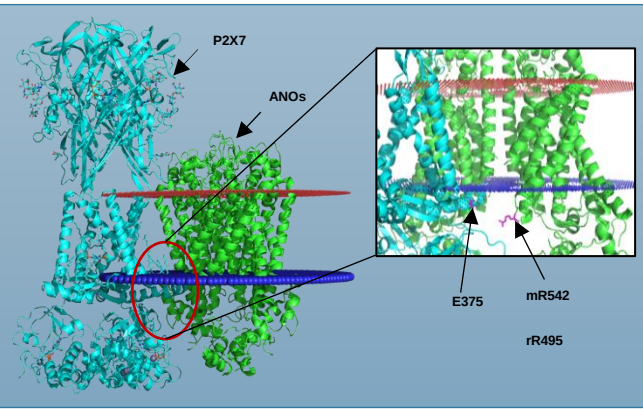

BOX 1 :

Given the additional 120 residues in the P2X7's C-terminus (cytoplasmic ballast), we hypothesised that the latter, might act as a docking site for anoctamin/TMEM16 family. In addition, this interaction might be modulated by the amino acid residue E375 situated on the cytoplasmic cysteine (C-cys) anchor of P2X7 and residue mR542 and rR495 located on transmembrane (TM) -4 and -5 of anoctamins.

Suite à cette découverte, nous avons ensuite évalué par modélisation moléculaire (réalisée par des collaborateurs) les résidus d'acides aminés pouvant être impliqués dans la modulation du complexe (voir ENCADRÉ1). Un examen approfondi du modèle moléculaire P2X7-ANO6 a identifié le résidu 375 d'aglutamate (E) situé dans l'ancre C-cys du récepteur P2X7, et une arginine (R) résidu 495 situé sur la transmembrane (TM) -4 et -5 dans ANO6, qui semblait être dans une très grande proximité (>100 A). Ces résidus ont donc été mutés via un site-directed mutagenèse générant E375R et R495E, afin d'observer, le cas échéant, charge-dépendante restauration de l'activité après transfection. En particulier, nous avons étudié le rôle de ces résidus dans la formation de macropores (comme mesure de l'absorption de colorant YOPRO-1) et phospholipides activité de brouillage (en fonction de l'intensité du fluorophore de l'annexine-V), abordant ainsi à la fois. Marques moléculaires des protéines P2X7 et ANO6. En plus de cela, nous avons également exploré si des corrélations entre les mécanismes ci-dessus ont pu être trouvées. Ce travail exigeant a été réalisée sur des lignées cellulaires ΔANO6 transfectées (lignées cellulaires HEK293T dans lesquelles. Le gène ANO6 a été génétiquement éliminé par la méthode CRISPR/Cas9) et le type sauvage HEK293T. Étonnamment, les résultats ont montré des réductions significatives dans les deux tests lorsque P2X7_E375R a été co-transfecté avec le résidu WT ANO6_R495R, et sauvé après l'échange de

résidus (c'est-à-dire, E375R_R495E). En conséquence, nous avons fourni pour la première fois des résidus potentiels, qui sont peut-être, responsable de la régulation de l'interaction complexe identifiant également les régions au sein de P2X7R qui peuvent être utilisés comme cibles pharmacologiques. Néanmoins, en raison de la réduction partielle des deux d'autres anoctamines et/ou protéines ne peuvent pas être déployées. Pour répondre à cette question, plusieurs Des expériences de qRT-PCR ont été réalisées, qui ont établi d'autres anoctamines exprimées dans Lignée cellulaire HEK293T : ANO-4-5-6-8 et -10.

Étant donné l'utilisation d'un système surexprimé (c'est-à-dire HEK293T), nous avons ensuite exploré si le complexe aidé dans la régulation de la mort cellulaire et l'inflammation dans les cellules immunitaires exprimant à la fois protéines de manière endogène. En utilisant des peptides HIV1-TAT conçus sur mesure pour pénétrer dans les cellules, nous avons démontré pour la première fois les implications potentielles de l'ancrage cytoplasmique P2X7 dans la régulation de l'activation de la caspase3/7 ainsi que dans la régulation des cytokines pro-inflammatoires, tels que TNFα et IL-1β dans les macrophages primaires et les macrophages RAW246.7, respectivement. Les deux représentent des caractéristiques importantes de l'inflammation. Cependant, les mécanismes et la physiologie l'importance de cette activité pro-inflammatoire inhabituelle survenant dans les microenvironnements sont actuellement insaisissables. Bien que des études aient dévoilé la structure mécanisme d'une nouvelle cascade activant la caspase - l'inflammasome. Ce dernier a été montré être fonctionnellement lié à l'activation du récepteur P2X7 couplée à la libération d'IL-1β et à d'autres cytokines. Ensemble, ces résultats fournissent des preuves d'un scénario intrigant, dans lequel le couplage entre ces deux protéines crée la base d'une initiation optimale de la réponse immunitaire. En conséquence, cette thèse de recherche a identifié des propriétés pharmacologiques prometteuses cibles pour le développement de médicaments anti-inflammatoires qui peuvent aider à mieux comprendre interactions immuno-tumorales et immunothérapie.

Les travaux futurs concernent des investigations plus approfondies sur les effets du TAT ciblé P2X7 peptides in vivo. En particulier, les récepteurs P2X7 jouent également un rôle important dans la neurodégénérescence conditions comme dans la sclérose en plaques (SEP). Il est très intéressant de noter que la physiopathologie

de la SEP est accumulation définie de macrophages et cellules inflammatoires s'infiltrant dans le SNC responsable pour la démyélinisation. Compte tenu de nos découvertes prometteuses dans les macrophages et de l'augmentation signalée immunoréactivité de P2X7 dans les macrophages/microglies activés, ainsi qu'une élévation de l'ATP niveaux liés à la libération d'IL-1β induite par la lésion de SEP. Ainsi, en explorant l'implication potentielle de L'ancre cytoplasmique P2X7 dans le modèle animal de SEP représenterait une étape clé de ce projet.

Reference List:

McCarthy AE, Yoshioka C, Mansoor SE. Full-Length P2X7 Structures Reveal How Palmitoylation Prevents Channel Desensitization. Cell. 2019 Oct 17;179(3):659-670.e13.

Feng S, Dang S, Han TW, Ye W, Jin P, Cheng T, Li J, Jan YN, Jan LY, Cheng Y. Cryo-EM Studies of TMEM16F Calcium-Activated Ion Channel Suggest Features Important for Lipid Scrambling. Cell Rep. 2019 Jul 9;28(2):567-579.e4.

Publications

2021

Dunning K, Martz A, Peralta FA, **Cevoli F**, Boué-Grabot E, Compan V, Gautherat F, Wolf P, Chataigneau T, Grutter T. P2X7 Receptors and TMEM16 Channels Are Functionally Coupled with Implications for Macropore Formation and Current Facilitation. Int J Mol Sci. 2021 Jun 18;22(12):6542.

Résumé en français suivi des mots-clés en français

Insérer votre résumé en français (1000 caractères maximum) suivi des mots-clés en français

Les récepteurs purinergiques P2X7 (P2X7R) sont des canaux cationiques non sélectifs dépendants d'un ligand, impliqués dans plusieurs conditions pathophysiologiques. L'activation des P2X7R est déclenchée par des concentrations élevées d'ATP extracellulaire, similaires à celles observées dans les lésions tissulaires, les inflammations chroniques, et dans le brouillage des phospholipides conduisant à l'hémorragie membranaire et à l'apoptose, survenant lors de l'entrée élevée d'ions Ca2+. Très récemment, une famille importante de scramblases régulées et de canaux chlorure activés par le calcium, connue sous le nom d'anoctamines/TMEM16s, a été proposée comme partenaire d'interaction prometteur des récepteurs P2X7. Dans cette thèse de recherche, nous avons démontré, pour la première fois, un couplage physique entre ces deux protéines et identifié des composants/régions régulateurs critiques pour la stabilité et l'interaction du complexe, contribuant ainsi à la caractérisation biophysique et moléculaire du complexe et explorant également ses implications dans les réponses immunitaires. Ainsi, nous avons pu découvrir de nouvelles cibles pharmacologiques potentielles.

Mots clés :

P2X7R, TMEM16F, FLIM-FRET Inflammation, Mort cellulaire, Immunité innée

Résumé en anglais suivi des mots-clés en anglais

Insérer votre résumé en anglais (1000 caractères maximum) suivi des mots-clés en anglais

Purinergic P2X7 receptors (P2X7R) are ligand-gated non-selective cation channels involved in several pathophysiological conditions. P2X7R activation is triggered following elevated concentrations of extracellular ATP, similarly to those observed in tissues injury, chronic inflammation, and in the scrambling of phospholipids leading to membrane blebbing and apoptosis, occurring during elevated entry of of Ca^{2+} ions. Very recently a major family of regulated scramblase and calcium-activated chloride channels, known as anoctamins/TMEM16s were proposed as promising interacting partner to P2X7 receptors. In this research thesis we demonstrated, for the first time, a physical coupling between these two proteins and identified regulatory components/regions critical to complex stability and interaction, contributing, as such to the biophysical and molecular characterisation of the complex also exploring its implications in immune responses. Thus, providing insights into novel potential pharmacological targets.

Keywords :

P2X7R, TMEM16F, FLIM-FRET, Inflammation, Cell death, Innate immunity, Cys Anchor.